STAR FORMATION IN MOLECULAR CLOUDS AND GLOBULAR CLUSTERS

By

DEAN E. McLAUGHLIN, B.Sc., M.Sc.

A Thesis

Submitted to the School of Graduate Studies

in Partial Fulfilment of the Requirements for the Degree

Doctor of Philosophy

McMaster University

STAR FORMATION IN MOLECULAR CLOUDS AND GLOBULAR CLUSTERS

DOCTOR OF PHILOSOPHY (1997)
(Astrophysics)

McMaster University
Hamilton, Ontario

TITLE: Star Formation in Molecular Clouds and Globular Clusters

AUTHOR: Dean E. McLaughlin
B.Sc. (University of Alberta)
M.Sc. (McMaster University)

SUPERVISOR: Dr. Ralph E. Pudritz

NUMBER OF PAGES: xiv, 233

Abstract

Giant molecular clouds (GMCs) and cores, which are the sites of star formation in the Galaxy today, are supported against their own gravity and an external pressure by a combination of thermal and magnetic pressures, and by an internal turbulence which is characterized by gas velocity dispersions that *increase outwards* within a given cloud. Until now, however, models of isothermal spheres (in which velocity dispersion is independent of radius) have been used as the starting point for theories of star formation. Thus, this thesis presents a generalization of the classic Bonnor-Ebert stability analysis of pressure-bounded, self-gravitating spheres of isothermal gas, to include clouds with *arbitrary* equations of state (EOS). The results are applied to GMCs and cores in order to model their internal structure. It is found that the simplest EOS which is consistent with all the salient features of these clouds is a "pure logotrope," in which $P/P_c = 1 + A\ln(\rho/\rho_c)$. Detailed comparisons with data are made to estimate the value of A, and an excellent fit to the observed dependence of velocity dispersion on radius in cores is obtained with $A \simeq 0.2$. This phenomenological model is then used to construct a new theory for gravitational collapse and star formation in turbulent molecular gas. Points of similarity and contrast between this and the collapse of an isothermal sphere are discussed. In particular, it is found that the rate of mass accretion onto a protostar in a logotrope increases with time (as $\dot{M} \propto t^3$), rather than remaining constant as in an isothermal sphere. Low-mass stars therefore take longer to form than previously suspected, while high-mass stars form more rapidly. This result has implications for the interpretation of observations of young stellar objects (the so-called "Class 0" protostars are discussed explicitly), for the origin and form of the stellar initial mass function, and for the process of star formation in clusters.

GMCs and cores are further characterized by a mass spectrum, $N(m) = dN/dm$, which

scales roughly as $m^{-1.5}$ and is reminiscent of the distribution of globular cluster masses in the globular cluster systems (GCSs) observed around most galaxies. This suggests that star formation in protogalaxies may have followed the same basic pattern that it does today, i.e., that globular clusters formed in clumps of gas embedded in much larger ($\sim 10^8 - 10^9 M_\odot$) protogalactic fragments. Within this framework, the first theory of the GCS $N(m)$ (which is directly related to the more frequently discussed globular cluster luminosity function, dN/dM_V) is developed here. A kinetic equation is formulated to statistically follow the collisional build-up and subsequent disruption (by the side-effects of internal massive-star formation) of protocluster clumps within a parent fragment, and solved for the mass spectrum which gives a detailed balance between the rates of these processes. This $N(m)$ agrees well with observations of the Milky Way, M31, and M87 GCSs, for cluster masses in excess of $\sim 10^5 M_\odot$. In addition, the theory naturally accounts for observations which suggest that, at least at these high masses, $N(m)$ is largely independent of galactocentric radius within any one GCS. The model makes specific predictions, regarding the lifetimes of cluster-forming cores, that should be applicable to present-day Galactic GMCs and cores as well.

Acknowledgements

I can only hope that this thesis reflects something of the influence that my supervisors present and past, Ralph Pudritz and Bill Harris, have had on me. With a generosity of intellect and an abundance of curiosity that I still find remarkable, these men have shown me what science, and scientists, can be. My hat is off to both of them.

Thanks are due Glen Petitpas and Christine Wilson for reading and commenting on individual chapters in this thesis, even though they were under no obligation to do so. I am also grateful to the rest of the Astronomy faculty here, for the past six years of instruction and discourse; to the Department staff, for guiding me with competence and unflagging cheerfulness through the labyrinthine workings of a University; and to what is now a long list of people who have passed through ABB 253, for never failing to provide me with much needed distraction.

GLAUCON: I am strongly in favor of [astronomy]. A heightened awareness of the seasons and the months and years will be useful both in agriculture and navigation, and still more in the art of war.

SOCRATES: You amuse me, Glaucon. You are so obviously concerned lest people think you are sanctioning studies that could turn out to be useless. Nonetheless, I realize your concern is not a trivial one. Only with greatest difficulty can one understand that every soul has that power of knowing that studies like these can refresh and purify. This holds true even if the soul's habitual behavior has left it blind and corrupt. Such a power is more precious than ten thousand eyes, for it is the only means we possess to see the truth. All who hold this belief will accept these words with deep conviction. But those others who are wholly unaware of such things will naturally call them nonsense, for they can see no profit in them. So you must decide, here and now, to which group you will address your argument. Or will you speak to none of them, pursuing the discussion rather for your own profit, while leaving others free to gain from it what they will?

GLAUCON: The latter. I speak and ask and answer questions mainly for my own sake.... And now, Socrates, as you rebuked the vulgar manner in which I praised astronomy before, my praise shall be given in your own spirit. For everyone, I think, must see that astronomy compels the soul to look upwards and leads us from this world to another.

PLATO, *The Republic [VII, 527-9]*

Contents

Abstract iii

List of Figures xii

List of Tables xiii

Preface xiv

1 Molecular Clouds in the Milky Way 1

1.1 Outline 1

1.2 Large-Scale Structure of the Interstellar Medium 2

1.3 Self-Gravitating Clouds Are Molecular 6

1.3.1 Interstellar Dust and Extinction 6

1.3.2 Criterion for Self-Gravitation 8

1.3.3 Molecule Formation and Destruction 9

1.4 Probing the Molecular ISM 13

1.4.1 The Importance of CO and NH_3 14

1.4.2 Temperatures, Linewidths, and Masses 16

1.5 Observations of Molecular Clouds and Cores 19

1.5.1 History 19

1.5.2 Distribution of CO and Associated Star Formation 21

1.5.3 Physical Conditions in Clouds and Cores 27

1.6 Theoretical Issues 38

2 The Internal Structure of Molecular Cores **44**

2.1 Introduction 45

2.2 Generalized Bonnor-Ebert Relations 46

2.2.1 Magnetic Equilibria 47

2.2.2 Stability: Critical Clouds 47

2.2.3 Magnetic Field Model 49

2.3 Polytropic Equations of State 49

2.4 The Logotrope 50

2.4.1 Comparison With Data: Molecular Cloud Cores 53

2.5 Summary 55

Appendices 55

References 59

3 Logotropic Collapse and Star Formation **60**

3.1 Introduction 61

3.2 Similarity Solutions 62

3.2.1 The Logotrope 62

3.2.2 Fluid Equations 64

3.2.3 Critical Points and the Expansion Wave 66

3.3 Accretion Timescales 67

3.4 Implications for Low-Mass Star Formation 69

3.5 Summary 72

Appendices 72

References 76

4 Globular Clusters **77**

4.1 A Clustered Mode of Star Formation 78

4.2 Observations of Globular Clusters 87

4.2.1 Magnitudes, Ages, Metallicities, and Masses 88

4.2.2 Globular Cluster Systems 92

4.3 Fossil Records or Chance Survivors? . . . 102
4.4 Globular Cluster Formation . . . 107
4.4.1 Supergiant Molecular Clouds . . . 112

5 The Globular Cluster Luminosity Function **122**
5.1 Introduction . . . 123
5.2 Observational Input . . . 124
5.3 A Steady State Agglomeration Model . . . 126
5.3.1 Basic Physics . . . 127
5.3.2 A General Equation . . . 128
5.3.3 Specifics . . . 130
5.3.4 Numerical Results . . . 131
5.4 Fitting the Luminosity Functions . . . 134
5.5 Timescales: Consequences for Galaxy Formation . . . 135
5.5.1 Collision Times . . . 135
5.5.2 Disruption Times . . . 137
5.6 Summary . . . 137
Appendices . . . 138
References . . . 141

6 Summary and Discussion **143**
6.1 Summary . . . 143
6.2 Logotropic Clouds and Collapse . . . 146
6.3 Cluster Formation . . . 148
6.4 The Low-Mass End of the GCLF . . . 149
6.5 Agglomeration and Fractal Cloud Structure . . . 153

A Computer Codes **161**
A.1 Hydrostatic Equilibrium . . . 161
A.1.1 poly.f . . . 162
A.1.2 ave.f . . . 177

A.2 Gravitational Collapse 182
A.2.1 sing.f 183
A.2.2 coll.f 191
A.3 Collisional Mass Spectra 193
A.3.1 spec.f 195
A.3.2 time.f 212

B Bureaucracy **214**

References **218**

List of Figures

1.1 Distribution of H I, H II, and H_2 in the Galaxy. 22

1.2 Molecular line maps of Orion A 25

2.1 Comparison of equations of state 51

2.2 Internal structure of a logotrope 52

2.3 $A = 0.2$ logotrope vs. observed linewidth profiles in GMC cores 54

3.1 Density profiles of critical-mass logotrope and isothermal sphere 63

3.2 Velocity fields in logotropic collapse solutions 66

3.3 Logotropic expansion-wave collapse (similarity variables) 68

3.4 Accretion timescales for protostars in $A = 0.2$ logotropes 69

3.5 Expansion-wave collapse of a solar-mass logotrope (physical variables) 70

4.1 Distribution of star formation in Taurus-Auriga 80

4.2 Distribution of star formation in Orion B 81

4.3 Globular clusters around M87 94

5.1 Distribution of globular cluster masses in the Milky Way and M31 124

5.2 Distribution of globular cluster masses in M87 125

5.3 Distribution of core masses in the Rosette and Maddalena GMCs 126

5.4 Effect of collision cross section on steady-state agglomeration mass spectra 132

5.5 Effects of other parameters on steady-state agglomeration mass spectra 133

5.6 Model fits to the M87 GCS 134

5.7 Model fits to the Milky Way and M31 GCSs combined 135
5.8 Dimensionless agglomeration timescales in the Milky Way and M87 136

List of Tables

1.1 Principal phases of the interstellar medium 4

1.2 Properties of molecular clouds and cores 27

2.1 Properties of critical logotropes 54

3.1 Properties of pressure-truncated $A = 0.2$ logotropes 63

3.2 Core mass vs. density normalization 65

3.3 Logotrope expansion wave 69

3.4 Polytrope expansion waves 75

4.1 Properties of SGMCs and cores in the Milky Way 115

5.1 Model parameters for observed GCS mass spectra 135

5.2 Computed quantities for $a = 1$ GCS models 136

5.3 Parameters for selected numerical models 139

Preface

The bulk of the original work in this thesis is presented in Chapters 2, 3, and 5. These include peer-refereed articles which were first published in The Astrophysical Journal and are reprinted here with the permission of the American Astronomical Society (see Appendix B). I hereby grant irrevocable, non-exclusive licence to McMaster University, and to the National Library of Canada, to reproduce this material as a part of the thesis.

As a general rule, I wrote each of these articles in its entirety, and performed all analytical and numerical calculations therein. The two exceptions to this are: (1) the Introduction to *The Formation of Globular Cluster Systems. I. The Luminosity Function* (Chapter 5), which was originally written by Ralph Pudritz; and (2) the calculation, in Section 3.1 of that same paper, of the expected shock cooling time for collisions between cores in "supergiant molecular clouds," which was carried out also by Ralph Pudritz. After peer reviews, and in preparation for publication, the papers were edited by myself and Ralph Pudritz. Acknowledgements of useful discussions with, or suggestions from, other individuals are given in the papers themselves.

I wrote any computer code required in the course of this work (Appendix A), although subroutines were frequently taken from *Numerical Recipes in Fortran, Second Edition* (Press et al. 1992).

Chapter 1

Molecular Clouds in the Milky Way

1.1 Outline

Star formation has been called the most important unsolved problem in astrophysics. At the very least, there can be little doubt that it is one of the few issues at the heart of the subject. Because they are host to planets, the formation of stars bears directly on the origins of life; because they are the building blocks of stellar clusters and galaxies, the formation of stars is inextricably linked to the origin and evolution of these more spectacular large-scale structures; because they are responsible for the production of heavy elements (i.e., essentially every element higher than helium on the Periodic Table), the formation of stars ultimately drives the chemical evolution of solar systems, galaxies, and the universe as a whole. The list could go on, but it is already clear from these few examples that, like many simple questions, the answer to this one — How do stars form? — has far-reaching consequences for our understanding of the universe around us. And, like most other simple questions, a complete answer to this one has proven frustratingly elusive.

This thesis represents an attempt to shed some new light on the question of star formation, from two complementary angles: first, from the point of view of initial conditions (what are the salient qualities of the gas which is now forming or will eventually form stars?); and second, from the point of view of final states (what is there to be learned from careful study of the end results of

the star-formation process?). We begin with the first of these approaches. The rest of this Chapter provides an introduction to our current knowledge of the star-forming gas in the Milky Way. Chapter 2 (McLaughlin & Pudritz 1996b) then goes on to develop a new theoretical picture of the initial, equilibrium structure of the so-called *clumps*, or *cores*, inside *giant molecular clouds*, and Chapter 3 (McLaughlin & Pudritz 1997) discusses their inevitable gravitational collapse. We then switch to the second mode of attack. Chapter 4 is a review of some fundamental properties of very massive and old *globular star clusters*, which have been found around nearly every galaxy in which they have been sought. Although their great sizes and ages might at first make globular clusters seem only marginally relevant to star formation in general, we argue that they are in fact the products of a most generic and commonplace aspect of the process. Chapter 5 (McLaughlin & Pudritz 1996a) then presents a theoretical model for the *globular cluster luminosity function*, which is one of the defining characteristics of the systems of globular clusters that inhabit galaxies. The theory is based on a recently developed physical framework for the formation of globular clusters, that itself incorporates the basic features of the star formation pattern in our Galaxy today. Finally, Chapter 6 summarizes the thesis and points to directions for further research.

1.2 Large-Scale Structure of the Interstellar Medium

Irrespective of any details, it is obvious that stars must condense out of the interstellar medium (ISM), which is the general term for the gas and dust spread between the stars in the disk of the Milky Way. Thus, in spite of the fact that the ISM presently constitutes only about 10% (i.e., $\sim 5 \times 10^9 M_\odot$)[1] of the visible mass of our Galaxy, an understanding of it is a critical prerequisite for any answer to the question of star formation.

Hydrogen is by far the most abundant element in the universe, and by *number* of nuclei it accounts for about 90% of the interstellar matter; the rest is primarily helium (~10%), with a scatter (~0.1%) of heavier elements. By *mass*, roughly 70% of the ISM is in hydrogen, 28% in helium, and 2% in all heavier elements. Van de Hulst (1945) first predicted that neutral interstellar hydrogen atoms (H I) should be observable, at radio wavelengths ($\lambda = 21$ cm; frequency $\nu = 1420$

[1]The mass of the Sun is $1 M_\odot = 1.99 \times 10^{33}$ g.

MHz), through the emission and absorption of radiation by transitions between states of parallel and antiparallel alignment of the spins in their constituent protons and electrons. This effect was first observed in astronomical gas by Ewen & Purcell (1951), and for some two decades thereafter served as the principal diagnostic of the ISM. Since the late 1960s and early 1970s, more extensive observations at radio, microwave, visible, ultraviolet, and X-ray wavelengths have combined to give what now appears to be an essentially complete inventory of the ISM, which includes ionized hydrogen (H II) as well as neutral H I, *and* a large amount of molecular gas.

Roughly half of the Galactic H I mass is concentrated into diffuse clouds, of typical temperature $T \sim 80$ K and particle number density $n \sim 10 - 100$ cm^{-3}, which occupy only a small fraction of the total volume of the ISM. This *cold neutral medium*, which is identified by absorption in the 21-cm "spin-flip" line mentioned above, is distributed within a disk that has an exponential scale height (half the average thickness) of ~150 parsecs (pc)[2] at the Sun's position in the Galaxy and that shows some flaring and warping further out.

The atomic H I clouds are surrounded by a much warmer ($T \sim 8000$ K), less dense ($n \lesssim 1$ cm^{-3}), and more pervasive *intercloud medium*. Much of this gas is also neutral hydrogen, and is therefore detected by 21-cm emission; its scale height is of order a few hundred pc in the solar neighborhood. There is also a significant amount of ionized hydrogen (H II) in the intercloud medium. This is detected primarily by emission of radiation resulting from the recombination of electrons and hydrogen nuclei; locally, it is confined to an average distance of ~1000 pc from the midplane of the Galaxy.

This much was already largely understood by the mid-1960s (e.g., Clark 1965). However, it was suggested very early on (Spitzer 1956) that H I clouds seen far above the plane might be confined by the pressure of a very hot ($T \sim 10^6$ K), low-density ($n \sim 10^{-3}$ cm^{-3}), highly ionized gaseous *corona*. The existence of this third component of the ISM was finally confirmed in the early 1970s, via observations of ultraviolet absorption lines of interstellar O VI (five-times ionized oxygen: Jenkins & Meloy 1974; York 1974) and diffuse X-ray emission (Williamson et al. 1974). The topology and volume filling factor of the hot corona are still matters of some debate, but it may have a scale height as large as several thousand pc, and take up as much as half the total volume of the ISM.

[2] A parsec is the distance at which the radius of the earth's orbit subtends an angle of one second of arc (i.e., 1/3600 of a degree) on the sky. It is equal to 3.09×10^{18} cm.

The hot corona, the intercloud medium, and the cold neutral medium are the three main components, or phases, of the *diffuse* ISM. A rough summary of their gross properties is given in Table 1.1 (e.g., Longair 1994); further details may be found in the texts of Longair (1994) and Mihalas & Binney (1981), or in the review of Kulkarni & Heiles (1988). (As we've suggested, the volume fractions of the corona and the intercloud medium are stilll somewhat controversial, and the numbers given here should be taken only as rough guides.)

Table 1.1: Principal Phases of the Interstellar Medium[a]

Phase	Main Constituent	Volume of Interstellar Medium	Fraction by Mass	n (cm^{-3})	Temp. (K)	Mean Visual Extinction
Corona	H II; e^-; highly ionized species	~50%	0.1%	$\sim 10^{-3}$	$\sim 10^6$	—
Intercloud Medium	H I, H II, e^-; ionization fraction 10–20%	40%	20%	0.1–1	8000	—
Cold Neutral Medium	H, C, O; some ions, C^+, Ca^+	5%	40%	1–100	80	< 1 mag
Molecular Clouds	H_2, CO, NH_3, CS, HCN, etc.	~0.5%	40%	> 100	10–30	~2–30 mag

[a]After Longair (1994)

It is worth taking note of the characteristic densities and temperatures for each of the components of the ISM mentioned thus far. The product of n and T is directly proportional to the *thermal* pressure of the gas, through the ideal gas law: $P_{\rm therm} = nkT$. Thus, even given the rough range of numbers in Table 1.1, it is apparent that there is at least an order-of-magnitude constancy of $P_{\rm therm}$ throughout the diffuse ISM, viz. $P_{\rm therm} \sim 10^3\ k\ {\rm cm}^{-3}\ {\rm K}$.[3] This basic fact is key to the current theoretical picture of a *multiphase ISM*. In its original incarnation (Field 1965; Field, Goldsmith, & Habing 1969), the idea was that the existence of thermal instability over a finite range of temperature in the ISM would lead to the coexistence of two *stable* phases of gas in

[3]The numerical value of Boltzmann's constant k is 1.38×10^{-16} erg K^{-1}.

pressure balance and thermal equilibrium at roughly the observed temperatures of the H I clouds and the intercloud medium. Later on, this picture was expanded, most notably by McKee & Ostriker (1977), to account for the inherent violence of the ISM and provide for the possibility of a hot corona produced by supernova shock waves. A good overview of the current theoretical and observational status of this picture is given by McKee (1995).

As it turns out, the total pressure in the diffuse ISM typically exceeds $P_{\rm therm}$ by about an order of magnitude: $P_{\rm ISM} = (2.8 \pm 0.4) \times 10^4\ k\ {\rm cm}^{-3}$ K, according to Boulares & Cox (1990), with roughly equal contributions from turbulent kinetic energy, magnetic fields, and cosmic rays. (Cosmic rays are charged particles — mostly protons — moving through the Galaxy at very high speeds, with kinetic energies $E \sim 10^9$ eV.) As we will see (§1.5.3 below, and McLaughlin & Pudritz 1996b), this pressure is important because it works to confine clouds in what is, from the star-formation point of view, the most important component of the interstellar gas.

As the last row of Table 1.1 indicates, nearly half of the mass of the Galactic ISM (i.e., $\sim 2.5 \times 10^9 M_\odot$) is contained in cold ($T \sim 10$ K), dense ($n > 10^2$ cm^{-3}) clouds of *molecular hydrogen* (H_2), which are distributed in the disk of the Galaxy with a scale height of ~75 pc. These clouds typically have overall diameters of ~40 pc, but they inevitably show internal structure — subcondensations referred to as *cores* or *clumps* — over a wide range of scales (down to ~0.1 pc) and densities (up to $10^5 - 10^6$ cm^{-3}). It is these cores which are now recognized as the true sites of star formation in the Milky Way. The rest of this Chapter therefore focuses mainly on the molecular ISM. As §1.5.3 discusses, molecular clouds and cores are typically very highly pressured, and are *not* in pressure equilibrium with the diffuse interstellar gas. Thus, as McKee (1995) points out, they cannot be incorporated into multiphase models of the ISM. Even though its net pressure is critical in defining the properties of star-forming clouds, the diffuse gas is therefore important to us only as a backdrop of sorts.

Before describing the observed distribution and physical properties of the molecular gas in any detail, however, we pause now to offer an argument (§1.3) as to why we should expect, *a priori*, that this component of the ISM alone be associated with star formation. Section 1.4 then roughly outlines the *way* in which molecular gas is observed, and §1.5 moves on to review the history and main results of these observations. Finally, §1.6 points out some of the important theoretical

questions that are raised by these data.

1.3 Self-Gravitating Clouds Are Molecular

Conditions in even the densest interstellar gas are still a far cry from those in stars themselves, where $n \sim 10^{24}$ cm^{-3}. Gravity is the only real candidate for a means to increase densities by the 20 orders of magnitude ultimately required to precipitate a star from the ISM; thus, *star-forming gas must be self-gravitating.* In light of this, we now demonstrate (following, e.g., Elmegreen 1985; McKee 1989, 1995) that, among all the phases of the ISM, it is exclusively the molecular clouds which have this vital property. Our argument will connect with the last column of Table 1.1, which lists the typical *mean visual extinctions* (denoted $\overline{\mathrm{A}}_V$) of neutral H I and molecular H_2 clouds.

1.3.1 Interstellar Dust and Extinction

Extinction is a measure, on the astronomical magnitude scale,[4] of the attenuation of radiation as it travels through the interstellar gas: if light of intensity I_0 at some wavelength λ enters a region of gas with a mean extinction $\overline{\mathrm{A}}_\lambda$ given in magnitudes, then it will emerge (and be observed) with intensity

$$\frac{I}{I_0} = 10^{-0.4\overline{A}_\lambda} \equiv e^{-\tau_\lambda} \ , \tag{1.1}$$

where $\tau_\lambda = 0.921\overline{\mathrm{A}}_\lambda$ is the *optical depth* of the gas.

For the case of interest here — the extinction observed towards H I and H_2 clouds — $\overline{\mathrm{A}}_\lambda$ is a function of wavelength (e.g., Mathis 1990), and $\overline{\mathrm{A}}_V$ refers specifically to the effect on (roughly yellow) light at $\lambda \simeq 5500$Å.[5] Attenuation is caused by scattering and absorption of the light by solid, silicon- and carbon-rich *dust grains* which exist in gas colder than about 10^3 K (at higher temperatures, the dust is effectively destroyed by collisions). These interstellar grains appear to contain a significant fraction of all the elements heavier than helium to be found in the ISM (it will be recalled [§1.2] that heavy elements account for ~2% of the total ISM mass). Light of a given

[4]The magnitude system puts energy fluxes on a logarithmic scale, such that the apparent brightness of an object is given, in magnitudes, by m_λ = constant $- 2.5 \log_{10}(L_\lambda/L_{\lambda,\odot})$, where L_λ is the energy radiated by the object, per second, at the wavelength λ; $L_{\lambda,\odot}$ is the energy radiated by the Sun at the same wavelength; and the additive constant is a function of the wavelength λ and the distance to the emitting object.

[5]One angstrom is 1Å $= 10^{-8}$ cm.

wavelength, λ, is most effectively scattered by particles with radii $a \gtrsim \lambda$, so the observed dependence of extinction on wavelength can be used to infer a distribution of grain radii. It is known, then, that grains range in size from $a \lesssim 3$Å to $a \sim 3000$Å, with a strong preference for the smaller radii [specifically, $N(a) \propto a^{-3}$ or so; see Mathis 1990, and references therein].

As light travels deeper into a cold cloud of gas, it will have more opportunities for encounters with dust grains. The total extinction $\overline{\mathrm{A}}_\lambda$ is therefore a function both of the average density n_d of grains in the cloud, and of the net distance traveled through it; specifically, $\overline{\mathrm{A}}_\lambda \propto N_d \propto \int n_d \, dl$. Here N_d is the *column density* (number of particles per cm^2) of the dust in the cloud; $\int dl$ is its depth; and the constant of proportionality depends on the scattering and absorption cross sections of the grains at wavelength λ. But now, N_d is itself proportional (for a constant gas-dust ratio) to the total column density of hydrogen *nuclei*, $N_H = N_{HI} + 2N_{H_2}$, so $\overline{\mathrm{A}}_\lambda$ can also be expressed in terms of this latter, more accessible quantity. With this in mind, Savage et al. (1977) derived the total H_2 column densities, and Bohlin, Savage, & Drake (1978) the total H I column densities, along the lines of sight to 109 stars with known visual extinctions $\overline{\mathrm{A}}_V$; they found (see also Spitzer 1978; Mathis 1990),

$$\overline{\mathrm{A}}_V = 5.36 \times 10^{-22} \left(\frac{N_H}{\mathrm{cm}^{-2}} \right) \ \mathrm{mag} \ , \tag{1.2}$$

or

$$N_H = 1.87 \times 10^{21} \left(\frac{\overline{\mathrm{A}}_V}{\mathrm{mag}} \right) \ \mathrm{cm}^{-2} \ . \tag{1.3}$$

Given these relations (which are equivalent to a gas-to-dust ratio of 100 : 1 by mass), the extinction $\overline{\mathrm{A}}_\lambda$ at any other wavelength may be derived from tabulated ratios of $\overline{\mathrm{A}}_\lambda / \overline{\mathrm{A}}_V$ (which are by now reasonably well determined, although they may vary from place to place in the Galaxy; Mathis 1990). In general, $\overline{\mathrm{A}}_\lambda$ increases towards shorter wavelengths: ultraviolet light is absorbed very efficiently indeed, while the extinction at millimeter and radio wavelengths in the Milky Way is effectively negligible.

It has to be noted that the numerical coefficient in equation (1.2) or (1.3) is strictly valid for relatively *diffuse* interstellar clouds ($\overline{\mathrm{A}}_V \lesssim 1.5$), since it is only there that H_2 can be observed directly (see §1.4 below). Nevertheless, it is common practice to assume that the $\overline{\mathrm{A}}_V$-N_H calibration pertains also to higher-extinction regions, so that this simple relation forms the basis of the analysis

in the rest of this Section.

1.3.2 Criterion for Self-Gravitation

The connection between column density and extinction allows us to use $\overline{\mathrm{A}}_V$ as a measure of the self-gravity of a cloud of gas (Elmegreen 1985; McKee 1989, 1995). This is because the gravitational energy of a cloud of mass M and radius R is given (in a spherical approximation) by

$$\mathcal{W} = -\frac{3a}{5}\,\frac{GM^2}{R}\ , \tag{1.4}$$

so that the energy density can be written as

$$\frac{\mathcal{W}}{V} = \frac{3}{4\pi R^3}\,\mathcal{W} = -\frac{9aG}{20\pi}\,\frac{M^2}{R^4} \equiv -3P_G\ . \tag{1.5}$$

The factor a here depends on the density stratification within the cloud; it is discussed further in Chapter 2 below, but is always of order unity. We have also defined a "gravitational pressure" P_G, after Bertoldi & McKee (1992). At this point, then, we can bring in the *mass* column density, $\Sigma \equiv M/\pi R^2$, such that

$$P_G = \frac{3a\pi}{20}\,G\Sigma^2 = \frac{3a\pi}{20}\,G(\mu m_H)^2 N_H^2\ , \tag{1.6}$$

where, as before, N_H is the total column density of hydrogen nuclei in the gas under question, and μ is the average mass *per H nucleus*, in units of m_H.[6] As was mentioned in §1.2, there is one helium atom (mass $4m_H$) to be found for every ten hydrogen nuclei (each of mass m_H) in the ISM, so we have that $\mu = 14/10 = 1.4$. In any event, equations (1.3) and (1.6) are equivalent to

$$P_G/k = 2.22 \times 10^3\ \mu^2 a\ \left(\frac{\overline{\mathrm{A}}_V}{\mathrm{mag}}\right)^2\ \mathrm{cm}^{-3}\ \mathrm{K}\ , \tag{1.7}$$

with k again denoting Boltzmann's constant.

Now, there are generally four kinds of energy associated with any interstellar cloud: an internal kinetic energy, $\mathcal{U} > 0$, which arises from random thermal and (usually more important)

[6] The mass of a hydrogen nucleus is $m_H = 1.67 \times 10^{-24}$ g, and the gravitational constant is $G = 6.67 \times 10^{-8}$ dyne cm^2 g^{-2}.

turbulent motions of the gas; the energy, $\mathcal{M} > 0$, of any mean magnetic field threading the cloud; a "compressive" energy, $\mathcal{C} = -3P_s V$, due to the pressure P_s exerted on the surface of the cloud by the more diffuse gas surrounding it; and the gravitational energy, $\mathcal{W} = -3P_G V$, just discussed. In the absence of $\mathcal{U}$ and $\mathcal{M}$, it is clear that $\mathcal{C}$ and $\mathcal{W}$ would combine to drive the cloud into collapse. In the absence of $\mathcal{C}$ and $\mathcal{W}$, the positive total energy of the cloud would lead to an overall expansion and eventual dispersal. More realistically, $\mathcal{C}$ and $\mathcal{W}$ work together to confine an *equilibrium* cloud. This leads us to consider the relative magnitudes of $\mathcal{C}$ and $\mathcal{W}$ — or, equivalently, of P_s and P_G — and to make a distinction between clouds which are confined more by their own gravity than by any surface pressure. *We designate as self-gravitating those clouds in which P_G is dynamically more important than P_s*:

$$\text{self-gravitating} \implies P_G \gtrsim P_s \,. \tag{1.8}$$

Given this rough criterion for self-gravitation; given that $P_s/k \simeq 2 \times 10^4$ cm^{-3} K on average in the intercloud ISM (Elmegreen 1989; Boulares & Cox 1990; McKee 1995);[7] and given equation (1.7) for P_G, we finally have that

$$\text{self-gravitating} \implies \overline{\mathrm{A}}_V \gtrsim \frac{3.0}{\mu\sqrt{a}} \text{ mag} \,. \tag{1.9}$$

With $\mu = 1.4$ and $a \approx 1$, then, interstellar clouds require $\overline{\mathrm{A}}_V \gtrsim 2.1$ in order to be self-gravitating. A quick glance back at Table 1.1 and the *observed* $\overline{\mathrm{A}}_V$ of H I and H_2 clouds shows that we do indeed expect only the latter to be self-gravitating; and thus, only they should be able to form stars.

1.3.3 Molecule Formation and Destruction

The preceding analysis offers the beginnings of an explanation for the association of star formation with molecular clouds; but it does not, by itself, exclude the possibility that there might be self-gravitating (and potentially star-forming) atomic clouds. And yet, as Table 1.1 suggests, H I clouds are *not* self-gravitating (they have $\overline{\mathrm{A}}_V \lesssim 1$, with typical values around 0.3 mag). Why are all high-$\overline{\mathrm{A}}_V$ clouds predominantly molecular in composition? The answer to this lies again with the interstellar dust grains.

[7] Only the contributions to $P_{\rm ISM}$ from magnetic fields and turbulence in the diffuse gas are important for cloud confinement; thus, $P_s \simeq (2/3)P_{\rm ISM}$; cf. §1.2.

One of the more important routes to molecule formation directly from atoms in astronomical gases is *radiative association* (e.g., Watson 1976; Duley & Williams 1984), in which two atoms collide to form an unbound "association" with positive total energy. Once this occurs, there is generally some small probability that some of the atoms' energy will subsequently be radiated away, allowing the pair to relax into a bound molecular state. If this mechanism of formation is to be at all viable, however, the radiative energy loss must take place quickly, before the atoms separate again of their own accord; in the language of quantum mechanics, the bound state must be reached through an electric dipole transition. This is possible for many of the molecules observed in the ISM — including the important carbon monoxide (CO) species — but it is *not* an option for the most abundant one, H_2.

Because H_2 consists of two nuclei with equal charge-to-mass ratios, its center of charge and center of mass are coincident, and it does not have an electric dipole moment (the same is true of any homonuclear molecule, like O_2 or N_2, and of symmetric species like methane, CH_4). Thus, formation of H_2 by the radiative association of two ground-state H atoms would rely on "forbidden" transitions (e.g., quadrupole radiation) to a bound molecular state, and these proceed far too slowly ever to be of any importance. Other possible gas-phase reactions to form H_2 involve the production of intermediate species like H^- or H_2^+, but this is efficiently done only when the temperature and ionization fraction of the gas are greater than what is observed in Galactic H I and H_2 clouds (Watson 1976).

These points lead to the conclusion that interstellar molecular hydrogen cannot be produced in any great quantities in a purely gaseous phase. Rather, *almost all of the H_2 in the ISM is likely formed on the surfaces of dust grains* (e.g., Hollenbach & Salpeter 1971; Watson 1976): A hydrogen atom collides with a solid grain and sticks to it until there is a collision with a second H atom. The two atoms then combine to form a single H_2 molecule, and the binding energy released in the process (4.48 eV)[8] is sufficient to evaporate the molecule, intact, off the surface of the grain and back into the gas itself. The rate of formation in this way depends on the collision rate between H atoms and grains, on the probability that an atom incident on a grain surface will be adsorbed (and remain with the grain until a second collision occurs), and on the probability that a molecule is

[8] An energy of one electron-volt (eV) is equal to 1.6×10^{-12} erg.

ejected after formation. A favorable balance between the collision rate (which should increase with the gas temperature) and the sticking probability (which decreases with increasing T) appears to be obtained for temperatures less than ~100 K (Hollenbach & Salpeter 1971), so that H_2 formation can proceed rapidly in typical interstellar clouds. Once H_2 is present in the gas phase, a suite of different molecular species can form through various exchange reactions that involve the transfer of charge or of atoms between colliding molecules, atoms, and ions (i.e., reactions of the type $AB+C \longrightarrow A+BC$). Many of these reactions are made possible through the ionization of H_2 by cosmic rays (which leads, for example, to formation of the important species H_3^+; see Herbst & Klemperer 1973; Duley & Williams 1988; Genzel 1992), a process which is also important as a heating mechanism for the gas (§1.5.3 below).

Evidently, then, dust grains are an indispensible catalyst for the formation of molecules in the ISM.[9] Once formed, however, a molecule is generally susceptible to rapid destruction by the process of *photodissociation*, in which a photon absorbed from the interstellar radiation field is energetic enough to break the molecule into its constituent atoms. The binding energies of many important molecules lie in the range $\sim 5 - 11$ eV (e.g., Lang 1980), so it is the ultraviolet (UV) background radiation in the Milky Way (at wavelengths $912\text{Å} \leq \lambda \lesssim 2400\text{Å}$, corresponding to energies $13.6 \text{ eV} \geq E \gtrsim 5$ eV) which is important in this context.[10] This UV background (Habing 1968; Jura 1974) is due almost entirely to radiation from hot ($T \sim 5000 - 45\,000$ K), massive ($M \sim 5 - 50 M_\odot$), O- and B-type stars in the Galaxy, and it is intense enough to dissociate exposed H_2 molecules almost as quickly as they form. The key to preserving H_2 molecules, and allowing for the formation of significant amounts of other species, is *shielding* from the destructive UV radiation field. When they are present in large enough quantities, dust grains contribute to this. A rough sketch of how this works is as follows (see Spitzer 1978 or Scheffler & Elsässer 1988 for a rigorous development):

---

[9] It is important to note, however, that, other than H_2, very few molecules now in the gas phase are likely to have formed directly on grain surfaces. The adsorption energies of most heavy molecules (with a few important exceptions like H_2O and ammonia, NH_3) tend to be quite large, so that when they do form on grains they are not easily evaporated back into the gas (e.g., Watson & Salpeter 1972a, b). This fact may account for the observed "depletion" of heavy-element abundances, relative to cosmic values, in the ISM (Spitzer 1978).

[10] In principle, radiation at shorter wavelengths ($\lambda < 912$ Å) would also be able to dissociate molecules. However, such light is also energetic enough ($E > 13.6$ eV) to directly ionize atomic hydrogen. It is therefore absorbed rapidly and efficiently over very short pathlengths in the ISM, and contributes very little to the pervasive "background" radiation.

The relative abundance of molecular hydrogen in a cloud, $n(H_2)/n(HI)$, is obtained from the statistical equilibrium condition $n(HI)R_{\rm form} = n(H_2)R_{\rm diss}$, where $R_{\rm form}$ is the formation rate of H_2 (in units of s^{-1}) and $R_{\rm diss}$ is the rate of photodissociation. These rates are discussed in detail by, e.g., Scheffler & Elsässer. For our purposes, the important points are that (1) $R_{\rm form}$ is proportional to the density of dust grains, which is itself proportional to $n(H) = n(HI) + 2n(H_2)$; and that (2) $R_{\rm diss}$ is proportional to the intensity $I_{\rm UV}$ of dissociative radiation able to penetrate the cloud. This latter quantity is in turn related to the overall background UV flux by $I_{\rm UV} = I_0 \exp(-\tau_{\rm UV})$ (cf. eq. [1.1]). Now, the mean extinction of the cloud at ultraviolet wavelengths is greater than that at visual wavelengths, by a factor of roughly $\overline{\rm A}_{\rm UV}/\overline{\rm A}_V \simeq 3.2$ (Mathis 1990). Thus, the optical depth is $\tau_{\rm UV} = 0.921\overline{\rm A}_{\rm UV} \simeq 3\overline{\rm A}_V$, so that, in equilibrium, $n(H_2)/n(HI) = R_{\rm form}/R_{\rm diss} \propto n(H) \exp(3\,\overline{\rm A}_V)$. Scheffler & Elsässer (1988) estimate $R_{\rm form}$ and $R_{\rm diss}$ explicitly for a typical diffuse cloud with $T = 100$ K, $n(H) = 25$ cm^{-3}, and $\overline{\rm A}_V$=0.3 mag. They then find a tiny $n(H_2)/n(HI) \simeq 2 \times 10^{-5}$, so if $R_{\rm form}$ is assumed to be roughly independent of temperature, we have that

$$\frac{n(H_2)}{n(HI)} = \frac{R_{\rm form}}{R_{\rm diss}} \approx 2 \times 10^{-5} \, \frac{n(H)}{25 \ {\rm cm}^{-3}} \, \exp\,[3(\overline{\rm A}_V - 0.3)] \qquad (1.10)$$

in general. [The neglect of any T-dependence in $R_{\rm form}$, and hence in $n(H_2)/n(HI)$, is justified because the H_2 formation rate depends on the product of the grain sticking coefficient and the characteristic thermal velocity of the gas particles. The former increases towards lower temperatures, while the latter decreases.]

This relation already shows that low-density, low-$\overline{\rm A}_V$, non-self-gravitating interstellar clouds are expected to be overwhelmingly atomic in composition. Further, if we define as molecular any cloud which has half or more of its total hydrogen mass in molecular form [i.e., $M(H_2)/M(HI) = 2n(H_2)/n(HI) \geq 1$], we now see that this is equivalent to

$$\text{molecular cloud} \implies \overline{\rm A}_V \gtrsim 3.0 \ {\rm mag} \qquad (1.11)$$

when an average $n(H) = 200$ cm^{-3} is also assumed (cf. Table 1.1, and Table 1.2 below).

This simple argument necessarily omits important details of molecular physics. It also ignores *self*-shielding of H_2 and the fact that extinction is a *cumulative* effect, i.e., that UV radiation

can only penetrate the outer few layers of a cloud with a mean $\overline{A}_V$ of even just a few magnitudes (so the dense inner regions of such clouds will always be almost totally molecular). Proper treatments of these points, and more detailed discussions of the atomic-molecular transition in interstellar clouds, may be found in, e.g., Hollenbach, Werner, & Salpeter (1971); Federman, Glassgold, & Kwan (1979); Elmegreen (1989); van Dishoeck & Black (1986); or (in a slightly different context) Tielens & Hollenbach (1985).

Nevertheless, a comparison of our equations (1.11) and (1.9) serves very well to make the basic point that self-gravitating, star-forming clouds in the Milky Way should in fact be molecular. How, then, are such clouds studied?

1.4 Probing the Molecular ISM

Aside from H_2, there is a vast array of molecules in the dense interstellar medium (see §1.5.1 below). By far, the majority of these are observed through their absorption or emission of radiation at long — millimeter to radio — wavelengths. One of the reasons for this is that, broadly speaking, there are three main "reservoirs" of energy in molecules (see, e.g., Bransden & Joachain 1989; or, in an astronomical context, Genzel 1992 and Scheffler & Elsässer 1988): (1) the configuration of the outer, or valence, electrons; (2) vibrations of the atomic nuclei about their mean positions; and (3) rotation of the nuclei about their common center of mass. Changes in the first of these are referred to as *electronic transitions*; they typically involve relatively large energy differences (of order a few eV), and thus the absorption or emission of light at optical or ultraviolet wavelengths. *Vibrational transitions* entail somewhat smaller energy changes, $\Delta E \sim 0.1$ eV, and tend to fall in the infrared region of the spectrum. *Rotational transitions*, however, usually correspond (just because of the typical size and mass scales involved) to very small $\Delta E \lesssim 10^{-3}$ eV, and thus $\lambda \gtrsim 1$ mm. In many cases, it is these low-energy transitions which are most easily effected at the typical densities ($n \gtrsim 100$ cm^{-3}) and temperatures ($T \sim 10$ K) of most of the molecular ISM. (Or, conversely, it is the preponderance of these transitions which points to such conditions in molecular clouds.) Aside from this, even when electronic transitions do occur, the high extinction at short wavelengths in molecular clouds (§1.3.3), coupled with the obscuring effect of short-λ transitions in the Earth's atmosphere, often makes them difficult or impossible to observe anyway. But extinction decreases

steadily with increasing wavelength (§1.3.1), and is essentially negligible for all $\lambda \gtrsim 0.25$ mm (Mathis 1990); thus, far-infrared and radio transitions are naturally selected for detection in dense gas.

Unfortunately, the molecular structure of H_2 (e.g., Shull & Beckwith 1982) is such that even its lowest-energy rotational transition — which has $\Delta E \simeq 0.04$ eV, corresponding to $\lambda \simeq 28$ μm and the far-infrared region of the spectrum — requires rather high densities and temperatures ($n \sim 10^2 - 10^3$ cm^{-3} and $T \sim 10^2 - 10^3$ K) to be excited (see also Genzel 1992); and any of its higher-energy transitions correspond to shorter wavelengths and more extreme excitation conditions. Thus, H_2 may serve as an effective probe of hot, shocked gas (e.g., Shull & Beckwith 1982), or perhaps of the UV-heated surfaces of molecular clouds, but *it cannot be observed directly* in the cold interiors of the high-$\overline{A}_V$ objects to which it is largely confined. Rather, the molecular gas in the Galaxy is, by and large, best mapped with "tracers" like (among many others) carbon monoxide (CO) and ammonia (NH_3). (Unless stated otherwise, when we refer to CO we mean its most common isotope, $^{12}C^{16}O$.)

1.4.1 The Importance of CO and NH_3

After H_2, CO is the most ubiquitous species in the molecular ISM: its fractional abundance in dense clouds, relative to H_2, is $\sim 10^{-4}$ (Genzel 1992, and references therein). As a diatomic molecule, it makes itself known primarily through its rotational transitions, which can be understood through a quantum mechanical analysis of the so-called *rigid rotator* (cf. Bransden & Joachain 1989): Two particles (atomic nuclei) with masses m_1 and m_2, separated by a distance r, orbit their center of mass with a total angular momentum L. The rotational energy of such a configuration is given by $L^2/2I$, where $I = \mu r^2$ is the moment of inertia; $\mu \equiv m_1 m_2/(m_1 + m_2)$ is the reduced mass (note that this μ is *not* the same as that discussed in §1.3.2 above); and L^2 is allowed to take on only certain discrete values, viz. $L^2 = \hbar^2 J(J+1), J = 0, 1, 2, \ldots$.[11] Thus, rotational energy states are referred to by their value of J, and transitions from an upper, or excited, level to a lower one involve the emission of energy according to $\Delta E(J+1 \rightarrow J) = (\hbar^2/I)(J+1)$; absorption of the same amount of energy would lead to a transition from the lower to the upper state. Since any molecule has a unique $\hbar^2/I$ which can be accurately measured in the laboratory, the presence of emission or

[11] Planck's constant is $h = 6.63 \times 10^{-27}$ erg s, and $\hbar \equiv h/2\pi$.

absorption features, or lines, at specific wavelengths in a rotation spectrum leads to the identification of the species present. For CO, $\hbar^2/I = 4.77 \times 10^{-4}$ eV, so that the two lowest-energy rotational lines appear at wavelengths of 2.6 mm ($J = 1 \rightarrow 0$) and 1.3 mm ($J = 2 \rightarrow 1$),[12] corresponding to frequencies $\nu = c/\lambda = 1.15 \times 10^{11}$ Hz and 2.30×10^{11} Hz.[13]

The fractional abundance of NH_3 is not as high as that of CO, but its polyatomic nature allows for many closely spaced energy levels, and so for many different transitions at similar wavelengths; thus, it can be observed under a wide variety of conditions in the ISM. A particularly important region of ammonia's spectrum is $\lambda \simeq 1.2 - 1.3$ cm ($\nu \simeq 2.3 - 2.5 \times 10^{10}$ Hz). Most of the lines here are produced by *inversion transitions* (Ho & Townes 1983), which are a class of the vibrational transitions mentioned above. Essentially, NH_3 has a pyramidal structure, in which the three H atoms define the molecule's "base," and the N atom its "apex." An inversion transition involves the *tunnelling* of the N atom from one side of the H-atom plane to the other.

Both CO and NH_3 ultimately trace H_2 because it is collisions with the latter particles which are largely responsible for putting significant numbers of the former into excited states ($J > 0$ for CO; N on the higher-energy tip of the pyramid for NH_3) in the first place — something which is obviously requisite for the subsequent radiative de-excitation that gives rise to any observed line. However, at a given temperature and H_2 density, the excited states of different molecules are populated with different efficiencies, and so CO and NH_3 trace different parts of the overall H_2 distribution.

The line emission in a given molecular transition is strongest when the populations of the upper and lower energy levels involved are *thermalized*; which is to say, when (1) the thermal energy kT of the gas is comparable to the energy (relative to the ground state) of the upper level of the transition, and (2) the total (mostly H_2) density exceeds a so-called *critical density*, $n_{\rm crit}$, at which the rate of collisional excitation to the upper level just balances the rate of de-excitation by spontaneous emission of radiation. When both these conditions are met, the higher-energy state will be sufficiently well populated, in statistical equilibrium, to allow for the emission of radiation with observable intensities.

Detailed calculations of the energies and critical densities for the various rotation levels of

[12]The rotational transitions of heteronuclear molecules generally proceed by electric dipole radiation, and as such are subject to the constraint that J change by only ± 1 in any single emission or absorption event. Thus, important lines in the spectrum of CO include $J = 1 \rightarrow 0$ and $J = 2 \rightarrow 1$, but not $J = 2 \rightarrow 0$.

[13]The speed of light is $c = 3.00 \times 10^{10}$ cm s^{-1}.

CO show that the $J = 1 \rightarrow 0$ and $2 \rightarrow 1$ lines are thermalized for $T \sim 10 - 20$ K and $n \gtrsim 10^2$ cm^{-3}. Thus, these millimeter transitions are good diagnostics of moderately cold and dense molecular gas. [More precisely, the critical density of a CO $J + 1 \rightarrow J$ line is $n_{\rm crit} \sim 4000(J + 1)^3/\tau$ cm^{-3}, and the optical depth τ, which is discussed below, is typically $\sim 10 - 100$ for the $1 \rightarrow 0$ line in the Milky Way; see Genzel 1992.] The $1.2 - 1.3$ cm inversion lines of NH_3 are thermalized at $T \sim 20 - 100$ K and $n \sim 10^4 - 10^6$ cm^{-3} and therefore can be used to probe warmer, denser regions (see Ho & Townes 1983).

1.4.2 Temperatures, Linewidths, and Masses

Spectral lines contain important information on the basic physical properties of the gas that forms them. A comprehensive discussion of how fundamental quantities like temperatures, velocity dispersions, and densities are derived from spectroscopic observations is well beyond the scope of this thesis, but we now mention some of the more important points.

First, the brightness of a line depends on the temperature of its source. An extended source (i.e., a cloud) that emits radiation in a line at wavelength λ against a uniform background will give rise to an excess in the observed intensity at that wavelength, according to

$$\Delta I_{\rm obs} = [I_\lambda({\rm source}) - I_\lambda({\rm background})]\,(1 - e^{-\tau_\lambda})\ , \tag{1.12}$$

where the optical depth, τ_λ (cf. eq. [1.1]), is now due to *line trapping* within the cloud, and *not* to extinction by dust grains as in §1.3.1. Line trapping occurs when radiation emitted during a downwards transition of some excited molecule in a cloud is reabsorbed, before it can escape and be observed, to excite another molecule of the same species elsewhere in the cloud. A line is said to be *optically thick* ($\tau_\lambda > 1$) when the probability of such a reabsorption event is high; it is *optically thin* ($\tau_\lambda < 1$) when radiation is more likely to escape the cloud unimpeded.

Now, the Rayleigh-Jeans approximation[14] can be used to write intensities in terms of *brightness temperatures*: $I_\lambda = (2kc/\lambda^4)T_b$. With this substitution, and in the limit of a *very optically thick*

[14]The Rayleigh-Jeans approximation describes the long-wavelength ($hc/\lambda \ll kT$) tail of the characteristic Planck spectrum for radiation from a blackbody of temperature T: $I_\lambda = (2hc^2/\lambda^5)[\exp(hc/\lambda kT) - 1]^{-1}$.

line [$\tau_\lambda \gg 1$, so that $(1 - e^{-\tau_\lambda}) \simeq 1$], equation (1.12) reduces to

$$\Delta I_{\rm obs} = \frac{2kc}{\lambda^4} [T_b(\text{source}) - T_b(\text{background})] \ . \tag{1.13}$$

The brightness temperature of a line source is equal to its more fundamental *kinetic temperature*, T, *if* the transition involved is thermalized and its upper level is populated mainly by collisions. As was suggested above, this is the case for the the $J = 1 \rightarrow 0$ line of CO in Galactic molecular clouds. Moreover, because of the high abundance of CO, this line is *universally optically thick* ($\tau_{1\rightarrow 0} \sim 10 - 100$) in these objects. Thus, one of the simplest ways to estimate kinetic temperatures in molecular clouds is to read them, as per equation (1.13), directly from observed intensities of the CO $J = 1 \rightarrow 0$ emission line. (There are, of course, complications in practice; see Genzel [1992] for a thorough discussion).

Second, the shape of a spectral line reflects the internal dynamics of the originating gas. Until now, we have been discussing lines as if they were infinitesimally thin "spikes" of emission or absorption at a single, well defined wavelength, λ_0, that corresponds exactly to the energy change involved in some molecular transition. However, there are a wide range of physical processes which act to broaden any spectral line, so that the intensity does not fall immediately to zero for wavelengths $\lambda \neq \lambda_0$. Several such mechanisms are discussed in detail by, e.g., Lang (1980). By far the most important of these, in the present context of the ISM, is *Doppler broadening*. This effect accompanies any internal motion in a cloud of gas, whether it be due to large-scale bulk flows like collapse or rotation, or to random velocities of the individual particles. In this latter case, the molecules will have a Maxwellian distribution of velocities, $N(v) \propto \exp[-(v - \langle v \rangle)^2/2\sigma^2]$, where $\langle v \rangle$ is the mean velocity of the cloud. For unsaturated, or optically thin, transitions, this results in a line with the same shape: $I_\lambda \propto N(v) \propto \exp[-(\lambda - \lambda_0)^2/2\sigma_\lambda^2]$. Thus, the peak of the line is at $\lambda_0 = \lambda_{\rm lab}(1 + \langle v \rangle/c)$, and its dispersion is

$$\frac{\sigma_\lambda}{\lambda_0} = \frac{\sigma}{c} \ . \tag{1.14}$$

Thus, the (one-dimensional) *velocity dispersions*, σ, of molecular clouds are inferred directly from measurement of the widths of their spectral lines. (The analysis of optically thick lines, which have non-Gaussian shapes, is more complicated than what we have suggested here [e.g., Genzel

1992]; but the basic idea is the same.) Throughout this thesis, we therefore use the term *linewidth* interchangeably with velocity dispersion to refer to σ.

A third fundamental parameter of any body of gas is its mass. This is usually inferred for molecular clouds from observations of their volume densities n, or column densities N, and their (effective) radii R. The most sophisticated analyses derive n from the observed intensities of different lines of a single molecular species to infer its level populations as a function of energy, which can then be used as conditions to solve the equations of radiative transfer and excitation in full. Difficulties with this approach can include the strong coupling of quantities like density, temperature, and optical depth (so that many different lines may need to be observed) and uncertainties in fundamental parameters such as collision cross sections (which are used in assuming a balance between the rates of collisional excitation and radiative de-excitation). In addition, the method is often best suited to the analysis of high-density tracers (like NH_3, with its many transitions at similar wavelengths), but (as is discussed in §1.5 below) these are really indicators of local conditions on small scales within molecular clouds; CO is still the best probe of the global properties in their larger-scale, lower-density regions. The difficulty is that, although CO necessarily traces H_2, its large optical depth means that *observable* emission in the low-J transitions can only come from the outer regions of clouds. Nevertheless, the use of CO $J = 1 \rightarrow 0$ observations to infer quantitative, *total* H_2 cloud masses is still valid, insofar as it can be justified empirically.

In practice, the total intensity of a $J = 1 \rightarrow 0$ line is expressed in terms of the quantity $W_{CO} \equiv \int T_b(v)dv$, wherein wavelengths are converted to velocities by $\Delta\lambda/\lambda_{lab} = v/c$; intensities are written as brightness temperatures (again, defined by the Rayleigh-Jeans approximation given above); and the integration covers the full extent of the broadened line. This quantity is then taken to scale with the H_2 column density — $N_{H_2} \equiv X_{CO}W_{CO}$ — so that the problem reduces to finding the constant of proportionality, X_{CO}, by independently estimating N_{H_2}. There are several ways in which this can be done: (1) Equation (1.3), relating visual extinction to the total hydrogen column density, is assumed to hold even in gas that is completely molecular. Measurements of W_{CO} and $\overline{A}_V$ along the same lines of sight then combine to yield X_{CO} (e.g., Dickman 1978; Young & Scoville 1982). (2) Lines of CO isotopes (such as $C^{18}O$ and, very often, ^{13}CO) can be optically *thin* (due to the lower abundances of these species), in which case their integrated intensities are just

proportional to the isotopic column densities, $N(^{13}CO)$ and $N(C^{18}O)$. But these latter quantities have been shown to correlate with N_{H_2}; thus the ^{12}CO intensity of a region can be compared with its ^{13}CO or C^{18}O emission to obtain $X_{\rm CO}$ (Dickman 1978; Frerking, Langer, & Wilson 1982). (3) The pervasive cosmic rays routinely collide with hydrogen nuclei to produce intermediate particles (π-mesons) which quickly decay into very energetic ($E \sim 3 \times 10^6 - 1 \times 10^9$ eV) gamma rays. The intensity of diffuse γ-radiation along the line of sight to molecular clouds therefore yields estimates of N_{H_2} for comparison with $W_{\rm CO}$ (e.g., Bloemen et al. 1986; Strong et al. 1988).

Each of these methods has its own built-in assumptions and practical limitations, and the CO-to-H_2 conversion is still uncertain by perhaps a factor of two. However, there are two important points to be made here. First, all of these procedures result in similar values for $X_{\rm CO}$; namely,

$$X_{\rm CO} \equiv \frac{N_{H_2}}{W_{\rm CO}} \simeq (3 \pm 1) \times 10^{20} \text{ cm}^{-2} \text{ (K km s}^{-1})^{-1} \tag{1.15}$$

(cf. Scoville & Sanders 1987; Combes 1991). This implies that CO $J = 1 \rightarrow 0$ intensity levels do in fact reflect total H_2 masses. Second, yet another method of estimating $X_{\rm CO}$ assumes that (large) molecular clouds are *virialized*, in order to derive N_{H_2} from CO $J = 1 \rightarrow 0$ observations of their linewidths and sizes (Dickman, Snell, & Schloerb 1986; Solomon et al. 1987; Scoville & Sanders 1987). The independent X-values thus obtained are again consistent with the others, and with equation (1.15). This fundamental result is discussed further in §1.5.3.

1.5 Observations of Molecular Clouds and Cores

1.5.1 History

So far, we have been taking for granted the fact that there is a significant amount of molecular gas in the Milky Way, and that it is collected into cold, dense clouds. In practice, of course, this realization was slow in coming, and the study of this important component of the ISM has taken most of this century to develop.

The first direct observation of interstellar gas seems to have been Hartmann's (1904) discovery of stationary, or "detached," absorption lines of calcium in the optical spectrum of the binary

star δ Orionis. These lines did not share in the periodic displacements (caused by orbital motions) of the other spectral features of the star, and were therefore inferred to arise from absorption in a cloud "at some point in space in the line of sight between the Sun and δ Orionis." Many other detached lines, most corresponding to transitions of calcium and potassium, were subsequently discovered in the spectra of other stars. Eventually, a number of unidentified detached lines were observed in the spectra of at least two different stars (Merrill 1934, 1936; Dunham 1937). Almost immediately after their measurement, it was suggested (Russell 1935; Eddington 1937; Saha 1937; Swings 1937; Swings & Rosenfeld 1937) that these might correspond to transitions between molecular, rather than atomic, energy states. Swings & Rosenfeld (1937), in particular, tentatively associated one of Dunham's (1937) lines with a rotational transition of CH. This identification was confirmed by Adams (1941), who also gave convincing evidence for the detection of interstellar cyanogen (CN) and (after McKellar 1940) of NaH.

These lines were all found in *optical* spectra, and as such had to have originated in diffuse gas with relatively low $\overline{A}_V$; for example, Bates & Spitzer (1951) found that observed (low) abundances of CH and CH^+ could be explained by an equilibrium between radiative association and photodissociation in regions of $n \sim 100$ cm^{-3} (which would correspond to the dense centers of H I clouds). Ultimately, the extinction factor meant that a full appreciation of the molecular ISM had to await the development of radio astronomy after World War II. The first interstellar molecule to be detected at radio wavelengths was hydroxyl (OH), by Weinreb et al. (1963). The second was NH_3, by Cheung et al. (1968). This was also the first polyatomic species to be discovered, and it marked the beginning of a flood of new identifications: Zuckerman & Palmer (1974) list 25 interstellar molecules known just 5 years later; Turner & Ziurys (1988) tabulate observed transitions for 68 different species; and Longair (1994) names 99, with the largest being the 13-atom complex $CH_{11}N$.

H_2 itself was not detected until rocket-borne observations saw some of its ultraviolet electronic transitions in absorption towards the star ξ Persei (Carruthers 1970). Given the difficulties with H_2 observations already discussed, this discovery was perhaps most important for showing that the column densities of H_2 and H I were roughly equal along the line of sight to ξ Per; the broader implication, that vast quantities of molecular gas might indeed exist in the Milky Way, was a significant step forward. Coincident with this development was the first identification of the 2.6-mm

CO $J = 1 \rightarrow 0$ line (Wilson, Jefferts, & Penzias 1970), which was used almost immediately to begin investigating the Galactic H_2 distribution in detail.

1.5.2 Distribution of CO and Associated Star Formation

The first large-scale CO surveys of the inner Galaxy were carried out by Schwartz, Wilson, & Epstein (1973), Burton et al. (1975), and Scoville & Solomon (1975). Many later studies both followed up on these initial observations and looked to the outer Galaxy, until Dame et al. (1987) were able to combine the data from 16 secondary surveys to construct a CO picture of ~20% of the sky. The designs and main results of most of the individual projects are discussed by Combes (1991). The large-scale distribution of CO (and therefore H_2) in the Milky Way is well reviewed by Scoville & Sanders (1987), and is essentially as follows:

Most of the CO emission in the inner Galaxy (i.e., inside the radius of the Sun's orbit, which is roughly $R_0 \simeq 8$ kpc = 8000 pc) is strongly concentrated in a thick *molecular ring* at Galactocentric radii $3 \lesssim R_{gc} \lesssim 7$ kpc (Scoville & Solomon 1975). The emission drops briefly interior to 3 kpc, before exhibiting a sharp rise again at radii $R_{gc} \lesssim 1.5$ kpc; beyond 7 kpc, the CO intensity falls steadily with increasing R_{gc}. Upon converting CO intensity to H_2 mass (as discussed above), it becomes clear that roughly 75% of all the molecular hydrogen in the Galaxy resides in the molecular ring. This is in marked contrast to the distribution of atomic H I, which has an essentially constant density throughout the disk (i.e., over $3 \lesssim R_{gc} \lesssim 15$ kpc), and most of whose mass is located at $R > R_0$. Thus, although the ISM is roughly equal parts atomic and molecular hydrogen (with $\sim 2.5 \times 10^9 M_\odot$ in each phase; cf. §1.2), the radial distributions of the two are completely different. On the other hand, the H_2 structure is in close agreement, particularly in terms of the ring feature, with the radial distribution of H II regions in the disk. These are essentially "bubbles" of ionized hydrogen around hot, young ($\lesssim 10^7$ yr), O and B (OB) stars; they are carved out by the intense UV radiation (at $E \geq 13.6$ eV, or $\lambda \leq 912$Å) from the stars themselves. As such, the overall correspondence between H II and H_2 is one direct piece of evidence that star formation is associated with molecular gas. Figure 1.1, which is taken from Scoville & Sanders (1987), illustrates these points quantitatively.

In addition to this, H_2 is rather closely confined to the disk of the Milky Way, with a scale height (mean half-thickness) which increases from ~35 pc at the Galactic center to ~130 pc at the

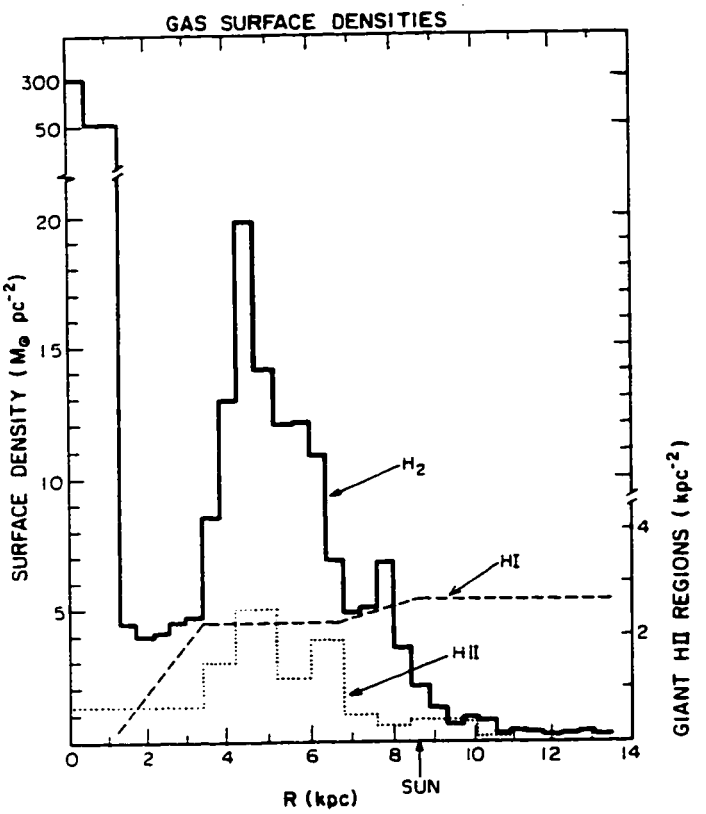

Figure 1.1: Distribution of H I, H II, and H_2 in the Milky Way. Vertical axis on the left marks the mass surface density (integrated perpendicular to the Galactic plane) of H I and H_2; on the right, number surface density of H II regions. The solar radius is taken here to be $R_0 = 8.5$ kpc. From Scoville & Sanders (1987).

Solar circle, and has an average value of $\simeq$75 pc (Cohen & Thaddeus 1977; Scoville & Sanders 1987). This is only half the scale height of the cold H I cloud layer, and less than one-tenth that of the warm intercloud gas (cf. §1.2); but it is quite comparable to the characteristic height ($\sim$50 pc; Blaauw 1991) that is observed in the distribution of OB associations. Again, then, and in a very global sense, the phenomena of star formation and molecular gas are clearly interrelated. Moreover, as our discussion in §1.3 led us to expect, this is most certainly *not* true of the H I component of the ISM.

Another important way in which the H_2 and H I distributions differ is in the degree of clumpiness they exhibit. This was clear almost from the beginning, when it was observed (e.g., Scoville & Solomon 1975) that CO spectra along any single line of sight towards the inner Galaxy exhibit several distinct peaks, but show no evidence for any widespread component of "diffuse"

emission between the peaks. This implies that the molecular gas is entirely confined to discrete clouds, i.e., there is no molecular intercloud medium. (Indeed, the low densities expected of any intercloud gas would seem to preclude the possibility that it could be molecular; cf. §1.3.3.) Such clouds are widely distributed throughout the disk, and are found to occupy the spiral arms and interarm regions of the Galaxy in roughly equal proportions (in terms of total CO emission; Solomon, Sanders, & Rivolo 1985). It is therefore possible to identify large numbers of molecular clouds as emission peaks in large-scale CO surveys, and then define each one down to some pre-set intensity (or brightness temperature) contour level. This approach lends itself particularly well to investigation of the statistical properties of a whole ensemble of clouds. Alternatively, clouds within a few kpc of the Sun can be identified individually — by the association of nebulosity and extinction with visible H II regions (as in, e.g., Orion, Taurus-Auriga, Ophiuchus, M17, and the Rosette Nebula) — and then mapped in CO to their outer boundaries. Whether they are defined statistically or individually, these clouds tend to show the same average properties in general (see Table 1.2 below): their kinetic temperatures are of order $T \sim 10$ K; total linewidths, $\sigma \sim 1 - 5$ km s^{-1}; radii, $R \sim 4 - 40$ pc; and masses, $M \sim 10^4 - 10^6 M_\odot$. Evidently, these are very large structures; in fact, roughly 80% of the total Galactic H_2 mass is contained in a few thousand clouds with $M \geq 10^5 M_\odot$ (e.g., Sanders, Scoville, & Solomon 1985). They are therefore usually referred to as *giant molecular clouds* (GMCs). (Here a distinction is made between GMCs and "optical" *dark clouds*. These are concentrated regions of high extinction — usually first identified in the course of photographic sky surveys [e.g., Barnard 1919; Lynds 1962] — with masses typically of order several hundred $M_\odot$. We will not discuss these objects in detail; reviews of their various properties can be found in Zuckerman & Palmer [1974], Ho & Townes [1983], and Leung [1985].)

A fundamental property of GMCs is their tendency to show internal substructure; *all molecular clouds contain dense clumps, or cores, on a wide range of scales.* Indirect evidence for this came initially from the fact that NH_3 can be observed *at all* in GMCs (e.g., Morris et al. 1973; Barrett, Ho, & Myers 1977): Since the inversion transitions of ammonia are sensitive to $n \gtrsim 10^4$ cm^{-3}, their detection obviously relies on the existence of very dense gas. On the other hand, CO observations imply mean H_2 densities of only $n \sim 10^2$ cm^{-3} on large scales in GMCs. To put this another way, if the $n \sim 10^4$ cm^{-3} required for NH_3 excitation were to obtain throughout an entire GMC with

typical radius $R \simeq 20$ pc, equation (1.2) would predict a visual extinction of order 1000 mag, rather than the $\overline{A}_V \simeq 9$ that is usually observed (cf. Table 1.2 below). Either way, consistency between the CO and NH_3 data requires that the NH_3 be tracing *small pockets* of high-density gas. More detailed arguments for this were made by Barrett et al. (1977) specifically for the Kleinmann-Low Nebula in Orion. These authors concluded that the NH_3 there had to be clumped on scales of $\sim$0.05 pc. Over time, radio studies made with increasingly higher spatial resolution have confirmed and extended these results, both in Orion and in other clouds. Many observations of NH_3 cores in a wide variety of GMCs and (smaller) dark clouds are reviewed by, e.g., Ho & Townes (1983) and Myers (1985). More recent progress has also come from the use of other high-$n_{\rm crit}$ species to identify very dense regions in clouds; a comprehensive overview of these results is given by Wilson & Walmsley (1989). It is now clear that small-scale clumpiness is ubiquitous in the molecular ISM. This is another feature which distinguishes H_2 from H I clouds, and it would therefore appear to be a key prerequisite for star formation.

The amount and spatial scale of any clumpiness seen in a cloud naturally depends on the resolution of the radio telescope used to make the observations, and on the physical conditions required to excite emission from the tracer molecule. This point is well illustrated by Fig. 1.2, which shows the Orion A (L1641) GMC mapped, at varying resolutions, in the $J = 1 \rightarrow 0$ line of ^{13}CO (which is usually optically thin, and is thus a *column* density tracer with $n_{\rm crit} \sim 10^3$ cm^{-3}); in the $J = 2 \rightarrow 1$ line of CS (an intermediate-density tracer); and in NH_3. Results such as these are the basis of the oft-stated assertion that molecular clouds show structure on all scales; indeed, high-resolution observations in both CO (e.g., Falgarone, Phillips, & Walker 1991) and higher-density tracers (Langer et al. 1995) have revealed the existence of clumps with well defined internal motions on scales as small as $\sim$0.02 pc. Such findings have led some (e.g., Scalo 1985, 1990) to argue that cores, and even entire clouds, are in some sense illusory artifacts, either of instrumental effects (such as limited resolution and dynamical range), or of "arbitrary" cloud definitions (i.e., the practice of mapping only down to some pre-determined lower limit of intensity or brightness temperature). In addition, claims of *self-similarity* in the structure of the molecular ISM, on $\sim 0.01 - 100$ pc scales, have led to descriptions of GMCs and cores as manifestations of a fractal geometry generated by turbulence (e.g., Scalo 1985, 1990; Falgarone 1995; Elmegreen & Falgarone 1996).

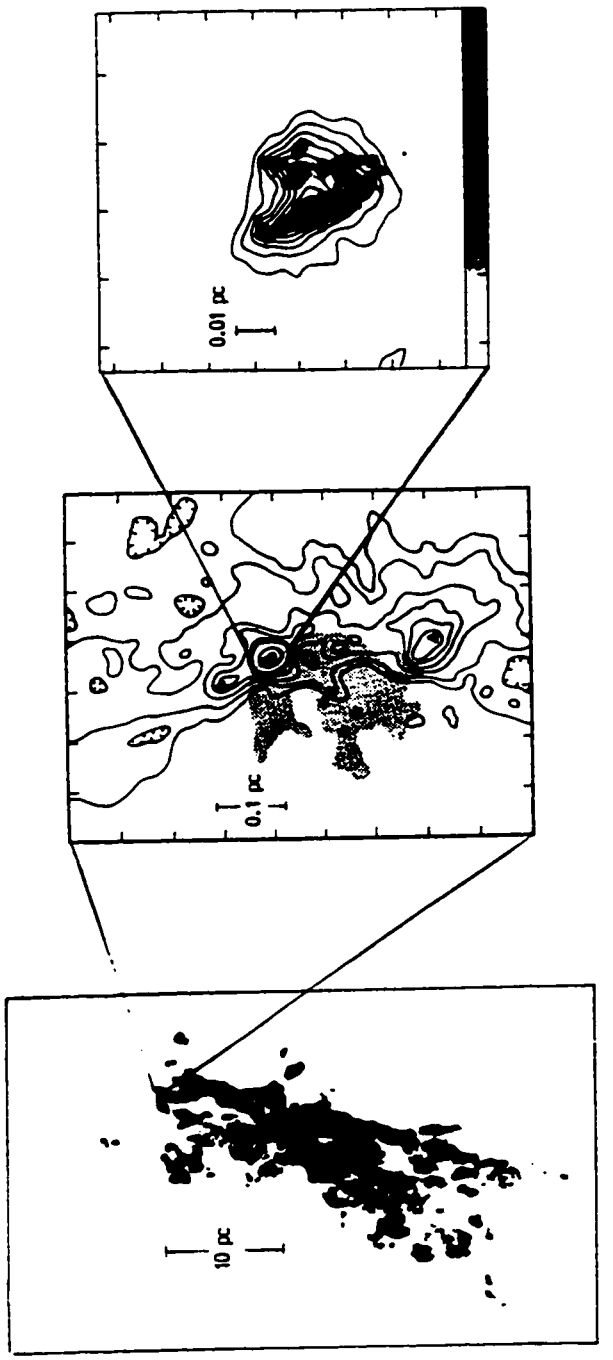

Figure 1.2: Molecular line maps of the Orion A molecular cloud. *Bottom panel*: ^{13}CO $J = 1 \rightarrow 0$ map with spatial resolution of 90″=0.19 pc. *Middle panel*: CS $J = 2 \rightarrow 1$ at a resolution of 7″.5=0.016 pc. Asterisks mark the OB stars of the Trapezium cluster; shaded region delineates the Orion A H II region. *Top panel*: Map of a 1.2-cm inversion line of NH_3, at 1″=0.002 pc and 2″=0.004 pc resolutions (grayscale and contours, respectively). From Genzel (1992).

We leave a discussion of fractal geometry in the ISM, and its connection with the conventional cloud-core picture that we pursue here, to Chapter 6. However, note that several lines of argument suggest that clouds and cores are indeed real, physically meaningful objects (e.g., Blitz 1991; Genzel 1992). Among these are the facts that (1) cores are not just random fluctuations of projected intensity in the plane of the sky, but have a limited extent in the *velocity* domain as well (e.g., Blitz & Stark 1986; Stutzki & Güsten 1990); (2) density contrasts between cores and the intercore material in GMCs are observed to be quite sizeable, viz. $\gtrsim 20 - 40$ (Stutzki & Güsten 1990; Williams, Blitz, & Stark 1995), suggesting again that the cores are distinct physical entities; and (3) no matter how they are identified, cores are observed to be associated with ongoing star formation. Indeed, the rather broad impression we have cultivated thus far — that star formation proceeds in molecular clouds — is both further validated and made much more precise when the dense substructure of GMCs is considered in detail.

Many specific examples of dense cores that are coincident, on a one-to-one basis, with compact H II regions, maser activity, or bright infrared emission (all byproducts of the early stages of star formation) are discussed by Ho & Townes (1983) and Wilson & Walmsley (1989). In addition, Myers & Benson (1983) observed 10 *low-mass cores* ($M \leq 10 M_{\odot}$), in the NH_3 inversion line, in the Taurus-Auriga GMC. They found all but one of these to be associated with obvious *groups* of young stars, and then extrapolated from their sample to estimate the total number of dense cores likely to be in all of Taurus-Auriga; compared this to the estimated rate of star formation there; and ultimately concluded that most of their NH_3 cores will form stars over the next $\sim 10^6$ years. Further, Beichman et al. (1986) were able to pair 47 of 95 nearby low-mass cores with IRAS satellite detections of infrared emission from heated dust grains around forming stars. In a similar vein, Lada, Bally, & Stark (1991a) used the CS $J = 2 \rightarrow 1$ line to identify 42 *high-mass cores* ($M \geq 10 M_{\odot}$) in the L1630 GMC (Orion B), and Lada (1992) showed that *96% of all the infrared sources associated with L1630 are contained within the four most massive cores there.* Phelps & Lada (1997) have also recently identified seven young *clusters* of stars in the Rosette GMC. Each cluster is still surrounded by molecular material, and each is associated with one of the ~ 70 high-mass cores identified in the Rosette by Williams, de Geus, & Blitz (1994) and Williams et al. (1995).

Much additional evidence along these lines is summarized by, e.g., Lada, Strom, & Myers

(1993); the idea of clustered star formation hinted at here is important in its own right, and is discussed further in Chapter 4 below. In any case, even though *not* all molecular cores necessarily contain stars at the present (in fact, there is one nearby GMC [Maddalena & Thaddeus 1985] that does not appear to be associated with any past or present star formation), all observations indicate that all sufficiently young stellar objects are associated with dense cores. Thus, as suggested in §1.2, it is the dense clumps in GMCs which are the real sites of ongoing star formation in the Milky Way; and, by extension, it is almost certain that they will play host to any such activity in the future. This makes it difficult to understand them as instrumental artifacts; rather, their observed properties, and those of their parent GMCs, serve to define the initial conditions for star formation.

1.5.3 Physical Conditions in Clouds and Cores

Table 1.2 summarizes the global characteristics of GMCs and cores in the Milky Way. Data on the clouds themselves have been distilled largely from the studies of Sanders et al. (1985) and Solomon et al. (1987), each of which analyzes $\sim$ 300 GMCs identified in the high-resolution (44″, corresponding to $\simeq$ 1 pc for a cloud at a distance of 4.5 kpc) Massachussetts-Stony Brook CO survey of the inner Galaxy (Sanders et al. 1986; Clemens et al. 1986). The indicated range of clump properties is chosen to be representative of dense NH_3 and CS cores (Myers 1985; Lada et al. 1991a; Stutzki & Güsten 1990), and is also *broadly* consistent with observations of ^{13}CO cores (Williams et al. 1994, 1995; Loren 1989a, b).

Table 1.2: Properties of Molecular Clouds and Cores

	Clouds		Cores	
Parameter	Range	Median	Range	Median
M / $M_\odot$	$10^4 - 10^6$	3.0×10^5	1–1000	260
R / pc	$4 - 40$	22	$0.02 - 0.65$	0.32
σ_{ave} / km s^{-1}	$1 - 5$	3.4	$0.2 - 1.5$	1.0
Σ / $M_\odot$ pc^{-2}	190	190	800	800
ρ_{ave} / $M_\odot$ pc^{-3}	$3.5 - 35$	6.5	$10^3 - 10^5$	1.9×10^3
N_{H_2} / 10^{21} cm^{-2}	8.4	8.4	35	35
$n(H_2)$ / cm^{-3}	$50 - 500$	93	$10^4 - 10^6$	2.7×10^4
T / K	$10 - 20$		$10 - 30$	

The rows in this Table list total masses M; effective radii $R = (\text{area}/\pi)^{1/2}$; total linewidth $\sigma_{\rm ave}$; total mass column densities $\Sigma = M/\pi R^2$; mean volume densities $\rho_{\rm ave} = 3M/4\pi R^3$; and the number densities N_{H_2} and $n(H_2)$ of hydrogen molecules, derived from Σ and $\rho_{\rm ave}$ under the assumption of a 10% helium abundance by number.

It is evident here that GMCs and cores both are distributed over fairly wide ranges in mass. In fact, this distribution takes the form of a (roughly) power-law *mass spectrum* (the number of objects with a given mass): $N(M) \propto M^{\gamma}$, where the exponent is consistently found to be in the range $\gamma \simeq -1.4$ to -1.7 for clouds and cores alike (e.g., Sanders et al. 1985; Blitz 1991). This fundamental result is discussed further in Chapters 4 and 5; but note that we have already made implicit use of it in claiming that 80% of the mass in GMCs is contained in clouds with $M \geq 10^5 M_\odot$.

The mass spectrum has also been used (with $\gamma = -1.5$ for definiteness) to evaluate the "median" cloud and core masses in Table 1.2; these are defined such that half of all the *mass* in clouds (or cores, as the case may be) is contained in those more massive than the median. Harris & Pudritz (1994) have also compiled a list of typical GMC and core properties which is, aside from some numerical differences, very similar to that given here. In particular, the ratios of median core and cloud densities, linewidths, and surface densities in Table 1.2 are

$$\widetilde{\rho} \equiv \frac{\rho_{\rm ave,core}}{\rho_{\rm ave,cloud}} \approx 290 \ , \qquad \widetilde{\sigma} \equiv \frac{\sigma_{\rm ave,core}}{\sigma_{\rm ave,cloud}} \approx 0.29 \ , \qquad \text{and} \qquad \widetilde{\Sigma} \equiv \frac{\Sigma_{\rm core}}{\Sigma_{\rm cloud}} \approx 4.2 \ , \tag{1.16}$$

which are within $\simeq$10% of those implied in Harris & Pudritz (1994). These characteristic ratios have been used by McLaughlin & Pudritz (1996b) to constrain a model for the internal structure of GMCs and cores.

Temperatures

An important aspect of GMCs and cores that has been mentioned several times now, and which appears again in Table 1.2, is their preference for kinetic temperatures $T \sim 10$ K. This is much lower than what is typically seen in H I clouds (Table 1.1), partly because their high $\overline{\rm A}_V$ shields the inner parts of molecular clouds from the hot Galactic UV background, and partly because a natural balance is struck between the cooling and heating processes in dense gas at around 10 K.

A cloud of gas inevitably loses energy whenever the line radiation from a downwards molec-

ular or atomic transition manages to escape it; any excited atom or molecule is therefore a potential coolant of the interstellar gas. Under the conditions characteristic of GMCs specifically, the most important of these by far is CO (including its isotopes), because it is abundant, it presents a large number of rotational levels to be excited, and it is easily thermalized. Goldsmith & Langer (1978) have made a detailed study of the cooling produced by line emission from a suite of molecular and atomic species. They find that, for kinetic temperatures in the range $T \sim 10 - 40$ K and total densities of order $n(H_2) \sim 10^2 - 10^4$ cm^{-3} — that is, throughout all but the very densest and smallest-scale regions of molecular clouds — the cooling by rotational transitions in all forms of CO dominates the cooling from all other species by factors of $\sim 5 - 10$. (Atomic carbon and molecular oxygen are the next most important species at these T and n.) To be specific, the total cooling rate due to rotational transitions of ^{12}CO and ^{13}CO in the temperature and density regimes considered here is approximately given by (see Genzel 1992)

$$\Lambda_{CO} \approx 10^{-24} \text{ erg s}^{-1} \text{ cm}^{-3} \left(\frac{T}{10 \text{ K}}\right)^{2.75} \left(\frac{n(H_2)}{10^3 \text{ cm}^{-3}}\right)^{0.3} . \quad (1.17)$$

Most of this cooling actually comes from high-J transitions, since the $J = 1 \rightarrow 0$ line of ^{12}CO is so optically thick.

In a static cloud, this loss of energy may be offset either by the heat released in the formation of H_2 or, more importantly, by cosmic ray ionization of H_2 (e.g., Goldsmith & Langer 1978; Genzel 1992). The latter process involves the liberation of energetic electrons that can contribute directly to heating of the gas. In the case of (essentially neutral) molecular clouds and cores, each cosmic ray ionization yields a free electron that ultimately provides about 7 eV of heat to the gas. With this and an estimate of the local cosmic ray flux, Genzel (1992) gives the cosmic ray heating rate in molecular gas as

$$\Gamma_{CR} = 9.4 \times 10^{-25} \text{ erg s}^{-1} \text{ cm}^{-3} \left(\frac{n(H_2)}{10^3 \text{ cm}^{-3}}\right) , \quad (1.18)$$

which is a factor of ~ 3 larger than the heating rate by H_2 formation (Goldsmith & Langer 1978). Comparison of equations (1.17) and (1.18) shows that, as Goldsmith & Langer also conclude, cosmic ray heating alone is sufficient to balance the gas cooling in clouds with kinetic temperatures $T \sim 10$ K and $n(H_2) \sim 10^2 - 10^4$ cm^{-3}. This very basic competition between CO and cosmic rays therefore

ensures that, generally speaking, most molecular clouds and cores will lie at similar temperatures. (However, some dense cores can be somewhat warmer if they contain hot young stars or are exposed to intense UV radiation such as that due to H II regions; small regions with T as high as $\sim$100 K do exist.)

Linewidths

At a temperature of 10 K, the *thermal linewidth* of a cloud or core is just $\sigma_{\rm T} = (kT/\mu m_H)^{1/2} = 0.19$ km s^{-1}. (Now μ is the mean mass *per particle* in the gas. Assuming its usual 10% abundance, one helium atom is found for every five H_2 molecules, so that $\mu = 14/6 = 2.33$.) It is immediately obvious, however, that the observed linewidths of GMCs are an order of magnitude larger than $\sigma_{\rm T}$. The velocity dispersions of individual cores are also *always* larger than this, although by an increasingly smaller margin as one moves towards lower masses ($\sigma_{\rm ave}/\sigma_{\rm T} \sim 1.2$ or less is not uncommon in low-mass cores).

What is the significance of these *superthermal* linewidths? An early suggestion (e.g., Goldreich & Kwan 1974) was that they reflected bulk radial motions in the clouds, due to their large-scale collapse. However, it is easily seen that this cannot be the case: *If every GMC were in a state of full-blown gravitational collapse, the star formation rate in the Galaxy would be some two orders of magnitude larger than what is observed* (cf. Zuckerman & Palmer 1974). To be specific, recall that the total mass in GMCs in the Milky Way is $M_{\rm tot} \simeq 2.5 \times 10^9 M_\odot$. Further, a typical cloud density is $\rho_{\rm ave} = 6.5 M_\odot$ pc^{-3} (Table 1.2), which corresponds to a free-fall time of $\bar{t}_{\rm ff} = (3\pi/32 G \rho_{\rm ave})^{1/2} \simeq 3.2 \times 10^6$ years. This is significant because once an object begins to collapse, it will complete the process within a few free-fall times: $t_{\rm coll} \lesssim 4.3\, \bar{t}_{\rm ff} \simeq 1.4 \times 10^7$ yr, according to McLaughlin & Pudritz (1997). If the collapse hypothesis were true, one should then expect to see a Galaxy-wide star formation rate of

$$S_{\rm coll} \gtrsim \frac{M_{\rm tot}}{t_{\rm coll}} \gtrsim \frac{2.5 \times 10^9 M_\odot}{1.4 \times 10^7 \ {\rm yr}} \sim 200\ M_\odot\ {\rm yr}^{-1}\ , \tag{1.19}$$

whereas the observed value (McKee 1989) is only

$$S_{\rm obs} \simeq 3\ M_\odot\ {\rm yr}^{-1}\ . \tag{1.20}$$

Thus, GMCs are most certainly not in free-fall collapse. This point is discussed more thoroughly by Zuckerman & Evans (1974), who address a number of serious observational difficulties with the notion of *any* widespread, systematic radial motion or infall, even at less than the free-fall rate, in GMCs. (Also important in this regard is the fact that the observationally inferred lifetimes of GMCs — which are variously estimated at anywhere between $\tau \simeq 4 \times 10^7$ yr and $\tau > 10^8$ yr — are generally longer than $t_{\rm coll} \sim 10^7$ yr; see, e.g., the review of Elmegreen 1991.) It therefore seems inevitable that *GMCs are somehow supported against their self-gravity on large scales.* On smaller scales, *some* cloud cores obviously must be collapsing to form stars; but even here, there is no evidence that collapse is very widespread or in an especially advanced stage (e.g., Myers & Benson 1983).

At the same time, if velocity dispersions everywhere were all at thermal levels, $\sigma_{\rm T} \sim 0.19$ km s^{-1}, most clouds and cores are so massive that they *would* have to collapse: The maximum mass of a sphere that can be supported entirely by thermal pressure against its self-gravity and an external surface pressure P_s is only $M = 2.59\ M_\odot\ (\sigma_{\rm T}/0.19\ {\rm km\ s^{-1}})^4\ (P_s/2 \times 10^4\ k\ {\rm cm^{-3}\ K})^{-1/2}$ (Ebert 1955; Bonnor 1956). Thus, we must conclude that the large linewidths in molecular regions are the signature of some internal mechanism of *nonthermal support* against their self-gravity.

It is interesting to estimate the total pressure, $P_{\rm ave}$, associated with the (mostly) nonthermal motions observed in GMCs. From Table 1.2, a typical cloud has a linewidth $\sigma_{\rm ave} = 3.4$ km s^{-1} and a density $\rho_{\rm ave} = 6.5\ M_\odot\ {\rm pc^{-3}}$; hence, $P_{\rm ave} = \rho_{\rm ave}\sigma_{\rm ave}^2 \simeq 3.7 \times 10^5\ k\ {\rm cm^{-3}\ K}$, which is a full order of magnitude larger than that of the intercloud H I ($P_{\rm ISM} \simeq 2 \times 10^4\ k\ {\rm cm^{-3}\ K}$; cf. §1.2). The fact that $P_{\rm ave}$ is larger than $P_{\rm ISM}$ is the reason why models of isobaric, multiphase ISMs cannot address the physics of molecular clouds in detail (§1.2); but why are the two pressures so widely different? Part of the discrepancy is likely related to the presence of massive amounts of low-density, atomic *intercore* gas in most GMCs (see Blitz 1991; Williams et al. 1995): The weight of this gas could well increase the effective pressure at the surface of the *molecular* part of a cloud by a factor of $P_s/P_{\rm ISM} \sim 7$ (e.g., Elmegreen 1989). The self-gravity of the GMC (and Table 1.2 does confirm that GMCs as a whole are self-gravitating, with $N_{H_2} = 8.4 \times 10^{21}\ {\rm cm^{-2}}$ and thus $\overline{\rm A}_V \simeq 9$ mag by eq. [1.2]) then leads naturally to $P_{\rm ave}/P_s \simeq 2.5$ in equilibrium (McLaughlin & Pudritz 1996b), and $P_{\rm ave}/P_{\rm ISM} \sim 18$ overall.

Virialization

The picture of the Orion A cloud in Fig. 1.2 is a clear example of the fact that, while cores are very often spheroidal in appearance, entire GMCs are usually elongated, and sometimes even filamentary, structures. Nevertheless, their typical dimensions are often reported, as in Table 1.2, in terms of an effective circular radius. Despite the crudeness of the approximation, simple models of spheres can serve very well to describe the average properties of GMCs.

One important example of this is the use of the *virial theorem* to estimate GMC masses (cf. §1.4.2). This theorem is given in full in §1.6; in the simplest case, it states that an equilibrium gas sphere will, *in the absence of rotation, magnetic fields, and surface pressure*, be supported against its own gravity by its internal pressure when

$$2\,\mathcal{U} + \mathcal{W} = 0\,. \tag{1.21}$$

Here $\mathcal{U} = (3/2)M\sigma_{\rm ave}^2$ is the kinetic energy of thermal and nonthermal random motions in the cloud; $\mathcal{W} = -(3a/5)GM^2/R$ is, as usual, the gravitational energy. As was mentioned in §1.3.2, the parameter a in $\mathcal{W}$ depends on the internal density profile of the cloud but is always of order 1. Under the assumption that equation (1.21) holds, then, the *virial masses* of GMCs are defined by setting $a = 1$, and thus

$$M_{\rm vir} \equiv \frac{5\sigma_{\rm ave}^2 R}{G}\,. \tag{1.22}$$

The virial masses of hundreds of GMCs with $M \geq 10^5 M_\odot$ in the Massachussetts-Stony Brook CO survey are computed by Solomon et al. (1987) and Scoville et al. (1987). These authors also calculate the corresponding H_2 column densities, $N_{H_2}^{\rm vir}$, and compare these to the observed $W_{\rm CO}$ in each cloud. Averaging over their entire sample, Solomon et al. thus find $X_{\rm CO}^{\rm vir} = N_{H_2}^{\rm vir}/W_{\rm CO} \simeq 3.3\times10^{20}$ cm^{-2} (K km s^{-1})$^{-1}$, while Scoville et al. obtain $X_{\rm CO}^{\rm vir} \simeq 3.0\times10^{20}$ cm^{-2} (K km s^{-1})$^{-1}$. The good agreement between these $X_{\rm CO}^{\rm vir}$ and the X-values obtained by independent methods (eq. [1.15]) implies that, indeed, *GMCs are "virialized," in the naive sense that* $2\,\mathcal{U} + \mathcal{W} \approx 0$. Thus arrived at, this conclusion might be considered uncertain by perhaps a factor of two, which is the same uncertainty afflicting $X_{\rm CO}$. However, numerous studies that use optically thin lines (like the $J = 1 \rightarrow 0$ transition of ^{13}CO) to estimate the densities of clouds and cores directly, and thus to compute

masses independently of any virialization assumption, also show that the masses of large clouds tend to lie at or near their virial values (1.22) in the mean (albeit with some scatter): for example, Larson (1981) finds $M/M_{\rm vir} \simeq 0.85 - 1.05$ for a set of clouds with $R \geq 10$ pc, while Myers & Goodman (1988b) obtain $M/M_{\rm vir} \simeq 1 \pm 0.5$ (estimated error) for clouds larger than 1 pc. Thus, it seems well established that the equilibrium condition embodied in equation (1.21) does hold among real molecular clouds. It is significant that the *total* linewidth $\sigma_{\rm ave}$ is always used to define $M_{\rm vir}$, indicating once again that the superthermal linewidths are crucial to cloud support.

One might still question whether conclusions based on spherical models are at all relevant to the true conditions in real, nonspherical GMCs. However, it was argued above, without any recourse to specific models, that GMCs must be stable against collapse on large scales; but it is exactly this kind of global support that the virial theorem is intended to describe. Thus, although it remains mysterious that spherical modelling should apply, the result $2\,\mathcal{U}+\mathcal{W} \approx 0$ is indeed physically meaningful for GMCs, and has to be taken seriously. The question of why this specific version of virialization (i.e., one in which the effects of magnetic fields and surface pressure are ignored) should be adequate to describe the stability of GMCs is rather more difficult to understand. After all, as we saw above, the external pressures P_s acting on GMCs can be quite sizeable; and as we show below, magnetic fields are a significant presence there as well. Why, then, can these things apparently be ignored?

We return to this theoretical question in §1.6. Meanwhile, the importance of surface pressure in particular is further pointed up by observations of cloud cores: In any given GMC, the most massive cores (which typically have $M \sim 10^2 - 10^3 M_\odot$) still generally follow the simple $2\,\mathcal{U}+\mathcal{W} \approx 0$ rule. All smaller cores, however, tend instead to show $2\,\mathcal{U} + \mathcal{W} > 0$; in fact, the ratio $2\,\mathcal{U}/|\mathcal{W}|$ can reach as high as 100 for some of these objects (cf. Bertoldi & McKee 1992, and references therein). This is often cited as evidence that cores are "not virialized;" but what it really means is that the assumptions of vanishing P_s and magnetic field break down in these objects. Indeed, Bertoldi & McKee (1992) have shown that the ratios $2\,\mathcal{U}/|\mathcal{W}|$ observed in cores can be quantitatively understood, *in terms of the full virial theorem*, if surface pressures are actually more significant than gravity in the confinement of these objects.

Larson's Laws

Evidently, GMCs exhibit a wide range of masses, radii, and total linewidths; and yet all are in approximate virial equilibrium. Thus, $\sigma_{\rm ave}$ and R must vary among them *in concert* with M: $\sigma_{\rm ave}^2 R \propto M$ if $M \simeq M_{\rm vir}$ is to hold in all clouds. Interdependences of this type were first convincingly demonstrated by Larson (1981), who analyzed data from the literature (mostly ^{13}CO studies) on the densities, radii, and velocity dispersions of ~50 GMCs, dark clouds, and cores with radii $R \sim 50-0.1$ pc to find that (cf. Table 1.2) $n(H_2) \simeq 53\ {\rm cm}^{-3}\ (R/22\ {\rm pc})^{-1.1}$ — corresponding to a nearly constant $N_{H_2} \approx 5 \times 10^{21}\ {\rm cm}^{-2}$ — and $\sigma_{\rm ave} \simeq 2.7\ {\rm km\ s}^{-1}\ (R/22\ {\rm pc})^{0.38}$. Several studies followed which confirmed the basic form of these scalings, at least among GMCs (e.g., Sanders et al. 1985; Solomon et al. 1987; Myers & Goodman 1988b; and references therein). The results of Solomon et al. specifically are quite typical *for GMCS*, and have been used in constructing Table 1.2; they show that

$$\sigma_{\rm ave} = 0.72\ {\rm km\ s}^{-1} \left(\frac{R}{\rm pc}\right)^{1/2} \qquad \text{and} \qquad M = 597\ M_\odot \left(\frac{R}{\rm pc}\right)^2 , \tag{1.23}$$

with uncertainties of ~10% in both the coefficients and the exponents.

Relations of this type between the *total* linewidths, radii, and masses of GMCs are now referred to as "Larson's laws." They imply that higher-mass clouds are progressively less dense, and have total linewidths which are increasingly larger than the thermal $\sigma_{\rm T}$ (i.e., nonthermal support is more important for larger structures). It is important that once $M \simeq M_{\rm vir}$ is independently established (i.e., not assumed), as Larson (1981) was able to do, then the assumption of either one of the relations (1.23) automatically implies the other, through equation (1.22). Thus, any theoretical derivation of Larson's laws — any, that is, which incorporates the version of virialization discussed above — only has to explain one of them.

Many attempts have been made to determine whether some version of Larson's laws also holds among cloud cores. These have met with qualified success: Global scalings of the type $M \propto R^2$ and $\sigma_{\rm ave} \propto R^{1/2}$ do describe the *most massive* cores in many clouds, but such correlations often break down when less massive cores are considered (Bertoldi & McKee 1992, and references therein). This is actually not surprising, given (1) the link between Larson's laws and the virialization condition of equation (1.21), and (2) the fact, already noted, that this condition is observed to apply only to

the largest cores.

Internal Structure of Cores

These considerations of M, R, and $\sigma_{\rm ave}$ do not speak at all to the internal density and (random) velocity-dispersion profiles of molecular cores; and yet, these are clearly an integral part of the full initial conditions required for star formation.

Unfortunately, it is difficult to determine accurate internal density profiles $\rho(r)$ [whether through molecular lines that trace density or column density, or through measurements of extinction profiles $A_V(r)$], because of uncertainties in excitation analyses, in molecular abundances, and in the conversion of column densities $N(r)$ to volume densities $n(r)$. Thus, many conflicting results have been reported in the literature; in a simple power-law approximation, $\rho \propto r^{-p}$, claims have been made for p anywhere in the range $1-3$ (e.g., Fuller & Myers 1992; Evans 1991; McLaughlin & Pudritz 1996b; and references therein). On the other hand, significant progress has recently been made in the empirical definition of linewidth profiles $\sigma(r)$ inside both low-mass ($M < 10M_\odot$; Fuller & Myers 1992) and high-mass ($M > 10M_\odot$; Caselli & Myers 1995) cores. Fuller & Myers and Caselli & Myers have mapped a total of 38 cores in lines of ^{13}CO and/or C^{18}O, CS, and NH_3. Since these species are sensitive to gas under different physical conditions (i.e., densities), they yield maps with different spatial extents (smallest for NH_3; largest for the CO isotopes) in any one core. In a single object, then, a plot of the linewidths measured by the different molecules, against their characteristic emission-contour radii, is equivalent to a plot of σ vs. r.

Taken together, the $\sigma(r)$ profiles thus inferred for the entire sample of Fuller & Myers (1992) and Caselli & Myers (1995) lead to three main conclusions: (1) *The total linewidth is superthermal at every radius observed in every core*, i.e., $\sigma > \sigma_{\rm T}$ for all $r \sim 0.03-1$ pc. (2) *The total linewidth in any core increases with increasing radius.* Given the temperature of a core, the nonthermal component of the linewidth can be isolated, viz. $\sigma_{\rm NT}^2 = \sigma^2 - \sigma_{\rm T}^2$, such that it is actually $\sigma_{\rm NT}$ that grows with r. (3) *The increase of $\sigma_{\rm NT}$ appears to differ quantitatively between low- and high-mass cores, at the radii observed.* Among the former objects, it is found that (roughly) $\sigma_{\rm NT} \propto r^{0.53\pm0.07}$ on average; in the latter, $\sigma_{\rm NT} \propto r^{0.21\pm0.03}$ (Caselli & Myers 1995). Extrapolation of this behavior, in either case, suggests that $\sigma_{\rm NT}$ must vanish at the centers of cores (but *only* at the centers), so that the

total linewidths there are due entirely to thermal motions. These results obtain for cores both with and without embedded stars, and as such must be prerequisites for, and not just side-effects of, star formation.

Rotation and Magnetic Fields

Rotation is mentioned here just to make the point that it is usually present only at fairly low levels in GMCs and cores. For example, Blitz (1991) quotes velocity gradients of $\Omega \simeq 0.1 - 0.2$ km s^{-1} pc^{-1} in four nearby GMCs. Similarly, Goodman et al. (1993) surveyed 43 dense cores for evidence of rotation and found a distribution of gradients (for just 29 objects which yielded positive detections) in the range $\Omega \sim 0.3 - 4$ km s^{-1} pc^{-1}, with the smaller values clearly being preferred. And Goldsmith & Arquilla (1985) review observations of velocity gradients in dark clouds which typically show $\Omega \sim 1$ km s^{-1} pc^{-1}. Thus, the angular frequency of rotation in molecular clouds, when it is present at all, would appear to be at the level of $\Omega \sim 10^{-14}$ s^{-1}. This corresponds to a ratio of rotational to gravitational energies that is typically $\mathcal{R}/|\mathcal{W}| \sim 0.1$ or less in these objects (Goldsmith & Arquilla 1985; Goodman et al. 1993). There are a few exceptions to this rule, and *any* amount of rotation must become important in a collapse situation, when Ω has to increase to conserve angular momentum ($L \propto \Omega R^2$); but it seems clear that, *in general, rotation is not an important aspect of the physics of the molecular ISM* before this point.

On the other hand, magnetic fields (**B**) are an integral part of the dynamics of dense interstellar clouds and cores. Even though accurate measurements of total *mean* (or ordered, or static, or uniform) field strengths ($B_{\rm ave}$) in molecular regions are difficult to make,[15] and reliable results are still few in number (see the reviews of Troland 1990; Heiles et al. 1993), it nonetheless would appear that *the mean magnetic field energies in GMCs and their most massive cores are in rough equipartition with the kinetic energies there.* That is, with $\mathcal{U} = (3/2)M\sigma_{\rm ave}^2$ and $\mathcal{M} \sim B_{\rm ave}^2 R^3/3$,

$$\mathcal{M} \approx \mathcal{U} \ . \tag{1.24}$$

[15]Currently the best way to investigate the large-scale properties of magnetic fields in molecular gas is through observations of the *Zeeman effect*, primarily in radio transitions either of OH or of the H I that is invariably associated with cloud complexes (Troland 1990; Heiles et al. 1993). This effect arises from a perturbation of the energy-level structure of an atom or a molecule placed in an external **B**-field. It therefore manifests itself by *splitting* some of the lines in a spectrum.

A number of arguments, some more direct than others, combine to support this claim: (1) Myers & Goodman (1988a) compare measured field strengths with kinetic energies in 9 objects with densities ranging from $n \sim 10^2 - 10^6$ cm^{-3}, to show directly that the *magnetic equipartition* of equation (1.24) holds to within a factor of two. (2) Crutcher et al. (1993) perform a statistical analysis on the measured line-of-sight field strengths — including some non-detections — in 12 dark clouds with $M \sim 10^3 - 10^4 M_\odot$, and come to the same conclusion. (3) The data of Goodman & Heiles (1993) indicate $\mathcal{M} \approx \mathcal{U}$ for the Ophiuchus GMC. And (4) Myers & Goodman (1988b) show that the observed virialization (of the type $2\,\mathcal{U} + \mathcal{W} \approx 0$; see above) of about 70 molecular clouds and *large* cores is *consistent* with magnetic equipartition, if it is assumed that the mean field strengths in all these clouds lie at roughly the same level, $B_{\rm ave} \simeq (30 \pm 15) \times 10^{-6}$ G $= 30 \pm 15$ μG. The handful of **B** measurements actually made in these clouds do appear to conform to this latter assumption (Myers & Goodman 1988b; Troland 1990).

It is significant that the claim here is for equipartition between $\mathcal{M}$ and the *kinetic* energy $\mathcal{U}$. Since virialized GMCs and large cores have $2\,\mathcal{U} \approx |\mathcal{W}|$, we might have argued instead that (to within the factor of two uncertainties that are common for individual $\mathcal{M}$ measurements) the data mentioned above are really suggesting $\mathcal{M} \approx |\mathcal{W}|$. However, Myers et al. (1995) contend that $\mathcal{M}$ and $\mathcal{U}$ are also similar in many *diffuse* clouds, where the gravitational energy $|\mathcal{W}|$ is quite small. As a specific example, they observe $\mathcal{M} \approx \mathcal{U} \gtrsim 300\ |\mathcal{W}|$ in the Ursa Major H I complex. Thus, equation (1.24) appears to be the more universal relation. It points to a fundamental connection between magnetic fields and the random motions in molecular (and, indeed, diffuse) clouds.

Finally, to be clear, equation (1.24), which ultimately involves the total linewidth $\sigma_{\rm ave}$, appears to apply in GMCs and *massive* cores, i.e., in regions where $\sigma_{\rm ave} \simeq \sigma_{\rm NT} \gg \sigma_{\rm T}$; in lower-mass cores the relation seems to break down, and $\mathcal{M} < \mathcal{U}$. This *may* mean that $\mathcal{M}$ is actually in equipartition with the *nonthermal* kinetic energy $\mathcal{U}_{\rm NT} = (3/2) M \sigma_{\rm NT}^2$, which is naturally smaller than the total $\mathcal{U}$ when $\sigma_{\rm ave} \approx \sigma_{\rm T}$ (Myers & Goodman 1988b). This conclusion is certainly aesthetically pleasing, and it may well be true; but the evidence for it seems to still be mostly circumstantial.

1.6 Theoretical Issues

The observations discussed in the last Section — which, as we have stressed, serve to set the parameters of the star-formation process — may be summarized as follows:

1. GMCs ($M \sim 10^4 - 10^6 M_\odot$) and their cores ($M \lesssim 10^3 M_\odot$) all have superthermal linewidths which work, to varying extents, to support them against their own gravity. Masses, radii, and linewidths scale *between* whole clouds as $M \propto R^2$ and $\sigma_{\rm ave} \propto R^{1/2}$. Scalings such as these also obtain between the *largest* clumps in a cloud, but not among its smaller cores.

2. All GMCs and many cores appear to be in some type of virial equilibrium, and specifically are not in any advanced stage of gravitational collapse overall. The largest cores, and entire GMCs, seem to obey the simple balance $2\,\mathcal{U} + \mathcal{W} \approx 0$, whereas smaller clumps are governed by a more sophisticated equilibrium condition.

3. Linewidths increase with increasing radius *inside* cores both with and without stars. In high-mass cores ($M > 10 M_\odot$), the nonthermal velocity dispersion grows as $\sigma_{\rm NT} \propto r^{0.2}$; in low-mass cores ($M < 10 M_\odot$), $\sigma_{\rm NT} \propto r^{0.5}$.

4. The mean, or ordered, magnetic field strengths in GMCs and the largest cores are such ($B_{\rm ave} \sim 30\ \mu$G) that their energy is in equipartition with the (mostly nonthermal) kinetic energy: $\mathcal{M} \approx \mathcal{U}$.

We now briefly address each of these major points, which together form the basis of the discussion in Chapter 2 (McLaughlin & Pudritz 1996b).

Nonthermal Linewidths

First, what is the source of the ubiquitous superthermal linewidths in GMCs and cores; that is, what is the underlying physical mechanism of support, beyond thermal pressure, in these objects? An obvious candidate might have been rotation; but, as we have just discussed, the observations show that this would fail by an order of magnitude if it had to counteract gravity on its own. Other possibilities that have been raised in the literature include: the injection of energy by outflows from young, low-mass (T-Tauri) stars into their parental gas (Norman & Silk 1980); random motions of,

and collisions between, smaller-scale substructure inside the objects (e.g., the cores within a GMC: Zuckerman & Evans 1974; Scalo & Pumphrey 1982); compressible turbulence driven by a cascade of angular momentum from Galactic to stellar scales (Fleck 1980, 1981; Henriksen & Turner 1984; Henriksen 1991); and hydromagnetic waves, or magnetohydrodynamic (MHD) turbulence (Arons & Max 1975; see the review of McKee et al. 1993).

Evidently, there has been no shortage of ideas concerning this important subject, and it is not our intention to address them all in detail. It has to be noted, however, that the currently favored option is the last one. Specifically, it is often proposed that large-amplitude *Alfvén waves* (i.e., transverse waves that travel along perturbed magnetic field lines) are responsible for the bulk of nonthermal motions in clouds and cores alike (Arons & Max 1975; McKee & Zweibel 1995, and references therein). The main observational impetus for this claim is the equipartition between *mean-field* magnetic and kinetic energies discussed above. By their very nature, Alfvén waves are actually identified (along with any other facet of MHD turbulence) with the *disordered* (or fluctuating, or time-dependent) component of a magnetic field, δB, rather than with its uniform component $B_{\rm ave}$. However, it is expected theoretically — and there is at least some observational support for this in the Ophiuchus GMC (Goodman & Heiles 1993) — that the energies of these two field components should evolve to equipartition. Thus, if GMCs and the largest cores are in fact stirred primarily by MHD turbulence, their total (mostly nonthermal) kinetic energy $\mathcal{U}$ can be expected to be in equipartition with the mean-field $\mathcal{M}$; for smaller cores, an equipartition between $\mathcal{M}$ and $\mathcal{U}_{\rm NT}$, as suggested by Myers & Goodman (1988a, b), would also be appropriate.

The Alfvén-wave picture is appealing on other grounds as well, including its allowance for simultaneous large-scale stability and small-scale instability in GMCs (Pudritz 1990). It can also reproduce the observed magnitude of the nonthermal linewidths in clouds and cores, as well as the scaling $\sigma_{\rm NT} \propto R^{1/2}$ — which, in large cores and whole clouds, where $\sigma_{\rm ave} \simeq \sigma_{\rm NT}$, is just one of Larson's laws — if it is true that the mean-field strength is roughly constant among them, at $B_{\rm ave} \simeq 30\ \mu$G (Mouschovias 1987).

Given all of this, it does seem plausible, and even likely, that MHD turbulence is the main cause of the superthermal linewidths in molecular regions; and Alfvén waves specifically could be the dominant manifestation of this. However, as McKee et al. (1993) discuss, there are still some

unresolved theoretical questions involving the dissipation of energy in magnetic clouds (i.e., can Alfvén waves be sustained for more than a cloud free-fall time?). Also, as Chapter 2 discusses at length, the derivation of Larson's $\sigma_{\rm ave} - R$ scaling from considerations of Alfvén waves is not unique; and there are, in any case, serious discrepancies between the observed structures of GMCs and predictions based on the assumption of support by Alfvén wave pressure alone.

The Virial Theorem and Larson's Laws

The (scalar) virial theorem was mentioned several times in §1.5.3, and a connection between the simple form $2\,\mathcal{U} + \mathcal{W} = 0$ and Larson's laws was implied there. This theorem (Chandrasekhar & Fermi 1953; Shu 1992; McKee et al. 1993) provides a *volume-averaged* description of a body of gas which is supported against its own gravity (potential ϕ) by a combination of internal random motions (total pressure P) and Lorentz forces (due to a mean magnetic field $\mathbf{B}$). It is derived by taking the first moment of the equation of motion for such a body. Thus,

$$\rho \frac{d\mathbf{v}}{dt} = -\nabla P - \rho \nabla \phi + \frac{1}{c}\,\mathbf{j} \times \mathbf{B} \tag{1.25}$$

becomes

$$\int_V \rho \frac{d\mathbf{v}}{dt} \cdot \mathbf{r}\, dV = -\int_V \nabla P \cdot \mathbf{r}\, dV - \int_V \rho \nabla \phi \cdot \mathbf{r}\, dV + \frac{1}{4\pi}\int_V [(\nabla \times \mathbf{B}) \times \mathbf{B}] \cdot \mathbf{r}\, dV\ , \tag{1.26}$$

where we have used the fact that the current $\mathbf{j} = (c/4\pi)(\nabla \times \mathbf{B})$, and where V is some arbitrary volume of integration, usually chosen to be the volume of the cloud itself. The velocity $\mathbf{v}$ on the left-hand side of these equations refers to any systemic velocity field (bulk motions) in the cloud, such as might arise from collapse or rotation. We have already seen that these are unlikely to be of much importance in interstellar clouds, but they are included here for the sake of generality. In any event, if spherical symmetry is assumed, then equation (1.26) may be written (after some algebraic manipulations involving Gauss' theorem and standard vector identities) as

$$\frac{1}{2}\frac{d^2 I}{dt^2} = -3P_s V + 3(P_{\rm ave} + P_{\rm bulk})V + \mathcal{W} + \mathcal{M}\ , \tag{1.27}$$

where $I \equiv \int \rho r^2 \, dV$ is analagous to a moment of inertia; P_s is the gas pressure at the surface of the cloud; $P_{\rm ave}$ is the volume-averaged internal pressure, $(1/V) \int P \, dV$; $P_{\rm bulk} \equiv (1/3V) \int \rho v^2 \, dV$ is the effective "pressure" of any bulk flows; the total gravitational energy of the cloud is $\mathcal{W} \equiv -\int \rho[Gm(r)/r] \, dV$; and the mean-field magnetic energy $\mathcal{M}$ is just the last term of equation (1.26).

Specializing now to the case of most relevance for molecular clouds (i.e., setting the acceleration term d^2I/dt^2 to 0 and letting $P_{\rm bulk} \ll P_{\rm ave}$), and making the straightforward substitutions $P_{\rm ave} = \rho_{\rm ave}\sigma^2_{\rm ave}$ and $\mathcal{U} = (3/2)M\sigma^2_{\rm ave}$, we finally have that

$$2\,\mathcal{U}(1 - P_s/P_{\rm ave}) + \mathcal{M} + \mathcal{W} \;=\; 0 \; . \tag{1.28}$$

Evidently, this form of the virial theorem is valid even in the presence of systemic velocities, so long as $\sigma_{\rm ave}$, and hence the average pressure and kinetic energy, are appropriately re-defined.

Two results are apparent here. First, consider an equilibrium cloud whose internal support is suddenly withdrawn completely (i.e., $P_{\rm ave}$ vanishes). One of two things will happen: If the mean magnetic field is strong enough that $\mathcal{M} > |\mathcal{W}|$, then it will be able to still support the cloud against gravitational collapse; such a cloud is referred to as *magnetically subcritical*. But if $\mathcal{M} < |\mathcal{W}|$, collapse is inevitable and unstoppable; the cloud is then said to be *magnetically supercritical*. Now, $\mathcal{M} \propto B^2_{\rm ave}R^3$; $|\mathcal{W}| \propto M^2/R$; and magnetic flux is defined as $\Phi \equiv \pi R^2 B^2_{\rm ave}$. Thus, the division $\mathcal{M} = |\mathcal{W}|$ between subcritical and supercritical clouds corresponds to a specific (global) *flux-to-mass ratio*, say $(\Phi/M)_{\rm crit} \equiv \mathcal{P}$. For a given flux Φ, then, clouds less massive than $M_\Phi = \Phi/\mathcal{P}$ are subcritical, while those with $M > M_\Phi$ are supercritical. (The numerical value of $\mathcal{P}$ depends on the geometry and mean-field configuration of the cloud in question.) This notion of sub- and supercritical clouds makes a brief appearance in Chapter 2.

Second, in the limit that $P_s/P_{\rm ave} \to 0$ and $\mathcal{M} \to 0$, equation (1.28) reduces to $2\,\mathcal{U} + \mathcal{W} = 0$, which is just the form of the virial theorem observed to hold among GMCs and very massive cores (§1.5.3). More generally, however, the ratio of kinetic to gravitational energies can be written as $2\,\mathcal{U}/|\mathcal{W}| = (1 - \mathcal{M}/|\mathcal{W}|)/(1 - P_s/P_{\rm ave})$. Thus, objects that are not strongly self-gravitating, and whose internal pressures $P_{\rm ave}$ are not much enhanced over the surface P_s, can have $2\,\mathcal{U}/|\mathcal{W}| > 1$ but still be in true virial equilibrium. Such objects are referred to as "pressure confined" by Bertoldi & McKee (1992), who argue that this is the case for all but the most massive cores in GMCs (cf. §1.5.3

above).

This last point is part of what makes the $2\,\mathcal{U} + \mathcal{W} \approx 0$ observed for very large cores and whole GMCs a rather subtle result: Why should surface pressures be important in the confinement of all but the few most massive cores? Moreover, why can mean magnetic fields be ignored altogether? The answer is that magnetic fields *cannot* be ignored in these objects; rather, we use the fact that $\mathcal{M} \approx \mathcal{U}$ to infer what we believe is the correct form of virialization observed there:

$$\mathcal{U} + \mathcal{M} + \mathcal{W} \approx 0\,. \tag{1.29}$$

Comparison with equation (1.28) immediately shows that if this is true, then the surface pressures on GMCs and their largest cores are not negligible either; $P_s/P_{\rm ave} \approx 1/2$ is required instead.

A thorough and general description of the conditions under which the relation (1.29) obtains in molecular clouds, and of its broader implications, is given in Chapter 2. There we also show how Larson's laws (eq. [1.23]) follow immediately from this relation, regardless of the source of the superthermal linewidths, if a roughly constant surface pressure P_s is assumed to apply at the surfaces of the clouds (Chièze 1987; Elmegreen 1989).

Internal Structure

Obviously, magnetic fields are a critical influence on the structure of interstellar clouds. Accordingly, there have been many theoretical studies, both analytical and numerical, of the structure of static gas clouds threaded by (poloidal) mean magnetic fields. Analytical work typically uses the *tensor* virial theorem,[16] with a prescribed magnetic field topology, to evaluate the global (i.e., necessarily volume-averaged) structures and stability properties of clouds (e.g., Strittmatter 1966; Zweibel 1990). Numerical models, on the other hand, are constructed by solving the full equations of magnetohydrodynamics at every point inside a cloud (e.g., Mouschovias 1976a, b; Tomisaka, Ikeuchi, & Nakamura 1988a, b, 1989); this obviously allows for a detailed view of the inner workings of magnetized bodies of gas.

[16]The tensor virial theorem takes account of off-diagonal matrix elements in the Maxwell stress tensor, $\mathbf{T} = \mathbf{BB}/4\pi - \mathbf{I}(P + B_{\rm ave}^2/8\pi)$, to take moments of the equation of motion $\rho\, d\mathbf{v}/dt = \nabla \cdot \mathbf{T} - \rho\nabla\phi$. The off-diagonal moments contain information on angular momentum conservation, while the diagonal moments sum to give equation (1.28); that is, the scalar virial theorem we employ is just the trace of the full tensor theorem (see, e.g., Shu 1992).

Such models are important, of course, because they clarify the role of mean magnetic fields in the support and structure of equilibrium clouds, and because they can be used to define the initial conditions for simulations of cloud collapse (see McKee et al. 1993 for a review). They also dispense with the assumption of spherical symmetry (this is replaced by an imposed axisymmetry), and are thus, in one sense, more faithful than the simplest spherical models to observations of real interstellar clouds. Generally speaking, however, they concern themselves *only* with the steady components of **B**-fields in clouds; the effects of disordered fields are rarely considered. More to the point, most studies to date (with the notable exception of the work by Lizano & Shu 1989) have involved the "addition" of a magnetic field to gas with an *isothermal (or ideal-gas) equation of state* (EOS): $P = nkT = \rho\sigma_{\rm T}^2$. The fact that the linewidths $\sigma_{\rm ave}$ observed in real GMCs and cores are usually larger than $\sigma_{\rm T}$ is not necessarily a problem here, since the *model* $\sigma_{\rm T}$ can be assigned any value whatsoever. The real difficulty with the use of an isothermal EOS is that, as its name suggests, it corresponds to a velocity dispersion that is *constant* throughout a cloud. Thus, any numerical or analytical model of magnetized molecular cores that assumes an equation of state of the form $P \propto \rho$ misses the fundamental point that linewidths are observed to increase with radius in these objects.

This is a serious inconsistency, albeit one that has only come into sharp relief with the very recent work of Fuller & Myers (1992) and Caselli & Myers (1995). The third main goal of Chapter 2, then, is to rectify this situation by *inferring* the gas EOS which best describes the observed internal $\sigma(r)$ of magnetized molecular cores. Although we fall back to a more idealized (semi-analytical and spherically symmetric) computational framework in order to do this, it should eventually prove possible to incorporate such an EOS as an accurate description of nonthermal motions (or disordered fields) in more realistic, nonspherical (and most likely numerical) realizations of magnetic molecular clouds and cores. However, even without such models it is possible to begin an investigation into the consequences of a realistic gas EOS for the gravitational collapse of molecular cloud cores, and star formation itself. This issue is taken up in Chapter 3 (McLaughlin & Pudritz 1997).

Chapter 2

A Model for the Internal Structure of Molecular Cloud Cores

THE ASTROPHYSICAL JOURNAL, 469:194–208, 1996 September 20

A MODEL FOR THE INTERNAL STRUCTURE OF MOLECULAR CLOUD CORES

DEAN E. MCLAUGHLIN AND RALPH E. PUDRITZ
Department of Physics and Astronomy, McMaster University, Hamilton, Ontario L8S 4M1, Canada; dean@physics.mcmaster.ca, pudritz@physics.mcmaster.ca
Received 1995 December 7; accepted 1996 April 11

ABSTRACT

We generalize the classic Bonnor-Ebert stability analysis of pressure-truncated, self-gravitating gas spheres to include clouds with arbitrary equations of state. A virial-theorem analysis is also used to incorporate mean magnetic fields into such structures. The results are applied to giant molecular clouds (GMCs), and to individual dense cores, with an eye to accounting for recent observations of the internal velocity-dispersion profiles of the cores in particular. We argue that GMCs and massive cores are at or near their critical mass and that in such a case the size–line width and mass-radius relations between them are only weakly dependent on their internal structures; any gas equation of state leads to essentially the same relations. We briefly consider the possibility that molecular clouds can be described by polytropic pressure-density relations (of either positive or negative index) but show that these are inconsistent with the apparent gravitational virial equilibrium, $2\mathscr{T} + \mathscr{W} \approx 0$, of GMCs and of massive cores. This class of models would include clouds whose nonthermal support comes entirely from Alfvén wave pressure. The simplest model consistent with all the salient features of GMCs and cores is a "pure logotrope," in which $P/P_c = 1 + A \ln(\rho/\rho_c)$. Detailed comparisons with data are made to estimate the value of A, and an excellent fit to the observed dependence of velocity dispersion on radius in cores is obtained with $A \simeq 0.2$.

Subject headings: equation of state — hydrodynamics — ISM: clouds

1. INTRODUCTION

Giant molecular clouds (GMCs; $M \sim 10^5$–$10^6\ M_\odot$) in the Galaxy are highly inhomogeneous: they are often filamentary in appearance, consisting of discrete clumps, or cores ($M \lesssim 10^3\ M_\odot$), which contain most of the mass of a cloud (including any young stars) and are surrounded by a more diffuse component of predominantly atomic gas (e.g., Williams, Blitz, & Stark 1995). Indeed, GMCs are clumpy on all scales observed and are possibly even fractal in nature (Falgarone, Phillips, & Walker 1991). Remarkably enough, however, the gross properties of cloud complexes are rather simply interrelated. Total masses, mean densities, and average velocity dispersions vary with sizes (effective radii) roughly as $M \propto R^2$, $\rho_{\rm ave} \propto R^{-1}$, and $\sigma_{\rm ave} \propto R^{1/2}$ (Larson 1981; Sanders, Scoville, & Solomon 1985; Solomon et al. 1987), with uncertainties in the exponents typically of order ± 0.1. The seeming universality of these results demands a physical explanation.

The relationship between size and line width (which term we use interchangeably with velocity dispersion) is further interesting because σ is observed to decrease toward smaller radii *inside* GMCs and within individual dense cores (Larson 1981; Miesch & Bally 1994; Fuller & Myers 1992; Caselli & Myers 1995). Since the total line widths of GMCs are mostly nonthermal (the clouds are stable against gravitational collapse on the largest scales, but have masses several orders of magnitude above the thermal Jeans value, so that their support must come largely from nonmagnetic or, very likely, MHD turbulence), this decrease reflects a move toward domination by thermal motions on the smallest scales. We should therefore expect the line widths of low-mass cores to have a smaller turbulent component than those of high-mass cores. This is indeed the case; in fact, the velocities nearest the centers of small cores are almost (to within a few percent) wholly thermal. However, it also happens (Caselli & Myers 1995) that the nonthermal velocity dispersion shows *a stronger dependence on radius in low-mass cores* (where $\sigma_{\rm NT} \propto r^{0.5}$) than in massive ones ($\sigma_{\rm NT} \propto r^{0.2}$). Because star formation is localized in the cores of GMCs, their overall structure—and this aspect specifically—bears strongly on our understanding of this most fundamental process.

The goal of this paper is to find a model for the internal structure of molecular cores (low- and high-mass both) that quantitatively matches their observed, internal velocity-dispersion profiles and that is also consistent with global properties (such as the observed mass-radius–line width relations) of large, self-gravitating clumps and even whole GMCs. Our approach is to reduce this problem to the specification of a (total) pressure-density relation—an equation of state—that, when used to solve the equation of hydrostatic equilibrium, results in a gas cloud with the required features. It is significant that the line width profiles of cores are insensitive to the presence or absence of young stars and thus may be viewed as one of the prerequisites for star formation (Fuller & Myers 1992; Caselli & Myers 1995). This justifies our focus on the structure of purely gaseous clouds.

To proceed, we shall resort to a virial-theorem treatment of molecular clouds that idealizes them as spheres of gas in hydrostatic equilibrium and satisfying Poisson's equation. This is appropriate enough for dense cores, which in many cases are roughly spheroidal (probably prolate: Myers et al. 1991), or even near spherical (e.g., Williams et al. 1995), overall. (Although their internal density distributions may not be especially smooth on very small scales, we concern ourselves here with a description of their *bulk* structure.) In addition, observations of very massive cores imply that they are self-gravitating and in approximate "gravitational virial equilibrium," $2\mathscr{T} + \mathscr{W} \approx 0$. This is not the case for low-mass cores, but these still appear to satisfy the full virial theorem if surface-pressure terms are included (Bertoldi & McKee 1992). Finally, even the total masses, radii, and line

widths of entire GMC complexes are generally consistent with virial-equilibrium models of spheres (e.g., Solomon et al. 1987; Elmegreen 1989); and it has been repeatedly confirmed that whole clouds tend to comply with $2\mathscr{U} + \mathscr{W} \approx 0$ (Larson 1981; Solomon et al. 1987; Myers & Goodman 1988b).

It should be noted that the correct, average mass-radius and size–line width relations can be recovered in a purely scale-free description of GMCs (e.g., Henriksen 1991). But the distinctly different scalings of velocity dispersion with radius inside low- and high-mass clumps is one indication that molecular clouds are in fact not entirely featureless. Other current models for these objects (such as isothermal spheres or negative-index polytropes) face similar difficulties in accounting simultaneously for their global properties and their internal structures.

Magnetic fields are an important presence in regions of star formation (e.g., Heiles et al. 1993), so we begin in § 2 by writing down the virial-theorem (or Bonnor-Ebert) relations between the masses and total line widths—including turbulent velocities—of magnetized spheres, truncated at radii such that the internal pressure just balances that of a diffuse surrounding medium. We then develop a stability criterion for such clouds that depends only on the assumption that their thermal line widths (i.e., kinetic temperatures) are invariant. When combined with the circumstantial evidence for equipartition between the kinetic and mean-field magnetic energies in GMCs and massive cores (Myers & Goodman 1988a, 1988b; Bertoldi & McKee 1992), this stability criterion leads to mass-radius–line width relations between critical-mass objects that agree with the observed scalings (both the exponents and the coefficients) among GMCs. Our analysis is therefore similar to those of, e.g., Chièze (1987), Fleck (1988), and especially Elmegreen (1989), but ours holds for clouds with an *arbitrary* equation of state. In addition, we find that critically stable clouds in magnetic equipartition should all satisfy $2\mathscr{U} + \mathscr{W} \approx 0$. We therefore conclude that GMCs and massive cores are approximately at their critical masses and magnetically supercritical, with $M_{\rm crit} \simeq 2M_\odot$ (see also McKee 1989; Bertoldi & McKee 1992). The generality of these results allows for the investigation of essentially any pressure-density relation as a potential description of the interiors of molecular cores, just so long as critically stable configurations are at all possible.

In § 3, we discuss polytropic equations of state: $P \propto \rho^\gamma$, with γ any positive number. Clearly, if $\gamma \geq 1$, then the total velocity dispersion ($\sigma^2 = P/\rho$) stays constant or decreases with decreasing density (increasing radius) inside a cloud. If instead γ is allowed to be less than 1 (e.g., Maloney 1988), then σ^2 increases with radius, as required. However, in our analysis, any such "negative-index" polytrope would be unconditionally stable against gravitational collapse; or equivalently (but independently of any stability criterion), it could not self-consistently satisfy the relation $2\mathscr{U} + \mathscr{W} \approx 0$. While this is not a problem for low-mass cores, it is inconsistent with what we know of very large clumps and GMCs overall. Thus, we argue that polytropic pressure-density relations give an incomplete picture of interstellar clouds. A corollary to this is that weakly damped Alfvén waves, for which $P \propto \rho^{1.2}$ (McKee & Zweibel 1995), cannot be invoked as the *sole* explanation of nonthermal line widths in GMCs.

Section 4 describes what is, in our view, a more suitable alternative. There we consider the possibility that pressure varies only logarithmically with density: $P/P_c = 1 + A \ln(\rho/\rho_c)$. We refer to the resulting gas cloud as a "pure" logotrope. This term was introduced by Lizano & Shu (1989; see also McKee 1989), who actually added a logarithmic term to an otherwise isothermal equation of state in an attempt to account for turbulent line widths. Such models have also been studied in detail by Gehman et al. (1996). Here, however, we dispense with the explicitly isothermal component, for two reasons: (1) Assuming $P = \rho\sigma_{\rm T}^2 + \kappa \ln(\rho/\rho_{\rm ref})$, with $\sigma_{\rm T}$ the thermal velocity dispersion and $\rho_{\rm ref}$ some reference density (Lizano & Shu 1989), the observational inference that line widths should be essentially purely thermal at the centers of cores requires that $\rho_{\rm ref} = \rho_c$. But then the internal $\sigma^2 = P/\rho$ *decreases* with increasing radius. (2) If now $P/P_c = \rho/\rho_c + \kappa \ln(\rho/\rho_c)$, then for large values of κ such as those suggested by Gehman et al. (1996), P vanishes for ρ/ρ_c rather near unity. Thus, real clouds would have to be almost uniform density, which again is not observed.

These difficulties do not extend to the specific equation of state that we examine. Instead, an outward increasing velocity-dispersion profile obtains for an equilibrium pure logotrope. Such a model can moreover account for the observed mass-radius and size–line width relations between GMCs. We also demonstrate that the line width measurements in both low- and high-mass cores, from a variety of molecular clouds, are quantitatively reproduced if $A \simeq 0.2$. The argument makes explicit use of the fact that small cores are *not* at their critical masses (while large ones generally are), but that they are still in approximate virial equilibrium when the effects of surface pressures are considered.

Although the logarithmic $P - \rho$ relation we advocate is phenomenological, its overall viability, along with the failings of other models, ultimately makes for a useful description of molecular clouds and their cores.

2. GENERALIZED BONNOR-EBERT RELATIONS

Interstellar clouds can be viewed as essentially "pressure-truncated" bodies of gas. (This term is meant to imply the existence, not of some radius where a gas cloud suddenly ends, but of one where it "blends in" with an ambient medium.) Thus, the boundary of a GMC is set by pressure balance with the surrounding, hot ISM. Note that even if there is no such balance initially, it will eventually obtain after an overall expansion or contraction of the cloud complex. The extent of a core within a GMC is similarly limited by the pressure of a tenuous interclump medium, as has been argued by Bertoldi & McKee (1992). The equilibrium structure of pressure-truncated isothermal spheres was first described by Ebert (1955) and Bonnor (1956) (see also McCrea 1957). Their expressions connecting the masses, radii, and line widths of the spheres follow from the assumption of hydrostatic equilibrium and Poisson's equation and therefore are written in terms of an internal pressure profile and gravitational potential. In Appendix A, we rederive these Bonnor-Ebert relations, but for clouds satisfying an arbitrary gas equation of state (eqs. [A4]–[A7]). We also provide a connection (eqs. [A8]–[A10]) with the more transparent and observationally convenient virial-theorem formulation given by equations (2.8a)–(2.8d) below. As various authors have noted (Chièze 1987; Fleck 1988; Maloney 1988; Elmegreen

1989), these relations in either guise provide a framework for an understanding of the standard "Larson's laws" for GMCs ($M \propto R^2$ and $\sigma \propto R^{1/2}$; Larson 1981).

The development of Appendix A refers specifically to "nonmagnetic" clouds, meaning only that no *ordered* (mean) magnetic field is considered to be present. We work on the assumption that the effects of disordered fields (MHD turbulence) can be separately dealt with, in an equivalent hydrostatic problem that makes use of an effective equation of state to describe *all* of the contributions to gas pressure as a function of density. Still, the effects of mean fields must also be considered in any applications to real interstellar clouds.

2.1. *Magnetic Equilibria*

In the absence of any analytic models for magnetohydrostatic clouds, we proceed by assuming spherical symmetry and turning to the scalar virial theorem:

$$2\mathscr{U}(1 - P_s/P_{ave}) + \mathscr{M} + \mathscr{W} = 0 . \tag{2.1}$$

Here the mass-averaged, total one-dimensional velocity dispersion of a cloud with radius R is related to its mean pressure and density by

$$\sigma_{ave}^2 = \frac{\int_0^R 4\pi r^2 \rho \sigma^2 dr}{\int_0^R 4\pi r^2 \rho \, dr} = \frac{P_{ave}}{\rho_{ave}} , \tag{2.2}$$

so that the kinetic (or internal), mean-field magnetic, and gravitational energies are given by the usual

$$\mathscr{U} = \tfrac{3}{2} M \sigma_{ave}^2 , \tag{2.3}$$

$$\mathscr{M} = \frac{1}{8\pi} \int B^2 \, dV + \frac{1}{4\pi} \oint (\boldsymbol{r} \cdot \boldsymbol{B}) \boldsymbol{B} \cdot d\boldsymbol{S} - \frac{1}{8\pi} \oint B^2 \boldsymbol{r} \cdot d\boldsymbol{S} , \tag{2.4}$$

and

$$\mathscr{W} = -G \int_0^R \frac{m \, dm}{r} \equiv -\frac{3}{5} a \frac{GM^2}{R} . \tag{2.5}$$

The parameter a is essentially a measure of the nonuniformity of a gas sphere, and as such it depends on the equation of state and the truncation radius (in terms of a fixed scale r_0; eq. [A8]). However, it is generally of order unity: for a power-law density profile $\rho \propto r^{-p}$, equation (2.5) gives $a = (1 - p/3)/(1 - 2p/5)$. We expect $1 \lesssim p \lesssim 2$ in a realistic GMC or core, and thus, $10/9 \lesssim a \lesssim 5/3$.

It is often more useful to work in terms of the virial parameter of Bertoldi & McKee (1992):

$$\alpha_{mag} \equiv \frac{5\sigma_{ave}^2 R}{GM} . \tag{2.6}$$

This *observable* quantity can also be written (see McKee & Zweibel 1992) as

$$\alpha_{mag} = 2a \frac{\mathscr{U}}{|\mathscr{W}|} = \frac{a}{1 - P_s/P_{ave}} \left(1 - \frac{\mathscr{M}}{|\mathscr{W}|}\right) .$$

Although this form of the virial theorem is appropriate for clouds of any shape, the corrective factors for spheroidal clouds are rather near unity (Bertoldi & McKee 1992), and we still allow only for spherical symmetry here. It is further convenient to distinguish between the virial parameters which would obtain for a cloud with and without a mean magnetic field; these are related by

$$\alpha_{mag} = \alpha_{non} \left(1 - \frac{\mathscr{M}}{|\mathscr{W}|}\right) . \tag{2.7}$$

Again, α_{mag} refers specifically to the combination (2.6) of observables. On the other hand, α_{non} applies to the $\mathscr{M} = 0$ (no mean field) counterpart of a given cloud; it is directly observable only in this special case (since then $\alpha_{mag} = \alpha_{non}$), but may always be calculated for a given gas equation of state, as outlined in Appendix A. Once this is known, α_{mag} follows with the specification of a mean field configuration (see § 2.3).

The connection (2.7) between α_{mag} and α_{non} is valid insofar as the ratio P_s/P_{ave} does not change drastically upon the "addition" of a mean magnetic field to a cloud that is already in hydrostatic equilibrium. This must hold along field lines anyway (force balance is required in that direction) and thus everywhere on the surface of a roughly spherical cloud. Defining $a_{eff} \equiv a(1 - \mathscr{M}/|\mathscr{W}|)$, such reasoning implies that $(\alpha_{mag} - a_{eff})/\alpha_{mag} = (\alpha_{non} - a)/\alpha_{non}$, so manipulation of the virial theorem gives the following:

$$M = 25 \sqrt{\frac{3}{20\pi}} \left(\frac{\alpha_{non} - a}{\alpha_{non}}\right)^{1/2} \frac{1}{\alpha_{mag}^{3/2}} \frac{\sigma_{ave}^4}{(G^3 P_s)^{1/2}} , \tag{2.8a}$$

$$R = 5 \sqrt{\frac{3}{20\pi}} \left(\frac{\alpha_{non} - a}{\alpha_{non}}\right)^{1/2} \frac{1}{\alpha_{mag}^{1/2}} \frac{\sigma_{ave}^2}{(GP_s)^{1/2}} , \tag{2.8b}$$

$$\Sigma = \sqrt{\frac{20}{3\pi}} \left(\frac{\alpha_{non}}{\alpha_{non} - a}\right)^{1/2} \frac{1}{\alpha_{mag}^{1/2}} \left(\frac{P_s}{G}\right)^{1/2} , \tag{2.8c}$$

and

$$\rho_{ave} = \frac{\alpha_{non}}{\alpha_{non} - a} \frac{P_s}{\sigma_{ave}^2} . \tag{2.8d}$$

These relations, of which only two are independent (they are contained, for example, in eqs. [9] and [10] of Elmegreen 1989), are also given by Harris & Pudritz (1994) for the specific case of critically stable isothermal spheres (as defined in § 2.2; $\alpha_{non} = 2.054$ and $a = 1.221$ at a cloud radius $R_{crit}/r_0 = 2.150$). As written here, they apply to any generic gas cloud, stable or unstable, isothermal or not.

Any cloud in hydrostatic equilibrium and satisfying Poisson's equation has a central region where the potential, density, and velocity dispersion are very nearly constant with radius. Equations (A8) and (A9) show that spheres truncated in or just outside this central region (i.e., at radii small enough that $P_s \approx P_c$) have $\alpha_{non} \gg a$, and thus, $\alpha_{mag} \propto M^{-2/3} \propto R^{-2}$ by equations (2.8a) and (2.8b). Roughly this scaling has been observed for the virial parameters of low-mass, high-α cores in several GMCs, leading Bertoldi & McKee (1992) to argue that such clumps can be viewed as truncated spheroids that are essentially in pressure equilibrium with an intracloud medium.

2.2. *Stability: Critical Clouds*

Given equations (2.8a)–(2.8d) for the equilibrium structure of pressure-truncated gas spheres, we are in a position to question their stability: Under what conditions will they be able to withstand the combined effects of self-gravity and surface pressure, and when will they be unstable to wholesale gravitational collapse? The answer to this depends, of

course, on any boundary conditions attached to a perturbation of the cloud. Obviously, the total mass should be unchanged by a contraction or expansion of the entire structure. In addition, following Maloney (1988), we suppose that the central velocity dispersion remains constant as the cloud radius, or the surface pressure, is varied. This stipulation is meant to reflect the fact that the turbulent line width decreases steadily toward smaller scales in cores and in entire GMCs. We therefore identify the central velocity dispersion with the thermal part of the total line width: $\sigma_c^2 = kT/\mu m_H$. Insisting that this be invariant amounts to recognizing the rough uniformity of kinetic temperatures $T \sim 10$ K (which to first order can be understood as a consequence of the competition between cosmic-ray heating and CO cooling) over a large range of scales in interstellar clouds. The stability criterion that follows ultimately leads to a set of results that self-consistently explain some important observational features of GMCs and massive cores.

A gas cloud will be stable against radial perturbations if the derivative $\partial P_s/\partial R$ (taken with σ_c and M held fixed) is ≤ 0: a slight decrease in the cloud radius then leads to an increase in the pressure just inside its boundary, which in turn leads to reexpansion. Appendix B shows that, for any equation of state, this condition is just

$$\left(\frac{\partial P_s}{\partial R}\right)_{M,\sigma_c} = -6\frac{P_s}{R}\left[\frac{1-(5/6)(\alpha_{non}-a)^{-1}}{3-\rho_{ave}/\rho_s}\right] \leq 0\,, \quad (2.9)$$

where ρ_s is the internal density at the edge of the cloud. Although this stability criterion has been derived without explicitly considering the effects of mean magnetic fields, we expect that it should not be greatly altered by their inclusion. (This is again implied by our assumption of approximate spherical symmetry, since eq. [2.9] must at least be satisfied along field lines at the boundary of a magnetized cloud.)

Depending on the equation of state, there may exist a radius for which a pressure-truncated cloud is marginally stable (the expression [2.9] is just 0) and beyond which it is unstable. It is these critical equilibria, which must have

$$\alpha_{non} - a = \tfrac{5}{6}\,, \quad (2.10)$$

that are of particular interest here. Once α_{non} and a are known as functions of radius (as in Appendix A), the satisfaction, if possible, of equation (2.10) sets the boundary R_{crit}/r_0 of the cloud. This in turn allows for evaluation of the coefficients in equations (2.8a)–(2.8d). Quite generally,

$$M_{crit} = \frac{25}{\sqrt{8\pi}}\frac{1}{\alpha_{non}^{1/2}\alpha_{mag}^{3/2}}\frac{\sigma_{ave}^4}{(G^3P_s)^{1/2}}\,, \quad (2.11a)$$

$$R_{crit} = \frac{5}{\sqrt{8\pi}}\frac{1}{\alpha_{non}^{1/2}\alpha_{mag}^{1/2}}\frac{\sigma_{ave}^2}{(GP_s)^{1/2}}\,, \quad (2.11b)$$

$$\Sigma_{crit} = \sqrt{\frac{8}{\pi}}\left(\frac{\alpha_{non}}{\alpha_{mag}}\right)^{1/2}\left(\frac{P_s}{G}\right)^{1/2}\,, \quad (2.11c)$$

and

$$\rho_{ave,crit} = \frac{6\alpha_{non}}{5}\frac{P_s}{\sigma_{ave}^2}\,. \quad (2.11d)$$

Equation (2.11c) shows that a nonmagnetic cloud ($\alpha_{mag} = \alpha_{non}$) on the verge of gravitational collapse has a mean column density that is fixed by the pressure of the surrounding medium, independently of any gas equation of state.

In general, the virial parameter of a given cloud is sensitive to its internal structure (through the equation of state) and its total radius. However, for a *critically stable* cloud we always have $\alpha_{non} = a + 5/6$. Since a is typically of order (but slightly greater than) unity, this implies $\alpha_{non} \approx 2$ and $1 - P_s/P_{ave} = a/\alpha_{non} \approx \frac{1}{2}$. The virial theorem (2.1) then becomes

$$\mathcal{U} + \mathcal{M} + \mathcal{W} \approx 0\,. \quad (2.12)$$

If there is equipartition $\mathcal{M} \approx \mathcal{U}$ between the magnetic and kinematic energies in such a cloud, then $2\mathcal{U} + \mathcal{W} \approx 0$ as well; thus, $\mathcal{M}/|\mathcal{W}| \approx \frac{1}{2}$, and the critical α_{mag} is expected to be of order unity (see eq. [2.7]; see also Elmegreen 1989 and McKee & Zweibel 1992).

Observations of molecular clouds show that $2\mathcal{U} + \mathcal{W} \approx 0$ (or equivalently, $\alpha_{mag} \approx 1$) and are *consistent* with $\mathcal{M} \approx \mathcal{U}$ (Myers & Goodman 1988a, 1988b), although actual magnetic-field measurements are few and uncertain. The most massive cores in GMCs similarly tend to show $2\mathcal{U} + \mathcal{W} \approx 0$ and α_{mag} near 1 (this is not the case for low-mass cores, however: e.g., Williams, de Geus, & Blitz 1994; Williams et al. 1995; see also § 4.1 below). Observations of them are also indicative of magnetic equipartition (Bertoldi & McKee 1992), though again the evidence is rather indirect and not necessarily conclusive. Having said this, it does seem that GMCs and massive cores both satisfy equation (2.12), which would imply that they are at or near their critical masses.

Thus arrived at, this conclusion depends on the criterion one adopts for cloud stability, i.e., it follows from the assumption that the thermal line width σ_c is held fixed during any radial perturbation (and from the additional proviso that $\mathcal{M} \approx \mathcal{U}$). Nevertheless, our analysis—which specifies no equation of state—provides a natural explanation for the fact that so many GMCs and large cores appear to be in simple "gravitational virial equilibrium" (i.e., $2\mathcal{U} + \mathcal{W} \approx 0$), even though they are threaded by appreciably strong mean magnetic fields.

There is also separate evidence for the criticality of massive molecular cores. For instance, Bertoldi & McKee (1992), in their study of the cores in four GMCs, argue that the most massive are at least magnetically supercritical, a necessary condition for gravitational instability. More fundamentally, star-forming regions clearly must be susceptible to gravitational collapse; but in the Rosette GMC at least, those cores that are most obviously associated with *IRAS* sources are also among the heaviest (Williams et al. 1995). As mentioned above, the largest cores in several GMCs also have the smallest virial parameters (as low as 1), so that this would seem to be a feature of clouds that are close to instability. The observation of a mean $\alpha_{mag} \approx 1$ for GMCs then implies that they, too, are near some critical mass and certainly in excess of the nonmagnetic Jeans or Bonnor-Ebert value (for which $\mathcal{M} = 0$ implies $\mathcal{U} + \mathcal{W} \approx 0$ and $\alpha_{mag} = \alpha_{non} \approx 2$). McKee (1989) has further argued that GMCs on the whole are magnetically supercritical, and of course they must be strongly self-gravitating in order to be molecular at all (e.g., Elmegreen 1985).

On a related note, McKee (1989) points out that GMCs must generally be near criticality because they show a P_{ave}

that is typically an order of magnitude larger than the total (thermal plus turbulent) pressure in the hot ISM. Given our stability criterion, equation (2.11d) shows that self-gravity can supply a maximal pressure enhancement $P_{\rm ave}/P_s \approx 2.5$ of a spherical cloud over its surrounding medium, and this only for a critical mass body. Even putting the nonsphericity of GMCs aside, however, it is important to note that the analysis here speaks only to the molecular, self-gravitating parts of GMCs and not to their diffuse, low-A_V H I components. Elmegreen (1989) has shown that the weight of these atomic "envelopes" can easily increase the pressure at the boundaries of the molecular parts of a cloud complex by a factor of 5 or more above the value in the ISM at large; overall, then, $P_{\rm ave}/P_{\rm ISM} > 10$.

If GMCs and their most massive cores are indeed critical mass objects, then they must all have the same dimensionless radii (although the physical scale r_0 will generally vary) and the same virial parameters. Aside from possible variations in P_s, which are discussed in detail by Elmegreen (1989), this causes the coefficients in equations (2.11a)–(2.11d) and (2.8a)–(2.8d) to be roughly constant and allows for well-defined mass-radius–line width relations between clouds. Moreover, we have argued that $\alpha_{\rm non} \simeq 2$ and, in the event of magnetic equipartition, $\alpha_{\rm mag} \simeq 1$ for critical clouds, regardless of the underlying equation of state. The coefficients in the $M - R - \sigma_{\rm ave}$ scalings are then independent of this detail, and the average properties of GMCs can shed no light on their internal structure. This both explains why critical, magnetized isothermal sphere models are successful in quantitatively accounting for the observed scalings (with $\alpha_{\rm non} = 2.054$ and $\alpha_{\rm mag} \simeq 1$: Elmegreen 1989; Harris & Pudritz 1994) and implies that the same agreement with the data comes with *any* model that provides for the existence of a critical mass (see eqs. [4.12a] and [4.12b] below).

Finally, equations (2.11a)–(2.11d) as written would suggest that all GMCs must be under similar surface pressures P_s if, for example, Σ is to be roughly the same among them. Other authors (e.g., McKee 1989; Mouschovias 1987; Myers & Goodman 1988b) have argued instead that either Σ itself (and hence $P_{\rm ave}$), or the mean field strength $B_{\rm ave}$, is the more fundamentally invariant attribute of GMCs. If so, then P_s could be eliminated from the critical Bonnor-Ebert relations in favor of any of these quantities, and our approach does not preclude the others.

2.3. *Magnetic Field Model*

Consider a cloud of radius R, threaded by a mean magnetic field approximated as uniform and of magnitude $B_{\rm ave}$. Outside the cloud, let B fall off as r^{-2} to a radius R_0, where it matches onto an ambient, uniform field of strength B_0 (Nakano 1984). Conservation of flux (or continuity of the normal component of $\boldsymbol{B}$ across the boundary of the cloud) demands $B_{\rm ave}R^2 = B_0 R_0^2$, and evaluating equation (2.4) at the surface $r = R_0$ gives

$$\mathscr{M} = \frac{B_{\rm ave}^2 R^3}{3}\left(1 - \frac{R}{R_0}\right).$$

Defining $\beta = 8\pi P_{\rm ave}/B_{\rm ave}^2$ and $\Phi = \pi B_{\rm ave} R^2$, we have

$$\frac{\mathscr{M}}{|\mathscr{W}|} = \frac{5}{9a\pi^2}\frac{\Phi^2}{GM^2}\left(1 - \frac{R}{R_0}\right) = \frac{2\alpha_{\rm mag}}{3a\beta}\left(1 - \frac{R}{R_0}\right), \quad (2.13)$$

so that equation (2.7) gives

$$\frac{1}{\alpha_{\rm mag}} = \frac{1}{\alpha_{\rm non}} + \frac{2}{3a\beta}\left(1 - \frac{R}{R_0}\right). \quad (2.14)$$

With $B_0 \simeq 3$ μG and $B_{\rm ave} \simeq 30$–40 μG for GMCs (Myers & Goodman 1988b), flux conservation gives $R/R_0 \simeq 0.3$; and $\mathscr{U} \simeq \mathscr{M}$ implies $\beta \simeq 1$. Thus, $\alpha_{\rm mag} \approx 1$ when $\alpha_{\rm non} \approx 2$, as expected.

Some indication of the reliability of equations (2.11a)–(2.11d) and (2.13), and of the approximations leading to them, can be had by comparing the critical masses they predict for magnetized, isothermal spheres ($a = 1.221$) with those obtained from self-consistent, axisymmetric numerical calculations. In particular, the mass M_Φ, which separates magnetically sub- and supercritical clouds, and for which $\mathscr{M} = |\mathscr{W}|$, is given by equation (2.13) as $0.18\Phi/G^{1/2}$, only a 50% overestimate of the exact result $M_\Phi \simeq 0.12\Phi/G^{1/2}$ (Mouschovias & Spitzer 1976; Tomisaka, Ikeuchi, & Nakamura 1988). Further, for $M \gtrsim 0.24\Phi/G^{1/2}$, the critical masses we obtain by using equation (2.7) in equation (2.11a) lie within a factor of 2 of those found by Tomisaka et al. (1988; see their eq. [4.7]). (In fact, our formula is more accurate in the weak field limit because it approaches the correct $M_{\rm crit} = 1.182\sigma^4/(G^3P_s)^{1/2}$ for the nonmagnetic, $\Phi = 0$ isothermal sphere.) And for the equipartition $\beta = 1$ seen in GMCs, setting $\alpha_{\rm mag} \approx 1$ in equation (2.13) implies $M_{\rm crit} \approx (5/6\pi^2)^{1/2}\Phi/G^{1/2}$. This is roughly 1.6 times our (approximate) M_Φ, and 2.4 times the exact value, for which the level of agreement is quite acceptable. In any case, we are led to expect that critical mass GMCs and cores are strongly magnetically supercritical, with $M_{\rm crit} \approx 2M_\Phi$—a result that has also been argued by McKee (1989) and Bertoldi & McKee (1992).

3. POLYTROPIC EQUATIONS OF STATE

The outward increase of line width both within giant molecular clouds as a whole (Larson 1981; Miesch & Bally 1994) and within individual dense cores (Fuller & Myers 1992; Caselli & Myers 1995), immediately suggests the class of negative-index polytropes as possible models for these structures. That is, if $P \propto \rho^{1+1/N}$, then for a polytropic index $N < -1$ we have P/ρ increasing for decreasing ρ, as required. Such models have been studied by, e.g., Viala & Horedt (1974) and Maloney (1988), and we derive the generalized Bonnor-Ebert relations for them in Appendix C. Although there are various physical arguments to support their use (e.g., Shu et al. 1972; de Jong, Dalgarno, & Boland 1980; McKee & Zweibel 1995), these polytropes turn out to be unlikely descriptions of real GMCs (and of course, a positive polytropic index is undesirable because it is inconsistent with a velocity dispersion that increases with radius).

Here we define $n = N/(N+1)$, so that $P \propto \rho^{1/n}$ and $n > 1$ for $N < -1$. From Appendix C, a nonmagnetic, negative-index polytrope that is truncated anywhere outside of its constant density central region (inside which, $a \simeq 1$ and $\alpha_{\rm non}$ increases without bound toward $r = 0$) will then satisfy

$$\alpha_{\rm non} - a = \tfrac{2}{5}(4n - 3).$$

Thus, an $n > 1$ polytrope has $(5/6)(\alpha_{\rm non} - a)^{-1} < 1$; and since its density profile is $\rho \propto r^{-p}$, with $p < 2$ everywhere for any n (Appendix C), we also find $\rho_{\rm ave}/\rho_s < 3$. According to equation (2.9), then, *a truncated, negative-index polytrope will always be stable and never critically so* (as was also

noted by Maloney (1988). Ultimately, the same steady increase of line width with radius that would recommend the polytropic equation of state in the first place also proves to be its undoing: the internal pressure gradient that results is so shallow as to stabilize a cloud under any external pressure. The concept of a critical mass is then irrelevant for these models, which casts doubt on their utility in describing real GMCs or high-mass cores. Any additional support from a mean magnetic field in the cloud obviously serves only to exacerbate this problem.

Again, this result follows to some extent from the constraint that the thermal line width σ_c be fixed during a perturbation of the cloud. By contrast, both Viala & Horedt (1974) and Chièze (1987) consider the possibility that the constant of proportionality in the relation $P \propto \rho^{1/n}$ is invariant and find that polytropes can become unstable for certain truncation radii. Still, our approach is closely related to a point that is *independent of any rule for cloud stability*:

The minimum value of the nonmagnetic virial parameter for a truncated polytrope is (eq. [C7])

$$\alpha_{\rm non} \geq \frac{5}{2}\frac{(4n-3)(2n-1)}{6n-5}.$$

As usual, this is a lower limit because $\alpha_{\rm non}$ can be very large indeed if the polytrope is truncated at a very small radius. In the event of equipartition $\mathscr{U} = \mathscr{M}$ between kinematic and magnetic energies, equation (2.7) and the identity $\alpha_{\rm mag} = 2\alpha\mathscr{U}/|\mathscr{W}|$ lead to

$$\alpha_{\rm mag} = \frac{\alpha_{\rm non}}{1+\alpha_{\rm non}/(2a)} = \frac{\alpha_{\rm non}}{1+(1/2)(1-P_s/P_{\rm ave})^{-1}},$$

in which case equation (C11) and $n > 1$ finally imply that

$$\alpha_{\rm mag} \geq 10\frac{(4n-3)(2n-1)}{(6n-5)(6n+1)} > \frac{10}{7}.$$

Thus, regardless of whether there exist any unstable modes for truncated polytropes, the virial parameters of such clouds are significantly larger than the $\alpha_{\rm mag} \simeq 1$ ($2\mathscr{U} + \mathscr{W} \approx 0$) seen in GMCs (Myers & Goodman 1988b) and in the most massive molecular cores (Bertoldi & McKee 1992; Williams et al. 1994, 1995), even if dynamically significant mean magnetic fields are allowed to be present. It is a property of our specific stability criterion that this fact implies the absence of critically stable equilibria.

The virial parameters of magnetized polytropes could be reduced to $\alpha_{\rm mag} \simeq 1$, for any n, if the mean field were such that $\mathscr{M} \simeq 2\mathscr{U}$. In this case, however, using equation (C11) for $P_s/P_{\rm ave}$ in the virial theorem (2.1) leads to $0.8 < \mathscr{M}/|\mathscr{W}| < 1$ for $n \geq 2$, which is difficult to reconcile with the rather higher degree of magnetic supercriticality that is observationally inferred for GMCs and massive cores ($\mathscr{M}/|\mathscr{W}| \lesssim 0.5$, and $M \simeq 2M_\odot$; see §§ 2.2 and 2.3).

One consequence of all of this is that the nonthermal line widths in GMCs, $\sigma_{\rm NT}^2 = \sigma_{\rm ave}^2 - kT/\mu m_{\rm H}$, cannot be attributed entirely to the pressure of weakly damped Alfvén waves, for which $P \propto \rho^{1/2}$ ($n = 2$, or $N = -2$; McKee & Zweibel 1995), and thus, $\alpha_{\rm mag} \gtrsim 1.65$ under magnetic equipartition. It seems almost certain that Alfvén waves do play a significant role in the support of GMCs and cores (e.g., Arons & Max 1975; Pudritz 1990); but, as McKee & Zweibel (1995) also note, they cannot be uniquely responsible for their large-scale stability. In this context, we note that the size–line width relation between clouds can be expressed in terms of a mean magnetic field strength, as in, e.g., Myers & Goodman (1988a). Specifically, equation (2.11d) can be used to write equation (2.11b) in terms of $P_{\rm ave}$ rather than P_s, and the definition of β (§ 2.3) relates $P_{\rm ave}$ to $B_{\rm ave}$. Then, with a mean mass per particle $\mu = 2.33$ and a kinetic temperature $T = 10$ K, we have

$$\sigma_{\rm NT} \simeq 0.60 \text{ km s}^{-1}(\alpha_{\rm mag}\beta)^{1/4}\left(\frac{B_{\rm ave}}{30\ \mu\text{G}}\right)^{1/2}\left(\frac{R}{1\text{ pc}}\right)^{1/2}.$$

The equality is not quite exact here, because the scalings with $B_{\rm ave}$ and R strictly apply to the total $\sigma_{\rm ave}$. Still, this relation is accurate in the typical case, $\sigma_{\rm NT}^2 \gg kT/\mu m_{\rm H}$; and for $\alpha_{\rm mag} = \beta = 1$, it is consistent with available data (see Myers & Goodman 1988a). Thus, although Mouschovias & Psaltis (1995) argue for an interpretation of this result in terms of Alfvén waves, we see here that it is independent of *any* assumptions on the physical origin of the nonthermal motions in GMCs (in principle, they need not even derive from magnetic fields).

Finally, it is clear that any simple "mixing" of two polytropes with different indices will still preclude the existence of a critical (or low-$\alpha_{\rm mag}$) cloud; even the superposition of an isothermal part, i.e., $P = C_1\rho + C_2\rho^{1/n}$, only admits one if it is essentially isothermal anyway ($C_1 \gg C_2$). Thus, we now turn to a different equation of state, in which the gas pressure varies only logarithmically with density.

4. THE LOGOTROPE

Many theoretical models of star forming clouds employ the singular isothermal sphere, in which $\rho \propto r^{-2}$. However, there is some evidence that H II regions are concentrated toward the CO centroids of their parent GMCs such that their three-dimensional number density is most consistent with an r^{-1} fall-off (Waller et al. 1987; Scoville et al. 1987). This suggests the possibility that, in a heavily smoothed, average sense, the internal density structure of molecular clouds is essentially $\rho \propto r^{-1}$ (see also Solomon et al. 1987). Further, extinction measurements indicate $\rho \propto r^{-1}$ or so in the outer parts of cores as well (Cernicharo, Bachiller, & Duvert 1985; Stüwe 1990).

Lizano & Shu (1989; see also Gehman et al. 1996) introduced the so-called logotropic equation of state for GMCs, $P = P_{\rm iso} + P_{\rm turb}$, with $P_{\rm iso} \propto \rho$ and $P_{\rm turb} \propto \ln(\rho/\rho_{\rm ref})$. If the central line width of a cloud is to be entirely thermal in origin, the reference density in $P_{\rm turb}$ must be $\rho_{\rm ref} = \rho_c$. However, P/ρ then *decreases* with radius, which is incompatible with the observations. We suggest that a more complete description of GMCs and cores is given instead by a "pure" logotrope:

$$P = \rho_c\sigma_c^2\left[1 + A\ln\left(\frac{\rho}{\rho_c}\right)\right], \tag{4.1}$$

with $A > 0$ a parameter to be adjusted. The assumption here is that any nonthermal motions, which presumably arise from MHD turbulence, add to the thermal pressure such that both are fully accounted for by the equation of state (4.1). This relation is shown schematically in Figure 1, along with an isothermal sphere combination and the polytropic $P \propto \rho^{1/2}$ for Alfvén waves. In the rest of our discussion, equation (4.1) is referred to simply as a logotrope.

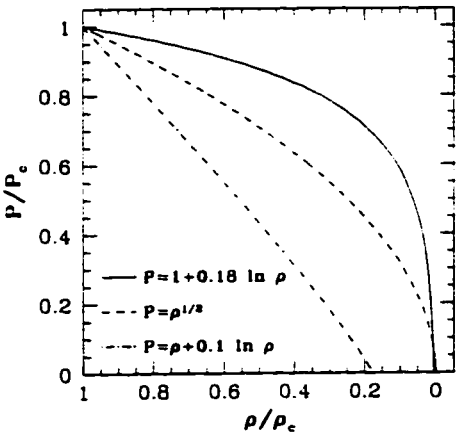

FIG. 1.—Comparison of the logotropic equation of state [$P/P_c = 1 + 0.18\ln(\rho/\rho_c)$] with those for Alfvén wave pressure [$P/P_c = (\rho/\rho_c)^{1/2}$] and a logotrope-plus-isothermal sphere combination [$P/P_c = \rho/\rho_c + 0.1\ln(\rho/\rho_c)$].

with the understanding that no further consideration is given to any mixed isothermal version.

Given equation (4.1), the equation of hydrostatic equilibrium (A1) integrates to

$$\frac{\rho}{\rho_c} = \frac{1}{1 + \psi/A}, \tag{4.2}$$

where $\psi = (\phi - \phi_c)/\sigma_c^2$ is a dimensionless gravitational potential. Substitution of this expression into Poisson's equation (A2) shows the existence of a singular solution,

$$\frac{\rho}{\rho_c} = \sqrt{\frac{2A}{9}}\left(\frac{r}{r_0}\right)^{-1}. \tag{4.3}$$

which describes the density profile of the bounded (finite ρ_c) solution at large radii. (The scale radius $r_0 = 3\sigma_c/[4\pi G\rho_c]^{1/2}$.) In spite of such a slowly decreasing internal density, a logotrope has only a finite extent, since for any positive A the pressure will eventually vanish. Assuming that A is *small* enough for the singular density profile to apply at the edge of the cloud, we have

$$\xi_{max} = \frac{R_{max}}{r_0} = \sqrt{\frac{2A}{9}}\, e^{1/A}. \tag{4.4}$$

The velocity dispersion, $\sigma^2 = P/\rho$, increases with radius inside the cloud until it reaches a maximum of

$$\sigma^2_{max}/\sigma_c^2 = Ae^{1/A - 1} \tag{4.5}$$

at $\xi = r/r_0 = e^{-1}\xi_{max}$, beyond which it falls again (to 0, at ξ_{max}).

A logotrope truncated by the pressure P_s of an external medium has precisely one critical mode for any given value of A. As discussed in Appendix B, if a cloud is truncated at a very small radius ξ, it will always be stable. But in the power-law part of the logotrope, equations (4.2) and (4.3) show that $d\psi/d\xi = (9A/2)^{1/2}$, so once ξ is so large that $P_s/P_c < A/4$, the cloud is unstable (see eq. [B6]). Thus,

$$\xi_{crit} = \frac{R_{crit}}{r_0} = \sqrt{\frac{2A}{9}}\exp\left(\frac{1}{A} - \frac{1}{4}\right) = e^{-1/4}\xi_{max}, \tag{4.6}$$

where we have again assumed that A is relatively small and the singular solution (4.3) holds at ξ_{crit}. (This expression shows that σ achieves its maximum *inside* ξ_{crit}, and the surface of the critical logotrope is cooler than its interior. McKee 1989 has suggested that such behavior might arise from the radiation of Alfvén waves into the ambient medium.) Now, evaluating the pressure (eq. [4.1]) and density (eq. [4.3]) at the radius (eq. [4.6]) yields, for any critically stable logotrope,

$$\left(\frac{\rho_s}{\rho_c}\right)_{crit} = \exp\left(\frac{1}{4} - \frac{1}{A}\right),$$
$$\left(\frac{\sigma_s^2}{\sigma_c^2}\right)_{crit} = \frac{A}{4}\exp\left(\frac{1}{A} - \frac{1}{4}\right),$$
$$\left(\frac{P_s}{P_c}\right)_{crit} = \frac{A}{4}. \tag{4.7}$$

Evidently, self-consistency in the use of equation (4.3) here requires $A \ll 4$. Equations (A7) and (2.2) can then be used to find

$$\left(\frac{\rho_{ave}}{\rho_s}\right)_{crit} = \frac{3}{2},$$
$$\left(\frac{\sigma^2_{ave}}{\sigma_s^2}\right)_{crit} = \frac{14}{9},$$
$$\left(\frac{P_{ave}}{P_s}\right)_{crit} = \frac{7}{3}, \tag{4.8}$$

independently of A.

A numerical solution for our logotrope with $A = 0.18$ (which we justify shortly) yields the internal density, pressure, and velocity-dispersion profiles shown in Figure 2. Equations (4.4) and (4.6) are valid here, as an r^{-1} density profile is realized well before the cloud ends (the vertical line in all four panels of the figure marks the radius ξ_{crit}). It is the steep pressure gradient near ξ_{max} that sets the logotrope apart from the negative-index polytropes and allows for a critical cloud with a small virial parameter.

The *total* velocity dispersion σ^2 in Figure 2 is roughly constant near the center of the cloud; and its rise with radius further on is consistent with $\sigma^2 \propto r^{2/3}$, which is essentially the scaling originally found for GMCs by Larson (1981). Identifying the central dispersion σ_c with the thermal part of the line width (so that thermal motions dominate on the smallest scales, as is observed), the nonthermal contribution to cloud support is $\sigma_{NT}^2 = \sigma^2 - \sigma_c^2$, which is also shown in Figure 2. At small to moderate radii, σ_{NT} naturally rises more steeply than the total σ, while at larger ξ the two are more comparable in magnitude. Roughly, then, our model has $\sigma_{NT}^2 \propto r$ over some range in radius before it flattens to $\sigma_{NT}^2 \propto r^{1/2}$ and eventually turns over (the maximum σ_{NT}^2/σ_c^2 is just $\sigma^2_{max}/\sigma_c^2 - 1$ and occurs at $\xi = e^{-3/4}\xi_{crit}$). It is found that $\sigma_{NT} \propto r^{0.5}$ within GMCs (e.g., Myers & Goodman 1988b), and low-mass molecular cores show the same general trend; high-mass cores are more suggestive of $\sigma_{NT} \propto r^{0.25}$ (Fuller & Myers 1992; Caselli & Myers 1995). A logotropic equation of state both for individual cores and for entire cloud complexes is consistent with these observations, provided that low-mass cores can be viewed as spheres that are pressure truncated at radii $\xi < \xi_{crit}$. We discuss this point further in § 4.1 below. As always, though, no matter how σ varies with r internally, the *average* rela-

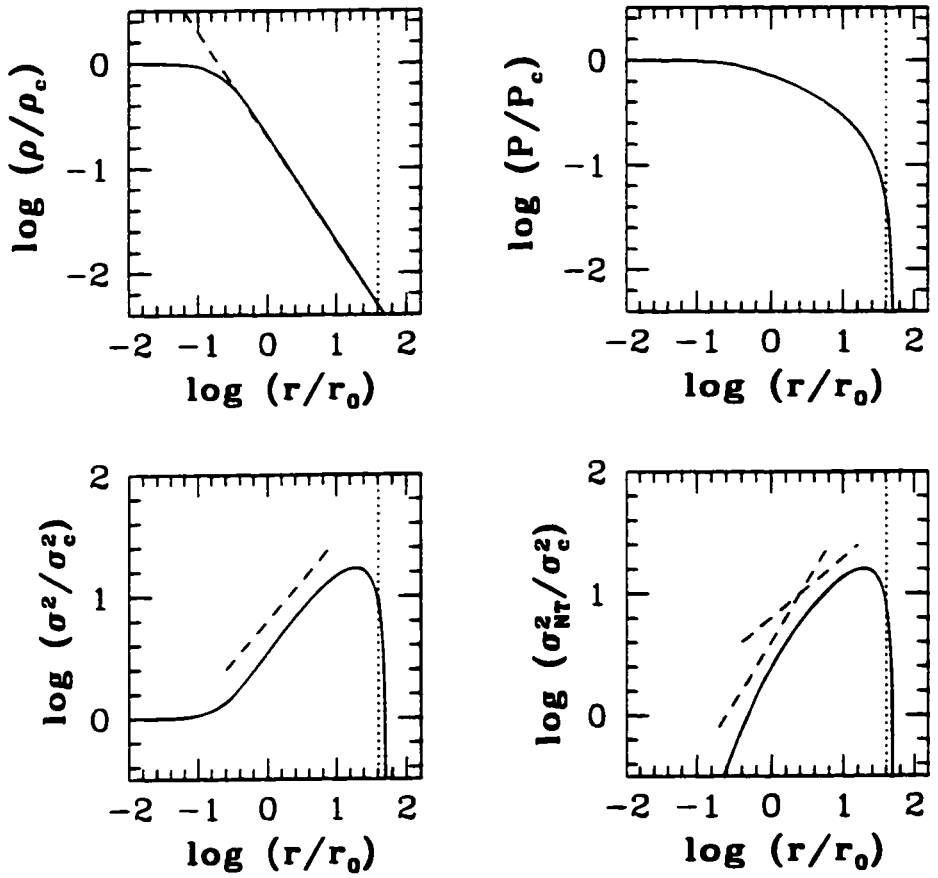

FIG. 2.—Structure of a logotropic gas sphere with $A = 0.18$. The vertical line in all four panels is at the truncation radius that makes for a critically stable cloud: $\xi_{crit} = 40.29$. The long-dashed line in the plot of ρ vs. r is the singular density profile of eq. (4.3); that in the plot of total line width (*bottom left*) represents $\sigma^2 \propto r^{2/3}$; and those in the plot of nonthermal line width (*bottom right*) trace $\sigma^2_{NT} \propto r$ and $\sigma^2_{NT} \propto r^{1/2}$. Recall that $r_0^2 \equiv 9\sigma_c^2/4\pi G\rho_c$.

tion $\sigma_{ave} \propto R^{1/2}P_s^{1/4}$ still holds for critical mass clouds, i.e., for GMCs.

A handle on an appropriate value of the parameter A for GMCs as a whole, can be gotten by reinventing them as smoothed out spheres with a number of distinct overdense regions (the cores) sprinkled throughout. The observed contrasts in mean density and velocity dispersion between GMCs and cores can then be related to the A of a model logotrope. Harris & Pudritz (1994; see their Table 2) list each of ρ_{ave}, σ_{ave}, and Σ for a GMC of mass $\bar{M}_{GMC} = 3.3 \times 10^5 M_\odot$ and a core with $\bar{M}_{core} = 5.4 \times 10^2\ M_\odot$. (Such values are "typical" in the sense that, *by mass*, half of all GMCs [cores] are larger than $\bar{M}_{GMC}$ [$\bar{M}_{core}$].) Defining $\tilde{\rho}$, $\tilde{\sigma}$, and $\tilde{\Sigma}$ as the core-to-GMC ratios of mean volume densities, line widths, and column densities, these data show that

$$\tilde{\rho} \simeq 240\ ,\quad \tilde{\sigma} \simeq 0.29\ ,\quad \tilde{\Sigma} \simeq 4.64\ . \tag{4.9}$$

Cores with $M = \bar{M}_{core}$ are among the most massive observed and are likely near critical. If they are also logotropes, then their ρ_{ave}/ρ_s, etc., should be roughly given by equation (4.8), regardless of whether $A_{GMC} = A_{core}$. Such large cores might further be expected to lie in very dense, cold, highly pressured regions of their parent clouds. Then the pressure P_s at the surface of a core is comparable to the GMC's P_c, and similarly for the density and velocity dispersion. These assumptions, together with the relation $\Sigma \propto P_s^{1/2}$ (eq. [2.11c]), result in

$$\tilde{\rho} \simeq \left(\frac{\rho_c}{\rho_s}\right)_{GMC}\ ,\quad \tilde{\sigma} \simeq \left(\frac{\sigma_c}{\sigma_s}\right)_{GMC}\ ,\quad \tilde{\Sigma} \simeq \left(\frac{P_c}{P_s}\right)^{1/2}_{GMC}\ . \tag{4.10}$$

Comparison of equations (4.9) and (4.7) then shows that the observed $\tilde{\rho}$, $\tilde{\sigma}$, and $\tilde{\Sigma}$ (only two of which are actually independent) are realized in a logotropic GMC with

$$A_{GMC} \simeq 0.175\ . \tag{4.11}$$

Although this procedure is highly idealized, it is perhaps telling that an A exists at all that gives at once the correct $\tilde{\rho}$ and $\tilde{\sigma}$. The logotrope appears to be the simplest barotropic equation of state that can account for these ratios *and* the small virial parameters (or the critical equilibrium) of GMCs and massive cores. For example, if GMCs and large cores were both $n = 2$ polytropes truncated at $\xi = r/r_0 \simeq 21.4$, then equation (4.9) could be roughly satisfied, but they would also have a large $\alpha_{non} = 5.37$, and hence, $\alpha_{mag} \simeq 1.75$ for magnetic equipartition (again, $\mathcal{M} \simeq 2\mathcal{U}$ is required to reduce α_{mag} to unity for a negative-index polytrope, but this

is not wholly satisfactory for other reasons; see § 3). Alternatively, adding an explicit $\rho^{1/2}$ term to equation (4.1) destroys the *simultaneous* correspondence between $\bar{\rho}$ and $\bar{\sigma}$ for critical clouds.

To this point, we have not accounted for any mean magnetic fields in GMCs and cores. However, these should have no effect on our estimate of $A_{\rm GMC}$ insofar as very massive clumps have the same $\alpha_{\rm mag} \approx 1$ as their parent clouds. More important is the assumption that the cores here lie at the rare, highest pressure peaks of cloud complexes; if instead they are found in less extreme regions, then equation (4.11) is an upper limit to $A_{\rm GMC}$. Even so, more direct estimates of $A_{\rm GMC}$ are in fairly good agreement with the representative value quoted above. For example, equations (4.7) and (4.8) can be combined to obtain an expression for $\sigma_{\rm ave}^2/\sigma_c^2$; comparison with observed values of the total $\sigma_{\rm ave}$ and the thermal σ_c in GMCs then suggests $0.12 \lesssim A_{\rm GMC} \lesssim 0.16$.

On a final note, since $\rho \propto r^{-1}$ at the edges of such logotropes, we have $a = (1 - 1/3)/(1 - 2/5) = 10/9$. With the ratio of mean kinematic and magnetic pressures $\beta \simeq 1$, equations (2.10) and (2.14) then give for the critical virial parameters,

$$\alpha_{\rm non} = 35/18 \text{ and } \alpha_{\rm mag} \simeq 1.07 .$$

These are near 2 and 1, as expected from general arguments and not far from the values 2.054 and 1.15 for a Bonnor-Ebert isothermal sphere. As alluded to earlier (§ 2.2), the mass-radius and size-line width relations among real GMCs can therefore be understood in terms of this model: equations (2.11b) and (2.11c) become

$$\frac{M}{R^2} = 147\ M_\odot\ \mathrm{pc}^{-2}\left(\frac{P_s}{P_{\rm ISM}}\right)^{1/2}\left(\frac{P_{\rm ISM}}{10^4 k\ \mathrm{cm}^{-3}\ \mathrm{K}}\right)^{1/2} \quad (4.12a)$$

and

$$\frac{\sigma_{\rm ave}}{R^{1/2}} = 0.37\ \mathrm{km\ s^{-1}\ pc^{-1/2}}\left(\frac{P_s}{P_{\rm ISM}}\right)^{1/4}\left(\frac{P_{\rm ISM}}{10^4 k\ \mathrm{cm}^{-3}\ \mathrm{K}}\right)^{1/4} . \quad (4.12b)$$

which agree well with observations (see Elmegreen 1989). Here P_s is the surface pressure on the *molecular part* of the GMC, while $P_{\rm ISM}$ is the total pressure of the hot, intercloud medium. The ratio of these two is typically around 5–10, due to the weight placed on a GMC by its UV-shielding atomic layer (Elmegreen 1989; see also § 2.2 above).

4.1. *Comparison With Data: Molecular Cloud Cores*

As a class, dense molecular cores seem somewhat more heterogeneous than their parent GMCs. First, many studies (Carr 1987; Loren 1989; Stutzki & Güsten 1990; Lada, Bally, & Stark 1991) show that the size-line width relation between cores can be significantly weaker than the virial, $\sigma_{\rm ave} \propto R^{1/2}$ scaling among GMCs and in some cases is difficult to discern at all. Second, in the L1630 GMC at least, the size-line width relation is considerably better defined for clumps that stand out more strongly against the interclump medium (see the comparison in Fig. 13 of Lada et al. between their "5 σ" and "3 σ" cores). And third, the virial parameters $\alpha_{\rm mag}$ of GMC cores are not restricted to values near 1, but rather can range as high as ≈ 100 (Bertoldi & McKee 1992; Williams et al. 1994, 1995).

This last point is particularly significant because the virial parameters of cores in a number of different clouds are seen to correlate with their size: low mass goes along with rather large $\alpha_{\rm mag}$ and high mass with more moderate $\alpha_{\rm mag} \approx 1$. Thus, as Bertoldi & McKee (1992) argue, the smallest clumps in GMCs are far removed from gravitational instability (surface pressure is more important than self-gravity in their confinement), while the largest are actually near criticality (strongly self-gravitating; see also § 2.2 above). Equivalently, a range in the masses of cores can be viewed, at least roughly, as a range in the dimensionless radii ξ—small for low mass and near $\xi_{\rm crit}$ for high mass—at which point they are truncated by the ambient pressure in a GMC (virial parameters generally decrease with ξ for any equation of state; Appendix A). This notion could account for the rather confused size-line width relation *between* cores (if ξ does not have a fixed value, then neither do $\alpha_{\rm non}$ and $\alpha_{\rm mag}$ in eq. [2.8b]) and ultimately must also have consequences for the interpretation of data on the radial variation of velocity dispersion *inside* cores.

If indeed very low-mass cores differ from very high-mass ones mainly in being truncated at $\xi_{\rm low} \ll \xi_{\rm high} \simeq \xi_{\rm crit}$, then the former must be less centrally condensed, have ratios P_s/P_c nearer unity and be generally less distinguishable from the intercore (GMC) gas than the latter. This results in the scale radius $r_0 = 3\sigma_c/(4\pi G\rho_c)^{1/2} \propto \sigma_c^2/P_c^{1/2}$ being *larger* for less massive clumps. To see this, compare the r_0 of a low-mass core, truncated at ξ small enough that $P_s \approx P_c$, with the r_0 of a near-critical, high-mass core. On average, any two cores should be under similar surface pressures P_s (this essentially being set by the internal $P_{\rm ave}$ of a parent GMC), so that

$$\frac{r_0(\text{high})}{r_0(\text{low})} \simeq \left(\frac{P_s}{P_c}\right)_{\rm high}^{1/2}\left[\frac{\sigma_c^2(\text{high})}{\sigma_c^2(\text{low})}\right] \simeq \sqrt{\frac{A}{4}}\left[\frac{\sigma_c^2(\text{high})}{\sigma_c^2(\text{low})}\right] , \quad (4.13)$$

where the second step follows from equation (4.7) if a logotropic equation of state applies. Thus, for σ_c not too widely different between the two cores, and for A small enough, the ratio (4.13) will be less than 1. The same *physical* radius r in high- and low-mass cores then corresponds to larger and smaller $\xi = r/r_0$, respectively. This result, which just reflects the fact that more strongly self-gravitating structures are more centrally concentrated, must be considered when attempting to match any model to any observations.

Returning now to the issue of internal velocity-dispersion profiles, Fuller & Myers (1992, hereafter FM) and Caselli & Myers (1995, hereafter CM) have compiled line width measurements in at least three different molecular lines for each of 14 low-mass and 24 massive cores. The resulting σ versus r profiles indicate that, over similar ranges $r \sim 0.1$–1 pc in all the clumps, and independently of whether or not stars are present within them, the velocity dispersion rises more steeply with radius in low-mass cores than in high-mass ones. In particular, nonthermal line widths in the former are consistent with $\sigma_{\rm NT} \propto r^{0.53}$; in the latter, $\sigma_{\rm NT} \propto r^{0.21}$ (CM). In our view, this situation is a direct result of the effect summarized by equation (4.13). That is, we consider the low-mass cores of FM to be eminently stable logotropes truncated at small ξ, while the high-mass clumps of CM are near critical stability and hence have smaller r_0. The two surveys target similar r within each type of core, so the massive-core data apply to larger dimensionless ξ and must sample the shallower parts of velocity-dispersion profiles like those in Figure 2.

To actually confront the predictions of our logotropic equation of state with the observations of FM and CM, we

again identify the (model) central velocity dispersion with the (observed) thermal line width: $\sigma_c^2 = \sigma_T^2 = kT/\mu m_H$, where T is taken from CM, and $\mu = 2.33$. CM assume $T = 10$ K for all the low-mass cores, and we further assume them all to have $P_s \approx P_c$; they should therefore have a common r_0, which may be easily estimated. Five of the FM cores are observed at radii r_{TNT} such that $\sigma_{NT} = \sigma_T$; among these, $\langle r_{TNT} \rangle \simeq 0.12$ pc (see Table 3 of CM). The related quantity $\xi_{TNT} = r_{TNT}/r_0$ in a model logotrope is just that point where $\sigma^2/\sigma_c^2 = (\sigma_{NT}^2 + \sigma_T^2)/\sigma_T^2 = 2$. If, for example, $A = 0.2$ in equation (4.1), we find $\xi_{TNT} = 0.51$, and thus,

$$r_0(\text{low}) \approx 0.25 \text{ pc} .$$

This result is then used in equation (4.13), along with $\sigma_c^2 \propto T$ and $A = 0.2$, to give

$$r_0(\text{high}) \approx 0.056 \text{ pc} \left(\frac{T_{\text{high}}}{10 \text{ K}} \right) ,$$

where 12 K $\leq T \leq$ 33 K for the massive cores (CM). The data may now be appropriately scaled and compared to theoretical $\sigma - r$ and $\sigma_{NT} - r$ curves.

Figure 3 is the result of such a comparison with three logotropes of different A. The good overall agreement between the models and data suggests that GMC cores are well described by

$$A_{\text{core}} = 0.20 \pm 0.02 ,$$

which is encouragingly close to A_{GMC} as given in equation (4.11) above. In Table 1 we list the radii and other properties (as calculated from eqs. [4.4]–[4.7] above) of critical logotropes with A near 0.2.

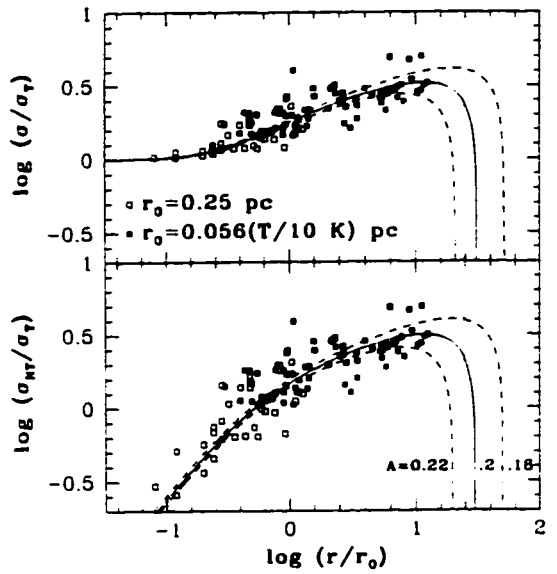

FIG. 3.—Comparison of observed internal velocity-dispersion profiles (total σ, thermal and nonthermal components σ_T and σ_{NT}) with logotropic models, for 38 GMC cores. Open squares correspond to low-mass cores (Fuller & Myers 1992) and filled symbols to high-mass cores (Caselli & Myers 1995; we omit four HCO^+ measurements). Cores both with and without stars are represented here, and each has been observed in three or more different molecular lines. The model curves are for $A = 0.20$ (best case; *solid line*), and $A = 0.18$, $A = 0.22$ (*dashed lines*); a larger A results in smaller maximum and critical radii r/r_0. The vertical line is at $\xi_{crit} = 24.37$ for an $A = 0.2$ logotrope.

TABLE 1

PROPERTIES OF CRITICAL LOGOTROPES

A	ξ_{max}	ξ_{crit}	ρ_s/ρ_c	σ_s^2/σ_c^2	$\sigma_{NT,s}^2/\sigma_c^2$	P_s'/P_c
0.18.....	51.73	40.29	4.96×10^{-3}	9.07	8.07	0.045
0.20.....	31.29	24.37	8.65×10^{-3}	5.78	4.78	0.050
0.22.....	20.83	16.22	1.36×10^{-2}	4.04	3.04	0.055

Some of the scatter in Figure 3 could arise if A does not have a common value for all cores, and any embedded stars could further complicate the situation. (Notably, FM and CM both find that starless cores alone show a tighter—but not different—line width–radius relation than do cores with stars, suggesting that the basic form seen here is one of the initial conditions for star formation.) However, some of the scatter is surely due to the fact that the cores in this sample do not reside in a single GMC, but come from diverse environments. (For instance, the low-mass cores here tend to be found in dark clouds of mass $\sim 10^4$–$10^5 M_\odot$ and the high-mass ones in somewhat larger GMCs.) Thus, there is no guarantee that every low-mass core observes $P_s \approx P_c$, or that every high-mass core is at its critical mass. It is the large number of cores available here that allows the mean trend in Figure 3, and the implied structural dichotomy between small and large clumps, to emerge.

As with our earlier consideration of core-to-GMC density and line width ratios, a fit of similar quality to the data in Figure 3 can be obtained with the model velocity-dispersion profile of an $n = 2$ polytrope that has a scale r_0 about a factor of two smaller than that used here. As we have stressed, however, there are other difficulties with the application of polytropic equations of state to GMCs and cores.

In summary, the approach we have taken self-consistently allows for purely thermal motions to dominate on the smallest scales in cores (and in GMCs); for an internal density structure ($\rho \propto r^{-1}$ in the outer parts of cores and much shallower near their centers) that is consistent with at least some observations[1] (Cernicharo et al. 1985; Stüwe 1990; André, Ward-Thompson, & Barsony 1993); and for a unified treatment of low- and high-mass cores. This is in contrast to the models of FM and CM (also Myers & Fuller 1992), which assume two distinct components of isothermal and nonthermal gas in cores and predict a $\rho \propto r^{-2}$ singularity at their centers. It should also be noted that the assumption $P_s \approx P_c$ in low-mass cores still allows for these noncritical clumps to show a fair degree of central concentration. For example, an $A = 0.2$ logotrope

[1] Williams et al. (1995) fitted the projected density profiles of many clumps in the Rosette GMC, with a function of the form $(1 + r_p/a)^{-n} - a$ being the projected half-power radius. They find $n \approx 1$ outside of unresolved central regions and suggest that this implies an intrinsic density profile of $\rho \propto r^{-2}$. However, because molecular cores have a finite extent, their density profiles in projection are not so simply related to their space densities. (For example, the surface density of a core with *any* ρ profile must decline steeply in the outermost regions, as less and less of the core material is intercepted by the line of sight.) Even a truncated logotrope, for which we might naively expect a flat surface-density profile, actually gives rise to something consistent with $n \approx -0.8$ to $n \approx -1.0$ over most radii in the fitting function of Williams et al.; and the projected half-power radius is only $a = 2.92 r_0 \sim 0.2$ pc for a critical, $A = 0.2$ core ($R_{crit} = 24.37 r_0$).

that is truncated at $\xi \simeq 0.1\xi_{crit}$ has $\rho_s/\rho_c < 0.09$, but $P_s/P_c \simeq 0.5$; thanks to the relatively weak dependence of P on ρ, we do not require, nor even expect, that all low-mass cores be uniform-density spheres. Our model is therefore consistent with the significantly non-uniform density profiles of low-mass cores ($\alpha_{mag} \gtrsim 3$) in the Rosette GMC (Williams et al. 1995).

5. SUMMARY

We have generalized the classic Bonnor-Ebert relations for isothermal spheres to give expressions for the masses, radii, and total velocity dispersions of magnetized, pressure-truncated gas clouds with any internal pressure-density relation. The analysis combines an exact approach, based on solving the equation of hydrostatic equilibrium, with a virial-theorem treatment to incorporate mean magnetic fields into the clouds. A stability criterion has been developed that relies only on the assumption of an invariant central velocity dispersion σ_c and is independent of the gas equation of state. Clouds that are just *critically* stable under this condition have mass-radius and size–line width relations that are effectively oblivious to their internal structure, i.e., to their equation of state.

These results have been applied to molecular cloud complexes and dense cores, leading to three main conclusions:

1. In spite of their nonspherical geometry, the gross features of GMCs are consistent with those of critical mass clouds in our analysis. (In the context of GMCs and cores, we identify the central velocity dispersion with the *thermal* part of the total [thermal plus turbulent] line width.) *Independently of the exact equation of state*, if equipartition between magnetic and kinetic energies obtains in a critically stable cloud, then it will appear to be in simple gravitational equilibrium, $2\mathscr{U} + \mathscr{W} \approx 0$ (equivalently, it will have a virial parameter $\alpha_{mag} \simeq 1$). These are observed features of real GMCs and their most massive cores. In addition, any of our critical mass spheres obey the same mass-radius and size–line width relations that hold among real GMCs. All of this implies that GMCs, and large clumps, are near criticality.

2. No polytropic (power-law) pressure-density relation can fully characterize GMCs or cores. A positive polytropic index leads to a velocity dispersion that decreases outward within a cloud, opposite to what is seen both in individual cores and in entire cloud complexes. Alternatively, a negative index (i.e., $P \propto \rho^\gamma$ with $\gamma < 1$) gives a line width that increases with radius, as required. However, such clouds do not show virial parameters near unity unless their mean fields are so strong that their magnetic and gravitational energies are comparable in magnitude, and this is again in conflict with observations of GMCs and large cores. Given our stability criterion, an equivalent statement is that pressure-truncated polytropes are unconditionally stable against gravitational collapse. Since weakly damped Alfvén waves satisfy $P \propto \rho^{1/2}$ (McKee & Zweibel 1995), this shows explicitly that they cannot fully explain the observed nonthermal support in molecular clouds.

3. The most successful model for the internal structure of molecular cores, and one that is also consistent with global properties of GMCs, is a "pure logotrope:" $P/P_c = 1 + A \ln(\rho/\rho_c)$. This relation is meant to account for *all* contributions to the total gas pressure, including the effects of disordered magnetic fields (MHD turbulence). Once it is recognized that low-mass cores are far below their critical masses (though still in virial equilibrium; they are essentially pressure-confined), and that high-mass cores are near criticality, the internal velocity-dispersion profiles of clumps from a variety of environments are seen to be consistent with a logotropic model with $A \simeq 0.2$. A similar value of A can also explain characteristic core-to-GMC ratios of mean densities and line widths, and any A is consistent with the observed size–line width relation between GMCs because the logotropic equation of state allows for critical equilibria. Finally, the equilibrium density profile of a logotrope has $\rho \propto r^{-1}$, outside of a constant-density central region. There is some observational support to be found for this prediction, in GMCs and cores both.

We would like to thank Phil Myers for his comments on an earlier version of this paper, and Charles Curry for valuable discussions. R. E. P. also acknowledges conversations with Paola Caselli and Gary Fuller. This work was supported in part by the Natural Sciences and Engineering Research Council of Canada.

APPENDIX A

PRESSURE-TRUNCATED EQUILIBRIA

For a spherical cloud in hydrostatic equilibrium, with kinematic (thermal plus turbulent) pressure $P = \rho\sigma^2$ (so that σ is the one-dimensional velocity dispersion) and a self-gravitational potential ϕ, we define

$$\psi = \frac{\phi - \phi_c}{\sigma_c^2}, \qquad r_0^2 = \frac{9\sigma_c^2}{4\pi G\rho_c}, \qquad \text{and} \qquad \xi = \frac{r}{r_0},$$

where a subscript "c" denotes evaluation of a quantity at the cloud center. The characteristic scale of a cloud is set by r_0; the factor of 9 in its definition identifies it with the projected half-power radius of an isothermal sphere (e.g., Binney & Tremaine 1987). The equation of hydrostatic equilibrium then reads

$$\frac{d}{d\xi}\left(\frac{P}{P_c}\right) = -\frac{\rho}{\rho_c}\frac{d\psi}{d\xi}, \tag{A1}$$

and Poisson's equation becomes

$$\frac{1}{\xi^2}\frac{d}{d\xi}\left(\xi^2\frac{d\psi}{d\xi}\right) = 9\frac{\rho}{\rho_c}. \tag{A2}$$

(Note that $\psi = d\psi/d\xi = 0$ at $\xi = 0$, and $\psi > 0$ for $\xi > 0$.) The mass enclosed within radius ξ is given by

$$M \equiv M(\xi) = 4\pi\rho_c r_0^3 \int_0^\xi \xi'^2 \frac{\rho}{\rho_c} d\xi' ,$$

so that, with the help of equation (A2),

$$M = \frac{4\pi}{9} \rho_c r_0^3 \left(\xi^2 \frac{d\psi}{d\xi}\right) = \frac{\sigma_c^2 r_0}{G} \left(\xi^2 \frac{d\psi}{d\xi}\right) . \tag{A3}$$

Following Ebert (1955) and Bonnor (1956), the surface of the cloud is defined by that radius ξ at which the internal pressure $P(\xi)$ just equals a confining pressure P_s due to a surrounding medium of negligible gravity. Equation (A3), the definition of r_0, and the identity $P_c = \rho_c \sigma_c^2$ then yield, for any equation of state relating P and ρ,

$$M = \sqrt{\frac{9}{4\pi}} \left(\xi^2 \frac{d\psi}{d\xi}\right) \left(\frac{P_s}{P_c}\right)^{1/2} \frac{\sigma_c^4}{(G^3 P_s)^{1/2}} . \tag{A4}$$

The physical radius of the cloud is $R = \xi r_0$:

$$R = \sqrt{\frac{9}{4\pi}} \xi \left(\frac{P_s}{P_c}\right)^{1/2} \frac{\sigma_c^2}{(G P_s)^{1/2}} . \tag{A5}$$

These relations combine to give

$$\Sigma \equiv \frac{M}{\pi R^2} = \sqrt{\frac{4}{9\pi}} \frac{d\psi}{d\xi} \left(\frac{P_s}{P_c}\right)^{-1/2} \left(\frac{P_s}{G}\right)^{1/2} \tag{A6}$$

and

$$\rho_{ave} \equiv \frac{3M}{4\pi R^3} = \frac{1}{3} \left(\frac{1}{\xi} \frac{d\psi}{d\xi}\right) \left(\frac{P_s}{P_c}\right)^{-1} \frac{P_s}{\sigma_c^2} . \tag{A7}$$

Given an equation of state, the integration of equations (A1) and (A2) determines $d\psi/d\xi$ and P_s/P_c at any truncation radius ξ. This fixes the coefficients in equations (A4)–(A7) and affords mass-radius and size–line width relations for pressure-truncated clouds. (Note that the scalings in these relations, $M \propto \sigma^4/P_s^{1/2}$, $R \propto \sigma^2/P_s^{1/2}$, etc., are *global* ones and do not necessarily reflect the radial dependence of any quantity *inside* a cloud.)

The definition of the nonuniformity parameter a (eq. [2.5]) allows it to be found as a function of radius:

$$a = \frac{15}{\xi^3} \left(\frac{d\psi}{d\xi}\right)^{-2} \int_0^\xi \xi'^3 \frac{d\psi}{d\xi'} \frac{\rho}{\rho_c} d\xi' ; \tag{A8}$$

and equation (A3) implies that the virial parameter $5\sigma_{ave}^2 R/GM$ for nonmagnetic clouds (i.e., $\alpha_{mag} = \alpha_{non}$) is just

$$\alpha_{non} = 5 \frac{\sigma_{ave}^2}{\sigma_c^2} \left(\xi \frac{d\psi}{d\xi}\right)^{-1} , \tag{A9}$$

which tends to be a nonincreasing function of ξ. Alternatively, equations (A7) and (2.8d) give

$$\alpha_{non} - a = 15 \left(\frac{d\psi}{d\xi}\right)^{-2} \left(\frac{P_s}{P_c}\right) . \tag{A10}$$

These results can be used to rewrite equations (A4)–(A7) in terms of α_{non}, a, and σ_{ave}; equations (2.8a)–(2.8d) (with $\alpha_{mag} = \alpha_{non}$) are then obtained. Also, once α_{non} is known as a function of radius in any cloud, the observable α_{mag} for a given magnetic field configuration may be calculated (e.g., § 2.3).

APPENDIX B

STABILITY CRITERION

We begin by recalling the definition of the scale radius r_0 from equation (A3):

$$r_0 = \frac{GM}{\sigma_c^2} \left(\xi^2 \frac{d\psi}{d\xi}\right)^{-1} ; \tag{B1}$$

and rearranging equation (A4):

$$P_s = \frac{9}{4\pi} \left(\xi^2 \frac{d\psi}{d\xi}\right)^2 \left(\frac{P_s}{P_c}\right) \frac{\sigma_c^8}{G^3 M^2} . \tag{B2}$$

The stability of a cloud truncated at radius R by the external pressure P_s is determined by the sign of the derivative $(\partial P_s/\partial R)$: this is negative for a stable equilibrium, 0 for the "critical" cloud, and positive for instability.

We now apply a perturbation $R \to R + dR$ while keeping the mass M and central (i.e., thermal) velocity dispersion σ_c of the cloud fixed, so that

$$\left(\frac{\partial P_s}{\partial R}\right)_{M,\sigma_c} = \left(\frac{\partial P_s}{\partial \xi}\right)_{M,\sigma_c}\left(\frac{\partial \xi}{\partial R}\right)_{M,\sigma_c} . \tag{B3}$$

Then $R = \xi r_0$ and equation (B1) give us

$$\begin{aligned}\left(\frac{\partial \xi}{\partial R}\right)_{M,\sigma_c} &= \frac{1}{r_0}\left[1 + \frac{\xi}{r_0}\left(\frac{\partial r_0}{\partial \xi}\right)_{M,\sigma_c}\right]^{-1} \\ &= \frac{1}{r_0}\left[1 - \xi\left(\xi^2\frac{d\psi}{d\xi}\right)^{-1}\frac{d}{d\xi}\left(\xi^2\frac{d\psi}{d\xi}\right)\right]^{-1} \\ &= \frac{1}{r_0}\left[1 - 9\xi\left(\frac{d\psi}{d\xi}\right)^{-1}\frac{\rho_s}{\rho_c}\right]^{-1} ,\end{aligned} \tag{B4}$$

where ρ_s is the density just inside the cloud edge and we have used Poisson's equation (A2). We also have, from equation (B2),

$$\begin{aligned}\left(\frac{\partial P_s}{\partial \xi}\right)_{M,\sigma_c} &= P_s\left(\frac{d\psi}{d\xi}\right)^{-1}\left(\frac{P_c}{P_s}\right)\left[\left(2\frac{d^2\psi}{d\xi^2} + \frac{4}{\xi}\frac{d\psi}{d\xi}\right)\left(\frac{P_s}{P_c}\right) + \left(\frac{d\psi}{d\xi}\right)^2\frac{d}{d\psi}\left(\frac{P_s}{P_c}\right)\right] \\ &= P_s\left(\frac{d\psi}{d\xi}\right)^{-1}\left(\frac{\rho_s}{\rho_c}\right)\left[18 - \left(\frac{d\psi}{d\xi}\right)^2\left(\frac{P_s}{P_c}\right)^{-1}\right] ,\end{aligned} \tag{B5}$$

where both equations (A1) and (A2) have been used.

Thus, equations (B3), (B4), and (B5) show that

$$\left(\frac{\partial P_s}{\partial R}\right)_{M,\sigma_c} = 18\frac{P_s}{R}\left[\frac{1 - (1/18)(d\psi/d\xi)^2(P_s/P_c)^{-1}}{(1/\xi)(d\psi/d\xi)(\rho_c/\rho_s) - 9}\right] . \tag{B6}$$

Now, from equations (A10) and (A7), we have

$$\frac{1}{18}\left(\frac{d\psi}{d\xi}\right)^2\left(\frac{P_s}{P_c}\right)^{-1} = \frac{5}{6}\frac{1}{\alpha_{\rm non} - a} \qquad \text{and} \qquad \frac{1}{\xi}\left(\frac{d\psi}{d\xi}\right) = 3\frac{\rho_{\rm ave}}{\rho_c} ,$$

so that finally,

$$\left(\frac{\partial P_s}{\partial R}\right)_{M,\sigma_c} = -6\frac{P_s}{R}\left[\frac{1 - (5/6)(\alpha_{\rm non} - a)^{-1}}{3 - \rho_{\rm ave}/\rho_s}\right] . \tag{B7}$$

Alternatively, for a *nonmagnetic* cloud, we can make use of equation (2.8c), with $\alpha_{\rm mag} = \alpha_{\rm non}$, to write

$$\left(\frac{\partial P_s}{\partial R}\right)_{M,\sigma_c} = -6\frac{P_s}{R}\left[\frac{1 - (\pi G\Sigma^2)/(8P_s)}{3 - \rho_{\rm ave}/\rho_s}\right] . \tag{B8}$$

This treatment is valid for *any* gas equation of state, so long as the cloud radius is perturbed in such a way that M and σ_c are unaffected. The result (B8) was also obtained by Ebert (1955) and Bonnor (1956), who specifically considered the stability of truncated isothermal spheres, and by Maloney (1988) in his study of negative-index polytropes.

Any virialized cloud truncated at small ξ (i.e., where ρ and σ^2 are approximately constant) will be stable. This is because, regardless of the equation of state, the potential ψ at small radii can always be expanded in a power series of the form: $\psi = (3/2)\xi^2 - \mathcal{O}(\xi^4)$ (see Appendix C for an example). Thus, referring to equation (B6) with $\rho_s \approx \rho_c$, we have $(\partial P_s/\partial R)_{M,\sigma_c} \approx -3P_s/R < 0$. Depending on the equation of state, there may or may not be a truncation at larger ξ, which results in $(\partial P_s/\partial R)_{M,\sigma_c} > 0$ and an unstable equilibrium.

APPENDIX C

POLYTROPES OF NEGATIVE INDEX

Consider the (nonmagnetic) equation of state:

$$P \propto \rho^{1 + 1/N} ,$$

where the polytropic index $N < -1$. Then we define $n = N/(N + 1)$ and write

$$P = \rho_c\sigma_c^2\left(\frac{\rho}{\rho_c}\right)^{1/n} , \qquad n \geq 1 , \tag{C1}$$

with $n = 1$ corresponding to isothermality. In order to evaluate the coefficients in equations (A4)–(A7) (or eqs. [2.8a]–[2.8d], with $\alpha_{mag} = \alpha_{non}$), we first use the relation (C1) to integrate the equation of hydrostatic equilibrium (A1) and find

$$\frac{\rho}{\rho_c} = [1 + (n-1)\psi]^{n/(1-n)}, \tag{C2}$$

so that Poisson's equation (A2) becomes

$$\frac{1}{\xi^2}\frac{d}{d\xi}\left(\xi^2\frac{d\psi}{d\xi}\right) = 9[1 + (n-1)\psi]^{n/(1-n)}. \tag{C3}$$

(Note that in the limit $n \to 1$, the right-hand side of eq. [C3] becomes $9e^{-\psi}$, just what is required for the isothermal sphere.) At the cloud center, $\psi = d\psi/d\xi = 0$, so for small ξ the potential ψ can be expanded in a power series:

$$\psi \to \frac{3}{2}\xi^2 - \frac{3n}{40}\xi^4 + \mathcal{O}(\xi^6), \tag{C4}$$

allowing for an integration of equation (C3). The result of this is a core-halo structure to the cloud: at very small radii, the solution is indistinguishable from that for an isothermal sphere, and the density and velocity dispersion are essentially constant with ξ, independently of n. Once $\xi \gtrsim$ a few, however, a power-law density profile obtains; for each n, there exists a singular solution to which the equilibrium cloud tends at large radii.

These singular solutions are readily found by substituting the prescription

$$\frac{\rho}{\rho_c} = K\xi^{-p}$$

into equation (C2) and solving equation (C3) for K and p. This gives

$$p = \frac{2n}{2n-1} \quad \text{and} \quad K = \left[\frac{2}{9}(p-1)(3-p)\right]^{p/2}, \tag{C5}$$

so that with $n \geq 1$ we have $1 < p \leq 2$, and these clouds are diffuse enough that they have no "natural" edge. That is, the density never vanishes, and any boundary to the cloud must be defined by the point at which the internal pressure matches that of an external medium. (It is again worth noting the exact correspondence to the singular isothermal sphere when $n = 1$ in eq. [C5]; see Chandrasekhar 1967.)

Consider now a polytrope of negative index, which is truncated at radius ξ large enough that the structure of the cloud is given by the singular solution. Then $d\psi/d\xi$ and P_s/P_c can be calculated analytically, and equation (A10) yields

$$\alpha_{non} - a = \tfrac{5}{8}(4n-3). \tag{C6}$$

We also know that $a = (1 - p/3)/(1 - 2p/5)$, so

$$\alpha_{non} = \frac{5}{2}\frac{(4n-3)(2n-1)}{6n-5}, \tag{C7}$$

and we have the following:

$$M = \sqrt{\frac{2}{\pi(4n-3)^3}}\left(\frac{6n-5}{2n-1}\right)^2\frac{\sigma_{ave}^4}{(G^3P_s)^{1/2}}, \tag{C8}$$

$$R = \sqrt{\frac{1}{2\pi(4n-3)}}\frac{6n-5}{2n-1}\frac{\sigma_{ave}^2}{(GP_s)^{1/2}}, \tag{C9}$$

$$\Sigma = \sqrt{\frac{8}{\pi(4n-3)}}\left(\frac{P_s}{G}\right)^{1/2}. \tag{C10}$$

and

$$\rho_{ave} = \frac{6n-3}{6n-5}\frac{P_s}{\sigma_{ave}^2}. \tag{C11}$$

Thus, regardless of where they are truncated by the surface pressure P_s, these model clouds can only ever represent modest enhancements over the intercloud medium. In particular, P_{ave}/P_s has a maximum of 3 (for isothermality, $n = 1$), but even for $n = 2$ (which gives the ρ dependence of Alfvén wave pressure; McKee & Zweibel 1995) is reduced to just 9/7.

As discussed in § 3, any truncation of a negative-index polytrope results in a stable cloud. This is because, with $\rho \propto r^{-p}$, we have that $\rho_{ave}/\rho_s = 3/(3-p)$, and the stability criterion (B7) becomes (with the help of eq. [C6]) $(\partial P_s/\partial R)_{M,\sigma_c} = -4P_s/R < 0$. In particular, this holds in the limit $n \to 1$, when the numerator and denominator of equation (B7) both vanish. What allows for the existence of critical and unstable equilibria for the bounded isothermal sphere, then, is the fact that its density profile

actually oscillates about the singular solution $\rho \propto r^{-2}$ at large radii (Chandrasekhar 1967). This does *not* occur for those polytropes with $n > 1$; instead, the bounded spheres follow the singular solutions exactly at large ξ.

Finally, it is worth noting that these results do not contradict the well-known instability (e.g., Shu 1977) of truly singular spheres, for which $\rho \propto r^{-p}$ all the way to the center and $\rho_c \to \infty$. In such cases, perturbation of the truncated cloud radius is performed with M, σ_c, *and* ρ_c all held fixed. Stability then depends only on the sign of $(\partial P_s/\partial \xi)_{M,\sigma_c}$ (eq. [B5]), which is always positive for these polytropes.

REFERENCES

André, P., Ward-Thompson, D., & Barsony, M. 1993, ApJ, 406, 122
Arons, J., & Max, C. E. 1975, ApJ, 196, L77
Binney, J., & Tremaine, S. 1987, Galactic Dynamics (Princeton: Princeton Univ. Press)
Bertoldi, F., & McKee, C. F. 1992, ApJ, 395, 140
Bonnor, W. B. 1956, MNRAS, 116, 351
Carr, J. S. 1987, ApJ, 323, 170
Caselli, P., & Myers, P. C. 1995, ApJ, 446, 665 (CM)
Cernicharo, J., Bachiller, R., & Duvert, G. 1985, A&A, 149, 273
Chandrasekhar, S. 1967, An Introduction to the Study of Stellar Structure (New York: Dover)
Chièze, J. P. 1987, A&A, 171, 225
de Jong, T., Dalgarno, A., & Boland, W. 1980, A&A, 91, 68
Ebert, R. 1955, Z. Astrophys., 37, 217
Elmegreen, B. G. 1985, in Protostars & Planets II, ed. D. Black & M. Matthews (Tucson: Univ. Arizona Press), 33
———. 1989, ApJ, 338, 178
Falgarone, E., Phillips, T. G., & Walker, C. K. 1991, ApJ, 378, 186
Fleck, R. C., Jr. 1988, ApJ, 328, 299
Fuller, G. A., & Myers, P. C. 1992, ApJ, 384, 523 (FM)
Gehman, C. S., Adams, F. C., Fatuzzo, M., & Watkins, R. 1996, ApJ, 457, 718
Harris, W. E., & Pudritz, R. E. 1994, ApJ, 429, 177
Heiles, C., Goodman, A., McKee, C. F., & Zweibel, E. G. 1993, in Protostars and Planets III, ed. E. H. Levy & J. I. Lunine (Tucson: Univ. Arizona Press), 279
Henriksen, R. N. 1991, ApJ, 377, 500
Lada, E. A., Bally, J., & Stark, A. A. 1991, ApJ, 368, 432
Larson, R. B. 1981, MNRAS, 194, 809
Lizano, S., & Shu, F. H. 1989, ApJ, 342, 834
Loren, R. B. 1989, ApJ, 338, 925
Maloney, P. 1988, ApJ, 334, 761
McCrea, W. H. 1957, MNRAS, 117, 562
McKee, C. F. 1989, ApJ, 345, 782
McKee, C. F., & Zweibel, E. G. 1992, ApJ, 399, 551
———. 1995, ApJ, 440, 686
Miesch, M. S., & Bally, J. 1994, ApJ, 429, 645
Mouschovias, T. Ch. 1987, in Physical Processes in Interstellar Clouds, ed. G. E. Morfill & M. Scholer (Dordrecht: Reidel), 453
Mouschovias, T. Ch., & Psaltis, D. 1995, ApJ, 444, L105
Mouschovias, T. Ch., & Spitzer, L. 1976, ApJ, 210, 326
Myers, P. C., & Fuller, G. A. 1992, ApJ, 396, 631
Myers, P. C., Fuller, G. A., Goodman, A. A., & Benson, P. J. 1991, ApJ, 376, 561
Myers, P. C., & Goodman, A. A. 1988a, ApJ, 326, L27
———. 1988b, ApJ, 329, 392
Nakano, T. 1984, Fund. Cosmic Phys., 9, 139
Pudritz, R. E. 1990, ApJ, 350, 195
Sanders, D. B., Scoville, N. Z., & Solomon, P. M. 1985, ApJ, 289, 373
Scoville, N. Z., Yun, M. S., Clemens, D. P., Sanders, D. B., & Waller, W. H. 1987, ApJS, 63, 821
Shu, F. H. 1977, ApJ, 214, 488
Shu, F. H., Milione, V., Gebel, W., Yuan, C., Goldsmith, D. W., & Roberts, W. W. 1972, ApJ, 173, 557
Solomon, P. M., Rivolo, A. R., Barrett, J., & Yahil, A. 1987, ApJ, 319, 730
Stutzki, J., & Güsten, R. 1990, ApJ, 356, 513
Stüwe, J. A. 1990, A&A, 237, 178
Tomisaka, K., Ikeuchi, S., & Nakamura, T. 1988, ApJ, 335, 239
Viala, Y. P., & Horedt, G. P. 1974, A&A, 33, 195
Waller, W. H., Clemens, D. P., Sanders, D. B., & Scoville, N. 1987, ApJ, 314, 397
Williams, J. P., Blitz, L., & Stark, A. A. 1995, ApJ, 451, 252
Williams, J. P., de Geus, E. J., & Blitz, L. 1994, ApJ, 428, 693

Chapter 3

Gravitational Collapse and Star Formation in Logotropic and Non-Isothermal Spheres

THE ASTROPHYSICAL JOURNAL, 476:750–765, 1997 February 20

GRAVITATIONAL COLLAPSE AND STAR FORMATION IN LOGOTROPIC AND NONISOTHERMAL SPHERES

DEAN E. MCLAUGHLIN AND RALPH E. PUDRITZ
Department of Physics and Astronomy, McMaster University, Hamilton, Ontario L8S 4M1, Canada;
dean@physics.mcmaster.ca, pudritz@physics.mcmaster.ca
Received 1996 June 21; accepted 1996 September 16

ABSTRACT

We present semianalytical similarity solutions for the inside out, expansion-wave collapse of initially virialized gas clouds with nonisothermal equations of state. Results are given for the family of negative-index polytropes ($P \propto \rho^{\gamma}$, $\gamma \leq 1$), but we focus especially on the so-called logotrope, $P/P_c = 1 + A \ln(\rho/\rho_c)$. In a separate paper, we have shown this to be the best available phenomenological description of the internal structure and average properties of molecular clouds, as well as dense clumps of both high and low mass. The formalism and interpretation of the present theory are extensions of those in Shu's standard model for accretion in self-gravitating isothermal spheres: a collapse front moves outward into a cloud at rest, and the gas behind it falls back to a collapsed core, or protostar. The infalling material eventually enters free-fall, so that the density profiles and velocity fields have the same shape ($\rho \propto r^{-3/2}$ and $-u \propto r^{-1/2}$) at both small radii in logotropic and isothermal spheres. However, several differences arise from the introduction of a new equation of state. The accretion rate onto a protostar is not constant in a logotrope, but grows as $\dot{M} \propto t^3$ during the expansion wave. Thus, the formation time for a star of mass M scales as $M^{1/4}$; low-mass stars are accreted over longer times, and high-mass stars over shorter times, than expected in isothermal clouds. This result has implications for the form and origin of the stellar initial mass function. In addition, the gas density behind an expansion wave increases with time in our theory, but it would decrease in an isothermal sphere. The infall velocities also grow, but at an initially much slower rate than that found in an isothermal collapse. These results apply to low- and high-mass star formation alike. We briefly discuss how they lead to older inferred collapse ages for Class 0 protostars in general and for the Bok globule B335 in particular.

Subject headings: hydrodynamics — ISM: clouds — ISM: general — ISM: globules — stars: formation

1. INTRODUCTION

One of the cornerstones in any theory of star formation has to be a correct description of the gravitational collapse of gaseous clouds. The pioneering studies of Bodenheimer & Sweigart (1968), Larson (1969), and Penston (1969) gave numerical integrations of the isothermal collapse of uniform-density spheres, and Larson and Penston both went so far as to derive semianalytical similarity solutions (descriptions of a fluid flow in which the densities and velocities approach invariant forms) for the evolution of their spheres. In a seminal paper that defined the current paradigm for "inside out" collapse and low-mass star formation, Shu (1977) derived a different, one-parameter family of similarity solutions for the isothermal problem. Hunter (1977) found still more, and Whitworth & Summers (1985) finally pointed out that there is in fact a two-dimensional continuum of such solutions. Common to all of these is the eventual formation of a central point mass that grows subsequently as the cloud continues to fall onto it. This *core* is naturally identified as a protostar (or star and disk).

One of Shu's (1977) solutions in particular—the so-called expansion wave—has played a central role in the development of the standard theory of star formation, as reviewed, for example, by Shu, Adams, & Lizano (1987). In part, this is because of the simple and intuitive nature of the expansion wave, and because it lends itself well to the (perturbative) inclusion of rotation (Tereby, Shu, & Cassen 1984) and mean magnetic fields (Galli & Shu 1993a, 1993b) in isothermal clouds. In addition, however, it is physically relevant because it describes the relatively gentle collapse, from the center out, of a sphere that is initially in virial equilibrium. As we discuss below, the idea that precollapse interstellar clouds are in equilibrium configurations is one that meshes with a variety of observations. There are contrary arguments (e.g., Bonnell, Bate, & Price 1996) that star-forming clouds should collapse from nonequilibrium, or even near-uniform conditions; but this is a violent process (the flow of Larson 1969 and Penston 1969 is everywhere highly supersonic) that would give rise to strong kinematic signatures that have never been observed. Rather, the most convincing claim to a direct detection of collapse has been made for the Bok globule B335, where molecular line profiles are consistent with the more moderate velocity field expected for an expansion wave (Zhou 1992; Zhou et al. 1993).

The standard theory has its difficulties, however. For instance, Shu's (1977) model describes the collapse of highly unstable, *singular* isothermal spheres, and is not necessarily applicable to more realistic clouds with finite central densities (such as the marginally stable Bonnor-Ebert sphere; Hunter 1977; Foster & Chevalier 1993). As another example, an isothermal expansion wave leads to a time-invariant protostellar accretion rate, $\dot{M} = 0.975\sigma^3/G$, which appears to be inconsistent with the observed luminosities of young stellar objects in the Taurus-Auriga star-forming region specifically (e.g., Kenyon et al. 1994). But most important is the fact that an isothermal equation of state, while a natural and instructive first approximation, is ultimately incompatible with observations of both giant molecular clouds (GMCs) and the subcondensations—the dense clumps where stars are ultimately born—within them.

As suggested above, GMC complexes and individual clumps are well described by models of (magnetic) virial-equilibrium spheres that are "truncated" by a constant surface pressure exerted by a diffuse external medium (e.g., Myers & Goodman 1988; Bertoldi & McKee 1992; Elmegreen 1989; McLaughlin & Pudritz 1996). (The dense clumps are often referred to as cores, but here we reserve that term for the central point mass, or protostar, which develops in a collapsing sphere.) The virial balance relies on superthermal random velocities that *increase outward* within any given clump. The nonthermal component σ_{NT} of the total velocity dispersion (line width) is larger in higher mass clumps (Caselli & Myers 1995), but it is present at even the smallest observed radii in low-mass clumps as well (Fuller & Myers 1992). Indeed, σ_{NT} grows more rapidly with increasing radius in low-mass clumps than in high-mass ones, and *no interstellar cloud obeys an isothermal equation of state.*

The first attempts to model the nonthermal line widths (e.g., Myers & Fuller 1992; Lizano & Shu 1989) tended to focus on the fact that σ_{NT} is small in low-mass clumps. Myers & Fuller, in particular, construct equilibrium, self-gravitating spheres from a gas equation of state (EOS) that is explicitly isothermal at small radii in a cloud and that becomes progressively "softer" (P depends less than linearly on ρ, so that $\sigma^2 = P/\rho$ increases with decreasing density) further out. Because the clumps in GMCs can be viewed as pressure-truncated spheroids, with truncation at a smaller radius corresponding to a lower mass, this approach effectively ensures that the low-mass clumps are still treated as (very nearly) isothermal spheres. Any consequences that the nonthermal support might have for collapse and star formation are then largely confined to the high-mass regime. For example, Myers & Fuller (1992) estimate the formation times of stars in their model, and conclude that high-mass stars are accreted relatively faster than they would be under an isothermal EOS, while low-mass stars grow at roughly the same rate.

By contrast, McLaughlin & Pudritz (1996, hereafter MP96) have adopted a phenomenological, *logotropic* EOS—$P/P_c = 1 + A \ln(\rho/\rho_c)$—for molecular clouds and clumps. This EOS provides a unified treatment of low- and high-mass clumps and entire GMCs. It can account quantitatively for (1) the global size line width and mass-radius relations (e.g., Larson 1981) *between* cloud complexes; (2) the typical mass and density contrasts between GMCs and the clumps within them; and (3) the observed dependence of line width on radius *inside* dense clumps of any mass. Moreover, the form of the EOS itself is never close, even on small spatial scales or in low-mass clouds, to the isothermal $P \propto \rho$. The details of *both* low- *and* high-mass star formation in a logotrope will therefore differ from the standard results for isothermal collapse. (It should be noted that our logotrope is different from that introduced by Lizano & Shu 1989, which essentially has $P \sim \rho + \ln \rho$ and cannot account for all three of the properties of interstellar clouds listed here.)

In this paper, then, we derive semianalytical similarity solutions for the collapse of nonmagnetic, nonrotating gas spheres with softer-than-isothermal equations of state. We concentrate on the case of a logotropic EOS as the most self-consistent description of the ubiquitous turbulence in interstellar clouds; but in a pair of Appendices, results are also given for the more general family of negative-index polytropes ($P \propto \rho^\gamma$, with $0 < \gamma \leq 1$). (Although the self-similar collapse of polytropes has previously been investigated by, e.g., Suto & Silk 1988, we also briefly discuss the accretion rates and star formation timescales in such spheres.)

Section 2 begins with a brief summary of the equilibrium structure of a logotrope (MP96), and then goes on to an analysis of its collapse. Our development owes much to the physical discussion of Shu (1977): we first find a class of collapse solutions for singular, $\rho \propto r^{-1}$ spheres that are very accurate approximations to more realistic, nonsingular logotropes, then we focus on the inside out, expansion-wave collapse of an initially virialized cloud. Two main features are a post-collapse density profile and velocity field that have the same free-fall shape ($\rho \propto r^{-3/2}$ and $-u \propto r^{-1/2}$ at small radii) found for an isothermal expansion wave, *but* a rate of accretion onto the collapsed core that is no longer constant in time; rather, here $\dot{M} \propto t^3$. These results allow for an evaluation, in § 3, of the formation times for stars of various masses. High-mass stars will be accreted more rapidly in a logotrope than in an isothermal sphere, but a low-mass star in a logotrope will appear later than a star of the same mass would in an isothermal sphere. This "squeezing" of formation timescales, which we estimate to be typically of order $1\text{–}3 \times 10^6$ yr, should have important implications for the origin and shape of the stellar IMF. In § 4, we consider the collapse of a 1 $M_\odot$ logotrope specifically, and we briefly discuss relevant observations of two young stellar objects, NGC 2071 and B335. We conclude that the age of B335 is probably greater than 10^6 yr, an order of magnitude older than suggested by the application of isothermal collapse models. Since B335 is one of the family of the youngest known, "Class 0" protostars (André, Ward-Thompson, & Barsony 1993), these objects might be considerably older, in general, than is currently believed.

2. SIMILARITY SOLUTIONS

2.1. *The Logotrope*

Our logotropic EOS (MP96) is

$$\frac{P}{P_c} = 1 + A \ln\left(\frac{\rho}{\rho_c}\right), \tag{1}$$

where P_c and ρ_c are the central pressure and density in a cloud, and A is essentially a free parameter. The total velocity dispersion $\sigma^2 = P/\rho$ increases outward from $r = 0$ until it reaches a maximum at some large radius, beyond which it decreases somewhat. Since line widths are essentially purely thermal on the smallest scales in real interstellar clouds, and are also observed to increase with radius (e.g., Fuller & Myers 1992; Caselli & Myers 1995), the central velocity dispersion in a logotrope is identified with the thermal value: $\sigma_c^2 \equiv P_c/\rho_c = kT/\mu m_H$. Once a value of A is specified, the EOS can be used to integrate a Lane-Emden type of equation for a self-gravitating, virialized gas sphere. This then allows for a quantitative comparison of the *internal* σ versus r profiles of real and model clouds. Good agreement with data on GMC clumps, of low and high mass alike, is obtained for $A \simeq 0.2 \pm 0.02$.

These points are discussed in more detail in MP96. Starting from the premise that interstellar clouds are pressure-truncated—their boundaries defined by a surface pressure P_s because of a more diffuse, surrounding medium—that paper develops expressions for the masses and densities of

virial-equilibrium gas spheres with arbitrary equations of state. Quite general arguments then imply that GMCs, and the *largest* clumps within them, are all at or near their critical masses: if they were any more massive, given their temperatures, surface pressures, and magnetic field strengths, they would be unstable to radial perturbations (see also McKee 1989; Bertoldi & McKee 1992). Although this conclusion is independent of the exact form of the gas EOS, not all equations of state provide for such a critical mass. For example, the family of negative-index polytropes (in which $P \propto \rho^{\gamma}$, with $\gamma < 1$) also have velocity dispersions that increase with radius, but are *always stable* against radial perturbations in the analysis of MP96. Put another way, and independently of any stability analysis, such polytropes cannot simultaneously account for the internal structure of molecular clumps and the global properties (Larson's [1981] laws: $M \propto R^2$ and $\sigma_{ave} \propto R^{1/2}$) of GMCs; the logotrope is the simplest EOS for which this is possible.

The critical mass of an $A = 0.2$ logotrope is given by equation (2.11) of MP96:

$$M_{crit} = \frac{250}{\alpha^{3/2}} M_{\odot} \left(\frac{T}{10\ \mathrm{K}}\right)^2 \left(\frac{P_s}{1.3 \times 10^5 k\ \mathrm{cm}^{-3}\ \mathrm{K}}\right)^{-1/2}, \quad (2)$$

where we have explicitly used the fact that $\sigma_c^2 = kT/\mu m_H$, and we have set the mean molecular weight to $\mu = 2.33$. The constant α here depends on the strength of any mean magnetic field threading the cloud. If there is equipartition between kinetic and mean magnetic energies, then $\alpha \approx 1$; in the absence of any mean field at all, $\alpha = 35/18$ for the logotrope and $M_{crit} \simeq 92\ M_{\odot}$ for this temperature and surface pressure. A smaller value of A results in a larger critical mass: for example, $A = 0.18$ would raise M_{crit} by a factor of about 2.5. MP96 also derive the mean density of a critical-mass logotrope:

$$\rho_{ave,crit} = 1.31 \times 10^{-20}\ \mathrm{g\ cm}^{-3} \left(\frac{T}{10\ \mathrm{K}}\right)^{-1} \times \left(\frac{P_s}{1.3 \times 10^5 k\ \mathrm{cm}^{-3}\ \mathrm{K}}\right). \quad (3)$$

The fiducial P_s chosen here is appropriate for dense clumps embedded in self-gravitating GMCs, which amplify the pressure of the hot ISM by about an order of magnitude (Elmegreen 1989; Bertoldi & McKee 1992); it is also similar to the value adopted by Shu (1977) in his study of isothermal collapse. It is significant that the logotropic M_{crit} is vastly greater than the $\sim 1\ M_{\odot}$ mass of a critical, $T = 10$ K isothermal sphere under the same surface pressure. This is part of what makes our model more consistent with observations of the ISM, and, in particular, with the arguments, mentioned above, that only the largest clumps in GMCs are at their critical mass, with smaller ones being in a stable virial equilibrium.

Because we are dealing with pressure-truncated spheres, a cloud's mass can be viewed as being set by the dimensionless "truncation radius" R/r_0 [where $r_0 \equiv 3\sigma_c/(4\pi G\rho_c)^{1/2}$] at which the internal pressure equals that of an ambient medium. That is to say, there is an EOS-dependent R/r_0 that corresponds to a critical mass cloud; any smaller R/r_0 is equivalent to a unique $M/M_{crit} < 1$. Indeed, R/r_0, along with a surface pressure P_s and kinetic temperature T, determine all the properties of a cloud (see Appendix A of MP96). An example of this is given in Table 1, where we list

TABLE 1

PROPERTIES OF PRESSURE-TRUNCATED $A = 0.2$ LOGOTROPES

R/r_0	ρ_c/ρ_s	P_c/P_s	ρ_{ave}/ρ_c	$\sigma_{ave}^2/\sigma_c^2$	$M_{tot}/M_{\odot}$[a]	$t_{ff}/10^5$ yr[a]
0.93	4.28	1.41	0.335	2.3	0.5	4.2
1.34	6.22	1.58	0.238	2.9	1	4.8
2.45	11.54	1.96	0.130	4.4	3	5.9
4.85	23.01	2.68	0.0655	6.7	10	7.1
9.40	44.63	4.16	0.0337	9.1	30	7.9
13.18.....	62.56	5.79	0.0240	10.0	50	7.9
17.02.....	80.77	8.22	0.0186	10.1	70	7.6
19.26.....	91.39	10.32	0.0164	10.0	80	7.2
21.26.....	100.88	12.95	0.0149	9.3	87	6.7
24.37[b].....	115.58	20.00	0.0130	9.0	92	5.8

[a] Calculated assuming no mean magnetic field; surface pressure $P_s = 1.3 \times 10^5 k\ \mathrm{cm}^{-3}$ K; and kinetic temperature $T = 10$ K.
[b] Truncation radius of a critically stable cloud, $M_{tot} = M_{crit}$.

the center-to-edge density and pressure contrasts, mean density, and mass-averaged line width (thermal plus nonthermal: $\sigma_{ave}^2 = P_{ave}/\rho_{ave}$) for logotropes with $A = 0.2$. The absolute values of the masses and free-fall times there [$t_{ff} = (3\pi/32G\rho_{ave})^{1/2}$] apply to purely hydrostatic spheres with no mean magnetic fields, since these are the types of objects that our collapse calculations will address directly. If P_s or T is changed, the mass and mean density of the critical cloud will be affected, as in equations (2) and (3). Then, because the dimensionless R/r_0 actually determines the mass and free-fall time relative to the critical values, these quantities will both change at every radius in Table 1 and by the same factors as in the critical cloud. In any case, it is significant that the total line width σ_{ave} is generally larger in bigger clouds. Lower mass objects are supported to a greater, *but not complete*, extent by thermal motions.

Figure 1 shows the density profile of a critical mass logotrope, and compares it with that of a critical mass, or Bonnor-Ebert, isothermal sphere (Bonnor 1956; Ebert

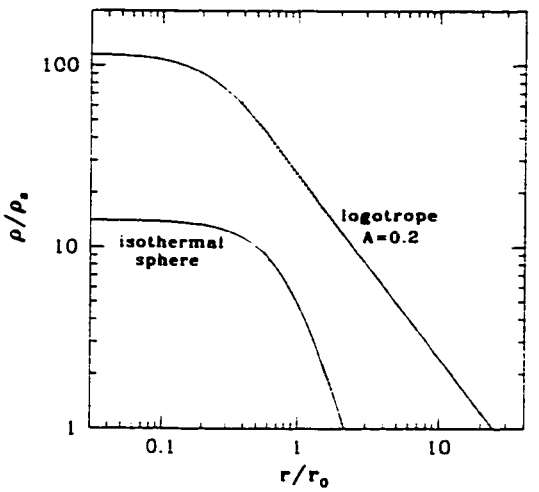

FIG. 1.—Density profiles of a pressure-truncated logotrope and the Bonnor-Ebert isothermal sphere. Both configurations are in hydrostatic equilibrium and correspond to critical mass clouds, i.e., an increased central concentration in either case would destabilize the equilibrium. Scale radius is $r_0 = 3\sigma_c/(4\pi G\rho_c)^{1/2}$, and ρ_s is the density at the cloud surface. Broken lines trace the singular profiles for each equation of state: note how such a solution mirrors the true behavior of the logotrope at most r but bears little resemblance to any stable isothermal sphere.

1955; McCrea 1957). The structure of less massive spheres can also be derived from this diagram: for example, the ρ versus r curve for a logotrope with $M/M_{\rm crit} \simeq 0.33$ is obtained by vertically shifting the curve in Figure 1 in such a way that $\rho/\rho_s = 1$ at $r/r_0 \simeq 9.4$ (cf. Table 1). Also shown in the figure (*dashed lines*) are the analytical singular solution to the equation of hydrostatic equilibrium for a self-gravitating logotrope (MP96),

$$\rho(r) = (AP_c/2\pi G)^{1/2} r^{-1} , \tag{4}$$

and the singular solution $\rho(r) = (\sigma_c^2/2\pi G) r^{-2}$ for an isothermal sphere. Equation (4) closely approximates the bounded logotrope (finite central density; *solid line*) at all $r/r_0 \gtrsim 0.4$, and thus adequately describes the structure even of stable low-mass spheres. On the other hand, the singular isothermal sphere bears very little relation to the Bonnor-Ebert configuration. (The logotropic prediction $\rho \propto r^{-1}$ is one with some observational support. This is discussed in MP96; here we note only that an observed column density profile $N \propto r^{-1}$, which is not uncommon, does *not* necessarily imply $\rho \propto r^{-2}$.)

Since a low-mass clump (for example, $M_{\rm tot} \sim 1\ M_\odot$) is expected to be globally stable against radial perturbations, how does it come to collapse and form a star? When magnetic fields are present, ambipolar diffusion should induce a slow contraction of the clump, during which its initial (time $t = -\infty$) central concentration will be enhanced and its density profile brought into agreement with the singular solution (eq. [4]) over essentially all radii—a configuration that is manifestly unstable (e.g., MP96). Alternatively, in a purely hydrodynamic situation, collapse could be initiated by the growth of a local density fluctuation; or the clump could be put out of equilibrium by the accretion of mass from the surrounding medium. The time at which a cloud becomes singular is labeled $t = 0$, and it corresponds to the formation of a central point mass (or core; physically, a protostar and disk). Following Shu (1977), it is the subsequent $t \geq 0$ evolution of nonmagnetic spheres that we now examine in detail.

2.2. *Fluid Equations*

We begin with the usual Eulerian equations for spherically symmetrical flow in a self-gravitating fluid (cf. Larson 1969; Shu 1977):

$$\frac{\partial u}{\partial t} + u\frac{\partial u}{\partial r} + \frac{GM}{r^2} + \frac{dP}{d\rho}\frac{\partial \ln \rho}{\partial r} = 0 \tag{5}$$

$$\frac{\partial M}{\partial t} + 4\pi r^2 \rho u = 0 \tag{6}$$

$$\frac{\partial M}{\partial r} - 4\pi r^2 \rho = 0 , \tag{7}$$

where $M(r, t)$ is the *total* mass (including any core) inside radius r at time t, and $u(r, t)$ is the instantaneous fluid velocity. The gas EOS influences the collapse through the pressure force $\rho^{-1}\partial P/\partial r$ in equation (5). For the most part, we confine our attention to the logotropic EOS (eq. [1]); but in Appendices A and B below, we also consider the more general family of negative-index polytropes.

We define a similarity variable

$$x = \frac{r}{a_t t} , \tag{8}$$

where a_t is a function of time with dimensions of velocity. Dimensionless density, velocity, and mass variables may then be set up as

$$\alpha(x) = 4\pi G t^2 \rho(r, t) , \quad v(x) = u(r, t)/a_t ,$$
$$m(x) = GM(r, t)/a_t^3 t . \tag{9}$$

Furthermore, because the square of the sound speed is $dP/d\rho = AP_c/\rho$ for this EOS, we are led to set

$$a_t = [AP_c(4\pi G t^2)]^{1/2} , \tag{10}$$

where $A \simeq 0.2$ for real interstellar clouds, and the constant P_c refers to the central pressure in the *initial*, precollapse ($t = -\infty$) cloud (as such, it reflects the constant pressure of the ambient medium and the total mass of the cloud; see, e.g., Table 1). Ultimately, the central core mass grows as $\dot{M}(0, t) \propto a_t^3 t \propto t^4$, and the accretion rate grows as $\dot{M}(0, t) \propto t^3$. This is in sharp contrast to an isothermal collapse, where the accretion rate is constant in time (see § 3 below for further discussion). In any case, straightforward manipulation of equations (5), (6), and (7) yields

$$\left[(2x - v)^2 - \frac{1}{\alpha}\right]\frac{d\ln\alpha}{dx} = \left[\frac{\alpha}{4} - \frac{2}{x}(2x - v)\right](2x - v) + [2(2x - v) + v] \tag{11}$$

$$\left[(2x - v)^2 - \frac{1}{\alpha}\right]\frac{dv}{dx} = \left[\frac{\alpha}{4}(2x - v) - \frac{2}{\alpha x}\right](2x - v) + \left[\frac{2}{\alpha} + v(2x - v)\right] \tag{12}$$

$$m = \frac{\alpha x^2}{4}(2x - v) . \tag{13}$$

These equations are written in a form similar to that of Shu (1977) for the isothermal sphere, which is included as a special case in the general development of Appendix A below.

There are two simple analytical solutions of equations (11), (12), and (13). The first has a uniform density,

$$\alpha = \frac{2}{3} , \quad v = \frac{2x}{3} , \quad m = \frac{2x^3}{9} , \tag{14}$$

and is equally valid for any polytropic EOS. Of more interest is the static (singular) solution,

$$\alpha = \frac{\sqrt{2}}{x} , \quad v \equiv 0 , \quad m = \frac{x^2}{\sqrt{2}} . \tag{15}$$

This corresponds to a time-independent density profile, $\rho(r) = (AP_c/2\pi G)^{1/2} r^{-1}$, which is just that found (eq. [4]) to satisfy the equation of hydrostatic equilibrium for a self-gravitating logotrope. As discussed in § 2.1, it also describes the large-radius structure of the bounded sphere—the type of cloud we expect to begin with at $t = -\infty$.

An entire class of singular solutions, valid at large radii or small (positive) times, can be found by taking α and $|v|$ to be much smaller than x in equations (11), (12), and (13). In this $x \to \infty$ limit, we have

$$\alpha \to \frac{C}{x} , \quad v \to -\frac{C}{2}\left(1 - \frac{2}{C^2}\right) , \quad m \to \frac{Cx^2}{2} . \tag{16}$$

For an inflow scenario ($v < 0$), the density normalization C must be greater than the hydrostatic equilibrium value $2^{1/2}$. Therefore, each $C > 2^{1/2}$ corresponds to the collapse of a logotrope that is initially just out of equilibrium, with densities (and pressures) everywhere enhanced by a factor $1 + \delta = C/2^{1/2}$. As in the equilibrium case, the cloud starts at $t = -\infty$ with a finite central density and ρ at large radii given by equation (16), and then contracts to follow that singular profile everywhere by $t = 0$. These solutions are the analogues of Shu's (1977) "minus solutions without critical points" for the singular isothermal sphere—although we show in § 2.3 that, in our case, some of the out-of-equilibrium flows *can* pass through critical points.

Although v is a finite constant at $t = 0$ here, the dimensional velocity $u \sim vt$ vanishes, and the cloud is essentially at rest at the time of core formation. This is consistent with a physical picture at $t < 0$ of quasistatic evolution toward the singular profile. As suggested above, such a slow contraction could be driven by ambipolar diffusion; therefore, we view the family of solutions (eq. [16]) as reasonable starting points for the post–core formation evolution of a collapsing logotrope. This is the same tack taken by Shu (1977) in his treatment of the isothermal sphere, but in one important way it is perhaps better justified for our EOS. If it happens that the mean magnetic field is initially weak and unable to significantly influence the evolution of a cloud, then the assumption of a gentle approach to the singular profile, as well as the validity of equation (16) in the $t = 0$ limit of the collapse, have to be questioned

The singular isothermal sphere is a poor description of the critical mass Bonnor-Ebert configuration, or of any less massive one (see Fig. 1). Thus, purely hydrodynamic collapse simulations of the latter clouds (e.g., Hunter 1977; Foster & Chevalier 1993) differ significantly from the results of Shu (1977). The approach to an r^{-2} profile at $t = 0$ is rather violent for them, and it involves appreciable fluid velocities that invalidate the main premise ($u = 0$ at $t = 0$) of the similarity solutions discussed here and by Shu. The subsequent $t > 0$ collapse then proceeds much more rapidly than for a singular sphere, with an accretion rate that decreases over time. In our case, the logotropic singular solution ($\rho \propto r^{-1}$: eq. [4] and Fig. 1) *does* describe the structure of bounded clouds of any interesting mass. The adjustment to a fully singular profile at $t = 0$ should then be a relatively easy one, and it is reasonable to expect that equation (16) adequately describes any collapsing logotrope at the point of core formation. This argument is consistent with numerical simulations (Foster & Chevalier 1993) for the collapse of a bounded isothermal sphere whose central concentration is ~ 70 times that of the Bonnor-Ebert value. Although such a cloud is highly unstable, it is well approximated at large radii by the singular isothermal sphere, and its accretion rate quickly approaches the constant value predicted by Shu (1977).

Turning now to the opposite limit of small radii, $x \to 0$, we find that $|v|$, $\alpha \to \infty$ for collapse, and therefore

$$\alpha \to 4\left(\frac{m_0}{2x^3}\right)^{1/2}, \quad v \to -\left(\frac{2m_0}{x}\right)^{1/2}, \quad m \to m_0, \qquad (17)$$

where the reduced mass m_0 of the collapsed core also serves to fix the accretion rate onto the core ($\dot{M}_0 \propto m_0 t^3$ by eq. [9]; see also § 3 below). The effects of shocks (e.g., Tsai & Hsu 1995) and radiation pressure (for massive stars; Jijina & Adams 1996) will invalidate this solution at very small x but should not affect our discussion of the area external to such disturbed regions, nor the value of m_0 itself.

The $x^{-3/2}$ and $x^{-1/2}$ scalings of α and v here are identical to the corresponding results for the isothermal sphere (Shu 1977), or any other polytrope with $0 < \gamma < 1$ (Appendix A). This reflects the fact that the ratio of gravitational and pressure forces,

$$\frac{GM/r^2}{\rho^{-1}dP/dr} = \frac{m\alpha}{x}\left(\frac{d\ln\alpha}{d\ln x}\right)^{-1} \to -\frac{4\sqrt{2}}{3}\frac{m_0^{3/2}}{x^{5/2}}, \qquad (18)$$

increases without limit as $x \to 0$, and the gas at very small radii approaches the core in free-fall. At any fixed time $t > 0$, the dimensional velocity field near the center therefore tends to $u = (2GM_0/r)^{1/2}$, and the density profile tends to

$$\rho(r) = \frac{\dot{M}}{4\pi r^2 u} = \frac{\dot{M}}{4\pi(2GM_0)^{1/2}} r^{-3/2}, \qquad (19)$$

which is equivalent to equation (17) for a spatially invariant accretion rate $\dot{M}$. When written this way, the effects of the gas EOS are completely contained in the values of $\dot{M}$ and M_0 at a given time; at least in the absence of rotation and magnetic fields, *observations of the shape of the density profiles or velocity fields in the central regions of a collapsing cloud are insufficient to constrain the underlying equation of state*. Any data that favor an $r^{-3/2}$ density profile in such objects (e.g., Butner et al. 1990, 1991) are qualitatively consistent with both the logotropic hypothesis and the isothermal one (quantitatively, however, the different accretion *histories* in the two models may well allow for an empirical discrimination between them; see § 4 below). By the same token, observations that suggest a different structure (e.g., André et al. 1993) are a challenge to both scenarios.

A full similarity solution for the collapse of overdense clouds, over all times $t \geq 0$ and all radii $r \geq 0$, begins at large x as in equation (16), and eventually tends to the form (eq. [17]) at small x. As such, there is a one-to-one relation between C and m_0. This is obtained by numerical integration of equations (11) and (12), and is laid out in Table 2. Evidently, the larger the overdensity $C/2^{1/2}$, the larger is the reduced core mass m_0, and the faster the accretion rate. The limit $C \to 2^{1/2}$ refers to the collapse of a logotrope that is initially arbitrarily close to hydrostatic equilibrium. In this

TABLE 2

CORE MASS VERSUS DENSITY NORMALIZATION

C	m_0
$\sqrt{2} + \epsilon$.....	0.000667
1.42.....	0.00173
1.4245	0.00248
1.43.....	0.00339
1.44.....	0.00507
1.46.....	0.00869
1.48.....	0.0127
1.50.....	0.0170
1.53.....	0.0243
1.56.....	0.0323
1.60.....	0.0444
1.70.....	0.0808
1.90.....	0.182
2.20.....	0.409
2.60.....	0.871

situation—which is the parallel of Shu's (1977) expansion-wave solution for the singular isothermal sphere—a collapse front propagates outward in a cloud at rest, with the material behind it falling away to the center.

2.3. *Critical Points and the Expansion Wave*

A look at equations (11) and (12) shows that when a collapse solution passes through a point $x_* \geq 0$ that has

$$2x_* - v_* - \alpha_*^{-1/2} = 0 , \tag{20}$$

the derivatives $d\alpha/dx$ and dv/dx will be undefined unless the quantities on the right-hand side of the fluid equations also vanish there. Any valid flow must therefore satisfy

$$\frac{\alpha_*^{1/2}}{4} + \frac{1}{x_*^{1/2}} - \frac{2}{x_*\alpha_*} + 2x_* = 0 \tag{21}$$

at such *critical points*. Mathematically, the $\alpha(x)$ and $v(x)$ that everywhere satisfy these two relations would present a third analytical similarity solution for our problem; but it is one that relies on a rather special interplay between the fluid variables, and one that we therefore neglect. Instead, physical flows must either avoid the line of critical points (or singular points, or sonic points) defined by equations (20) and (21), or else pass right through it.

Whitworth & Summers (1985) elaborate on the topology of critical points and the implications for a self-similar, isothermal collapse, and we refer the interested reader to that paper for an excellent discussion of such issues. Here we note that, for any gas EOS, a linearization of the fluid equations in the neighborhood of any critical point x_* leads to three pairs of eigenvalues for the slopes $d\alpha/dx$ and dv/dx there, and, therefore, to three eigensolutions for $\alpha(x)$ and $v(x)$. One of these is physically inadmissible but the other two, corresponding to the "minus" and "plus" solutions of Shu (1977), have the velocity either decreasing or increasing toward smaller x. They are described quantitatively, for the logotrope and for negative-index polytropes, in Appendix B.

It is the minus solutions, for which $v \to -\infty$ as $x \to 0$, that are of most interest in the collapse context. The velocity fields for some representative examples are shown as solid lines in Figure 2. Also shown there are the locus of critical points (*dash-dotted line*) defined above, as well as a few plus solutions (*dashed lines*). We will not discuss the plus solutions, other than to say that (1) their time-reversed counterparts could be of interest in a wind problem, and (2) in the limit $x \to \infty$, they have $\alpha \sim x^{-4}$, $v \sim x^2$, and $\alpha v^2 = \rho u^2/AP_c = 2$.

Our Figure 2 should be compared to that of Shu (1977). The heavy black line is the expansion-wave solution mentioned above. It passes through the critical point $x_* = 0.02439$, and it is the limit of two different sequences of minus solutions. Those that pass through critical points $x_* < 0.02439$, to the left of the expansion wave, go on to a stagnation point ($v = 0$) at some finite x, beyond which there is outflow. Therefore, these solutions are of no interest to us, although they might be useful in modeling the effects of accretion shocks (see Tsai & Hsu 1995). If they were to be simply truncated at the point where $v = 0$, they would have vanishingly small spatial extent at $t = 0$, which is unacceptable; and, as in the isothermal case, the static solution (eq. [15]) cannot be used to continue such flows to infinite x because there is a mismatch in the densities at the stagnation point. The densities and velocities still follow the power laws of equation (17) at small x, although with a core mass m_0 that is uniquely defined by the location of the critical point x_* and is always less than the expansion-wave value.

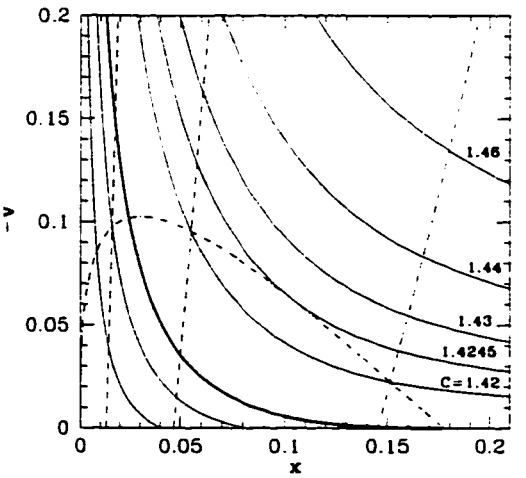

FIG. 2.—Velocity fields for various logotrope collapse solutions. Solid curves are minus solutions, and broken lines are plus solutions; the dash-dot line traces the locus of critical points. Heavy solid line represents the expansion wave, which continues to $x = \infty$ with $v = 0$ and densities given by the hydrostatic singular solution. Minus solutions to the left of the expansion wave reach $v = 0$ at some finite x, and therefore have vanishingly small spatial extent at $t = 0$. Minus solutions to the right of the expansion wave follow the collapse of spheres that are initially out of hydrostatic equilibrium. Expansion wave is the limit of both sequences.

Fundamentally, the expansion wave is identified as an extreme member of this family of solutions because its stagnation point is also a critical point, $x_* = x_{ew}$. In this case (see Appendix B),

$$x_{ew} = \frac{1}{4\sqrt{2}} \Rightarrow \alpha_{ew} = 8 , \quad v_{ew} = 0 ,$$

$$m_{ew} = \frac{1}{32\sqrt{2}} , \quad m_0 = 6.67 \times 10^{-4} . \tag{22}$$

These results agree with the static cloud profile (eq. [15]) at $x = x_{ew}$, and the core mass m_0 corresponds to that in the $C \to 2^{1/2}$ collapse (cf. Table 2 above), so an extension to arbitrarily large x is obtained by simply joining the two solutions in the obvious way. In fact, the logotropic expansion wave comes into x_{ew} from the left with velocity and density derivatives, $(dv/dx)_{x_{ew}} = 0$ and $(d\alpha/dx)_{x_{ew}} = -1/32(2)^{1/2}$, respectively, which also agree with those of the static profile—i.e., the flow is *continuous* at x_{ew}. This is the case for any polytropic EOS with $\gamma \leq \frac{3}{5}$, but when $\gamma > \frac{3}{5}$ (including the isothermal $\gamma = 1$) there is a discontinuity at the matching point (see Appendix B).

Physically, as discussed above and by Shu (1977), an expansion wave corresponds to the inside out collapse of a cloud that is in hydrostatic equilibrium at the moment ($t = 0$) of core formation. At any point in time (before the expansion wave reaches the initial cloud surface), a total reduced mass of m_{ew} is involved in the collapse, with a small fraction $m_0/m_{ew} \simeq 0.03$ of that having already fallen onto the central core. It may also be shown (for any gas EOS)

that, since the point x_{cw} is fixed in similarity space, the wave propagates into the cloud always at the *local* speed of sound, $(dP/d\rho)^{1/2}$.

However, the logotrope differs from the isothermal sphere, in that its expansion wave passes through two critical points: $x_* = 0.02439$ and $x_* = x_{cw}$. (For an isothermal EOS, the expansion-wave v is just tangent to the locus of critical points at x_{cw}, and it does not cross it anywhere.) It is the presence of these two distinct critical points—*both* with $v_* \leq 0$—that also marks the expansion-wave flow as the limit of a second sequence of minus solutions, namely, the out-of-equilibrium collapse profiles encountered in § 2.1 (eq. [16]). Several of these are drawn on Figure 2 to the right-hand side of the expansion wave, and labeled by their density normalizations C. Evidently, for C close enough to the hydrostatic-equilibrium value of $2^{1/2}$, such solutions—which have $v < 0$ everywhere—also pass through two critical points. This is again in contrast to the isothermal situation, in which all out-of-equilibrium collapses are free of critical points. On some level, however, this is just a mathematical issue; there is nothing intrinsically unphysical or artificial about flow through a critical point.[1]

3. ACCRETION TIMESCALES

Once numerical solutions to the self-similar fluid equations have been obtained and the reduced mass m_0 has been found for any minus solution, we have a description of the growth of the central core in a collapsing cloud. The formation times for stars of various masses can then be computed. Again, we focus on the results for logotropic expansion waves in this section. Generalizations to out-of-equilibrium collapses, as well as to more general polytropic equations of state, are fairly straightforward (cf. Appendix A).

From equation (13) for the dimensionless mass m and equation (17) for our similarity solutions at small radii, the central core mass is given by

$$M(0, t) \equiv M_0 = [AP_c(4\pi G)]^{3/2} \frac{m_0 t^4}{G} = A^{3/2}\left(\frac{3\pi^2}{8}\frac{\rho_c}{\rho_{ave}}\right)^{3/2} \frac{t^4}{\bar{t}_{ff}^3}\frac{m_0 \sigma_c^3}{G} . \quad (23)$$

Here ρ_c and ρ_{ave} are the central and mean densities of the initial ($t = -\infty$) cloud; $\bar{t}_{ff}$ is its mean free-fall time, $(3\pi/32G\rho_{ave})^{1/2}$; and it will be recalled that $A = 0.2$ in the logotropic EOS is most appropriate for real molecular clumps and GMCs. The ratio ρ_c/ρ_{ave} and the free-fall time are referred to their values in the nonsingular cloud because these are then related to the surface pressure, kinetic temperature, and total mass (by, e.g., Table 1 above), which fundamentally control the collapse. As also discussed in § 2.1, σ_c is just the thermal line width, $(kT/\mu m_H)^{1/2}$. The logotropic EOS already accounts for the presence of turbulence in the initial cloud, and σ_c is therefore *not* to be interpreted as the type of "effective" sound speed discussed by, e.g., Shu et al. (1987). The accretion rate is therefore

$$\dot{M}_0 = 4A^{3/2}\left(\frac{3\pi^2}{8}\frac{\rho_c}{\rho_{ave}}\right)^{3/2}\left(\frac{t}{\bar{t}_{ff}}\right)^3 \frac{m_0\sigma_c^3}{G} = 4\langle\dot{M}_0\rangle , \quad (24)$$

where $\langle\dot{M}_0\rangle$ is the mean rate M_0/t. As we discuss further in § 4, the time dependence of this quantity is the most important consequence of the move away from an isothermal EOS, which gives a constant $\dot{M}_0 = \langle\dot{M}_0\rangle = 0.975\sigma_c^3/G$ for the expansion wave (Shu 1977; also Appendix A below). $\langle\dot{M}_0\rangle$ increases with time in our case, and in any negative-index polytrope, because density profiles shallower than r^{-2} put more mass at larger radii in a cloud.

Now we consider a pressure-truncated logotrope that is in hydrostatic equilibrium and large enough that the singular r^{-1} density profile holds at the edge of the cloud. The analysis of MP96 gives the total mass and radius as

$$M_{tot} = \frac{(3A)^{3/2}}{\pi}\left(\frac{\rho_c}{\rho_{ave}}\right)^{3/2}\bar{t}_{ff}\frac{\sigma_c^3}{G} \quad (25)$$

and

$$R = \frac{2(3A)^{1/2}}{\pi}\left(\frac{\rho_c}{\rho_{ave}}\right)^{1/2}\bar{t}_{ff}\sigma_c . \quad (26)$$

Apart from corrections for the presence of mean magnetic fields (MP96), these expressions are valid for a cloud of any mass, as long as the r^{-1} profile is achieved inside it. In turn, as we have seen (cf. Fig. 1), this occurs for the full range of clump masses—from less than 1 to several hundred $M_\odot$—seen in GMCs. As the expansion wave moves outward in a logotrope, equations (23) and (25) give for the fractional core mass (independently of the EOS parameter A)

$$\frac{M_0}{M_{tot}} = \frac{\pi^4}{16\sqrt{2}}\left(\frac{t}{\bar{t}_{ff}}\right)^4 m_0 , \quad (27)$$

where, again, $m_0 = 6.67 \times 10^{-4}$. Also, the definition of a_t (eq. [10]) locates the boundary of the cloud in similarity space:

$$X \equiv \frac{R}{a_t t} = \frac{4\sqrt{2}}{\pi^2}\left(\frac{t}{\bar{t}_{ff}}\right)^{-2} . \quad (28)$$

Since the head of the expansion wave is at $x_{cw} = 1/[4(2)^{1/2}]$ for the logotrope, equation (28) shows that it reaches the surface of a collapsing cloud (of any mass) at

$$t_{cw} = \frac{4\sqrt{2}}{\pi}\bar{t}_{ff} , \quad (29)$$

i.e., after $\simeq 1.80$ initial free-fall times. At that point, equation (27) (or the ratio m_0/m_{cw} from eq. [22]) gives $M_0/M_{tot} \simeq 0.03$. If the similarity solution continues to hold after this time, then the entire cloud will be accreted onto the core (i.e., $M_0/M_{tot} = 1$ in eq. [27]) by

$$t_{end} = \frac{2}{\pi}\left(\frac{\sqrt{2}}{m_0}\right)^{1/4}\bar{t}_{ff} \simeq 4.32\bar{t}_{ff} . \quad (30)$$

The inside out collapse described by the expansion-wave solution is the gentlest possible, and, therefore, also the

[1] Figure 2 shows that the $C \simeq 1.4245$ collapse just brushes the locus of critical points at a single $x_* \simeq 0.1034$. Solutions for $C > 1.4245$ then bypass all critical points, while those with $2^{1/2} < C \leq 1.4245$ encounter two critical points (one less than 0.1034, and one greater). In the language of Whitworth & Summers (1985), the points with $x_* < 0.1034$ are *saddles*; those with $x_* > 0.1034$ are *nodes*; and $x_* = 0.1034$ itself is degenerate. (The direction of stable numerical integration is away from a saddle but toward a node, and only a pure plus or minus solution can pass through a saddle, while any function can cross a node.) The degeneracy moves toward larger x for increasing polytropic index γ, and occurs at $x_* = 1 = x_{cw}$ in the limit $\gamma = 1$. This is why the isothermal expansion wave is only ever tangent to the line of critical points, and why the overdense collapse solutions ($C > 2$ in that case) do not involve critical points at all.

slowest. Solutions of the type seen in equation (16), with $C > 2^{1/2}$ for a sphere that is initially denser than allowed for equilibrium, lead to faster accretion because of an increase in m_0 (Table 2) and M_{tot} (by a factor $(C/2^{1/2})^{3/2}$; see Appendix A).

Realistically, once the expansion wave reaches the boundary of a cloud that is under a constant surface pressure, it should be reflected and driven back into the cloud as a compression wave. Thus, our similarity solution cannot be exact beyond t_{ew}, and the resulting estimate of t_{end} might be something of an upper limit. However, it does seem likely that more than one additional free-fall time is required to complete the collapse after t_{ew}, because the accreting gas is in free-fall only deep inside the expansion wave (at $x < 0.1x_{ew}$; cf. eq. [18]). In the absence of detailed numerical simulations, then, the most secure conclusion is that the collapse of a (near-) equilibrium logotrope lasts for $t_{end} > t_{ew} + \bar{t}_{ff} \approx 3\bar{t}_{ff}$ after core formation. However, if the isothermal sphere is any guide, then the simulations of Boss & Black (1982) and Foster & Chevalier (1993) suggest that the correct time to $M_0 = M_{tot}$ for a logotrope may in fact be fairly close to our equation (30): the core in Boss & Black's numerical collapse of a nonrotating, equilibrium singular sphere grows at roughly the expansion-wave rate, even after t_{ew}; and the results of our Appendix A can be used to compute a t_{end} that is only ~20% longer than the total accretion time in Foster & Chevalier's "$\xi_{max} = 40$" run for a cloud that is overdense by 10% and has high but finite concentration at $t = -\infty$.

Figure 3 shows the density profile and velocity field, in similarity space, for a full expansion-wave solution. The thick black lines lie inside the head of the expansion wave,

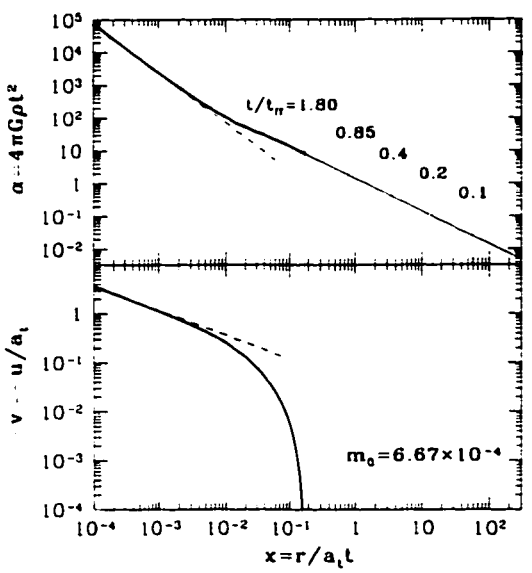

FIG. 3.—Density profile and velocity field, in similarity variables, of the expansion-wave solution for a collapsing logotrope. Heavy black lines trace out the region of dynamical collapse inside the expansion wave, like the same line type in Fig. 2, while the thin solid line in the top panel is the hydrostatic singular solution $\alpha = 2^{1/2}/x$. Dashed lines are the expected free-fall solutions $\alpha \sim x^{-3/2}$ and $v \sim x^{-1/2}$. Vertical (*dotted*) lines show the time-dependent location $X = R/a_t t$ of the cloud's outer radius.

which is at $x_{ew} \simeq 0.177$. At larger x, the density profile is given by the hydrostatic singular solution $\alpha = 2^{1/2}/x$. This is shown as the thin solid line in the top panel, where the *continuous* matching of densities across x_{ew} is evident. The velocity field also joins continuously to the static $v \equiv 0$ at x_{ew}. Table 3 lists α, v, and the mass m as functions of x inside the head of the expansion wave. The initial radius R of the cloud is fixed in real space (at least, until the expansion wave reaches it), and so over time it moves steadily inward in similarity space. The vertical lines in Figure 3 are placed at $X = R/a_t t$ (eq. [28]) for the times $t/\bar{t}_{ff}$ shown. As discussed above, $X = x_{ew}$ after 1.80 free-fall times. Finally, the dashed lines in both panels of the figure are just the free-fall profiles of equation (17). Clearly, they do not describe the flow until the gravitational attraction of the core exceeds the pressure-gradient force, at $x < 0.01$ or so.

A dimensional version of Figure 3 is given in § 4, but now we examine the dimensional core masses M_0 and accretion rates $\dot{M}_0 = 4\langle\dot{M}_0\rangle$ as functions of time in logotropes of various total masses. These are obtained from equation (27):

$$M_0 = 5.41 \times 10^{-6}\, M_\odot \left(\frac{M_{tot}}{M_\odot}\right)\left(\frac{\bar{t}_{ff}}{4.8 \times 10^5\ \mathrm{yr}}\right)^{-4}\left(\frac{t}{10^5\ \mathrm{yr}}\right)^4$$

$$\dot{M}_0 = 2.16 \times 10^{-10}\, M_\odot\ \mathrm{yr}^{-1}\left(\frac{M_{tot}}{M_\odot}\right) \times \left(\frac{\bar{t}_{ff}}{4.8 \times 10^5\ \mathrm{yr}}\right)^{-4}\left(\frac{t}{10^5\ \mathrm{yr}}\right)^3 . \quad (31)$$

It will be recalled (from Table 1 above) that $\bar{t}_{ff} = 4.8 \times 10^5$ yr is appropriate for a solar-mass, $A = 0.2$ logotrope with temperature $T = 10$ K and surface pressure $P_s = 1.3 \times 10^5 k$ cm^{-3} K. The free-fall time of a logotrope with any other M_{tot}, P_s, or T can be computed (as discussed in § 2.1) in such a way that equation (31) is quite generally applicable. The first of these relations is plotted in Figure 4 for a number of different initial cloud masses. In a $C > 2^{1/2}$ collapse, our M_0 and $\dot{M}_0$ should each be multiplied by $(C/2^{1/2})^{3/2}[m_0/(6.67 \times 10^{-4})]$, with m_0 taken, for example, from Table 2. What was already apparent from equation (27) is made more explicit here: a protostar in a collapsing logotrope gathers fully one-half of its mass M_0 over the last $1-(0.5)^{1/4} \simeq 16\%$ of its accretion phase. By far, the majority of a star's total formation time is spent waiting out a period of very slow and relatively unproductive infall in its parent cloud.

Also shown in Figure 4 is the line $M_0 = 0.155\, M_\odot (t/10^5\ \mathrm{yr})(T/10\ \mathrm{K})^{3/2}$ for a singular isothermal sphere of *any* total mass. There are at least three points of interest in a comparison between this and the logotropic curves:

1. Any isothermal sphere has the *same* time-invariant accretion rate, while more massive logotropes eventually accrete much more rapidly than clouds of lower M_{tot}. This is because a softer-than-isothermal EOS generally gives rise to larger nonthermal motions on larger scales, i.e., to higher σ_{ave} in higher-mass clouds (cf. § 2.1). Since $\dot{M} \sim \sigma^3/G$, the mass originating from larger radii in bigger clouds will therefore fall faster onto the core.

2. Generally speaking, low-mass stars take longer to accrete in a logotrope than in an isothermal sphere, while high-mass stars form on relatively shorter timescales. The extent of the discrepancy between the two models depends

TABLE 3

LOGOTROPE EXPANSION WAVE

x	α	$-v$	m
0	∞	∞	0.000667
0.001	2395	1.115	0.000668
0.002	879	0.760	0.000671
0.003	497	0.599	0.000675
0.004	335	0.500	0.000680
0.005	249	0.431	0.000686
0.010	106	0.254	0.000728
0.015	68.9	0.175	0.000793
0.020	52.4	0.129	0.000884
0.025	43.2	0.0988	0.00100
0.030	37.2	0.0781	0.00115
0.035	32.9	0.0630	0.00134
0.040	29.6	0.0515	0.00156
0.045	27.0	0.0425	0.00181
0.050	24.9	0.0354	0.00211
0.055	23.1	0.0296	0.00244
0.060	21.5	0.0248	0.00280
0.065	20.2	0.0208	0.00321
0.070	18.9	0.0175	0.00366
0.075	17.9	0.0146	0.00414
0.080	16.9	0.0122	0.00466
0.085	16.0	0.0102	0.00522
0.090	15.2	0.00846	0.00582
0.095	14.5	0.00697	0.00646
0.100	13.9	0.00570	0.00713
0.105	13.3	0.00463	0.00784
0.110	12.7	0.00371	0.00859
0.115	12.2	0.00294	0.00938
0.120	11.7	0.00230	0.0102
0.125	11.2	0.00176	0.0111
0.130	10.8	0.00132	0.0120
0.135	10.4	0.000965	0.0129
0.140	10.1	0.000680	0.0139
0.145	9.74	0.000457	0.0149
0.150	9.42	0.000289	0.0159
0.155	9.12	0.000168	0.0170
0.160	8.84	8.50×10^{-5}	0.0181
0.165	8.57	3.41×10^{-5}	0.0193
0.170	8.32	8.35×10^{-6}	0.0204
0.175	8.08	2.86×10^{-7}	0.0217
$1/4\sqrt{2}$	8	0	$1/32\sqrt{2}$

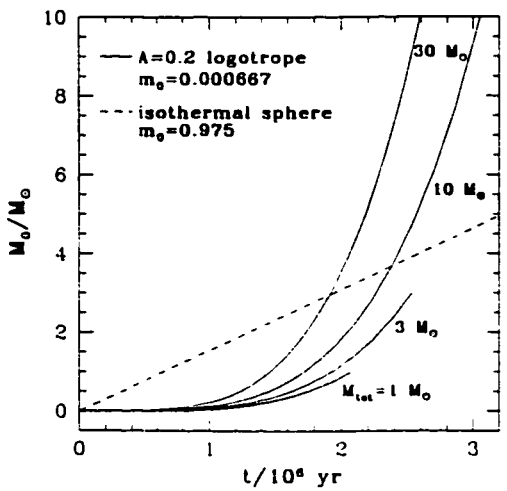

FIG. 4.—Expansion-wave accretion timescales for stars in an $A = 0.2$ logotrope and a singular, $T = 10$ K isothermal sphere. Low-mass stars take longer to form in the logotrope, while more massive ones accrete more rapidly.

on the initial mass of the logotrope. Indeed, because of the effect noted in point (1), even the stellar mass for which the total accretion times coincide depends on M_{tot}.

3. This being so, there is a much smaller spread in star-formation times in logotropes than in isothermal spheres. This is because of the weak mass dependence in the free-fall time of a logotrope (Table 1), and because $M_0 \propto (t/t_{ff})^4$. Specifically, stars of mass $0.3\ M_\odot \lesssim M_0 \lesssim 30\ M_\odot$ all tend to form within $1\text{–}3 \times 10^6$ yr, in logotropes of essentially any M_{tot}. In an isothermal collapse, where $M_0 \propto t$, the accretion times would differ by a factor of 100.

It has to be recalled that these results are based on the assumption that the self-similar collapse solution continues to hold even after the expansion wave has been reflected from the boundary of a cloud. As discussed above, Figure 4 may then represent upper limits to the true star formation times in logotropes. On the other hand, this effect may not be very large; in any case, it will be offset to some extent by the (outward) radiation pressure from stars larger than a few solar masses (Jijina & Adams 1996). Our analysis should then be a reasonably accurate first-order approximation to a rather complicated situation.

These points could have some bearing on the formation of bound clusters, which requires that a large fraction ($\gtrsim$30%: Hills 1980; Lada, Margulis, & Dearborn 1984; Elmegreen & Clemens 1985) of the protocluster gas be converted to stars before the remainder is dispersed by supernovae or H II regions. In light of Figure 4 and the short accretion times of high-mass stars, this would seem to demand that high-mass stars *start* collapsing *after* the low-mass stars do—a conclusion that also has ramifications for the form and origin of the stellar IMF.

Myers & Fuller (1992; also Myers & Fuller 1993; Caselli & Myers 1995) have introduced a thermal plus nonthermal (TNT) model of molecular clumps, which has an EOS that is explicitly isothermal at small radii but becomes essentially polytropic (with $\gamma < 1$) at large r. They use this model to estimate approximate accretion times for stars of various masses. Although our logotropic model is preferable to the TNT construction (because the latter has density singularities at the centers of even precollapse, $t = -\infty$, clouds), the M_0 versus t relation of equation (31) and Figure 4 may profitably be compared with that of Myers & Fuller. In particular, although our t_{esd} for clouds of various masses tend to be somewhat longer than the TNT estimates—which bypass an exact treatment of the expansion wave, and which are almost isothermal for low-mass clumps anyway—they have roughly the same order of magnitude. More importantly, the rather narrow range in accretion times and the fairly rapid formation of high-mass stars are common to both sets of results; indeed, these are generic features of any softer-than-isothermal EOS.

4. IMPLICATIONS FOR LOW-MASS STAR FORMATION

Our analysis has concentrated on spherical infall in a logotrope, and ignored the effects of *mean* magnetic fields (to whatever extent disordered fields contribute to the turbulence in interstellar clouds, they are already accounted for by the EOS), rotation and circumstellar disks, and radiation pressure from the forming star. All of these have been studied analytically or numerically for accretion in isothermal clouds (e.g., Galli & Shu 1993a, 1993b; Tereby et al. 1984; Boss & Black 1982; Jijina & Adams 1996, and refer-

ences therein). In addition, some connection has to be made with the issues of fragmentation and binary formation (see, e.g., Myhill & Kaula 1992). Clearly, the present study can only be viewed as one step toward a full theory of nonisothermal collapse.

Nevertheless, some fairly robust conclusions can be drawn. In particular, although others have considered the effects of softer-than-isothermal, and even logotropic, equations of state on massive star formation (e.g., Myers & Fuller 1992; Jijina & Adams 1996), the most important new point to be made here is that even low-mass ($\sim 1\ M_\odot$) molecular clumps can be described by a logotropic EOS. Their collapse is therefore rather gentler than in the isothermal case, and their accretion rates must be much smaller at early times.

Figure 5 shows the time evolution, from $t = 5 \times 10^4$ to $t = 8.6 \times 10^5$ yr, of the density profile and velocity field in an expansion wave moving through an initially hydrostatic $A = 0.2$ logotrope with a total mass of 1 $M_\odot$, a kinetic temperature $T = 10$ K (hence, $\sigma_c = 1.88 \times 10^4$ cm s^{-1}), and a constant surface pressure $P_s = 1.3 \times 10^5 k$ cm^{-3} K. The velocity scale a_τ (eq. [10]) can be evaluated at any time, given the surface pressure and the fact (cf. Table 1) that $P_c/P_s = 1.58$ in the nonsingular cloud at $t = -\infty$; the dimensional r, ρ, and u of Figure 5 then follow immediately from the x, α, and v of Figure 3. At the point $t = 0$ of core formation, the cloud is everywhere at rest and follows the singular density profile $\rho(r) = 1.3 \times 10^{-20}$ g cm^{-3} $(r/R)^{-1}$. At later times, this profile still holds outside of the expansion wave; it is sketched as the broken line in the top panel of Figure 5. For reference, we also have that the initial free-fall time of this cloud is $\bar{t}_{ff} = 4.8 \times 10^5$ yr (Table 1), the initial ratio of central and mean densities is $\rho_c/\rho_{ave} = 4.20$, and the initial radius is $R = 2.9 \times 10^{17}$ cm (eq. [26]; this is within a factor 2 of the radius of a solar-mass isothermal sphere under the same surface pressure). We have only plotted the densities and velocities for $t \leq 8.6 \times 10^5$ yr $= 1.80\bar{t}_{ff}$, i.e., prior to the time t_{ew} when the head of the expansion wave meets the initial boundary of the cloud.

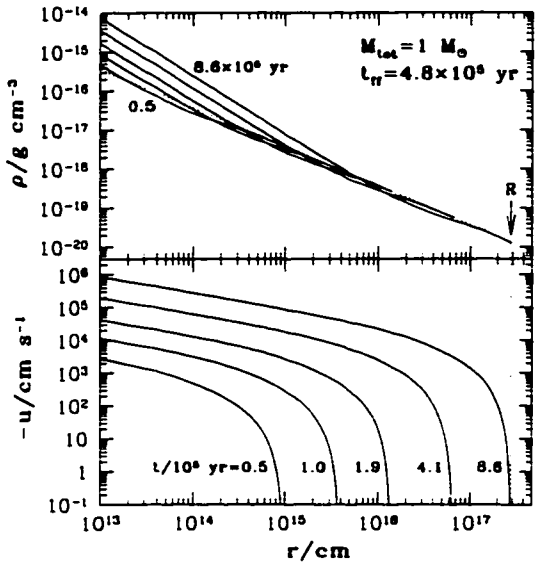

FIG. 5.—Time evolution (from left to right), in dimensional variables, of the density profile and velocity field for a collapsing logotrope of 1 $M_\odot$, with a kinetic temperature $T = 10$ K, and under a surface pressure $P_s = 1.3 \times 10^5 k$ cm^{-3} K. Solid curves lie in the interior of the expansion wave (and therefore correspond to the heavy black lines in Figs. 2 and 3), and the broken line in the top panel traces the hydrostatic r^{-1} density profile out to the boundary R of the initial cloud. Times shown are roughly the same $t/\bar{t}_{ff}$ used to locate X in Fig. 3.

A cloud that is initially rotating at a constant rate Ω will depart from the spherical expansion-wave solution at small $r \lesssim R_C$, where R_C is the *centrifugal radius* at which the circular speed $(GM_0/r)^{1/2}$ just equals the infall velocity $-u$. For an $M_{tot} = 1\ M_\odot$ logotrope with the surface pressure and temperature we have assigned here, it is given by

$$R_C = \frac{\Omega^2 M_0}{2\pi A P_c} = 3.0 \times 10^{10}\ \text{cm} \left(\frac{\Omega}{10^{-14}\ \text{s}^{-1}}\right)^2 \left(\frac{t}{10^5\ \text{yr}}\right)^4 . \tag{32}$$

The first of these equalities comes from Jijina & Adams (1996; note the slightly different notation); the second equality comes from our equation (31), along with $A = 0.2$ and the fact that $P_c = 1.58 P_s$ for this specific example. Thus, a disk of 100 AU in extent will be built up within $\sim 1.5 \times 10^6$ yr in our model, as compared to $\simeq 7.5 \times 10^5$ yr for a singular isothermal sphere at $T = 10$ K. Scaling of this result for clouds with different total masses, surface pressures, and temperatures involves a change in the coefficient of M_0, as described after equation (31), and a change in P_c/P_s (see Table 1). In any case, the magnitude of R_C at a specified age t gives some indication of the radial range in which the results of Figure 5 are valid in an initially rotating cloud. Calculation of the analogous length scale for a magnetized sphere—the so-called magnetic radius of Galli & Shu (1993a, 1993b)—will also be important, but it is beyond the scope of this paper.

There are two main points to Figure 5. The first is that the densities far behind the head of the expansion wave are well in excess of the initial hydrostatic values (see also Fig. 3 above), and are *increasing* with time. This is in stark contrast to an isothermal collapse, where $\rho(r)$ falls below its equilibrium value and decreases with time at small radii (cf. Fig. 3 of Shu 1977). The difference stems in part from the increasing M_0 in our case, but more fundamentally from the fact that the initial r^{-1} density profile of the logotrope is shallower than the final $r^{-3/2}$ that must obtain near the central core; there is relatively more mass in the outer regions of the static cloud than in the collapsing one, so a backlog of sorts develops at small radii. The opposite is true of a singular isothermal sphere, which begins with a static r^{-2} density profile. More quantitatively, the scaling $\alpha \propto x^{-3/2}$ implies $\rho(r, t) \propto r^{-3/2} t$ for the logotrope, but $\rho(r, t) \propto r^{-3/2} t^{-1/2}$ for an isothermal EOS.

This situation calls to mind observations of the far-infrared emission of the NGC 2071 region in Orion B (Butner et al. 1990). Radiative-transport models are consistent with a central star of around 5 $M_\odot$ there and a $\rho \propto r^{-3/2}$ density profile at radii $r \geq 2000$ AU. However, the value of the density at 2000 AU given by Butner et al.'s radiative-transport analysis (and also suggested by independent molecular data) is at least one full order of magnitude *larger* than that expected for an isothermal expansion-wave collapse. One explanation for this is that 2000 AU is deep inside the expansion wave for an isothermal collapse age of

$\simeq 5 \times 10^5$ yr (which follows from an assumed $T = 35$ K and $M_0 = 5\ M_\odot$), such that significant depletion would have occurred there. There is no such depletion, but rather an enhancement in our logotropic model, and these data could therefore provide an important test of it. However, a proper analysis of NGC 2071 would require a self-consistent treatment of radiation pressure and rotation, as well as a reliable feel for the initial total mass involved; it is too detailed to be undertaken here.

The second point of Figure 5 is that, naturally, the infall velocity at any given radius also grows over time, *but* it does so at a rate that is quite different from that in an isothermal sphere. In particular, since $u \propto (M_0/r)^{1/2}$ at small radii, we have that $u \propto r^{-1/2}t^2$ in a logotrope, while $u \propto r^{-1/2}t^{1/2}$ in the isothermal case. At any fixed r, the velocities in the two models will agree at some t; the logotropic u must then be smaller than the isothermal one at earlier times and larger later on. With $M_{\rm tot} = 1\ M_\odot$, specifically, a comparison of Figure 5 and Shu's (1977) Figure 3 shows that we are firmly in the former, lower velocity regime at all radii and throughout the entire duration $t \leq t_{\rm ew}$.

For example, let us focus on the scale $r = 10^{16}$ cm $\simeq 0.003$ pc. Our model gives infall velocities there (and at larger radii) that are *less than the thermal line width*, $\sigma_c \simeq 0.2$ km s^{-1}, for all $t \leq 8.6 \times 10^5$ yr. By contrast, a solar-mass, singular isothermal sphere attains $-u \simeq \sigma_c$ at the same radius by $t = 6 \times 10^4$ yr. This is one example of how the systematic velocity field at observable radii in a logotrope of *any* mass will be effectively swamped by random velocities for a significant fraction of the duration of its collapse; even a molecular clump that is well into the accretion phase can appear to be in virial equilibrium. Because the accretion rate increases with time, at any instant the majority of clumps will be in a fairly inconspicuous evolutionary state. This could explain the apparent paucity of obviously collapsing regions of the ISM. Similarly, for those clouds that do show observable signatures of collapse, the adoption of a logotropic EOS leads to larger inferred dynamical ages than an isothermal model would suggest.

Currently, the best direct, kinematic evidence for collapse is in the isolated Bok globule B335, where molecular line profiles appear consistent with infall velocities $-u \sim 1.2$ km s^{-1} at radii $r \sim 5 \times 10^{15}$ cm (Zhou et al. 1993). Given that $-u = (2GM_0/r)^{1/2}$ deep inside any expansion wave (the radial scaling of which is also consistent with the B335 data), this implies the existence of a central protostar (or star plus disk) with mass $M_0 \simeq 0.25\ M_\odot$. Also, 1.3-mm continuum measurements of dust emission indicate a circumstellar envelope of about 0.8 $M_\odot$ (Bontemps et al. 1996). The physical parameters that we have specified in deriving Figure 5 therefore seem particularly suited to a discussion of B335.[2] In particular, *model-independent* considerations suggest that $M_0/M_{\rm tot} \sim 0.25$ in this object. If it is undergoing a logotropic collapse, then it must be older than $t_{\rm ew} = 8.6 \times 10^5$ yr, because our similarity solution gives a much smaller $M_0/M_{\rm tot} = 0.03$ at that time. (In addition, Fig. 5 shows that $-u$ is rather less than the observed value at $r = 5 \times 10^{15}$ cm for all $t \leq t_{\rm ew}$.) That is to say, *the expansion wave should already have been reflected from the boundary of B335*.

If B335 is much older than $t_{\rm ew}$, then it will no longer follow its original r^{-1} density profile: the entire cloud should be taken up in the collapse and the free-fall $\rho \propto r^{-3/2}$ should hold essentially throughout. In fact, this is consistent with the study of Zhou et al. (1990), who conclude that the densities in the inner regions of the globule are best described by an $r^{-1.5}$ power law. (As a test of the isothermal collapse theory specifically, they go on to argue that at large radii the densities are consistent with $\rho \propto r^{-2}$. However, there is no *direct* evidence for this, or for any other power law but -1.5; the data are "insufficient to determine independently the parameters of a density distribution with two power-law regimes;" Zhou et al. 1990.)

Just how old is B335? Equation (31), given $M_0 = 0.25\ M_\odot$, predicts a collapse age of $t = 1.5 \times 10^6$ yr (if our fiducial surface pressure is correct here), and, therefore, a time-averaged accretion rate of $\langle \dot{M}_0 \rangle = M_0/t = 1.7 \times 10^{-7}\ M_\odot$ yr^{-1}. These numbers are, moreover, quite robust against any uncertainties in the initial total mass: even if $M_{\rm tot} = 10\ M_\odot$ (in which case $M_0/M_{\rm tot} \sim 0.03$ and the expansion wave would have just reached the edge of the cloud), we find $t \simeq 1.2 \times 10^6$ yr. By contrast, Zhou et al. (1993) discuss their data in terms of the isothermal expansion-wave model and estimate $t = 1.5 \times 10^5$ yr, $\dot{M}_0 = 2.8 \times 10^{-6}\ M_\odot$ yr^{-1}, and $M_0 = 0.4\ M_\odot$. It seems inevitable that our model requires an age for B335 that is nearly an order of magnitude older, with a time-averaged accretion rate much smaller than previously thought.

B335 is an example of the low-mass Class 0 sources recently identified by André et al. (1993) and André & Montmerle (1994). These typically have (cold) single blackbody spectral energy distributions but are invisible at short wavelengths $\lambda \lesssim 10\ \mu$m. This is attributed to veiling by a circumstellar envelope the mass of which exceeds that of the central protostar—a conclusion that is supported by direct, millimeter-continuum measurements of the envelope masses—and, therefore, implies that these objects are in the earliest stages of collapse yet to be observed. Indeed, the theory of isothermal accretion applied to the Class 0 sources generally implies ages of a few 10^4 yr (e.g., Barsony 1994; Pudritz et al. 1996). Although B335 might then be somewhat older than average, even in the context of isothermal models, it seems likely that the relative age increase we deduce for it should also be applied to other Class 0 sources. Note, however, that most of this age increase is required to accommodate an early period of very gentle infall, with small central source masses and low accretion luminosities. *Most* of a 1 $M_\odot$ star is accreted over a period of only ~ 2–3×10^5 yr in a logotrope. This is much smaller than the total collapse time (cf. Fig. 4) and is still consistent, for example, with empirical estimates of the formation time of visible T Tauri stars in the Taurus-Auriga complex (Myers & Benson 1983; Myers et al. 1987).

Finally, if our low mean accretion rate in B335 is typical, then it should have some bearing on the "luminosity problem" of young stellar objects in Taurus-Auriga. Very briefly, the bolometric luminosities of Class I sources there (which are embedded in less massive circumstellar envelopes than Class 0's, and, therefore, appear to be in later stages of collapse; André & Montmerle 1994) are gen-

[2] In fact, Zhou et al. (1990) favor a kinetic temperature of 13 K for B335. A $T = 13$ K logotrope with no mean magnetic field has a critical mass of 155 $M_\odot$ and a free-fall time of 6.6×10^5 yr, by equations (2) and (3). Thus, B335 has $M_{\rm tot}/M_{\rm crit} \simeq 0.0064$ and therefore a truncation radius $R/r_0 \simeq 1$ from Table 1. This in turn implies $t_{\rm ff}/t_{\rm ff,\,crit} \simeq 0.74$, or $t_{\rm ff} = 4.9 \times 10^5$ yr. Our timescale estimates, which apply strictly to a $T = 10$ K solar-mass logotrope with $t_{\rm ff} = 4.8 \times 10^5$ yr, are then relevant to B335 as well.

erally about an order of magnitude smaller than expected from number-count arguments (Kenyon et al. 1990; Kenyon et al. 1994) and fits to individual spectral energy distributions (Kenyon, Calvet, & Hartmann 1993; see also Adams, Lada, & Shu 1987). A similarly low luminosity has also been noted for the prototypical Class 0 source VLA 1623 (Pudritz et al. 1996). The problem results, in large part, from the isothermal assumption of a time-independent accretion rate $\dot{M}_0$, and Kenyon et al. note that it could be alleviated if stars accumulate most of their mass on timescales that are short compared to the total duration of their embedded phase. We have seen that such a situation arises naturally in the collapse of a logotrope. A revision of the assumed EOS in molecular clouds may therefore play an important part in the eventual resolution of this issue.

5. SUMMARY

McLaughlin & Pudritz (1996) have shown that a logotropic equation of state, $P/P_c = 1 + A \ln(\rho/\rho_c)$ and $A = 0.2$, provides the most self-consistent description of the internal, equilibrium structure of both low- and high-mass dense clumps within GMCs, as well as of the global properties (Larson's laws) of the giant cloud complexes themselves. We have now used this model to investigate the collapse of interstellar clouds. There are a number of consequences for issues of not only high-mass, but also low-mass star formation.

We have derived similarity solutions for the collapse of a gaseous logotrope. These solutions are analogous to those of Shu (1977) for the collapse of singular isothermal spheres; in particular, an expansion-wave solution—the inside out collapse of a cloud that is initially in virial equilibrium—is identified as the one of most physical interest. The predicted density profile is $\rho \propto r^{-1}$ for gas that has not yet been reached by the expansion wave, and $\rho \propto r^{-3/2}$ far behind the collapse front, where infall velocities approach their free-fall values $-u = (2GM_0/r)^{1/2}$. These latter scalings are model independent, as they follow directly from the presence of a central point mass (protostar) M_0. However, the core accretion rate in a logotrope increases with time (as $\dot{M}_0 \propto t^3$, so that $M_0 \propto t^4$), while it is constant for an isothermal sphere.

This implies that $\dot{M}_0$ in a logotrope will be smaller than the isothermal value at early times and larger at late times. Low-mass stars therefore take longer to form, while high-mass stars are built up much more rapidly. With t_{ff} the mean free-fall time of a logotrope (typically of order 5×10^5 yr), our similarity solutions are strictly valid for $t < 1.8t_{ff}$. At that point, the expansion wave reaches the edge of a cloud—with only 3% of the total initial mass having been accreted onto the core—and hydrodynamical simulations will likely be required to exactly describe the later stages of evolution in which most of the final mass of a star is accreted. Nevertheless, a simple extrapolation of our present results suggests that if a cloud of any mass were to completely collapse to a single star, it would do so by $t = 4.3t_{ff}$. A weak dependence of t_{ff} on mass in logotropes, together with the result $M_0 \propto t^4$, guarantees that the accretion times of stars of widely disparate masses differ only slightly: stars of anywhere from 0.3 to 30 $M_\odot$ are all expected to form within ~ 1–3×10^6 yr. This conclusion, which is similar to that reached in other studies of nonisothermal collapse, has important implications for cluster formation and the stellar IMF.

Another clear difference between the logotropic and isothermal models lies in the evolution of the density at small radii in a cloud: ρ ultimately increases with time at any given radius in our model, but it would decrease in a singular isothermal sphere. Infall velocities u, on the other hand, grow with time in any collapse model, but the *rates* at which they do so are quite dependent on the assumed equation of state. Early on in its collapse, the logotrope can have much smaller u than an isothermal sphere. Therefore, it takes longer for observable systematic velocities to develop at observable radii within a cloud, and collapse will initially be harder to detect directly. This implies that (1) early on in its accretion phase, a logotrope will effectively appear to still be in virial equilibrium, such that the number of molecular clumps that are in fact undergoing collapse could be much larger than previously suspected; and (2) current estimates for the ages of (low-mass) young stellar objects, which are based on isothermal collapse models, should be subject to a significant upward revision. In the Bok globule B335 specifically, we find an age that is certainly greater than 8.6×10^5 yr—probably $\sim 1.5 \times 10^6$ yr—older by perhaps an order of magnitude than suggested by the isothermal expansion-wave theory. This result could have wider implications for the ages of Class 0 protostars (of which B335 is one) in general.

This work was supported in part by the Natural Sciences and Engineering Research Council of Canada.

APPENDIX A

COLLAPSING POLYTROPES

A1. SIMILARITY SOLUTIONS

In many ways, the isothermal sphere and the logotrope are profitably viewed as opposite extremes of the family of *negative-index polytropes*, which have $P \propto \rho^\gamma$ with $0 < \gamma \leq 1$. Although incomplete as models of real interstellar clouds, these have been considered, for example, by Maloney (1988), McKee & Zweibel (1995), and MP96. The case $\gamma = 1$ gives an isothermal equation of state, while most features of the logotrope are recovered by formally setting $\gamma = 0$ in what follows. The "negative-index" label refers to standard polytropic notation, which has $\gamma = 1 + 1/N$. An isothermal EOS then corresponds to $N \to -\infty$, and the logotrope corresponds to $N \to -1$.

To derive similarity solutions for collapsing polytropes, we write the EOS as

$$P = K\rho^\gamma . \tag{A1}$$

The similarity variable x, the dimensionless density α, the velocity v, and the mass m are all defined as in equations (8) and (9);

since $dP/d\rho = K\gamma\rho^{\gamma-1}$, the appropriate velocity scale is just

$$a_t = [K\gamma(4\pi G t^2)^{1-\gamma}]^{1/2} . \tag{A2}$$

As discussed in § 2.1, we are concerned with the evolution of a cloud only *after* the time ($t = 0$) when a core has formed at its center. The density structure is then singular throughout, and K is a constant in space and time, with the value $\sigma_c^2\rho_c^{\gamma-1}$ it had in the initial ($t = -\infty$) cloud.

If we write

$$\beta \equiv (2-\gamma)x - v , \tag{A3}$$

then equations (5), (6), and (7) give the following:

$$[\beta^2 - \alpha^{\gamma-1}]\frac{d\ln\alpha}{dx} = \left[\frac{\alpha}{4-3\gamma} - \frac{2}{x}\beta\right]\beta + (1-\gamma)[2\beta + v] \tag{A4}$$

$$[\beta^2 - \alpha^{\gamma-1}]\frac{dv}{dx} = \left[\frac{\alpha}{4-3\gamma}\beta - \frac{2\alpha^{\gamma-1}}{x}\right]\beta + (1-\gamma)[2\alpha^{\gamma-1} + v\beta] \tag{A5}$$

$$m = \frac{\alpha x^2}{4-3\gamma}\beta . \tag{A6}$$

Setting $\gamma = 1$ in equation (A2) onward recovers the results of Shu (1977) for the isothermal sphere; if, instead, $\gamma = 0$ (but $K\gamma$ is replaced by AP_c), then the equations in § 2.2 are obtained. No constraint has yet been imposed on the value of γ, and, in particular, it could well be greater than 1 at this point. In this regime, treatment of the case $\gamma = 4/3$ evidently requires some care. We do not discuss this point further, but we note that it relates to the instability of positive-index polytropes with $1 < \gamma < 4/3$ (e.g., Chandrasekhar 1967). Goldreich & Weber (1980) have studied the *homologous* collapse of a $\gamma = 4/3$ polytrope, in connection with the evolution of degenerate iron cores in supernovae. More generally, Suto & Silk (1988) solve equations for the self-similar collapse of polytropes with arbitrary indices γ. The physical requirement K = constant identifies our equations (A4) and (A5) with equation (15) of Suto & Silk, in their "$n = 2 - \gamma$" case.

Still without restricting the value of γ, equations (A4), (A5), and (A6) admit two analytic solutions. One of these is the same uniform-density case given by equation (14); the other is the static solution,

$$\alpha = C_{\rm HSE}\, x^{-2/(2-\gamma)} \qquad v \equiv 0 \qquad m = \frac{2-\gamma}{4-3\gamma}\, C_{\rm HSE}\, x^{(4-3\gamma)/(2-\gamma)} , \tag{A7}$$

where the density normalization is

$$C_{\rm HSE} = \left[\frac{2(4-3\gamma)}{(2-\gamma)^2}\right]^{1/(2-\gamma)} . \tag{A8}$$

The singular density profile obtained is an exact solution of the equation of hydrostatic equilibrium for a self-gravitating polytrope of any (negative) index (cf. MP96). Again, if $\gamma = 0$ here, the logotropic result (eq. [15]) obtains; while if $\gamma = 1$, we have $\alpha = 2/x^2$ and $m = 2x$, in agreement with Shu (1977) for the singular isothermal sphere.

In the context of interstellar clouds, we are interested only in the range $0 < \gamma \leq 1$—and, in particular, the $\gamma = 0$ limit of the logotrope—since the velocity dispersion P/ρ then increases with radius. For such a γ, equations (A4), (A5), and (A6) in the limit $x \to 0$ (late times or small radii) and $|v| \gg x$ give

$$\alpha \to (4-3\gamma)\left(\frac{m_0}{2x^3}\right)^{1/2} , \qquad v \to -\left(\frac{2m_0}{x}\right)^{1/2} , \qquad m \to m_0 , \tag{A9}$$

which are minus solutions. In the opposite limit $x \to \infty$ (early times or large radii) and $|v| \ll x$, instead we have

$$\alpha \to Cx^{-2/(2-\gamma)} , \qquad v \to -\frac{2-\gamma}{4-3\gamma}C\left[1 - \left(\frac{C_{\rm HSE}}{C}\right)^{2-\gamma}\right]x^{-\gamma/(2-\gamma)} , \qquad m \to \frac{2-\gamma}{4-3\gamma}\, Cx^{(4-3\gamma)/(2-\gamma)} . \tag{A10}$$

The density normalization C is essentially a free parameter, but it must exceed the hydrostatic equilibrium value $C_{\rm HSE}$ (eq. [A8]) for inflow ($v < 0$). As usual, therefore, this family of solutions represents the collapse of nonequilibrium spheres that are everywhere denser (by a factor $C/C_{\rm HSE}$) than a virialized one with the same volume. There is also a one-to-one relationship between C and m_0 for a complete solution that extends from $x = \infty$ (the moment of core formation) to $x = 0$ (the end of accretion), and the limit $C \to C_{\rm HSE}^{+}$ corresponds to the expansion-wave solution. (Note that these asymptotic solutions differ from those cited by Larson 1969, which hold for plus solutions where $|v|$ increases at large x but is still $\ll x$. A sufficient, though not necessary, condition for the existence of such solutions is $\gamma > 1/3$.)

A2. ACCRETION RATES

The reduced core mass m_0 translates, by equations (A2) and (9), to a dimensional

$$M_0 = \gamma^{3/2}\left(\frac{3\pi^2}{8}\frac{\rho_c}{\rho_{\rm ave}}\right)^{3(1-\gamma)/2}\frac{t^{4-3\gamma}}{t_{\rm ff}^{3-3\gamma}}\frac{m_0\sigma_c^3}{G} , \tag{A11}$$

where $t_{\rm ff}$ is the free-fall time evaluated at the initial mean density $\rho_{\rm ave}$, and where we have used the fact that $K = \sigma_c^2\rho_c^{1-\gamma}$. By

construction, the line width σ_c at the center of a cloud is taken to be purely thermal ($\sigma_c^2 = kT/\mu m_H$) and the EOS automatically accounts for nonthermal motions elsewhere. In any case, the mass accretion rate is therefore

$$\dot{M}_0 = (4-3\gamma)\gamma^{3/2}\left(\frac{3\pi^2}{8}\frac{\rho_c}{\rho_{ave}}\right)^{3(1-\gamma)/2}\left(\frac{t}{t_{ff}}\right)^{3(1-\gamma)}\frac{m_0\sigma_c^3}{G} = (4-3\gamma)\langle\dot{M}_0\rangle\ , \tag{A12}$$

and only the singular isothermal sphere has an accretion rate $\dot{M}_0 = \langle\dot{M}_0\rangle = m_0\sigma_c^3/G$ that is constant in time. Formally, the results of § 3 above are recovered by substituting $A^{3/2}$ for $\gamma^{3/2}$ and setting $\gamma = 0$ elsewhere in these expressions.

Now by manipulating the results given in Appendix C of MP96, the total mass and radius of a *singular* pressure-truncated polytrope can be written as

$$M_{tot} = \frac{8}{\pi}\left(\frac{3\gamma}{4-3\gamma}\right)^{3/2}\left(\frac{4-3\gamma}{6-3\gamma}\right)^{3\gamma/2}\left(\frac{C}{C_{HSE}}\right)^{3/2}\left(\frac{\rho_c}{\rho_{ave}}\right)^{3(1-\gamma)/2} t_{ff}\,\frac{\sigma_c^3}{G} \tag{A13}$$

and

$$R = \frac{4}{\pi}\left(\frac{3\gamma}{4-3\gamma}\right)^{1/2}\left(\frac{4-3\gamma}{6-3\gamma}\right)^{\gamma/2}\left(\frac{C}{C_{HSE}}\right)^{1/2}\left(\frac{\rho_c}{\rho_{ave}}\right)^{(1-\gamma)/2} t_{ff}\,\sigma_c\ , \tag{A14}$$

which should be compared to equations (25) and (26) in the logotropic limit $\gamma = 0$. The factor C/C_{HSE} here is required for consideration of the collapse (eq. [A10]) of a sphere that is everywhere denser than a virial-equilibrium configuration with the same radius R and temperature σ_c. Where the expansion wave is concerned, of course, the initial cloud is taken to be exactly virialized, and $C = C_{HSE}$.

Given these results, the central point mass builds up as

$$\frac{M_0}{M_{tot}} = \frac{\pi}{8}\left(\frac{\pi^2}{8}\frac{4-3\gamma}{2-\gamma}\right)^{3(1-\gamma)/2}\left(\frac{1}{2-\gamma}\frac{C}{C_{HSE}}\right)^{-3/2}\left(\frac{t}{t_{ff}}\right)^{4-3\gamma} m_0\ , \tag{A15}$$

and the boundary $X = R/a_i t$ is given by

$$X = \frac{4}{\pi}\left(\frac{8}{\pi^2}\frac{2-\gamma}{4-3\gamma}\right)^{(1-\gamma)/2}\left(\frac{1}{2-\gamma}\frac{C}{C_{HSE}}\right)^{1/2}\left(\frac{t}{t_{ff}}\right)^{\gamma-2}\ . \tag{A16}$$

If our similarity solution is taken to hold at all times, then equation (A15) gives the time to accrete an entire cloud onto the core ($M_0/M_{tot} = 1$). For the expansion wave, with $C = C_{HSE}$, this ranges between $t_{end} \simeq 2.61 t_{ff}$ for $\gamma = 1$, and $t_{end} \simeq 4.32 t_{ff}$ for $\gamma = 0$. (The relation between γ and m_0 is given by Table 4 in Appendix B.) Strictly speaking, however, boundary effects are important at late times in finite spheres; in particular, the expansion wave will reach the edge of a cloud when $X = x_{ew}$ (eqs. [B3], [B4]), i.e., at

$$t_{ew} = \frac{4\sqrt{2-\gamma}}{\pi}\,t_{ff} < t_{end}\ . \tag{A17}$$

APPENDIX B

CRITICAL POINTS

Collapse flows in polytropes with $\gamma \le 1$ (where again γ is set to 0 for the logotrope) may involve passage through a critical point, $x_* \ge 0$, where the velocity $v_* \le 0$ and density α_* satisfy

$$(2-\gamma)x_* - v_* = \alpha_*^{(\gamma-1)/2}\ . \tag{B1}$$

Equations (A4) and (A5) then demand that

$$\frac{\alpha_*^{(\gamma+1)/2}}{4-3\gamma} + (1-\gamma)\alpha_*^{(\gamma-1)/2} - \frac{2}{x_*}\alpha_*^{\gamma-1} + (1-\gamma)(2-\gamma)x_* = 0 \tag{B2}$$

in order for $(d\alpha/dx)_{x_*}$ and $(dv/dx)_{x_*}$ to be finite.

The critical point x_{cw} for which $v_* = 0$ has, by equation (B1),

$$x_{cw} = \frac{\alpha_{cw}^{(\gamma-1)/2}}{2-\gamma}\ , \tag{B3}$$

so that equation (B2) gives

$$x_{cw} = 2(4-3\gamma) = \left[\frac{2(4-3\gamma)}{(2-\gamma)^2}\right]^{1/(2-\gamma)} x_{cw}^{-2/(2-\gamma)}\ . \tag{B4}$$

which agrees with the static solution (eqs. [A7], [A8]) of the fluid equations at x_{cw}. The collapse solution that begins with $v \to -\infty$ at $x = 0$, and goes on to pass through x_{cw} with $v = 0$, may therefore be continued to larger x by attaching the static

TABLE 4

POLYTROPE EXPANSION WAVES.

γ	x_*	x_{cw}	m_0	m_{cw}
0.....	0.0244	0.17678	0.000667	0.022097
0.1.....	0.0340	0.21384	0.00156	0.039756
0.2.....	0.0472	0.25806	0.00356	0.070502
0.3.....	0.0658	0.31061	0.00797	0.12287
0.4.....	0.0917	0.37276	0.0175	0.20964
0.5.....	0.128	0.44583	0.0373	0.34835
0.6.....	0.181	0.53111	0.0774	0.55970
0.7.....	0.259	0.62964	0.156	0.86089
0.8.....	0.380	0.74183	0.301	1.24939
0.9.....	0.585	0.86668	0.558	1.67391
1.....	1	1	0.975	2

solution. This composite flow is just the expansion wave.

We now confine our attention to critical points $x_* \le x_{cw}$, so that $v_* \le 0$ and $\alpha_* \ge \alpha_{cw}$. In general, given x_*, it is a simple matter to find α_* and v_* from equations (B2) and (B1). Then we set

$$\alpha(x) = \alpha_* + a_1(x - x_*) + \mathcal{O}[(x - x_*)^2] \quad \text{and} \quad v(x) = v_* + b_1(x - x_*) + \mathcal{O}[(x - x_*)^2]$$

in some neighborhood of x_*. Substitution of this first-order expansion in equations (A4) and (A5) leads to a pair of coupled quadratic equations for the slopes a_1 and b_1. Under the constraint (eq. [B2]), these yield a single cubic equation for a_1, and, therefore, three eigensolutions for the flow through a critical point. The first of these satisfies the simple relation

$$b_1 = (2 - \gamma) + \frac{1 - \gamma}{2} a_1 \alpha_*^{(\gamma - 3)/2}, \tag{B5}$$

which serves only to move the flow along the locus (eq. [B1]) of critical points. Such a propagation of singularities is so contrived as to be unphysical, and therefore we discard this solution. This leaves us with

$$a_1 = -\left[\frac{k_1 \pm \sqrt{k_1^2 - 4(1 + \gamma)k_2}}{2(1 + \gamma)}\right]\alpha_*^{(3 - \gamma)/2}$$

$$b_1 = -2(1 - \gamma) + \frac{2}{x_*}\alpha_*^{(\gamma - 1)/2} + a_1\alpha_*^{(\gamma - 3)/2}, \tag{B6}$$

where

$$k_1 \equiv -(9 - 7\gamma) + \frac{8}{x_*}\alpha_*^{(\gamma - 1)/2}$$

$$k_2 \equiv \alpha_* + 2(1 - \gamma)(5 - 3\gamma) - \frac{4(4 - 3\gamma)}{x_*}\alpha_*^{(\gamma - 1)/2} + \frac{6}{x_*^2}\alpha_*^{\gamma - 1}. \tag{B7}$$

For $x_* \le x_{cw}$ and $0 \le \gamma \le 1$, a_1 is always real and negative. If the minus sign is taken to solve for it in equation (B6), we find $b_1 \ge 0$, and such solutions have v more negative at smaller x. Therefore, these correspond to the minus solutions of Shu (1977), or the type 2 solutions of Hunter (1977) and Whitworth & Summers (1985). In the isothermal limit of $\gamma = 1$, the result is $a_1 = -2/x_*^2$ and $b_1 = 1/x_*$. If, instead, the addition sign is taken in equation (B6), then $b_1 \le 0$ and we recover the plus (or type 1) solutions; in the isothermal case, $a_1 = 2/x_* - 6/x_*^2$ and $b_1 = 1 - 1/x_*$. The plus solutions for this or any other γ have $|v|$ growing for $x > x_*$ and vanishing at some nonzero $x < x_*$. In addition, they are underdense at large x, relative to the singular hydrostatic profile, and may, therefore, be of interest as (time-reversed) wind solutions.

The slopes a_1 and b_1 at x_{cw} can be found analytically, given any γ, for both the minus and the plus solutions that flow through that point; again, the minus solution at x_{cw} is the expansion wave. Using equations (B3) and (B4) in equations (B6) and (B7), we have the following:

$\frac{1}{5} < \gamma \le 1$, *minus solution*:

$$a_1 = \frac{3\gamma - 5}{1 + \gamma}\alpha_{cw}^{(3 - \gamma)/2} < 0 \quad \text{and} \quad b_1 = \frac{5\gamma - 3}{1 + \gamma} > 0. \tag{B8}$$

Although α_{cw} and v_{cw} match the density and velocity of the corresponding static solution at x_{cw}, the derivatives do *not* agree there (in particular, $dv/dx \equiv 0$ for the static outer cloud). The density profile and velocity field of an expansion wave in this range of γ—which includes the isothermal sphere—are therefore discontinuous at x_{cw}.

$0 \le \gamma \le \frac{1}{5}$, *minus solution*:

$$a_1 = -2\alpha_{cw}^{(3 - \gamma)/2} < 0 \quad \text{and} \quad b_1 = 0. \tag{B9}$$

Now these (left) derivatives do match the (right) derivatives of the static solution at the head x_{cw} of the expansion wave (see eq.

[A7]), and the full flow is everywhere continuous. The logotrope corresponds to $\gamma = 0$, and therefore shows this behavior.

The plus solutions at x_{ew} for $\gamma > \frac{1}{3}$ have the same a_1 and b_1 as the minus solutions for $\gamma \leq \frac{1}{3}$, and the plus solutions at x_{ew} for $\gamma \leq \frac{1}{3}$ have the same derivatives as the minus solutions for $\gamma > \frac{1}{3}$.

Equations (B8) and (B9) also show that, for $\gamma < 1$, the velocity slope b_1 of the expansion wave at x_{ew} is always shallower than the gradient dv_s/dx_s of the locus (eq. [B1]) of critical points there, and the infall velocity of the material just inside the head of the wave is less than the critical value. However, $|v|$ increases without bound toward $x = 0$ for a minus solution, so any gas EOS that is softer than isothermal (including logotropic; § 2.3) leads to an expansion-wave flow that eventually crosses a second critical point $x_s < x_{ew}$. Since the expansion wave also stands as the limit of out-of-equilibrium collapse solutions ($C > C_{HSE}$; Appendix A), some of these must also pass through two critical points. By contrast, in the isothermal case the expansion wave is just tangent to the locus of critical points at $x_{ew} = 1$, and all $C > 2$ infall solutions avoid it altogether.

Finally, it is clear that the head x_{ew} of the expansion wave, its second, inner critical point x_s, and the core mass/central accretion rate m_0 are all uniquely defined by the specification of the polytropic index γ. These connections are shown in Table 4. Also given there is the total mass m_{ew} interior to x_{ew} (from eq. [A7]). The ratio m_0/m_{ew} is the fraction of infalling material that is already taken up in the central core itself.

REFERENCES

Adams, F. C., Lada, C. J., & Shu, F. H. 1987, ApJ, 312, 788
André, P., & Montmerle, T. 1994, ApJ, 420, 837
André, P., Ward-Thompson, D., & Barsony, M. 1993, ApJ, 406, 122
Barsony, M. 1994, in ASP Conf. Ser. 65, Clouds Cores and Low Mass Stars, ed. D. P. Clemens & R. Barvainis (San Francisco: ASP), 197
Bertoldi, F., & McKee, C. F. 1992, ApJ, 395, 140
Bodenheimer, P., & Sweigart, A. 1968, ApJ, 152, 515
Bonnell, I. A., Bate, M. R., & Price, N. M. 1996, MNRAS, 279, 121
Bonnor, W. B. 1956, MNRAS, 116, 351
Bontemps, S., André, P., Tereby, S., & Cabrit, S. 1996, A&A, 311, 858
Boss, A. P., & Black, D. C. 1982, ApJ, 258, 270
Butner, H. M., Evans, N. J., Harvey, P. M., Mundy, L. G., Natta, A., & Randich, M. S. 1990, ApJ, 364, 164
Butner, H. M., Evans, N. J., Lester, D. F., Levreault, R. M., & Strom, S. E. 1991, ApJ, 376, 636
Caselli, P., & Myers, P. C. 1995, ApJ, 446, 665
Chandrasekhar, S. 1967, An Introduction to the Study of Stellar Structure (New York: Dover)
Ebert, R. 1955, Z. Astrophys., 37, 217
Elmegreen, B. G. 1989, ApJ, 338, 178
Elmegreen, B. G., & Clemens, C. 1985, ApJ, 294, 523
Foster, P. N., & Chevalier, R. A. 1993, ApJ, 416, 303
Fuller, G. A., & Myers, P. C. 1992, ApJ, 384, 523
Galli, D., & Shu, F. H. 1993a, ApJ, 417, 220
———. 1993b, ApJ, 417, 243
Goldreich, P., & Weber, S. V. 1980, ApJ, 238, 991
Hills, J. G. 1980, ApJ, 235, 986
Hunter, C. 1977, ApJ, 218, 834
Jijina, J., & Adams, F. C. 1996, ApJ, 462, 874
Kenyon, S. J., Calvet, N., & Hartmann, L. 1993, ApJ, 414, 676
Kenyon, S. J., Gomez, M., Marzke, R. O., & Hartmann, L. 1994, AJ, 108, 251
Kenyon, S. J., Hartmann, L. W., Strom, K. M., & Strom, S. E. 1990, AJ, 99, 869
Lada, C. J., Margulis, M., & Dearborn, D. 1984, ApJ, 285, 141
Larson, R. B. 1969, MNRAS, 145, 271
———. 1981, MNRAS, 194, 809
Lizano, S., & Shu, F. H. 1989, ApJ, 342, 834
Maloney, P. 1988, ApJ, 334, 761
McCrea, W. H. 1957, MNRAS, 117, 562
McKee, C. F. 1989, ApJ, 345, 782
McKee, C. F., & Zweibel, E. G. 1995, ApJ, 440, 686
McLaughlin, D. E., & Pudritz, R. E. 1996, ApJ, 469, 194 (MP96)
Myers, P. C., & Benson, P. J. 1983, ApJ, 266, 309
Myers, P. C., & Fuller, G. A. 1992, ApJ, 396, 631
———. 1993, ApJ, 402, 635
Myers, P. C., Fuller, G. A., Mathieu, R. D., Beichman, C. A., Benson, P. J., Schild, R. E., & Emerson, J. P. 1987, ApJ, 319, 340
Myers, P. C., & Goodman, A. A. 1988, ApJ, 329, 392
Myhill, E. A., & Kaula, W. M. 1992, ApJ, 386, 578
Penston, M. V. 1969, MNRAS, 144, 425
Pudritz, R. E., Wilson, C. D., Carlstrom, J. E., Lay, O. P., Hills, R. E., & Ward-Thompson, D. 1996, ApJ, 470, L123
Shu, F. H. 1977, ApJ, 214, 488
Shu, F. H., Adams, F. C., & Lizano, S. 1987, ARA&A, 25, 23
Suto, Y., & Silk, J. 1988, ApJ, 326, 527
Tereby, S., Shu, F. H., & Cassen, P. 1984, ApJ, 286, 529
Tsai, J. C., & Hsu, J. J. L. 1995, ApJ, 448, 774
Whitworth, A., & Summers, D. 1985, MNRAS, 214, 1
Zhou, S. 1992, ApJ, 394, 204
Zhou, S., Evans, N. J., Butner, H. M., Kutner, M. L., Leung, C. M., & Mundy, L. G. 1990, ApJ, 363, 168
Zhou, S., Evans, N. J., Kömpe, C., & Walmsley, C. M. 1993, ApJ, 404, 232

Chapter 4

Globular Clusters

In the preceding Chapters, we have discussed the initial conditions for star formation in the Milky Way, as embodied in the observed properties of molecular clouds and cores; developed a new theoretical description of these conditions (the logotropic equation of state; McLaughlin & Pudritz 1996b); and investigated one of the most immediate consequences of our model for the star formation process itself (i.e., non-isothermal collapse; McLaughlin & Pudritz 1997).

The discussion of McLaughlin & Pudritz (1997) specifically focuses on the issue of *infall to a single protostar* at the center of a spherical gas cloud. The explicit simplifications that enable the analysis there (spherical symmetry, lack of rotation, neglect of mean magnetic fields) are certainly justifiable in what is still, at some level, an exploratory stage of the theory — although they should just as certainly be abandoned in future work. However, there is also a more subtle underlying simplification here, as there is in almost all of star-formation theory as it stands today: the emphasis is on the formation of a single star. This is obviously an important process, and it poses problems that must be solved; and yet, myriad observations have made it clear that, in fact, *most stars do not form in isolation.* Whether they be labelled as associations, complexes, or outright clusters, many — perhaps even most — stars are now, and were in the past, born in groups.

Thus, the rest of this thesis seeks to better understand one manifestation of this important aspect of star formation, namely, the old ($\tau \sim 15 \times 10^9$ yr $= 15$ Gyr) and massive ($m \simeq 2 \times 10^5 M_\odot$ on average) *globular clusters* of stars that can be found, sometimes by the thousands, in nearly any

galaxy of sufficient size (with more than 70 systems beyond the Milky Way surveyed to date; e.g., Harris 1991). The great age of these objects puts their birth firmly in the protogalactic era, so that any theory for globular cluster formation must directly address questions of galaxy formation as well. The hope is that at least some of the fundamentals of star formation have not changed significantly from that time to the present; and that the study of globular clusters can indeed reveal something of these fundamentals, and thereby lead to a fuller appreciation of the process as it operates now.

4.1 A Clustered Mode of Star Formation

A simple comparison between the masses of molecular cores and those of the stars they produce is sufficient to show that most stars today actually are *forced* to form in groups. As was mentioned in §1.5.3, cores have masses between roughly 1 and 1000 $M_\odot$, and are distributed throughout this interval according to a *mass spectrum*, $N(m) = dN/dm$, which takes the form of a power law. That is, the number of cores with masses between m and $m + dm$ is $N(m) \propto m^\gamma$, with $\gamma \simeq -1.5 \pm 0.2$ (Blitz 1991; McLaughlin & Pudritz 1996a, and references therein). This result is observed to hold, over one or two decades in mass, among the cores in a large number of different clouds. Stars, on the other hand, range in mass from $\sim 0.1 - 100 M_\odot$; and for our purposes, their mass spectrum is also reasonably approximated as a power law $N(m) \propto m^\gamma$, but now with $\gamma \simeq -2.35$ (Salpeter 1955; Miller & Scalo 1979; Scalo 1986). Once $N(m)$ is known for any collection of objects, it is a simple matter to compute where most of the total mass in the population is located: does it lie mostly in the few largest objects? in many very small ones? or is it more evenly distributed between all of them? We can now ask these questions of cores and of stars.

The total mass of a group of objects that follow a power-law mass spectrum, $N(m) = Am^\gamma$ with $m_\ell \leq m \leq m_u$, is just $M_{\rm tot} = \int_{m_\ell}^{m_u} mN(m)\, dm = A\int_{m_\ell}^{m_u} m^{1+\gamma}\, dm$. Similarly, the mass contained just in those objects *more* massive than some $m_f \geq m_\ell$ is $M_f \equiv A\int_{m_f}^{m_u} m^{1+\gamma}\, dm$. By construction, $M_f/M_{\rm tot} \equiv f < 1$, so upon performing the integrals we have that

$$m_f^{2+\gamma} = (1-f)\, m_u^{2+\gamma} + f\, m_\ell^{2+\gamma} \,. \tag{4.1}$$

Thus, we can readily compute the mass range $m_f \leq m \leq m_u$ of objects that together account for

any chosen fraction f of the total mass $M_{\rm tot}$.

We first apply this procedure to cores, with $m_\ell = 1M_\odot$, $m_u = 1000M_\odot$, and $\gamma = -1.5$, to find that $f = 0.5$ corresponds to $m_f = 266M_\odot$; i.e., half of all the mass in GMC cores is contained in those more massive than $\sim 260M_\odot$ (cf. §1.5.3 and Table 1.2). The mass spectral parameters appropriate to stars are (to be conservative) $m_\ell \sim 0.3M_\odot$, $m_u \sim 50M_\odot$, and $\gamma = -2.35$; thus, $f = 0.5$ in this case implies a much smaller $m_f = 1.40M_\odot$. This difference is striking, and it is made more so when more extreme mass fractions f are considered. For instance, we find that

$$\begin{aligned} \text{cores:} \quad f = 0.8 \quad &\Longrightarrow \quad m_f = 50.8\ M_\odot \\ \text{stars:} \quad f = 0.2 \quad &\Longrightarrow \quad m_f = 6.91\ M_\odot\ . \end{aligned} \tag{4.2}$$

That is, *by mass, 80% of the star-forming gas in the Galaxy is found in cores with* $m \gtrsim 50M_\odot$, *while 80% of stars have* $m \lesssim 7M_\odot$.

This simple result stems almost entirely from the different mass *spectra* of cores and stars — specifically, from the fact that $\gamma > -2$ in one case but $\gamma < -2$ in the other — rather than from any difference in their mass *ranges*, which actually overlap significantly. Although its origin is not at all understood, this contrast in the indices γ for cores and stars is a fundamental, and apparently universal, finding. The conclusion, then, is that stars are most commonly born in cores that are much more massive than any single one of them; the implication is that stars typically have to form more than one at a time.

As was suggested in §1.5.2 above, there is much direct observational evidence that this really is the case (e.g., Lada et al. 1993; Larson 1993). For example, even the nearby Taurus-Auriga molecular cloud, which has long been regarded as the prototypical environment of "isolated" low-mass star formation, actually forms loose *groups* of stars (e.g., Larson 1982; Myers & Benson 1983; Kenyon et al. 1990). This is illustrated in Fig. 4.1, which is taken from the fairly complete census of young stellar objects (YSOs) in Taurus by Kenyon et al. (1990). While it is clear that YSOs are widely spread throughout this cloud ($\sim$100 YSOs within a $\sim$300 pc^2 area on the sky), a significant amount of clustering is obvious even to the eye; star formation in Taurus is undoubtedly *distributed*, but it is not at all clear that it is random or isolated in any real sense (see Gomez et al. 1993 for a quantitative discussion of this). More impressive is the situation in the $\sim 600M_\odot$ core of the (also

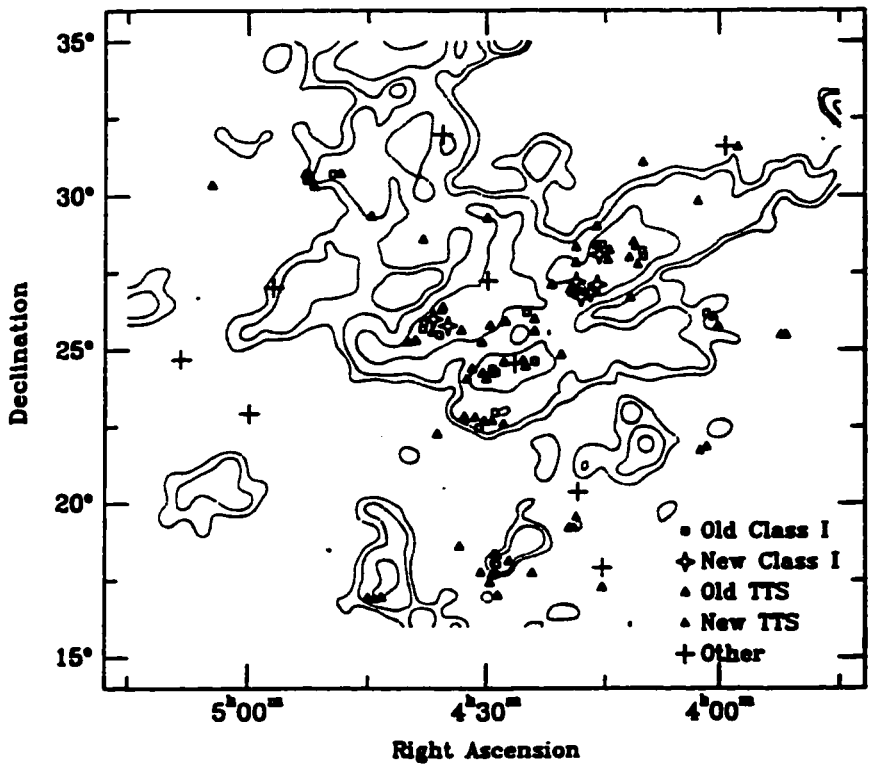

Figure 4.1: Distribution of star formation in the Taurus-Auriga molecular cloud. Symbols correspond to embedded (Class I) infrared sources and optically visible T Tauri stars. Contours trace equal integrated intensities of CO emission. The distance to the Taurus cloud is 140 pc, such that an angular scale of 1′corresponds to 0.04 pc. From Kenyon et al. (1990).

nearby) ρ Ophiuchus cloud, where another ~100 YSOs are packed into an area of only 2 pc^2 or so, and where the ratio of star-to-gas mass implies a star formation efficiency of at least 25% (e.g., Wilking, Lada, & Young 1989). But most revelatory has been the detailed study, in recent years, of the stars and gas in the Orion molecular cloud complex. In Orion A (L1641), obvious clusters (including the famous Trapezium cluster; see Fig. 1.2 above) account for 85% of all the YSOs known to be associated with the cloud (Lada et al. 1993); and 96% of the ~450 YSOs in the Orion B (L1630) cloud are contained in only 4 cores, each which has $M \gtrsim 300 M_\odot$ (Lada 1992). This remarkable situation is reflected in Fig. 4.2, which compares the integrated intensity of CS emission with the surface density of YSOs in L1630, as found by Lada et al. (1991b). The high degree of clustering in the YSOs, and their close association with the dense CS cores, is evident.

Numerous other examples of young ($\lesssim 10^7$ yr) stellar clusters that are still embedded in

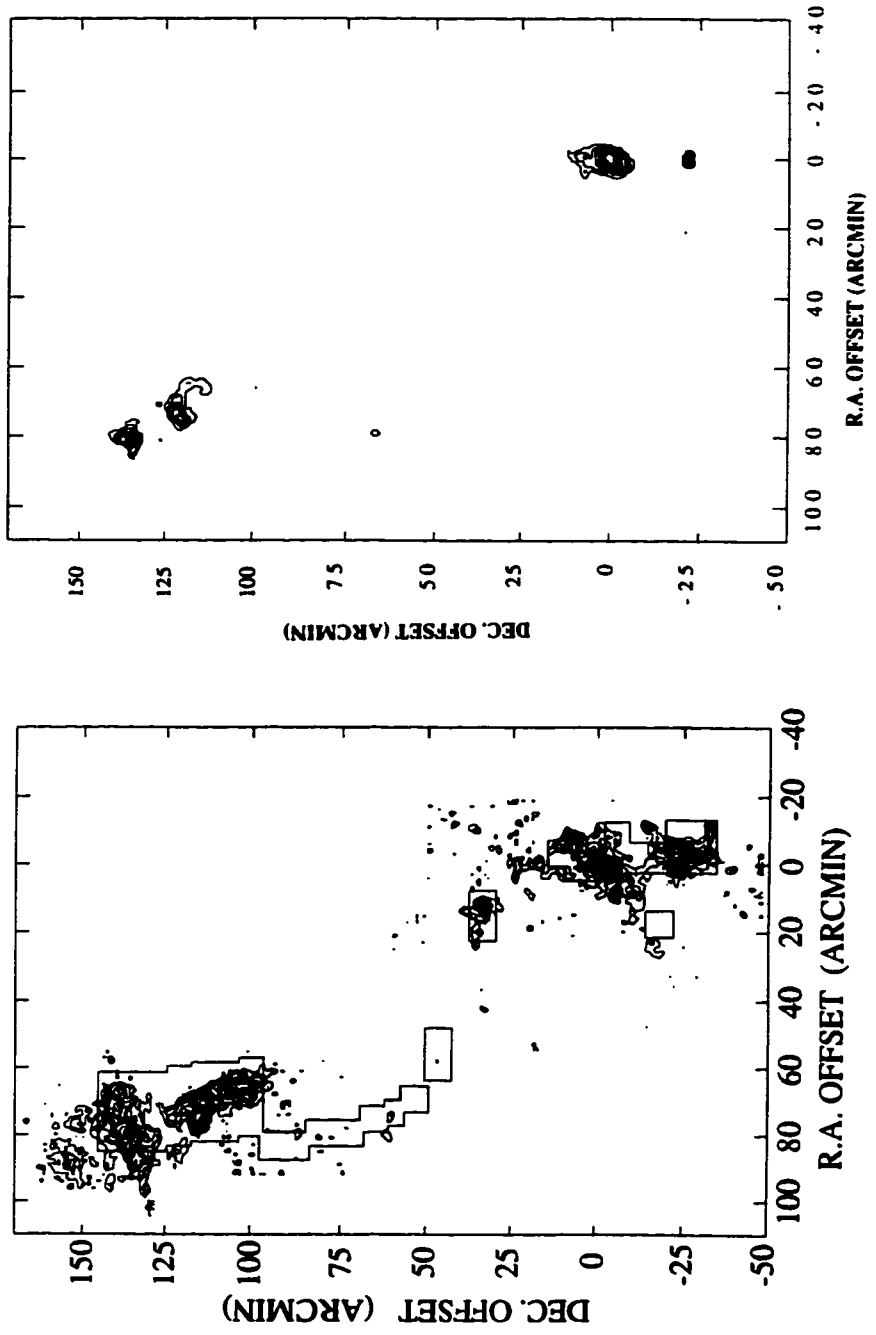

Figure 4.2: Distribution of star formation in the Orion B (L1641) GMC. *Bottom panel*: Integrated intensity contours in the CS $J = 2 \rightarrow 1$ line. Boxes show the boundaries of a complete near-infrared survey for YSOs. *Top panel*: Equal-surface density contours (number per arcmin^2) for the YSOs associated with this cloud. For a distance to Orion of 450 pc, $1' \simeq 0.13$ pc. From Lada et al. (1991b).

copious amounts of gas and dust throughout the Milky Way are discussed by, e.g., Zinnecker, McCaughrean, & Wilking (1993). The few specific examples mentioned here — all of which come from relatively nearby molecular clouds, where low-mass YSOs and the molecular gas can both be surveyed relatively completely — are clearly indicative of a very general trend in star formation. The observations of Orion are particularly important, because this massive complex (which has $m \sim 10^5 M_\odot$, compared to $m \sim 10^4 M_\odot$ for Taurus and Ophiuchus) may be representative of the conditions in most GMCs. If so, then it would seem that a predominantly clustered mode of star formation is the norm in the Milky Way today.

Of course, this is *not* to say that all stars form as members of gravitationally *bound* clusters that survive as coherent dynamical units for any length of time; after all, whatever substructure there is among the general field stars of the Galaxy (e.g., Efremov 1995; Majewski, Hawley, & Munn 1996) usually appears on scales considerably greater than those of molecular cores and clouds. Instead, most cores are destined to form unbound groups or associations of stars that eventually drift apart and blend into a more uniform stellar background. The reason for this is that star formation necessarily involves an element of feedback, wherein outflows, winds, ionization in H II regions, and supernova explosions from the more massive (O and B) stars forming in a GMC core eventually conspire to evaporate or blow out the remaining gas around them. On a global scale, the combined effect of all the OB stars in a typical GMC would appear able to destroy the entire cloud within a few 10^7 yr after the formation of the stars (e.g., Leisawitz, Bash, & Thaddeus 1989; Williams & McKee 1997). More locally, any group of stars inside any individual core [which will include not only a few highly destructive, massive members, but many low-mass ones as well, all distributed according to $N(m) \propto m^{-2.35}$] must itself be affected by the gas loss it engenders. If too much of the total mass of a star-forming core is still in gaseous form when blow-out occurs, then the concomitant loss of gravitational binding energy can leave the stars with a collective total energy that is positive ($\mathcal{E}_{\rm stars} = \mathcal{U}_{\rm stars} + \mathcal{W}_{\rm stars} > 0$), so that they ultimately emerge as an unbound association. If this is to be avoided, and the new stars to remain as a gravitationally bound cluster after gas loss, the cumulative *star formation efficiency* of the core, SFE $\equiv M_{\rm stars}/(M_{\rm stars} + M_{\rm gas})$, has to be quite high (e.g., Hills 1980).

To see this, consider the typical situation in which one of the most massive cores in a GMC

is forming a group of stars. Such a core will roughly satisfy (cf. Chapters 1 and 2) the simple virialization condition $2\,\mathcal{U}_0 + \mathcal{W}_0 = 0$, where $\mathcal{U}_0 = (3/2)M_0\sigma^2_{\rm ave,0}$ and $\mathcal{W}_0 = -(3a/5)GM_0^2/R_0$ as usual, and where $M_0 = M_{\rm gas} + M_{\rm stars}$ is the total mass initially in the core. Thus, this mixture of gas and stars has a velocity dispersion of

$$\sigma^2_{\rm ave,0} = \frac{a}{5}\frac{GM_0}{R_0}\ . \tag{4.3}$$

Now assume that this core is at that point in its evolution where just enough massive stars have formed to completely clear the region of gas. This blow-out will put the purely stellar system left behind out of virial equilibrium; but if it occurs suddenly, there will be no immediate change in the stars' collective velocity dispersion and radius. The total energy of the stars alone, just after gas loss, is then

$$\mathcal{E}_{\rm stars} \;=\; \mathcal{U}_{\rm stars} + \mathcal{W}_{\rm stars} \;=\; \frac{3}{2}\,M_{\rm stars}\,\sigma^2_{\rm ave,0} \;-\; \frac{3a}{5}\,\frac{GM^2_{\rm stars}}{R_0}\ . \tag{4.4}$$

Eventually, the radius and velocity dispersion of the stellar system will relax to a new virial equilibrium, in which $2\,\mathcal{U}_{\rm stars} + \mathcal{W}_{\rm stars} = 0$. The total energy (4.4) will be conserved as this goes on, so if $\mathcal{E}_{\rm stars} < 0$ immediately after gas loss, then re-virialization results in the formation of an equilibrium, bound cluster. But if $\mathcal{E}_{\rm stars} > 0$, then our core has produced a group of stars whose virialization formally requires expansion to infinity, i.e., dispersal into the field. Thus, substitution of equation (4.3) into (4.4) shows that the criterion for the production of a bound star cluster is just

$$\mathcal{E}_{\rm stars} \;\leq\; 0 \quad\Longrightarrow\quad {\rm SFE} \;\equiv\; \frac{M_{\rm stars}}{M_{\rm stars} + M_{\rm gas}} \;\geq\; \frac{1}{2}\ . \tag{4.5}$$

This constraint on SFE can be made slightly less stringent if gas loss from the core is allowed to take place over a sufficiently long time (so that the adjustment from a star-plus-gas equilibrium to a purely stellar one is more gradual, and less traumatic; see Hills 1980), or if the mean magnetic field in the initial core is taken explicitly into account (Elmegreen & Clemens 1985); but even then, SFE $\gtrsim 30\%$ is still typically required.

The number of massive cores forming multiple stars with any given SFE is obviously difficult to estimate, but it is clear that few ever reach the critical $\sim$50% threshold. For example, Elmegreen

(1983) suggests that the *average* SFE in star-forming cores is perhaps ~10%, so that the mass fraction $f_{\rm cl}$ of cores which can actually achieve the high SFE required to form a bound cluster must be less than 1. That $f_{\rm cl}$ is likely very much smaller than unity is hinted at by the fact that even the most impressive stellar groupings in Orion B correspond to local efficiencies of $30-40\%$ in their parent cores (Lada 1992), which may or may not be high enough to result in a (loosely) bound cluster.

A global value of $f_{\rm cl}$, effectively averaged over many GMCs, may be roughly estimated as follows: First, Elmegreen & Clemens (1985) place the rate of formation of bound *open clusters* (which are defined by masses $m \sim 10^2 - 5 \times 10^3 M_\odot$ and ages $\tau \lesssim 5 \times 10^8$ yr) within a few kpc of the Sun at $(2.5 \pm 1) \times 10^{-7}$ clusters kpc^{-2} yr^{-1}; thus, assuming an average cluster mass of $700 M_\odot$, the local star formation rate in bound clusters is $S_{\rm cl} = (1.8 \pm 0.7) \times 10^{-4} M_\odot$ kpc^{-2} yr^{-1}. Second, the *total* rate of star formation in the solar neighborhood is $S_{\rm tot} \simeq 4.5 \times 10^{-3}\ M_\odot$ kpc^{-2} yr^{-1} (e.g., McKee 1989). And third, these quantities, which involve *stellar* masses, are related to the fraction $f_{\rm cl}$ of the total *gas* mass in cluster-forming cores by noting that stars born in clusters are, by definition, appearing in environments with $\mathrm{SFE_{cl}} \gtrsim 0.5$, while the average star comes to a core with $\mathrm{SFE_{tot}} \sim 0.1$ (Elmegreen 1983). Thus,

$$f_{\rm cl} \;=\; \frac{S_{\rm cl}}{\mathrm{SFE_{cl}}} \times \frac{\mathrm{SFE_{tot}}}{S_{\rm tot}} \;\approx\; (2-11) \times 10^{-3}\ . \tag{4.6}$$

Together, equations (4.2) and (4.6) therefore suggest that (1) star formation in the Milky Way proceeds almost exclusively in a clustered mode, i.e., in groups inside dense and massive molecular cores, but that (2) only a select few active cores, perhaps $f_{\rm cl} = 0.1 - 1\%$ by mass, are able to achieve a critical, "binding" local SFE of better than ~50% before their gas is lost to the effects of massive-star winds, ionization, and supernovae.

These considerations involve the ongoing formation of stars locally, and in groups of total mass $< 10^3 M_\odot$, which is the typical size of the largest cores in Galactic GMCs today. Nevertheless, the situation is not much different when we look to the open cluster population in the Milky Way as a whole, and to the much older ($\tau \sim 15$ Gyr) and more massive ($m = 2 \times 10^5 M_\odot$ on average) globular clusters. There are currently about 1200 open clusters known in the Galactic disk. Some two dozen globular clusters are also associated with the disk (Zinn 1985), or perhaps with the nuclear

bulge region (Minniti 1996), and another ~130 are found in the more extended, roughly spherical stellar *halo* of the Milky Way (Harris & Racine 1979; Djorgovski 1993). The combined mass of the globulars dominates that of the open clusters by two orders of magnitude, but still accounts for only a small fraction, $f_{\rm cl}^{\rm glob} \sim 10^{-3}$, of the total stellar mass of our Galaxy. Since bound clusters can still be destroyed in the long term, by their evolution in the gravitational field of the Galaxy (see §5.3 below), this mass fraction might have been slightly higher in the past. However, the clusters most susceptible to such destruction are the least massive ones, and their loss is unlikely, even when accumulated over 15 Gyr, to change $f_{\rm cl}^{\rm glob}$ by even a factor of two. Thus, $f_{\rm cl}^{\rm glob} \sim 10^{-3}$ is actually a reasonable measure of the *formation* efficiency, by mass, of large bound clusters in the early Milky Way. The similarity of this result to the estimate of $f_{\rm cl}$ in equation (4.6), which applies to the formation of much smaller and younger open clusters, is one strong indication that *the fundamental mechanism of star and cluster formation has not changed significantly over the life of the Milky Way.*

Nor is this mechanism peculiar to our Galaxy. Hodge (1988) provides a census of the known star clusters (young, old, open, and globular) in galaxies within the Local Group,[1] and extrapolates on the number observed to estimate a total population of ~20 000. His results for the Andromeda Nebula, or M31 — which is the nearest spiral galaxy resembling the Milky Way — are of particular interest, as he places the current rate of open cluster formation there at roughly 3300±1700 clusters per 10^8 yr. With an average mass of $\sim 10^3 M_\odot$ for these young clusters (based on the mass range $10^2 - 10^4 M_\odot$ specified by Hodge), this corresponds to a global $S_{\rm cl} \sim 0.033 \pm 0.017\ M_\odot\ {\rm yr}^{-1}$ throughout M31. At the same time, the global rate of *all* star formation there is probably similar to the Milky Way value (McKee 1989; eq. [1.20] above), $S_{\rm tot} \simeq 3\ M_\odot\ {\rm yr}^{-1}$. (Note that this level of $S_{\rm tot}$ does appear to obtain generally in other spiral galaxies like ours; Kennicutt 1983.) Thus, if we take ${\rm SFE_{cl}} \gtrsim 0.5$, and assume ${\rm SFE_{tot}} \simeq 0.1$ as above, we find that $f_{\rm cl}^{\rm M31} \sim (1-3) \times 10^{-3}$, which is similar to the Galactic value (eq. [4.6]).

Another key feature of ongoing cluster formation is that, as Larson (1990, 1993, 1996) has stressed, it occurs within much larger star-forming complexes, such that the typical ratio of a young

[1]The Local Group is the gravitationally bound collection of about 30 galaxies lying within ~ 1 Mpc $= 10^6$ pc of the Milky Way. Its most prominent members are the Milky Way itself, M31 (Andromeda), and M33, which are all spiral galaxies. Other members are small irregulars (like the Large and Small Magellanic Clouds) and dwarf elliptical galaxies; most of these are satellites of either the Milky Way or M31.

cluster's mass to the total mass of gas in its immediate vicinity is of order 10^{-3}. This is obviously the case in the Milky Way, where we have already seen that clusters currently form in the dense cores (typical mass $260M_\odot$; cf. Table 1.2) of GMCs (typical mass $3 \times 10^5 M_\odot$). It is also true in more extreme situations. For example, the most massive young cluster of stars in the Local Group is R136, which lies at the center of the giant 30 Doradus H II region in the Large Magellanic Cloud. This compact ($R \sim 3$ pc) cluster has an age of $\tau \sim 5 \times 10^6$ yr and a mass of $m \sim 3 \times 10^4 M_\odot$ (Hunter et al. 1995), and is associated with $\sim 10^8 M_\odot$ of gas in a region of space about 2 kpc across (Larson 1993). Spectacular as the conditions in R136 are, it has become clear in recent years that they are quite representative of the circumstances attending the formation of massive clusters in a number of galaxies outside the Local Group: Literally hundreds of young ($\tau \sim 10^7 - 10^8$ yr) clusters, with sizes and masses at least as great as those of R136 and with similarly large quantities of associated gas, have now been observed by the Hubble Space Telescope in at least 18 different galaxies. These galaxies were originally selected for observation either because they are currently merging, or have recently merged, with others (e.g., Holtzman et al. 1992; Richer et al. 1993; Whitmore et al. 1993; Whitmore & Schweizer 1995; Schweizer et al. 1996; Holtzman et al. 1996), or because they show other evidence for intense recent star formation (i.e., starbursts: O'Connell, Gallagher, & Hunter 1994; O'Connell et al. 1995; Meurer et al. 1995; Watson et al. 1996). As such, they represent a strong enhancement of the more leisurely star formation occurring in quiescent galaxies like the Milky Way; but observations of them and their clusters are nevertheless of quite general significance, in at least three ways.

First, these data clearly indicate that the clustered mode of star formation is a universal phenomenon; although it is not known how many, or which, of the clusters in these galaxies will remain bound once they are fully formed and rid of their gas, the simple fact is that great numbers of stars in the local universe are forming within massive groups. Second, the young clusters are often associated with large (~kpc-scale), dense, "clumpy" substructures or knots in the galaxies (e.g., Meurer et al. 1995; Whitmore & Schweizer 1995), which suggests that they are part of a simple extension, to larger scales, of the local cloud-core system of star formation. Any clouds involved here are evidently much larger than any individual cluster: Larson (1996) summarizes direct evidence that a mass ratio of $\sim 10^{-3} - 10^{-2}$ between clusters and their surrounding gas again applies in some

specific extragalactic systems; and in many galaxies, clusters appear to form in groups of several at a time, within a number of spatially distinct regions (e.g., Whitmore & Schweizer 1995; Meurer et al. 1995; and especially O'Connell et al. 1995). And third, *the luminosities and radii of these clusters are generally such that they are expected to evolve, over the next 15 Gyr, into objects closely resembling the globular clusters in our Galaxy and others* (cf. the references cited above).

This last fact, especially, provides the point of departure for the rest of this Chapter and the next, as we turn now to study the generic properties of the old globular clusters in many different galaxies. These clusters are obviously bound, and they represent a small fraction $f_{\rm cl} \sim 0.001 - 0.01$ of the total product of early star formation. Nevertheless, they are relevant to the study of star formation in general, simply because they are part of what is now understood to be a spatially and temporally ubiquitous aspect of it. The advantage to studying globulars, as opposed to younger embedded groups or open clusters, is that the former are much more massive than the latter, and thus are visible in a great number of very distant galaxies. The advantage of globulars over the extreme young clusters in merging and starburst galaxies is that the former can be found in almost all *normal* systems. Thus, these objects offer a unique opportunity to obtain a far-reaching and global view of the end results of star formation.

4.2 Observations of Globular Clusters

The presence of globular clusters in the Milky Way has been appreciated at least since the late 18th century, when Charles Messier included 29 of them in his famous catalogue of obviously nonstellar celestial bodies; the first scientific descriptions of some of these, as large (although fairly compact), regular (roughly spherical) swarms of stars, came in the first half of the 19th century, with the work of W. Herschel and J. Herschel. With the advent of photographic techniques later in that same century, globulars were subjected to increasingly systematic analyses, including the first attempts to use detailed star counts to infer the internal structures and dynamical states of self-gravitating stellar systems. Throughout the 20th century, individual globular clusters have continued to be the focus of concentrated observational and theoretical study; good overviews of the history of this discipline can be found in, e.g., Meylan & Heggie (1997) or Harris & Racine (1979).

As was mentioned above, roughly 150 globular clusters have now been identified in the Milky

Way. (Although this count is undoubtedly nearly complete, there may well be a few overlooked clusters still waiting to be recognized; e.g., Harris et al. 1997.) By far, the majority of these belong to the halo of the Galaxy, which is the general term for the spatially extensive, low-density, old, metal-poor, and roughly spherical component of its stellar population. As such, most globulars are situated far away from the obscuring gas and dust in the disk. This, together with the fact that most are also very massive and intrinsically bright, makes them rather easily observable in general.

4.2.1 Magnitudes, Ages, Metallicities, and Masses

As was mentioned in §1.3.1 above, astronomical convention puts the measured brightness of an object, at some wavelength λ, onto a logarithmic *absolute magnitude* scale, defined by $M_\lambda = C_\lambda - 2.5\,\log_{10}(L_\lambda/L_{\odot,\lambda})$. By and large, globular clusters are studied by straightforward photometry and spectroscopy at optical wavelengths; thus, we confine ourselves here to a discussion of magnitudes in the common V bandpass, which is a standard filter centered on $\lambda = 5500$Å. In this case, the constant C_λ is rather arbitarily assigned a value of $C_\lambda = 4.83$, such that

$$M_V \equiv 4.83 - 2.5\,\log_{10}(L_V/L_{\odot,V})\ , \tag{4.7}$$

and the absolute magnitude of the Sun is $M_V = 4.83$. (Note that this definition assigns numerically smaller absolute magnitudes to intrinsically brighter objects.) Now, the observed flux from a body of luminosity L located a distance D away is given by $L/(4\pi D^2)$, and a logarithmic measure of this quantity is provided by the *apparent magnitude* (in the V bandpass):

$$V = 4.83 - 2.5\,\log_{10}\left[\frac{L_V/D^2}{L_{\odot,V}/(10\ \mathrm{pc})^2}\right] = M_V + 5\,\log_{10}(D/10\ \mathrm{pc})\ , \tag{4.8}$$

where the choice of 10 pc as a reference distance is again arbitrary. This relation between apparent magnitude V, absolute magnitude M_V, and distance D can be used to either (1) infer the distance to an object with measured V, if its intrinsic luminosity L_V (and hence M_V) is known *a priori*; or (2) derive the intrinsic M_V of an object with measured V and D. The difference $(V - M_V)$ is referred to as a *distance modulus*.

Globular clusters in the Milky Way are nearby enough that they can be resolved into their

individual member stars. Thus, the distance to a Galactic globular is generally obtained by comparing the apparent magnitudes measured for a subsample of its stars — typically either faint, main sequence stars (see below) or brighter, pulsating stars known as RR Lyrae variables — to the absolute magnitudes measured for field stars of the same type but with independently determined distances. A recent review of cluster distance determinations, and of the uncertainties still associated with them, is given by, e.g., VandenBerg, Bolte, & Stetson (1996). Once its distance D from the Sun is known, some of the most fundamental properties of a cluster can be immediately derived. For example, its integrated apparent magnitude is converted into a total absolute magnitude, corresponding to the summed luminosity of all its stars, by way of equation (4.8). The range of M_V among Galactic globulars (e.g., Djorgovski 1993), and among those in many other galaxies (see below), is $-1.7 \geq M_V \geq -10.1$, with a mean $\langle M_V \rangle \simeq -7.4$, corresponding to total cluster luminosities of $409 L_\odot \lesssim L \lesssim 9.38 \times 10^5 L_\odot$ and $\langle L \rangle \simeq 7.8 \times 10^4 L_\odot$. (From now on, V-band luminosities L_V and $L_{\odot,V}$ are written simply as L and $L_\odot$.) In addition to this, the observed angular extent θ of a cluster on the sky can be converted to a physical radius r through the trivial relation $r = D\theta$. Again, there is a range of total radii r_t among Galactic globulars: 10 pc $\lesssim r_t \lesssim$ 100 pc, with $\langle r_t \rangle \simeq 35$ pc (Djorgovski 1993). An observationally and physically more robust characterization of clusters uses their *half-light* radii, which are nearly immune to dynamical evolution. Typically, 1 pc $\lesssim r_h \lesssim$ 20 pc and $\langle r_h \rangle \simeq 4$ pc.

The age of a cluster can also be directly determined once its distance is known. A detailed discussion of the current status of this procedure, which has evolved from an original suggestion by Sandage (1953), is given by VandenBerg et al. (1996). The basic idea is that the individual stars in a globular cluster are all essentially coeval, and differ only in terms of their total masses. Now, for most of their lives, stars shine by fusing hydrogen nuclei into helium in their dense central regions (see Kippenhahn & Weigert 1990). While this core H-burning goes on, stars appear somewhere within a well defined area, known as the *main sequence*, in a plot of absolute magnitude vs. color (a color-magnitude diagram, or CMD).[2] Exactly where along the main sequence a given star will fall depends on its mass: larger stars are intrinsically brighter and bluer. At the same time, the rate at

[2]The color of an object is defined as the difference in its magnitudes (either absolute or apparent) at two different wavelengths; thus, it is equal to 2.5 times the logarithm of the ratio of luminosities at those wavelengths. In the context of this discussion, color is mainly an indicator of stellar temperature: hotter stars are "bluer," i.e., they emit relatively more light at shorter wavelengths.

which a star burns the hydrogen in its core also depends on its mass, as larger stars exhaust their central fuel supplies and evolve away from the main sequence before smaller ones do. Thus, to state the situation very simply, the observed absolute magnitude M_V of the brightest stars still on the main sequence in a globular cluster CMD is used to infer the mass of the largest stars in the cluster that are still undergoing core hydrogen burning. Given their mass, stellar evolution theory is then able to predict the age of these stars, and hence the age of the cluster as a whole.

The derivation of absolute cluster ages in this way is intricate work that involves many pieces of often disparate and sometimes uncertain physics, and is further subject to uncertainties in transformations between theoretical and observable quantities (i.e., between temperatures and colors, or masses and magnitudes). But once the ages of a few clusters are known with confidence, there are numerous dating techniques that rely on differential comparisons between the CMDs of two or more clusters to estimate fairly precise relative ages for them (see Stetson, VandenBerg, & Bolte 1996 for a review). Thus, it is known that most globular clusters in the Milky Way have ages $\tau \simeq 15 \pm 3$ Gyr, and that there is a significant *age spread* of $\Delta\tau \sim 3-4$ Gyr among them (Sarajedini & King 1989; VandenBerg, Bolte, & Stetson 1990; Chaboyer, Demarque, & Sarajedini 1996; Richer et al. 1996).

There are several ways to infer the abundances of heavy elements (again, everything higher than helium on the Periodic Table) in the stars of a globular cluster (see, e.g., Zinn & West 1984). All of these methods ultimately rely on spectroscopic observations, either of individual bright (giant) stars in the cluster itself or of similar stars in the field, simply because the strengths of the absorption lines in a stellar spectrum depend on the relative atmospheric abundances of the elements responsible for the lines. Heavy-element abundances, or *metallicities*, are usually expressed as mass fractions, Z, and are referred to the solar value, $Z_\odot = 0.02$ (i.e., heavy metals account for 2% of the Sun's mass). There are two important aspects to the metallicities of Galactic globulars. First, spectra of individual giants show that $Z/Z_\odot$ generally varies from star to star within any one cluster by much less than 10% (with the notable exceptions of the massive objects M22 and ω Centauri, where sizeable internal metallicity spreads are present; Suntzeff 1993); that is, in general, *globular clusters are internally chemically homogeneous.*[3] And second, photometric and spectroscopic estimates of

[3]To be precise, it should be noted that this claim really only applies to the abundances Z_{Fe} of iron-peak elements.

the average metallicities of entire clusters show that there is a rather wide spread in abundances *between* Galactic globulars, which have a mean $\langle Z/Z_\odot \rangle \simeq 0.03$ but span a range from $Z/Z_\odot = 0.0026$ to $Z/Z_\odot > 1$ (Zinn & West 1984).

Finally, the spectra of individual stars in a cluster also yield their velocities along the line of sight to an observer, as the central wavelengths of absorption lines are Doppler shifted from their laboratory values. If the velocities of several stars are measured in this way, then the mean line-of-sight velocity of the entire globular can be measured, along with its internal velocity dispersion (as a function of radius), $\sigma(r)$. This latter quantity is a critical element of the internal dynamics of a cluster, and can be used in conjunction with the observed spatial distribution of its stars to constrain the steady-state structure of a complicated, self-gravitating, N-body system. This is a fruitful line of research, although not one that we will discuss here; for a comprehensive review, see Meylan & Heggie (1997). Simply speaking, however, the measured velocity dispersion σ_c at the center of a cluster can be used to obtain a straightforward estimate of its total mass (e.g., Richstone & Tremaine 1986). Essentially, the idea is to evaluate the structural parameter $r_0 \equiv 3\sigma_c/(4\pi G\rho_c)^{1/2}$ of a cluster (cf. McLaughlin & Pudritz 1996b), by fitting scaled theoretical models (e.g., King 1966; Gunn & Griffin 1979) of luminosity density $\mathcal{L}/\mathcal{L}_c$, as a function of radius r/r_0, to photometric observations of $\mathcal{L}$ vs. r. This yields both the central luminosity density $\mathcal{L}_c$, in units of $L_\odot$ pc^{-3}, and the combination $\sigma_c/\rho_c^{1/2}$, with ρ_c the central *mass* density (in $M_\odot$ pc^{-3}) for the cluster. With σ_c known independently the (central) mass-to-light ratio $\Upsilon_c = \rho_c/\mathcal{L}_c$ follows immediately. It can then be assumed that this ratio of stellar mass (in $M_\odot$) to light emitted (in $L_\odot$) applies globally, to the cluster as a whole. Thus, in a rough analysis, the mass of a cluster is given by $m/M_\odot = \Upsilon_c(L/L_\odot)$. Most Galactic globulars are found to have mass-to-light ratios $\Upsilon \simeq 2M_\odot/L_\odot$ in the V band, with a range of $\sim 1-4$ allowed (Mandushev, Spassova, & Staneva 1991; Pryor & Meylan 1993), and perhaps with a weak tendency for the ratio to increase weakly with increasing cluster mass (Mandushev et al. 1991). A cluster with $M_V = -2$ therefore has a total mass of $m \simeq 1100M_\odot$, while one with $M_V = -10$ has $m \simeq 1.7 \times 10^6 M_\odot$.

In summary, globular clusters in the Milky Way exhibit a fairly wide, although relatively well defined, spectrum of properties: They range in luminosity from $\sim 500 - 10^6 L_\odot$ (mean $\langle L \rangle \simeq$

The abundances of other, lighter elements (e.g., $Z_{\rm CNO}$) are not always so constant throughout a cluster (see Suntzeff 1993; Kraft 1994), possibly reflecting evolutionary processes within the stars themselves.

$8 \times 10^4 L_\odot$), in mass from $\sim 10^3 - 2 \times 10^6 M_\odot$ (mean $\langle m \rangle \simeq 1.6 \times 10^5 M_\odot$), and in size from $r_h \sim 1$ pc to $r_h \sim 20$ pc (mean $\langle r_h \rangle \simeq 4$ pc); their heavy elements are distributed homogeneously among their member stars, but total abundances vary significantly from cluster to cluster, with $Z \sim 0.002 - 1.5 Z_\odot$ (mean $\langle Z \rangle \simeq 0.03 Z_\odot$); and they are all uniformly old, but not equally aged: $\tau \sim (12 - 16) \pm 3$ Gyr.

4.2.2 Globular Cluster Systems

Individual globular clusters are of considerable interest in their own right, as convenient laboratories for stellar evolution and N-body gravitational dynamics. But in addition to this, it has long been realized (at least since the pioneering effort to locate the center of the Galaxy by Shapley 1918) that the collective properties of the entire *globular cluster system* (GCS) can serve as effective probes of everything from the current structure, orbital dynamics, and mass of the Milky Way (e.g., Harris 1976; Hartwick & Sargent 1978; Frenk & White 1980), to the formation history and chemical evolution of its halo (Searle & Zinn 1978). This is so, simply because the clusters are as widely distributed and as ancient as they are. It is perhaps not surprising, then, that the GCSs of other galaxies, too, have increasingly been the targets of research over the past two decades.

Hubble (1932) was apparently the first to explicitly recognize extragalactic globular clusters, when he suggested that ~140 small objects projected against the disk of M31 were in fact some of its globulars; this identification was confirmed when Baade (1944a, b) was able to partially resolve some of these objects into their constituent stars. Studies of GCSs beyond the Local Group began when Baum (1955) first noticed an excess of faint, starlike objects gathered around M87, the giant cD galaxy[4] at the center of the 16-Mpc distant Virgo Cluster of galaxies. Later observations of these faint objects, by Racine (1968a, b) and, especially, Hanes (1971, 1977a, b), confirmed their identity as globular clusters, and essentially gave birth to a new subdiscipline of observational astronomy.

Observations of extragalactic GCSs are even simpler, in some respects, than those of Galactic globulars. A typical diameter of 10 pc subtends an angle of only $0''.5$ at a distance of 4 Mpc from the Milky Way, and clusters further out than this cannot be resolved into stars with ground-based

[4]Large galaxies tend to fall into one of three broad morphological classes: spirals (like the Milky Way and M31), ellipticals (like most of the galaxies which have been surveyed for GCSs), and cD galaxies. The members of this last group are characterized by a large, bright, elliptical "body" embedded in a larger (sometimes up to ~1 Mpc in size), diffuse "envelope" of starlight.

telescopes; globulars at "interesting" distances of 16 Mpc (e.g., in the Virgo Cluster) lie just at the resolution limits of even the Hubble Space Telescope (Elson & Schade 1994). Thus, these objects are normally identified as excesses of faint, starlike objects superimposed on the image of a galaxy. Their physical association with the galaxy is established if they show a significant increase in density (number per unit area on the sky) towards its center, and their identity as true globulars is established if they show a range in absolute magnitude and color that is consistent with what is seen in the Galactic GCS. Faint stars in the Milky Way that lie by chance in the line of sight to any galaxy will also be projected near it on the sky, however, as will distant small galaxies that lie behind the observed target. Thus, it is generally not possible to say, on a one-by-one basis, *which* of the stellar images around a galaxy is one of its globular clusters; analyses of extragalactic GCSs are necessarily statistical in nature. This loss of definition is offset by the great distances to which globular clusters can be seen (an object of $M_V = -10$ can still be observed without excessive difficulty at $D = 100$ Mpc and an apparent $V = 25$), and by the fact that a major portion of a distant galaxy's GCS can often be fit into one field of view. To illustrate this, Fig. 4.3 shows an image, taken through the V filter, of the M87 galaxy and its GCS (McLaughlin, Harris, & Hanes 1993, 1994).

Direct age measurements are precluded for extragalactic globulars, and in general it is simply assumed (with supporting evidence from their integrated photometric colors and spectra) that they are as old, $\tau \gtrsim 10$ Gyr, as the Milky Way globulars. Similarly, it is impossible to take individual spectra of their stars, and even integrated spectra are exceedingly difficult to obtain (although this latter situation is rapidly changing for the better with the advent of large, 8-m class telescopes). Thus, internal V-band mass-to-light ratios are usually assumed to be similar to the $\Upsilon \simeq 2M_\odot/L_\odot$ that obtains in Galactic globulars, and cluster metallicities are most often estimated by extrapolating on empirical correlations between photometric colors and $Z/Z_\odot$ in the Milky Way GCS. (This latter ploy relies on the fact that more metal-rich, or higher-Z, clusters are "redder." They emit more of their light at longer wavelengths, because the stronger heavy-element lines in their stars' atmospheres block more short-wavelength light.) And finally, GCSs are most readily studied in spiral galaxies whose disks are oriented nearly edge-on to the line of sight (so that the globulars run less of a risk of being projected against the disk and obscured by dust or confused with bright young clusters there) or in giant elliptical galaxies (where the cluster systems are intrinsically quite populous and easily

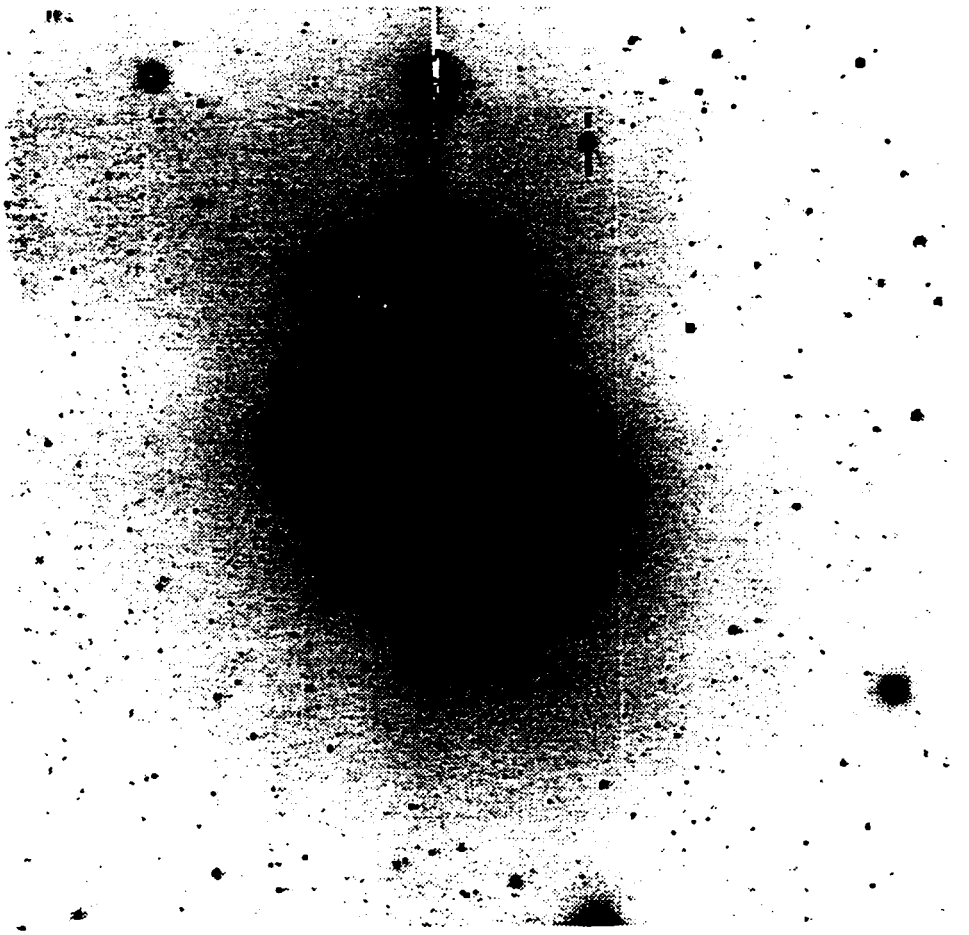

Figure 4.3: Globular clusters around M87, the central cD galaxy in the Virgo Cluster. Most of the starlike objects around the galaxy are its globular clusters. These number 15 000 in total for M87, with perhaps 20% of them visible on this image. The scale of the frame is approximately 14′ on a side, corresponding to 65 kpc at the distance (16 Mpc) of M87. From McLaughlin et al. (1993, 1994).

picked out from foreground and background objects).

Despite these limitations, much has been learned about the generic properties of GCSs, whose cluster populations number in the hundreds to thousands and are widely spread throughout the old halos (up to galactocentric radii $R_{\rm gc} \sim 100$ kpc) in galaxies of all types. Harris (1991) gives what is still a reasonably current overview of the observational status of this field, and we now summarize those results that, in our view, should be brought most to bear on theories of globular cluster and star formation.

Luminosity Functions

The number of globulars with absolute magnitude between M_V and $M_V + dM_V$ in any given GCS is denoted by $\phi(M_V) = dN/dM_V$, and is referred to as the *globular cluster luminosity function*, or GCLF, of the system. Since M_V reflects the intrinsic luminosities, and hence the masses, of globular clusters, the GCLF is directly related to the underlying mass spectrum, $N(m) = dN/dm$ of a GCS. This fundamental quantity is the main topic of Chapter 5 below (McLaughlin & Pudritz 1996a), and is discussed in detail there. Here we note just a few of the main features of GCLFs.

First, it has long been known that $\phi(M_V)$ *is a peaked function*, both in the Milky Way (see Harris & Racine 1979) and in other galaxies (Harris 1991); that is, the relative number of globulars with given M_V increases at first towards fainter M_V, but eventually decreases again. The *turnover magnitude* at which ϕ peaks in the Milky Way is $M_V^0 = -7.4$, which corresponds to a cluster mass of $m_* \simeq 1.6 \times 10^5 M_\odot$. The *apparent* turnover magnitude V^0 of any other GCLF, in any galaxy at a known distance, can then be converted to an absolute M_V^0 and compared to the Milky Way value (via eq. [4.9]; see Jacoby et al. 1992 for a review of distance measurement techniques). In every galaxy where this can been done reliably, it is found that the GCLF turnover is in agreement with the Galactic $M_V^0 = -7.4$ (cf. Harris 1991). (There have been recent suggestions [e.g., Fleming et al. 1995; Durrell et al. 1996] that M_V^0 might vary slightly, but systematically, between spiral, elliptical, and dwarf elliptical galaxies; however, given the observational errors involved, any claimed differences in M_V^0 are not significant.) Thus, M_V^0, or m_*, is a fundamental characterization of globular cluster systems. A side benefit of this is that the GCLF is of use as a distance indicator in its own right (Hanes 1977a; Hanes & Whittaker 1987; Jacoby et al. 1992; Secker 1992; Secker &

Harris 1993).

It is often the case that only the most visible members of extragalactic GCSs — which usually means those globulars brighter than M_V^0 and at R_{gc} greater than a few kpc — are directly observed. For clusters in these specific regimes, there is overwhelming evidence that the basic *shape* of the GCLF is similar (though *not exactly identical*) in all galaxies (e.g., Harris 1991). To repeat, this claim can be applied with strict confidence only to bright clusters outside the central regions of most galaxies; but in the handful of cases where GCLFs have been traced explicitly to magnitudes fainter than M_V^0 and/or to small R_{gc}, they still appear to conform to a roughly common base form that resembles that of the Milky Way GCLF (see McLaughlin & Pudritz 1996a for specific examples). Thus, although more extensive observations are required to be sure, it seems likely that GCLFs are similar in their entirety in different galaxies. When combined with the near-exact constancy of M_V^0, one of the immediate consequences of this is that the observed *range* of globular cluster masses in the Milky Way, viz. $10^3 - 10^6 M_\odot$ or so, appears to be typical of all GCSs.

In addition to this, there are strong hints that the turnover magnitude and the shape of the GCLF in any single GCS may *both* be identical among subsets of globulars at different galactocentric radii throughout the system (although see Kavelaars & Hanes 1997). This is certainly the case in the well studied Virgo cD M87 (McLaughlin et al. 1994; Harris, Harris, & McLaughlin 1997; Whitmore et al. 1995; see also McLaughlin & Pudritz 1996a). The conclusion relies most heavily on observations of the clusters brighter than the GCLF peak there, but appears to hold for the fainter ones as well.

Finally, as was mentioned just above, the GCLF is readily converted into a GCS mass spectrum. A detailed discussion of the connection between these two quantities, which respectively count the number of clusters appearing in given magnitude (or *logarithmic* mass) and linear mass intervals, can be found in McLaughlin (1994). Significantly, it has recently been noted (Harris & Pudritz 1994; McLaughlin & Pudritz 1996a; and references therein) that, above the mass $m_* \simeq 1.6 \times 10^5 M_\odot$ corresponding to M_V^0, GCS mass spectra can be reasonably described by power laws, $N(m) \propto m^\gamma$ with $\gamma \simeq -1.6$ to -2.0, that are reminiscent of those observed among Galactic GMCs and cores (cf. §5.1). Again, this point is discussed in more detail by McLaughlin & Pudritz (1996a).

Spatial Structures

It has always been clear that the surface density of globulars (i.e., the number projected into a unit area on the sky) decreases in a regular way with increasing distance R_{gc} from the center of any galaxy; that is, GCSs are centrally concentrated subsystems of galaxies. However, it also happens that GCS densities often fall off more slowly at large radii ($R_{gc} \gtrsim 5$ kpc) than do the surface densities of unresolved, non-cluster field stars in their parent galaxies (Harris & Racine 1979; Harris 1986). In fact, this structural contrast between GCSs and stellar halos is almost a defining characteristic of giant elliptical systems.[5] Meanwhile, at smaller $R_{gc} \lesssim 5$ kpc, evidence is mounting that most GCSs, in all types of galaxies, have *core radii* (the galactocentric distance at which the density of objects falls to half its central, $R_{gc} = 0$ value) that are significantly larger — by factors of $\sim 2 - 10$ — than those of the underlying stellar components of halos (see Lauer & Kormendy 1986 and McLaughlin 1995 for a discussion of this effect in M87; Grillmair et al. 1994 for the cD galaxy NGC 3311; Harris et al. 1991 for 3 elliptical galaxies in Virgo; Djorgovski & Meylan 1994 for the Milky Way; Durrell et al. 1995 for the dwarf elliptical near the isolated galaxy NGC 3115; and Forbes et al. 1996 for a sample of 14 ellipticals). Interestingly, the data of Forbes et al. (1996) indicate that GCS core radii may even be systematically larger in brighter galaxies. Taken together, the *larger core radii* of GCSs and the (often) *shallower slopes* of their number density profiles at large R_{gc} show that, by comparison with the underlying field-star populations of galaxies, GCSs on the whole are relatively distended; globular clusters are preferentially *less* centrally concentrated than the surrounding galaxy light of field stars.

Another important aspect of the spatial structure of GCSs, but one that has only recently been investigated in any detail, involves their overall shapes and the extent to which they agree or disagree with those of their parent galaxies. M87 is the best studied system in this regard: McLaughlin et al. (1994) find that the major-to-minor axis ratio of the globular cluster density distribution in this galaxy increases with increasing R_{gc}, and the GCS quickly becomes flatter, or more elliptical, than the distribution of underlying field stars. On the other hand, similar (though less

[5] In the Milky Way and some other small galaxies, though, the GCS and halo density profiles can be in close agreement (e.g., Harris 1976; Kissler-Patig 1997). At the other end of the scale, GCSs in the outer, envelope regions of large cD galaxies also tend to follow the general starlight rather faithfully; but this is likely saying something very specific about the unique formation history of these truly extreme objects (McLaughlin et al. 1995).

extensive) case studies of other systems (e.g., McLaughlin et al. 1995; Hilker & Kissler-Patig 1996; Kissler-Patig, Richtler, & Hilker 1996; Minniti, Meylan, & Kissler-Patig 1996; Forbes et al. 1996) tend to show better agreement between the shapes of GCSs and their galaxies' stellar halos. In all cases, the orientation of the GCS major axis appears to coincide with that of the galaxy as a whole. The implications of these results are not entirely clear; we mention them here only to suggest that a systematic study of GCS shapes should probably be carried out, and could prove especially interesting if many more systems like M87 are uncovered.

Specific Frequencies

Distant GCSs can rarely be observed in their entirety, due to a combination of (necessarily) incomplete spatial coverage of their parent galaxies, and instrumental limits on the detection of very faint objects. However, once the GCLF and spatial distribution of the brighter clusters in a system have been determined, they can be integrated to fainter magnitudes and larger galactocentric radii, to yield an estimate of the total population $N_\oplus$ of a GCS. Once this is had, the number of clusters can be compared to the total magnitude M_V^T of the parent galaxy (as some indication of the number of field stars there) to evaluate the so-called *specific frequency* (Harris & van den Bergh 1981):

$$S_N \equiv N_\oplus \times 10^{0.4(M_V^T+15)} . \tag{4.9}$$

The factor $10^{0.4M_V^T}$ here is just inversely proportional to the total luminosity $L_{\rm gal}$ of the galaxy, by equation (4.7), while the additive constant 15 is chosen, for convenience, to give S_N values that are of order unity rather than 10^{-8}.

Evidently, S_N is proportional to the number of clusters per unit galaxy light, and hence is a measure of the fraction of a galaxy's halo mass contained in bound clusters. To see this more explicitly, $N_\oplus$ can be related to the total mass in globular clusters, and $L_{\rm gal}$ to the total mass in all the stars of a galaxy (see also Harris & Pudritz 1994). First, it was mentioned above that the shape of the GCLF is similar in all galaxies, and its peak M_V^0 specifically is a near-universal constant. The average globular cluster mass in any galaxy is therefore similar to that ($\langle m \rangle \simeq 2 \times 10^5 M_\odot$) in the Milky Way, and the total mass of any GCS is just $M_\oplus = \langle m \rangle N_\oplus$. Second, the typical V-band mass-to-light ratio of the old halo stellar population in any galaxy is $\Upsilon \simeq 8 M_\odot/L_\odot$ (e.g., Faber

& Gallagher 1979; Binney & Tremaine 1987); hence, $M_{\rm gal}/M_\odot \simeq 8\,L_{\rm gal}/L_\odot$, and equation (4.7) is equivalent to $M_V^T = 7.09 - 2.5\,\log_{10}(M_{\rm gal}/M_\odot)$. Thus, equation (4.9) becomes

$$f_{\rm cl}^{\rm glob} \equiv \frac{M_\oplus}{M_{\rm gal}} \simeq 2.92 \times 10^{-4}\ S_N\ . \tag{4.10}$$

Harris (1991) and Durrell et al. (1996) summarize the S_N values typically observed for spiral and elliptical (including dwarf) galaxies. In the former, when the "total" $L_{\rm gal}$ is corrected to include only the light from the old halo (i.e., to avoid contributions from the younger stars in galactic disks, where globulars are generally not present in large numbers), $\langle S_N\rangle_{\rm Sp} \simeq 2 \pm 0.5$; in the latter types, $\langle S_N\rangle_{\rm E} \simeq 2.5 \pm 0.5$ (although with some standout exceptions) for galaxies that belong to sparse groups, and $\langle S_N\rangle_{\rm E} \simeq 5.5 \pm 0.5$ for members of rich clusters. There appears to be at least a weak correlation between a galaxy's S_N and its environment (specifically, the local number density of neighboring galaxies: West 1993; Kumai, Hashi, & Fujimoto 1993b). This effect may just be a restatement of the difference between the mean $\langle S_N\rangle$ of spirals and ellipticals, simply because the latter tend to be found in much denser regions of space than the former (Dressler 1980). A much wider range of specific frequency is seen in large cD galaxies, which are always located at high-density peaks in galaxy clusters (Beers & Geller 1983), and which have S_N values of anywhere from 4 to 20 (corresponding to total GCS populations as high as 20 000; see McLaughlin et al. 1994; Harris, Pritchet, & McClure 1995).

The factors influencing these variations in S_N between galaxies — and particularly the extreme values observed in many cD systems — are, in our view, not at all understood (although see West 1993, Kumai et al. 1993b, and West et al. 1995 for suggestions). But at the same time, it is rather striking that measured S_N are always similar at a rough, order-of-magnitude level (i.e., no GCS is known to have a specific frequency of 0.001, or of 1000). Specifically, with $S_N \sim 2 - 20$ over the whole spectrum of galaxies, equation (4.10) yields, for the halo mass fractions in bound clusters,

$$f_{\rm cl}^{\rm glob} \approx (0.6 - 6) \times 10^{-3}\ , \tag{4.11}$$

which is remarkably similar to the estimated mass fraction of molecular cores forming bound clusters (albeit less massive ones) in the disk of the Milky Way today (eq. [4.6]).

Finally, it should be noted that the S_N values we have been discussing here are global ones that compare the total mass in globular clusters to that in other stars throughout entire galaxies. However, in galaxies with large cluster populations, and hence good number statistics, it is also possible to compute *local* specific frequencies which compare the number of globulars at some specific galactocentric radius, to the brightness of the galaxy light just at that same $R_{\rm gc}$. This has been done for M49 and M87 (Harris 1991; McLaughlin et al. 1994), both of which are members of the Virgo Cluster. In these galaxies it is found that S_N, *and hence* $f_{\rm cl}^{\rm glob}$, *increases with increasing* $R_{\rm gc}$. That this is actually expected to be a generic feature of many GCSs can be seen from the definition (4.9) of S_N and the fact, noted above, that GCSs tend to have larger core radii and shallower density fall-offs than the light from halo field-star populations. Again, then, globular clusters are preferentially found at larger distances (relative to field stars) from the centers of galaxies.

Metal Abundances

It was mentioned above that the average metallicites of globular clusters can be estimated from their integrated photometric colors. Especially useful in this regard has been the so-called Washington system of filters; in particular, the $(C-T_1)$ index — the difference between magnitudes in a blue filter (C) and a redder one (T_1) — is well known (Geisler & Forte 1990; Geisler, Lee, & Kim 1996) to sensitively and accurately reflect the overall Z-values of individual globulars in the Milky Way and other galaxies. Thus, observations of Washington $(C-T_1)$ colors have recently been used to investigate the metallicity systematics in several extragalactic GCSs (see Geisler & Forte 1990; Harris et al. 1992; Ostrov, Geisler, & Forte 1993; Lee & Geisler 1993; Secker et al. 1995; Zepf, Ashman, & Geisler, 1995; Geisler et al. 1996; Durrell et al. 1996). The results of these studies, along with those of many others that use different photometric systems to estimate cluster metallicities (see Harris 1991, and references therein), point to at least three more main features of GCSs.

First, the mean metallicity $\langle Z\rangle_{\rm GCS}$ of the clusters in a GCS is found to depend on the total luminosity of its parent galaxy, roughly as $\langle Z\rangle_{\rm GCS} \propto L_{\rm gal}^{0.4}$ (van den Bergh 1975; Brodie & Huchra 1991; Secker et al. 1995; Forbes et al. 1996). The compilation of data by Forbes et al. (1996), in particular, shows that this relation holds in galaxies of all types and sizes, from dwarf ellipticals with $M_V^T \sim -14$ and $\langle Z\rangle_{\rm GCS} \sim 0.01 Z_\odot$, through the spirals and giant ellipticals, and on to cD galaxies

with $M_V^T \sim -23$ and $\langle Z\rangle_{\rm GCS}/Z_\odot$ as high as 1. The power-law exponent of the $\langle Z\rangle_{\rm GCS} - L_{\rm gal}$ relation is identical to that of a similar scaling between the luminosities and the mean Z of entire galaxies (Brodie & Huchra 1991).

Second, the individual clusters in most GCSs are *not* confined to a narrow interval about the mean $\langle Z\rangle_{\rm GCS}$ but exhibit a wide range of metallicities. It will be recalled, for instance, that the Milky Way globulars show $0.002 \lesssim Z/Z_\odot \lesssim 1$. Two other good examples of this are provided by the cD galaxy NGC 3311 (Secker et al. 1995), for which $\langle Z\rangle_{\rm GCS} \simeq 0.5Z_\odot$, but whose clusters span a range of $0.01 \lesssim Z/Z_\odot \lesssim 5$ (with fully *one-third* of the globulars having $Z > Z_\odot$); and by the giant elliptical M49 (Geisler et al. 1996), which has $\langle Z\rangle_{\rm GCS} \simeq 0.1Z_\odot$ and, again, $0.01 \leq Z/Z_\odot \leq 5$. It has recently become apparent (e.g., Zepf & Ashman 1993; Lee & Geisler 1993; Secker et al. 1995; Zepf et al. 1995; and especially Geisler et al. 1996) that the broad ranges of metallicities in the GCSs of individual ellipticals are often due to the presence of at least two distinct (and roughly equally populated) groups of globulars in the galaxies, that have abundances clustered around significantly different mean Z-values. This is also seen in the Milky Way, where the clusters associated with the disk (or the bulge) are systematically metal-richer than those firmly in the halo (Zinn 1985). Thus, most GCSs may comprise separate metal-poor and metal-rich subsystems. It has been suggested (Ashman & Bird 1993; Forbes, Brodie, & Grillmair 1997) that the former typically have $\langle Z\rangle_{\rm poor} \sim 0.05Z_\odot$ in *any* galaxy; the latter, with $\langle Z\rangle_{\rm rich} \sim 0.3 - 1.5Z_\odot$ depending on the size of their host galaxy, would then effectively drive the total $\langle Z\rangle_{\rm GCS} - L_{\rm gal}$ correlation. This interesting possibility needs to be investigated further.

And third, the interiors of globular clusters beyond the Local Group are mostly unobservable at the present time, so that the internal chemical homogeneity that is seen in most Galactic globulars cannot be directly confirmed in many other systems. Nonetheless, it is significant that there is no relation, of any kind, in any galaxy, between the metallicities and luminosities (or masses) of globular clusters. This indicates that most globulars are *not* self-enriched objects;[6] rather, their heavy metal contents had to have been set while they were still largely gaseous, and before their stars formed. (If this were not true, then metal abundance would be expected to increase with cluster mass, simply

[6]Self-enrichment refers to the process in which very massive stars in a young cluster (i.e., one that is still partly gaseous and forming stars) inevitably explode as supernovae, thereby spilling the elements synthesized in their interiors into the cluster at large, and raising the average metallicity of any stars that form afterwards.

because more massive self-enriched objects are better able both to form very massive stars early on and to ultimately retain their metal-enriched supernova ejecta.) This in turn suggests, albeit somewhat indirectly, that internal chemical homogeneity is likely the rule among most globular clusters (see also Murray & Lin 1990).

There are other intriguing, if rather more mysterious, aspects of GCS metallicities. For example, the mean cluster metallicity decreases with increasing galactocentric radius in some systems, but remains constant throughout others (see, e.g., Ajhar, Blakeslee, & Tonry 1994; Forbes et al. 1996, 1997; Harris 1996a). Also, the globular clusters in many giant and dwarf ellipticals appear to be metal-poorer, by a factor of perhaps 3 in the mean, than the general field populations of the galaxies (Harris 1991; Durrell et al. 1996). However, this is clearly not a universal phenomenon, as the mean abundance of the Milky Way GCS is essentially coincident with that of its unclustered halo stars (Laird et al. 1988). The origins of these metallicity gradients and offsets in GCSs are not clear at the present time; nor is there any general consensus as to why they appear in some galaxies and not in others. In any case, the cluster-to-cluster *spread* in Z, in any GCS, is always larger than any radial gradient or offset from the halo in the clusters' *mean* $\langle Z \rangle$.

4.3 Fossil Records or Chance Survivors?

To summarize the observations just discussed, we believe that the following traits of GCSs are firmly enough established, in a sufficient number of diverse systems, that they should serve as general constraints on any complete theory of cluster formation:

1. The frequency distribution of globular cluster numbers per unit magnitude — the GCLF — peaks at a well defined $M_V^0 \simeq -7.4$, corresponding to a cluster mass of $m_* \simeq 1.6 \times 10^5 M_\odot$, that appears to be a near-universal constant between and within galaxies. At magnitudes brighter than M_V^0 (masses greater than m_*) and galactocentric radii greater than ~ 5 kpc, and probably also for fainter M_V and smaller R_{gc}, the shape of the GCLF is *similar in different galaxies* (although differences in detail do exist, and have to be accounted for), and is *independent of* R_{gc} *within individual systems.* The total spread in cluster masses is similar ($m \sim 10^3 - 10^6 M_\odot$) in all galaxies, and the mass spectra $N(m)$ that correspond to GCLFs are similar, above m_*,

to those seen in Galactic GMCs and cores.

2. Globular clusters are spatially concentrated towards the centers of the galaxies in which they are found. But at the same time, GCSs typically have larger core radii, and often show shallower density profiles overall, than field stars do; i.e., the number density of globular clusters falls off more slowly towards larger $R_{\rm gc}$ than does the density of unclustered halo stars in galaxies.

3. The global specific frequencies of most GCSs (with a typical $S_N \sim 5$, and a range of $2 \lesssim S_N \lesssim 20$) correspond to cluster-to-field star mass fractions of $f_{\rm cl}^{\rm glob} \sim 1.5 \times 10^{-3}$ [with limits of roughly $(0.6 - 6) \times 10^{-3}$], which is similar to the mass fraction of cores that are currently forming bound clusters in the Milky Way. Local specific frequencies, or $f_{\rm cl}^{\rm glob}$, tend to increase with radius inside galaxies.

4. The average metallicity of globulars in a GCS correlates with their parent galaxy's luminosity, roughly as $\langle Z \rangle_{\rm GCS} \propto L_{\rm gal}^{0.4}$, and the clusters in any one GCS are distributed over a wide range in total abundance; globular clusters exist with Z anywhere between 1/1000 and 5 times the solar value. Internally, individual clusters appear to be chemically homogeneous in general.

We now offer a brief justification of our view that these features do indeed reflect something of the *formation* process of clusters, and have not resulted entirely from their evolution in the galaxies they have inhabited for the last 15 Gyr.

There can be no doubt that the metallicities of globular clusters are determined at some very early stage in their lives. This is particularly true if the degree of chemical homogeneity in these objects is generally as high (and that of self-enrichment as low) as we have argued, since then cluster Z-values necessarily reflect those of the gases from which they condensed. The interpretation that globular cluster abundances are relics of their formation epoch is unequivocal, and the implication is that the presence of heavy metals is in no way an impediment to this mode of star formation. *Metallicities should therefore not play a primary role in cluster formation theories.*

Similarly, given the order-of-magnitude level at which it is found to be the same in all galaxies, the specific frequency of a GCS, or the fraction $f_{\rm cl}^{\rm glob}$ of a galaxy's stellar mass contained in globulars, must be a reflection of the early *formation* efficiency of bound clusters. Even if dynamical

evolution (see below) has destroyed a large *number* of low-mass clusters in GCSs over the past 15 Gyr, the form of the GCLF, or mass spectrum, is such that the total *masses* of cluster systems should not have decreased by more than a factor of $\sim$2 from their initial values (e.g., Harris & Pudritz 1994). The smaller (but important) variations in S_N between galaxies of different types or in different environments most likely also stem largely from initial conditions; but even if they are instead affected by any number of specific evolutionary processes in the individual galaxies, these clearly can effect only secondary fluctuations on a base $f_{\rm cl}^{\rm glob} \sim 2 \times 10^{-3}$. The fact that $f_{\rm cl}^{\rm glob}$ is always comparable to the current $f_{\rm cl}$ for open cluster formation in the Milky Way (and apparently M31 as well; cf. §5.1) implies, once again, that *the formation of old globular clusters may have just been the earliest realization of a truly generic process that has not much changed, other than in terms of scale, to the present day.* General cluster formation theories should therefore aim to account for the typical value of $f_{\rm cl}$, and for its observed increase with radius inside most galaxies.

Our claim that GCS density profiles and luminosity functions also still reflect their initial conditions requires a slightly more detailed defence, simply because globular clusters live in galaxies, where they are necessarily subjected to numerous internal and external evolutionary influences that can work to destroy them on Gyr timescales. In general, these influences vary in strength depending on the mass of a cluster and its location within a galaxy; thus, they could conceivably alter the spatial structures and mass spectra of GCSs.

It has long been recognized that, even in isolation, and even if their stars were not destined to eventually burn out, globular clusters cannot be infinitely long-lived. The main cause of the demise of an idealized, isolated cluster would be its inevitable *evaporation* (e.g., Johnstone 1993; Spitzer 1987, and references therein): gravitational encounters between stars within the cluster drive the system towards a Maxwellian (or Gaussian) distribution of velocities, such that some of the stars reach high enough velocities and kinetic energies to enable their escape from the gravitational field of the cluster. The high-velocity "tail" of the Maxwellian is continuously repopulated, and the stars there lost, until the cluster more or less just fades away. Much the same process goes on, although with some quantitative adjustments, in the more realistic situation where a cluster is embedded in the external gravitational field of a galaxy (e.g., Spitzer & Chevalier 1973; Oh & Lin 1992; Lee & Goodman 1995). In addition to this, however, several other effects are potentially important.

Quite generally, if the cluster on its orbit encounters an impulsive force due to a dense component of its parent galaxy, the *tidal shock* it experiences will increase its total internal energy (recall that bound stellar systems have a total $\mathcal{E}_{\rm stars} \leq 0$). If enough strong shocks are received over time, their cumulative effect is to boost $\mathcal{E}_{\rm stars}$ above 0, and disrupt the cluster. Such shocks can occur when a globular passes through the disk of a galaxy (Ostriker, Spitzer, & Chevalier 1972; Aguilar, Hut, & Ostriker 1988), or through its dense central bulge region (Aguilar et al. 1988; Ostriker, Binney, & Saha 1989; Charlton & Laguna 1995). Also, the nuclei of most galaxies of all types may harbor *supermassive black holes* (with $M_\bullet \sim 10^6 - 10^9 M_\odot$; Kormendy & Richstone 1995) which are capable of scattering and shocking globulars that stray too close (Gerhard & Binney 1985; Ostriker et al. 1989; Capuzzo-Dolcetta 1993). And finally, the unclustered field stars in a galaxy exert a kind of gravitational drag on any dense object, such as a globular cluster, that moves through them. This *dynamical friction* acts as a sink of angular momentum for the cluster, causing it to spiral in towards the center of a galaxy (Tremaine, Ostriker, & Spitzer 1975; Tremaine 1976; Pesce, Capuzzo-Dolcetta, & Vietri 1992).

Given such a varied list of theoretical destruction mechanisms, it seems at least vaguely surprising that many globular clusters have survived to the present time. Indeed, the first comprehensive study of the combined effects of most of these processes, on globular clusters in the Milky Way specifically (Aguilar et al. 1988), concluded that disruption is so easily effected that "the present globular cluster population is but a shadow of its former self," with perhaps $20 - 80\%$ of the initial Galactic GCS (by number) having been destroyed over the past $\sim$10 Gyr. Rather alarmingly, more recent evaluations of evaporation and of tidal-shock "heating" (e.g., Weinberg 1994a, b, c; Kundić & Ostriker 1995; Gnedin & Ostriker 1997) have suggested that these processes are even more powerful than previously thought. At first glance, this would seem to imply that, as was apparently first suggested by Fall & Rees (1977; see also Caputo & Castellani 1984), GCSs have been sculpted largely by dynamical forces within their parent galaxies, and that their systemic properties therefore reflect their evolution more than their formation. This premise has served specifically to guide various theoretical attempts to explain both the present-day luminosity function of the Galactic globular clusters (Surdin 1979; Okazaki & Tosa 1995; Vesperini 1997) and the sizes of the GCS core radii in M87 and other elliptical galaxies (Ostriker et al. 1989; Capuzzo-Dolcetta 1993; Murali & Weinberg

1997).

In spite of all this, however, *the large core radii of most GCSs and the observed shapes of their GCLFs cannot be ascribed entirely to the cumulative influence of cluster destruction mechanisms.* It is hard to imagine that these theoretically powerful processes could be of *no* consequence in reality, and this is not what we claim; certainly tidal shocks, evaporation, and the like are important in the lives of some — even most — globular clusters. But the simple *observed* fact is that the features of GCSs isolated specifically in points (1) and (2) above are exceedingly regular, and appear in many galaxies of many different types. Thus, for example, any attempt to explain them as the result of disk shocking must fail, since not all galaxies contain disks. Similarly, any claim that dynamical friction plays a dominant role in the long-term evolution of GCSs has to be viewed with suspicion, simply because this process should cause denser clusters at smaller galactocentric radii to sink more rapidly to the centers of their galaxies, and thereby create *unobserved* radial gradients in the bright, or high-mass, tails of GCLFs. (Moreover, in the Milky Way at least, there is a dearth of massive clusters at large $R_{\rm gc} \gtrsim 10$ kpc, where dynamical friction would have allowed them to survive; e.g., Caputo & Castellani 1984.)

Encounters with stellar bulges and nuclear black holes most efficiently destroy low-mass clusters at small galactocentric radii ($R_{\rm gc} \lesssim 5$ kpc or so; see the references cited above), and are therefore unable to account for the characteristic shapes of GCLFs above M_V^0 throughout galaxy halos. Such shocks do work to erode GCSs from the inside out, however, and thus might still be thought responsible for enlarging their core radii relative to their galaxies' underlying stellar light. We would caution against this interpretation, however, as it has yet to be shown that this process is independent enough of the specific local conditions in different parent galaxies to account for the apparent universality of the core radius discrepancy. In fact, the most recent work on this topic (Murali & Weinberg 1997) claims that the GCSs in bright elliptical galaxies should evolve more slowly than those in fainter ones, because larger galaxies are well known to be less dense in their central regions (e.g., Djorgovski & Davis 1987; Faber et al. 1987). If it is hypothesized that all GCSs were born with core radii equal to those of their parent galaxies, this would suggest that brighter galaxies should now show better agreement between the core radii of their GCSs and their unclustered halos. However, the ratios of GCS-to-galaxy core radii in 14 ellipticals studied by

Forbes et al. (1996) do not show *any* obvious correlation with galaxy luminosity. Although further observations and more general theories are required, it seems inevitable that the large core radii of GCSs have to date back, at least in part, to their formation.

More generally, if any feature common to most GCSs is to be at all explained through the destruction of clusters, the mechanisms responsible must be able to work independently of local external conditions to destroy globulars uniformly across galaxies of all types. The only real candidates for such mechanisms are those driven by processes *internal* to the clusters themselves, namely, evaporation and the loss of mass from individual member stars during the natural course of their evolution (e.g., Chernoff & Shapiro 1987; Chernoff & Weinberg 1990). We discuss the possible influence that evaporation specifically has had on GCLFs in Chapter 6. Here we note only that the universality of the GCLF turnover, at $M_V^0 \simeq -7.4$ or $m_* \simeq 1.6 \times 10^5 M_\odot$, strongly hints that it is fundamental in nature, and not evolutionary in origin. Similarly, the facts that present-day GCLFs vary so little between galaxies, and are so similar above m_* to the mass spectra of GMCs and cores, argue for the interpretation that they have been left essentially untouched, *at least* at large cluster masses or bright magnitudes, from the time of their formation.

In summary, it seems clear that the four general traits of GCSs listed at the beginning of this Section must reflect something of the cluster formation process. This conclusion does appear to be mysteriously at odds with some theoretical calculations of globular cluster evolution; but even without understanding the origin of this conundrum, or being able to foresee its solution, an attempt to formulate a theory of cluster formation that can ultimately use these observations as constraints is well justified.

4.4 Globular Cluster Formation

Before discussing the particular model of globular cluster formation that McLaughlin & Pudritz (1996a) explore in detail, we briefly review some of the more prominent theories that have been proposed in the past for these objects. Following Fall & Rees (1988), these theories can be classified as primary, secondary, or tertiary, according to whether they place the globular cluster formation era before, during, or after the epoch of large-scale collapse and overall star formation in a gaseous protogalaxy.

The main idea of primary models, which are motivated largely by the observed consonance of *some* aspects of GCSs (such as the peak of the GCLF) from galaxy to galaxy, is that globular clusters were the first, or among the first, gravitationally bound systems to have condensed in the early universe. In their simplest form (Peebles & Dicke 1968), such models posit that all clusters were born when the universe was only $\sim 3 \times 10^7$ yr old and had a temperature $T \sim 10^4$ K, so that the critical Jeans mass for gravitational instability was $m \sim 10^5 - 10^6 M_\odot$ (see also eq. [4.12] below). The principal flaw in this idea is probably that it predicts *too* uniform a spectrum of globular cluster properties: since they are supposed to form before galaxies by definition, it is difficult to account quantitatively for observations that GCSs are spatially concentrated to the centers of galaxies; for the fact that their elliptical shapes and orientations are often similar to those of their parent galaxies; for the possibility that their core radii increase with galaxy luminosity; or for their mean metallicities $\langle Z \rangle_{\rm GCS}$, which again depend on galaxy luminosity, and which lie far above primordial, $Z \simeq 0$ values anyway. *Globular clusters had to have been aware, at some level, of the galaxies around which they formed*, and thus could not have appeared too far ahead of them. More recent considerations of pregalactic formation (e.g., Peebles 1984; Rosenblatt, Faber, & Blumenthal 1988) address some of these issues to some degree, but ultimately rely on the adoption of specific cosmological frameworks that involve poorly constrained model parameters and that may or may not prove to be correct in the long run. These theories also predict that individual globulars should be surrounded by massive halos of non-stellar dark matter, which may not be the case (Moore 1996; but see also Taillet, Salati, & Longaretti 1996). An interesting contribution by West (1993) aims specifically to explain the variation in GCS specific frequencies among galaxies in different environments via a slightly less cosmology-dependent argument that represents globulars as statistical density fluctuations whose numbers are enhanced near larger peaks (i.e., in denser regions) in the overall primeval density field. While this approach does seem reasonably able to reproduce observed, systemic S_N values, it may again be hampered by predicting too much uniformity among individual cluster properties in different galaxies.

The only tertiary model that has received serious consideration in recent years (see Harris 1991 or Harris et al. 1995 for a critique of earlier tertiary formation schemes) advances the idea that a significant fraction of the globular clusters in large elliptical galaxies — which, taken together,

account for most of the known globulars in the universe — were preferentially formed at the hot, dense interfaces of colliding clouds or streams of gas during merger events that involved *pre-existing* galaxies (presumably spirals) and that were also responsible for the formation of the larger galaxies themselves (Schweizer 1987; Ashman & Zepf 1992; Zepf & Ashman 1993; see also Kumai, Basu, & Fujimoto 1993a). While it is clear that globular-like clusters do form in galaxy mergers (cf. §5.1), the view that most of them (and most elliptical galaxies) formed in this way is certainly too extreme. Quantitatively, the current version of the merger model appears to face serious difficulties in accounting for detailed observations of GCS systematics (e.g., Geisler et al. 1996; Forbes et al. 1997); and more fundamentally, the formation of hundreds or thousands of typical, $m \sim 10^3 - 10^6 M_\odot$ globular clusters during mergers would require, given that $f_{\rm cl}^{\rm glob} \sim 10^{-3}$, the involvement of vast amounts ($\sim 10^{10} - 10^{11} M_\odot$) of gas. This necessarily pushes the cluster formation epoch back to that of galaxy formation itself, which is the only time when such quantities of gas were available as a matter of course; but then the "merger" idea is indistinguishable from any secondary formation model that allows for the *collapse of protogalaxies from clumpy initial conditions* (see Harris 1995).

Over the past decade, the work of Fall & Rees (1985) has served as the starting point for many theories of globular cluster formation. This model, which is of the secondary class, is similar to the primary models mentioned above, in that it focuses on the search for an appropriate epoch at which a "characteristic" cluster mass of $\sim 10^6 M_\odot$ was naturally selected. Rather than placing this era in the pregalactic universe, however, Fall & Rees (1985) argue that globular clusters should form during the gaseous collapse of protogalaxies. Essentially, the original theory, which was applied specifically to the Milky Way, relies on a two-phase model of the protogalactic gas that is similar to those (cf. §1.2 above) which have been applied to the present-day diffuse ISM in the Galaxy: Hot, diffuse gas with a *virial temperature* of $T_h \sim 2 \times 10^6$ K (obtained by equating its thermal and kinetic energies) and a density of $n_h \sim 0.15$ cm^{-3} (at a Galactocentric radius of 10 kpc), is spread throughout the gravitational well of the early Galaxy and supposed to be thermally unstable, such that density fluctuations in it rapidly develop, *under conditions of constant pressure* nkT, into colder ($T_c \sim 10^4$ K), denser ($n_c \sim 30$ cm^{-3}) condensations. The hot halo gas naturally exerts a surface pressure $P_s \sim 3 \times 10^5\ k$ cm^{-3} K on these *purely thermally supported clouds*, such that their critical, Bonnor-Ebert (or Jeans) mass at $R_{\rm gc} = 10$ kpc is [see Fall & Rees 1985; or eq. (2.11a) of McLaughlin

& Pudritz 1996b, for an isothermal equation of state and $\sigma_{\rm ave} = \sigma_{\rm T} = (kT/\mu m_H)^{1/2}$]

$$m_{\rm crit} \simeq 2.5 \times 10^6 \; M_\odot \left(\frac{T_c}{10^4 \; {\rm K}}\right)^2 \left(\frac{P_s}{3 \times 10^5 \; k \; {\rm cm^{-3}} \; {\rm K}}\right)^{-1/2} . \qquad (4.12)$$

The surface pressure P_s here is expected to decrease systematically towards larger Galactocentric radii, as is n_h; specifically, for an isothermal protogalaxy, $P_s \propto n_h \propto R_{\rm gc}^{-2}$.

The rough similarity that the result (4.12) bears to the largest globular cluster masses led Fall & Rees (1985) to suggest that the critical-mass cold clouds in this type of early two-phase medium could be the progenitors of the globulars, *so long as a characteristic temperature of* $T \sim 10^4$ K *could be maintained in them.* Much of the original Fall & Rees paper is therefore devoted to a discussion of the various heating and cooling mechanisms *in essentially metal-free gas* ($Z \lesssim 0.01 Z_\odot$), in an attempt to show that this temperature condition could plausibly be met. They conclude that cooling by molecular and atomic processes in the clouds could be balanced, at a temperature around $T \sim 10^4$ K, by heating from the absorption of X-ray radiation from the hot phase of the halo gas, if molecular hydrogen was present in only trace amounts [specifically, for $n(H_2)/n(HI) \sim 10^{-5}$, which is expected in an equilibrium between the rates of its dissociation and formation in the gas phase, and is similar to the result of eq. (1.10) above]. However, it was soon realized (Shapiro & Kang 1987; Palla & Zinnecker 1988; Ashman 1990) that H_2 should form efficiently under *non-equilibrium* conditions in these types of clouds, such that $n(H_2)/n(HI) \sim 10^{-3} - 10^{-2}$. The radiation from line transitions in such large amounts of H_2 would lead to rapid cooling to temperatures as low as $T \sim 100$ K, corresponding to $m_{\rm crit} \sim 10^2 - 10^3 M_\odot$ by equation (4.12); even in the absence of any metals at all, there would be no long-lived phase at $T \sim 10^4$ K and $m_{\rm crit} \sim 10^6 M_\odot$, and the entire "Jeans-mass" interpretation of globular clusters would be vitiated. This problem only worsens if the inevitable presence of significant amounts of heavy metals in the protocluster clouds is acknowledged, and the additional cooling by their line radiation taken into account. Attempts to circumvent these difficulties (e.g., Kang et al. 1990; Murray & Lin 1992) rely on the supposed presence of additional *external* sources of strong heating for the clouds (mostly in the form of dissociating ultraviolet radiation, such as might arise from activity in a protogalactic nucleus, or from shocks in the hot phase of the collapsing halo) to offset the molecular and metal-line cooling and allow the clouds to "hang" at 10^4 K long enough to be imprinted with masses of order $10^6 M_\odot$.

As Murray & Lin (1992, 1993) stress, it does seem inevitable that some additional source of support is required to sustain protocluster clouds for timescales longer than those on which their thermal energy is radiated away by internal atomic and molecular processes. This is simply because it is thought that if a cloud cools too rapidly — specifically, on less than a gravitational free-fall timescale — it will become unstable to fragmentation (Rees & Ostriker 1977; Silk 1977), and form individual stars before it can contract as a whole to contain them and form a bound stellar cluster. However, even at their most generous, realistic external heat sources appear able to balance cooling well enough to allow the formation of globular-sized clusters only if $Z \lesssim 0.1 Z_{\odot}$; but this fails to account for a very large fraction of the globulars in galaxies other than the Milky Way. In addition, such external heating mechanisms are bound to be galaxy-specific, and thus run the risk of introducing strong, and unobserved, environmental dependences into such quantities as globular cluster masses. An alternative to external sources of protocluster support (Harris & Pudritz 1994) is discussed below.

A rather more conceptual, but no less important, difficulty with the Fall & Rees (1985) model is that, as was mentioned above, it is based on the explicit assumption that there is such a thing as a "characteristic" cluster mass. That is, the theory specifically associates *only* the critical-mass clouds at $T \sim 10^4$ K with the progenitors of globular clusters, and assumes that the wide *range* in the masses (and other properties) of globular clusters today have resulted from the erosion of some very narrow initial distribution. However, as we suggested in §5.3, and as McLaughlin & Pudritz (1996a) also argue, this mass range, $m \sim 10^3 - 10^6 M_{\odot}$, and the distribution of clusters throughout it, are more likely relics of the formation epoch. This suggests that there is *no* "preferred" globular cluster mass (also see Harris & Pudritz 1994), in which case any theoretical insistence on a correspondence between globulars and critical clouds at a single Jeans mass, at any temperature, may be somewhat specious. Moreover, even if globular clusters were all descended from gas clouds with masses given by equation (4.12), then the dependence of $m_{\rm crit}$ on P_s would cause this "typical" cluster mass to vary significantly throughout any galaxy (according to $m_{\rm crit} \propto P_s^{-1/2} \propto R_{\rm gc}$, under the assumption of isothermality in the hot halo gas), as well as between systems (the value of P_s depends on the virial temperature T_h, which increases in direct proportion to the total mass of a halo).

A more recent, and more realistic (although still only semi-quantitative), discussion of this

issue is given by Murray & Lin (1993), who argue that the Jeans mass in the Fall & Rees framework only places an upper limit on allowed globular cluster masses. But the fact remains that *models of this type examine a mechanism of cluster formation that bears little, if any, relation to the star-formation process as it occurs today*: GMCs and cores in the Galaxy *cannot* be understood as components of a multiphase ISM in pressure equilibrium with more diffuse gas, and they are *never* supported entirely by their internal thermal pressures (cf. §1.5.3). To be fair, it has to be noted that such a dissimilarity is quite consciously built into these theories, which take the express point of view that the formation of old globulars was indeed a special process that has seen no true counterpart since the protogalactic era. However, we do not see that there is any particularly compelling need for such an assumption. On the contrary, as we have stressed throughout the discussion here, stars still form in groups in the Milky Way today, where they emerge as bound clusters with an efficiency $f_{\rm cl}$ similar to that which obtained in GCSs 15 Gyr ago; and young clusters very much like globulars are, in fact, commonplace in many other galaxies around us (§5.1). A deliberate attempt to explain the formation of old globular clusters without any reference to these facts — or vice versa — seems, to us, to bring an unnecessary element of complexity into the problem.

4.4.1 Supergiant Molecular Clouds

Larson (1988, 1993, 1996), especially, has argued forcefully that a broader view of globular clusters can and should be taken. In particular, he suggests a move away from the idea that these objects formed as discrete and essentially isolated units of $m \sim 10^3 - 10^6 M_\odot$ scattered throughout hot protogalaxies with $M_{\rm gal} \sim 10^{11} M_\odot$, and towards the idea that, like the clusters and groups of stars being born today, old globulars everywhere formed in the densest parts of much larger, *but still subgalactic* ($m \sim 10^8 - 10^9 M_\odot$), star-forming complexes. This possibility provides neatly for a framework within which all of the systematics of GCSs outlined in §5.2.2 can be addressed, in a way that relates directly to the observed pattern of star formation in GMCs and cores today. Moreover, as we briefly discuss below, such a framework meshes well with evidence suggesting that the formation of most large galaxies involved at least some amount of chaotic merging and accretion of gaseous protogalactic "fragments" over an extended period of time (Larson 1992).

The globular cluster formation theory of Harris & Pudritz (1994) is built on a more detailed

statement of these ideas. The theory is again of the secondary type, as it envisages bound globular clusters forming at around the same time as the bulk of their parent galaxies' stars. It also still assumes, similar to the stipulation of Fall & Rees (1985), that protogalaxies are already defined on large scales, as gravitational potential wells containing some amount of hot, virialized gas (e.g., with $T_h \sim 2 \times 10^6$ K and $P_s \sim 3 \times 10^5\ k$ cm^{-3} K at $R_{gc} \sim 10$ kpc in the early Milky Way specifically), when star formation begins in them. However, this virialized component of the halo gas is now supposed to envelop discrete clouds that are much more massive than any one globular cluster. These clouds are not the direct precursors of single globulars, but serve as the analogues of the GMCs in the Galaxy today; thus, they are referred to as *supergiant molecular clouds* (SGMCs). [It has to be stressed that the term "molecular" should not necessarily be taken literally here; the actual molecular abundance $n(H_2)/n(HI)$ in any given SGMC will depend on its metallicity Z, on its dust-to-gas ratio, and on the level of background flux in dissociating X-ray or UV radiation; cf. the brief mention of H_2 abundances above, and §1.3.3. These objects are called SGMCs primarily to advertise their connection with star-forming clouds as we know them today.] The SGMCs are taken to be self-gravitating (and therefore *not* in exact pressure equilibrium with the hot halo), and internally virialized in the simple sense that $2\,\mathcal{U} + \mathcal{W} = 0$ (as is observed among present-day GMCs; cf. Chapter 1 above).

Given the possibility, mentioned above, that a significant amount of H_2 — perhaps one part in 100 or 1000 — could be built up under non-equilibrium conditions in protogalactic gas, these SGMCs are expected to have temperatures of order ~100 K or so (the exact T in any given cloud will depend on its dust content and its metal abundance, which could be at or above solar levels). And yet, as we've just suggested, they are hypothesized to have $m \gg 10^5 M_\odot$ in general. If they are to be stable structures, then, equation (4.12) shows that they must be supported on large scales by something other than their thermal pressures. In a sense, this parallels the need for extra heating of the cold protocluster clouds in the Fall & Rees picture. However, in the Harris & Pudritz (1994) scheme, the burden of cloud support is removed from external, environment- and metallicity-dependent (and still thermal) factors, and placed instead with the internal physics of the clouds themselves. Thus, *SGMCs are supposed to be supported against their self-gravity by a significant nonthermal component of internal pressure* — again, like GMCs in the Galaxy are today. Moreover,

Harris & Pudritz suggest that the source of the nonthermal motions in SGMCs ultimately lies with the same mechanism operating currently in Galactic clouds and cores, i.e., probably with disordered magnetic fields and MHD turbulence. The mean components of fields, which are expected to be in equipartition with the kinetic energy $\mathcal{U}$, then also contribute to cloud support, as discussed in Chapter 1 above and in McLaughlin & Pudritz 1996b. Together with the assumed $2\,\mathcal{U} + \mathcal{W} = 0$ for these objects, this implies that *protogalactic SGMCs were all at their critical masses*, as was discussed by McLaughlin & Pudritz (1996b) for regular GMCs.

Just how large were SGMCs, then? To answer this question, one further analogy with the current situation in the Galaxy is drawn, to suggest that *protogalactic star formation was restricted to small, dense cores within SGMCs*, and that some of these were ultimately responsible for the production of bound globular clusters. Presumably, the cores of SGMCs were also in virial equilibrium (although not necessarily all at their critical masses), but again colder than $T \sim 10^4$ K; thus, they should also have been supported by internal turbulence. Clearly, there should have been a range of core masses in SGMCs, just as there is a significant spread in globular cluster masses and in the masses of GMC cores now. However, the expected properties of a *median* protocluster core (defined as for the GMC cores in Table 1.2 above, i.e., so that half of all the mass in the cores of an SGMC is contained in those more massive than the median) can be used to, first, represent the properties of cores in general and, second, constrain the properties of their parent SGMCs (see also Harris & Pudritz 1994).

Thus, note that, under this definition, the median globular cluster mass in the Milky Way (and other galaxies) today is roughly $m_{\rm glob} \simeq 4.6 \times 10^5 M_\odot$ (which is larger than the *mean* mass of $\langle m \rangle \simeq 2 \times 10^5 M_\odot$). The gaseous protocluster core corresponding to such an object was likely more massive by a factor of $1 - 2$, since it had to have lost some of its mass ($\lesssim$50%, according to eq. [4.5]) to gas blowout during star formation, and some during the subsequent evolution of the cluster. For definiteness, the mass of the median core in a typical SGMC is therefore set at $m_{\rm core} \simeq 1.5\, m_{\rm glob} \simeq 7 \times 10^5 M_\odot$. Then the observed ratio of median core-to-cloud mass in Galactic GMCs (see Table 1.2 above, or Harris & Pudritz 1994) can be used to infer that the median SGMC should have been larger than this by a factor of $\sim 10^3$. (This is also suggested by the observations of currently forming massive clusters in merging and starburst galaxies, as discussed in §5.1.) Next,

for the case of the proto-Milky Way specifically, a surface pressure of $P_s = 3 \times 10^5\ k\ \mathrm{cm}^{-3}\ \mathrm{K}$ is assumed to be exerted by the hot, virialized halo gas on the SGMCs at a galactocentric radius $R_{\rm gc} \sim 10$. The column density $\Sigma = m/\pi R^2$ of a median SGMC is then obtained from equation (2.11c) of McLaughlin & Pudritz 1996b (with a model-independent $\alpha_{\rm non} \simeq 2$ and $\alpha_{\rm mag} \simeq 1$), and its total linewidth $\sigma_{\rm ave}$ from equation (2.11a) of that paper. The rest of the median cloud and core properties follow either from definitions or from the observed ratios $\widetilde{\rho}$, $\widetilde{\sigma}$, and $\widetilde{\Sigma}$ of the average densities, linewidths, and column densities in typical Galactic cores and GMCs (i.e., eq. [1.16] above, or eq. [4.9] of McLaughlin & Pudritz 1996b). The results of this exercise are given in Table 4.1, and are almost identical to those obtained, in a slightly different manner, by Harris & Pudritz (1994). These authors show that mean magnetic field strengths of order $B_{\rm ave} \sim 40\ \mu$G are required to keep SGMCs with the properties listed in Table 4.1 in equipartition and equilibrium. Such strengths could arise naturally in the dense clouds of any protogalaxy, from the amplification of a background primordial field at the level of $B_0 \sim 2\ \mu$G.

Table 4.1: Properties of Local SGMCs and Cores in the Milky Way

Parameter	Median Cloud	Median Core
m / $M_\odot$	7×10^8	7×10^5
R / pc	910	14
$\sigma_{\rm ave}$ / km s^{-1}	26	7.5
Σ / $M_\odot$ pc^{-2}	270	1200
$\rho_{\rm ave}$ / $M_\odot$ pc^{-3}	0.22	65

We stress that the numbers given in this Table apply to the properties of *median* SGMCs and their star-forming cores, and more specifically to those at galactocentric radii of $R_{\rm gc} \sim 10$ kpc in the early Milky Way. Again like normal GMCs and cores, however, SGMCs should have come with a variety of masses (perhaps $m_{\rm SGMC} \sim 10^7 - 10^9 M_\odot$), and so should the cores inside them (roughly speaking, $m_{\rm core} \sim 10^3 - 10^6 M_\odot$). But since all SGMCs are expected to have been at their critical masses, their average properties scale simply with their mass — or with P_s, as this changes within or between protogalaxies — according to Larson's laws (i.e., eqs. [2.11] of McLaughlin & Pudritz 1996b). These scalings are used explicitly by McLaughlin & Pudritz (1996a) to discuss globular

cluster formation in the Milky Way, M31, and M87 within the general context of the SGMC model. And finally, as was mentioned above, cores should have been in virial equilibrium, and supported to a significant extent by internal nonthermal motions. To be more specific, note that a total linewidth of $\sigma_{\rm ave} = 7.5$ km s^{-1}, as in Table 4.1, would correspond, if it were just thermal in origin, to $T \sim 10^4$ K; but, as discussed above, this is hotter than should have been allowed. (The thermal linewidth at $T = 100$ K is only $\sigma_{\rm T} \simeq 0.8$ km s^{-1}.)

This supergiant cloud-core picture forms the basis of a theory of globular cluster formation whose macroscopic initial conditions are obtained by a straightforward scaling-up of those that govern ongoing star formation in our Galaxy. The theory stands to address each of the four points listed at the beginning of §5.3, as follows:

First, as we have stated, the cores in SGMCs should not have all had a common mass. In fact, as Harris & Pudritz (1994) point out, the mass spectrum of protocluster cores specifically should translate more or less directly to the initial GCLF in a galaxy, simply because $\gtrsim$50% of the cores' gas had to be turned into stars in order to produce bound globular clusters. Given the general similarity between the GCLFs in many galaxies and the mass spectra of GMCs and cores in the Milky Way, Harris & Pudritz suggest that GCLFs were established, in a very general fashion, by the building up of SGMC core masses as a result of binary collisions within their parent clouds — an idea which was originally applied to Galactic GMCs by, e.g., Field & Saslaw (1965) and Kwan (1979).

Second, Harris & Pudritz propose that the large core radii of GCSs might be due to the inhibition of cluster formation in the central regions of galaxies, as large SGMCs could essentially be shredded by strong gravitational tides at small $R_{\rm gc}$. This possibility could be investigated further. However:

Third, the more fundamental property of GCSs, in our view, is the tendency for local specific frequencies (i.e., $f_{\rm cl}^{\rm glob}$) to grow with galactocentric radius inside systems. That is, a systematic increase towards larger $R_{\rm gc}$ in the formation efficiency of bound clusters would *automatically guarantee* the formation of GCSs with larger core radii, and shallower density profiles overall, than the underlying field stars of galaxies. It may therefore prove more fruitful to first try and understand the origins of the typical $\sim 10^{-3}$ order of magnitude of $f_{\rm cl}$ in general (eqs. [4.6], [4.11]), and to see if this

quantity can indeed be expected to increase with R_{gc} *ab initio*. In this context, it is worth remarking (after Harris & Pudritz 1994) on the interpretation of S_N within the SGMC framework. Thus, recall (from Table 4.1) that a typical SGMC has $m_{SGMC} = 7 \times 10^8 M_\odot$. Also, the *mean* core mass in a cloud should be something like 1.5 times the mean globular cluster mass today (following the same type of argument used to estimate the median core mass in Table 4.1), so that $\langle m \rangle_{core} \simeq 3 \times 10^5 M_\odot$. This means that a typical SGMC consisted of around $2000 - 3000$ individual cores. Given that a typical (global) specific frequency of $S_N \sim 5$ corresponds to $f_{cl}^{glob} \sim 0.002$, it is then expected that only a handful of cores — roughly speaking, perhaps $(f_{cl}^{glob} m_{SGMC})/\langle m \rangle_{core} \sim 5$ — in any given SGMC would have actually been able to form bound globular clusters; the rest would have been responsible for the unclustered field stars in galaxies. This is just another way to see that specific frequencies can be understood in terms of the probability that any given core will attain a cumulative star formation efficiency of $\gtrsim 50\%$ before its young stars clear out the remaining gas. When this probability and its variations within and between galaxies are understood, so will S_N be. Such understanding will, of course, come only with detailed investigations of the star formation process inside massive cores. *Whether this is carried out specifically in a protogalactic or a present-day context would seem to be of little importance*, given that f_{cl} is so similar in the two cases.

And fourth, the idea that globular clusters formed in many separate, $m_{SGMC} \sim 10^7 - 10^9 M_\odot$ *pieces* of protogalaxies, rather than directly as parts of much larger and more cohesive bodies of gas, naturally accounts for the large spread of cluster metallicities in most GCSs: each SGMC would essentially have undergone its own chemical evolution (as was first discussed for the Milky Way, in a slightly different context, by Searle & Zinn 1978), and thus would have produced individual clusters — as well as field stars — with metallicities independent of those in other clouds. At the same time, the internal turbulence supporting individual SGMC cores would have led to an efficient mixing of the protocluster gas, thus ensuring the formation of clusters that were internally chemically homogeneous (Murray & Lin 1990; Harris & Pudritz 1994; Vietri & Pesce 1995). And because the main source of SGMC and core support was nonthermal, it was also independent of metallicity, so that globulars were allowed to form with essentially any Z. (On a larger scale, however, the global scaling $\langle Z \rangle_{GCS} \propto L_{gal}^{0.4}$ has yet to be fully explained in this, or any other, globular cluster formation model.)

Much work remains to be done on the microscopic level at which individual cores in SGMCs — or anywhere else, for that matter — collapse and fragment to form multiple stars (see, e.g., Murray & Lin 1989a, b; but note that these analyses work specifically with very low metallicities, $Z \simeq 0.002 Z_{\odot}$). Nevertheless, the theory outlined here can account, at least in principle, for the most important *global* aspects of old globular cluster systems. At the same time, its basic set-up is such that it can both draw on and contribute to the understanding of star and cluster formation in the densest regions of large star-forming clouds of gas at any epoch.

One of the quantitative successes of this picture is that it naturally reproduces the observation (van den Bergh, Morbey, & Pazder 1991) that the half-light radii of Galactic globular clusters scale with Galactocentric position as $r_h \propto R_{\rm gc}^{1/2}$. (This follows directly from Larson's laws for the SGMCs, the variation $P_s \propto R_{\rm gc}^{-2}$ in the pressure of the hot gas in an isothermal halo, and the fact that SGMC and core masses are invariant with $R_{\rm gc}$; see Harris & Pudritz 1994, and McLaughlin & Pudritz 1996a). As a second test of the model, Chapter 5 below goes on to develop the first detailed theory of the GCLF. There we take up the suggestion of Harris & Pudritz that this arose as the result of collisions and agglomeration among the gaseous cores in SGMCs. As part of our theory, we are able to draw some inferences on the star-formation lifetimes of SGMC cores that should apply generally to the molecular clouds and cores in the Galaxy today.

SGMCs and Galaxy Formation

As we have presented them here, supergiant molecular clouds arise naturally as part of a hypothesis specifically intended to link the mechanisms of present and long-past star formation. However, it is important to note that quite an independent line of reasoning, based on considerations of the overall *galaxy* formation process, leads again to the conclusion that most protogalaxies must have incorporated several independent, and probably SGMC-sized, bodies of gas.

In some historical sense, models for the formation of large galaxies can be divided into two distinct classes: one involving the relatively ordered, dissipative collapse of a single, $m \sim 10^{11} M_{\odot}$ cloud of gas, and one envisioning a more drawn-out and stochastic process of merging and accretion among many smaller clumps, or protogalactic "fragments." As regards the formation of the Milky Way specifically, a pioneering physical picture of the first type was provided by Eggen, Lynden-Bell,

& Sandage (1962; see also Sandage 1990), while an influential model of the second type was offered by Searle & Zinn (1978). An excellent review of these two basic kinds of scenarios, cast in more modern terms and considered in the light of evidence gleaned from the general properties of spiral and elliptical galaxies alike, is given by Larson (1992). The main point to be made here is that the balance of detailed evidence from the kinematics and chemistry in the halo of our own Galaxy now points clearly to a prolonged history of interactions, merging, and accretions of *subgalactic* bodies (see also Majewsky 1993). In fact, this process is still ongoing, as the recent discovery of the Sagittarius system — a dwarf galaxy ($m \sim 10^9 M_\odot$) that is even now being assimilated into the Milky Way — attests (Ibata, Gilmore, & Irwin 1994). This is not to say that no element of coherent collapse was involved in the formation of the Galaxy (gaseous dissipation is required to produce a disk, for example), only that a long period of rather more chaotic evolution was at least as important. And, since the story of the Milky Way is not a unique one, the formation of *any* large galaxy is likely to have involved some amounts of both gaseous collapse *and* mergers between smaller subunits very early on (possibly followed by later accretion of smaller galaxies; see Larson 1992). These "subunits," however they arose, are obvious candidates for counterparts to the SGMCs discussed here.

Here we mention just two specific pieces of empirical evidence that appear to favor this interpretation: (1) The fact that most of the dwarf galaxies in the Local Group are clearly concentrated around either the Milky Way or M31, implies that many of them may be building blocks left over from — or yet to be used in — the formation of these larger systems (e.g., Zinn 1980, 1993). In the case of the Milky Way in particular, it is striking that the number density of dwarf satellites increases towards the Galactic center, from $R_{\rm gc} \sim 300$ kpc on in, until they appear to vanish altogether at $R_{\rm gc} \sim 70$ kpc (Zinn 1993; although note his caveat regarding selection effects for faint dwarf systems at smaller $R_{\rm gc}$). It is significant, then, that dwarf galaxy masses typically lie in the range $m \sim 10^8 - 10^9 M_\odot$. And (2) outside the Local Group now, Pascarelle et al. (1996) have discovered, through a combination of ground- and space-based observations, a collection of 18 very distant, compact, star-forming, and subgalactic clouds of gas. These objects are all at a common distance of about 13 billion light years, and are thus being observed now as they were when the universe was only $\simeq$2 Gyr old. They are clustered into several groups of a few, and the groups

together occupy a $\sim$0.5 Mpc^2 area of space. As Pascarelle et al. point out, it seems obvious that these clouds may well go on, over the next $2-3$ Gyr, to form a few large galaxies of Milky Way proportions. Thus, it is significant that each cloud is only of order 1 kpc in size. A broad extrapolation of these results would suggest that galaxies typically formed from fragments with masses and sizes (to repeat, $m \sim 10^8 - 10^9 M_\odot$ and $R \sim 1$ kpc) similar to those outlined above for SGMCs.

This impression appears to be at least qualitatively borne out in current theories of galaxy formation. These theories rely on the fact that most of the mass in the universe is contained in the form of unseen (and still unidentified) dark matter, which appears to dominate everywhere except in the innermost regions of galaxies, and which typically outweighs the visible stars and gas in individual galaxies by a factor of $\sim$10 : 1 (see the review of Trimble 1987). The growth of structure from uniform conditions in the early universe is therefore thought to have been driven by the gravitational force of the dark matter. In this context, visible galaxies are expected to have formed when gas fell into pre-existing, galaxy-sized potential wells (maintained by dark matter, and possibly built up through a process of hierarchical clustering and merging), and then cooled and attained sufficently high densities, in places, to allow stars to form (White & Rees 1978; White & Frenk 1991). It is these dark matter wells that provide the gravitational backdrop for the globular cluster formation theories of both Fall & Rees (1985) and Harris & Pudritz (1994). (For example, they contain the virialized component of the protogalactic gas.) As White & Rees (1978) point out, this road to galaxy formation requires some type of dissipative collapse if the observed properties of galaxies today are to be reasonably well reproduced. More generally, and independently of any model, if the primeval gas was initially distributed like the dark matter, then it was not self-gravitating, and could not form stars until it condensed considerably within the galaxy-sized dark matter wells that are known to exist (and that almost certainly predate the visible parts of galaxies; see Larson 1992).

It is the details of this inevitable dissipation that are perhaps of most interest here. Katz & Gunn (1991) and Katz (1992) have performed a number of numerical simulations of the evolution of dark matter and gas together in single, galaxy-sized potential wells. These calculations begin from smooth initial conditions, and end with the formation of objects having the gross characteristics of typical spiral galaxies. Specific results are dependent on various choices of parameters within the overall cosmological framework adopted, and on necessarily prescriptive treatments of star formation.

Generally speaking, however, Katz & Gunn (1991) and Katz (1992) find that their spiral galaxies go through an early chaotic stage in which the gas is organized into *self-gravitating clumps* that individually form "stars" with some small efficiency (note that each "star" here — i.e., each particle in these numerical simulations — is assigned a mass of $5 \times 10^6 M_\odot$), and then go on to merge and build up the halos and disks of the galaxies overall. This sequence of events is very much like that proposed by Harris & Pudritz (1994) in the context of GCS formation; and at least some of the clumps in the simulations of Katz (1992) are as massive as $10^8 - 10^9 M_\odot$.

It therefore seems clear that galaxy formation generally had to have involved, at some level, collapse and star formation in a collection of discrete clouds of gas; and it is quite plausible that such fragments could have had $m \sim 10^8 - 10^9 M_\odot$ and $R \sim 1$ kpc. But if these objects were at all like star-forming clouds are today, then they should have also exhibited smaller-scale substructure. Thus, we arrive again at the idea of SGMCs and cores with roughly the properties listed in Table 4.1. There can be little doubt that the question of how star formation proceeds within subgalactic clouds of gas is relevant to issues of galaxy formation, globular cluster formation, and ongoing star formation alike.

Chapter 5

The Formation of Globular Cluster Systems. I. The Luminosity Function

THE ASTROPHYSICAL JOURNAL, 457:578–597, 1996 February 1

THE FORMATION OF GLOBULAR CLUSTER SYSTEMS. I. THE LUMINOSITY FUNCTION

DEAN E. MCLAUGHLIN AND RALPH E. PUDRITZ
Department of Physics and Astronomy, McMaster University, Hamilton, Ontario, Canada, L8S 4M1;
dean@physics.mcmaster.ca, pudritz@physics.mcmaster.ca
Received 1995 February 13; accepted 1995 July 14

ABSTRACT

We present a numerical model for the globular cluster luminosity function (GCLF) which characterizes globular cluster systems (GCSs) around galaxies. This model is based on the idea that globular clusters formed in the cores of self-gravitating, magnetized, supergiant molecular clouds (SGMCs). A distribution of core masses is built up through a series of collisions within a parent SGMC. Massive cores are assumed to be destroyed (at a mass-dependent rate) by the act of star formation, allowing for the establishment of a unique, steady state mass spectrum. The model, which allows only for coalescent collisions between cores, fits observed GCS mass spectra very well above the GCLF peak mass $m_* \simeq 1.6 \times 10^5\ M_\odot$, which is remarkably constant from galaxy to galaxy. We suggest that it represents the critical mass above which the cores of SGMCs become susceptible to internal disruption. Our fits to the mass spectra of the Milky Way, M31, and M87 GCSs predict that, in a given SGMC, the lifetimes of such cores should decrease at higher masses. The crucial factor in determining the shape of the GCLF is the ratio β of characteristic core disruption and collision timescales. It is shown that β does not differ between SGMCs in a single protogalaxy; this accounts for observations that GCLFs are independent of galactocentric radius. However, β does differ, and the overall shape of the GCLF along with it, between GCSs. Finally, our model suggests an "inside-out" sequence of GCS formation.

Subject headings: galaxies: formation — galaxies: luminosity function, mass function — galaxies: star clusters — globular clusters: general

1. INTRODUCTION

One of the concerns in understanding how galaxies formed is our lack of an adequate theory of star formation (see the review by Silk & Wyse 1993). It is therefore difficult to predict exactly when or how star formation began within the assembling dark matter potential wells of galaxies. There are, however, a few basic characteristics of star formation in the interstellar medium (ISM) of our Galaxy and its neighbors which must also have been of importance in the protogalactic epoch. First, star formation in Local Group galaxies takes place within massive, cold, self-gravitating (primarily molecular) clouds whose temperatures are so low that thermal pressure fails by an order of magnitude in staving off gravitational collapse (Scoville & Sanders 1987). Measurements show, instead, that magnetic fields within clouds have the required energy density to provide the needed pressure support (McKee et al. 1993; Heiles et al. 1993). Second, star formation within molecular clouds is confined to small, overdense (high-pressure) subregions, known as cores. Infrared camera observations have recently revealed that these molecular cloud cores produce stellar groups and clusters (e.g., Lada, Bally, & Stark 1991). While the efficiency of star formation within these cores can be very high (as much as 40% in some instances), the overall efficiency is low (at the level of a few percent) when averaged over an entire cloud. Finally, there is excellent evidence that the observed properties of nearby molecular clouds can be derived from the virial relations for pressure-truncated, magnetically supported, self-gravitating objects (Elmegreen 1989a).

Perhaps the most significant clue about protogalactic star formation is locked into the characteristics of globular cluster systems (GCS) within the halos of galaxies (for a review see Harris 1991). One of the fundamental observables of any GCS is the globular cluster luminosity function (GCLF) ϕ, which is the number of globulars seen per unit magnitude. This distribution is the first moment of the GCS mass spectrum (dN/dm, the number of clusters per unit mass). Rather remarkably, the form of the mass spectrum for globular clusters is nearly identical to the mass function of molecular cloud cores (Harris & Pudritz 1994, hereafter HP; also § 2 below). This can be simply understood by noting that regions which form *bound* star clusters must be better than 50% efficient in converting gas into stars. The mass functions of bound clusters and their natal cores ought then to be nearly identical.

One caveat is that external gravitational shocks and internal relaxation processes may have caused mass loss and even disruption of fully formed globular clusters as they evolved within the tidal fields of their parent galaxies. In principle, this dynamical evolution of a GCS would cause its mass spectrum to change with time and vary with galactocentric radius. However, this effect has not been observed; globular cluster luminosity functions are independent of galactocentric radius. Therefore, the observed two-decade range of globular cluster masses is likely to be a fossil of the original protoglobular cloud mass function rather than the erosion product of some initial distribution.

The difference in mass scale between presently forming star clusters in molecular cloud cores and the old globular clusters may reflect the predominance of gas rather than stars in protogalaxies. Thus, early interstellar media in protogalaxies consisted of 10^{11} rather than $10^9\ M_\odot$ of gas, implying that vastly larger and more massive complexes of self-gravitating (and possibly even molecular) clouds could have been built up. HP showed that the physics of self-gravitating, magnetized clouds provides an excellent framework for understanding many properties of globular cluster systems.

Whatever the gas supply, and however it was facilitated, ultimately the formation of a collection of self-gravitating clouds is a prerequisite for star formation in any galaxy. Smoothed particle hydrodynamics (SPH) simulations (e.g., Katz, Hernquist, & Weinberg 1992) suggest that while a significant amount of gas associated with dark matter wells is shock heated and virialized to high temperatures, gas that falls in early is nonetheless able to cool and exist as discrete cold clouds. Thus, regardless of whether mergers of gas-rich galaxies (Ashman & Zepf 1992), the cooling of early gas clouds on dynamical timescales (Rees & Ostriker 1977; Silk 1977), or, indeed, any other gasdynamical process dominated the scene, the gaseous medium in a dark matter well probably settled into a state consisting of (1) a hot, virialized component and (2) an ensemble of much colder clouds that ultimately become self-gravitating.

In this paper we extend the work of HP and construct a more detailed theory of the GCS mass spectrum. The physical picture that we (as did HP) investigate involves a number of self-gravitating clouds moving through a hot tenuous medium within the dark matter halo of a galaxy. The inevitable collision and agglomeration of small gas parcels in these large clouds produce a collection of cores, some of which will form stars with the high efficiency required to produce bound, globular clusters. Our model for the core mass spectrum which characterizes the globulars is based on numerical solutions to a kinetic equation that describes the collisional evolution of a generic ensemble of clouds. This is a statistical equation which works under the assumption that a group of cores is able to reach a steady state equilibrium between the rates of collisional growth and internal disruption (brought on by star-formation). Such a statistical treatment does not require any assumptions on the detailed workings of the star-formation process in protocluster cores. Accordingly, we do not deal with this problem: the theory is not one of individual globular cluster formation *per se*, but instead addresses a more global aspect of globular cluster *systems* in quite a general way. We find an excellent fit to the GCS mass spectra in a variety of galaxies, for cluster masses in excess of $\sim 10^5\ M_\odot$. Our model also explains, from first principles, why GCLFs are independent of galactocentric radius.

In the next section we use some of the best defined GCLFs (those of the Milky Way, M31, and M87) to infer some basic observational constraints that must be satisfied by any successful theory for the GCS mass spectrum. We then go on (§ 3) to construct a family of theoretical mass spectra for the cluster-forming cores. In § 4, fits to the observed GCS mass spectra in M87, the Milky Way, and M31 are used to constrain some fundamental parameters in these models. Finally (§ 5), we use our results to deduce some fundamental timescales and put interesting constraints on the details of globular cluster formation and, therefore, galaxy formation.

2. OBSERVATIONAL INPUT

There are three closely related but individually important functions which describe the distribution of mass in globular cluster systems (GCSs). The directly observed quantity is the globular cluster luminosity function (GCLF, $\phi \sim dN/dM_V$). Derived from this are the more fundamental luminosity (or mass) *spectrum* $N(L) = dN/dL$ (HP), and the luminosity-weighted luminosity function (LWLF, $\psi \sim L\phi$; Harris 1991), which is the summed luminosity or mass of all globulars per unit magnitude. The relationship between these three functions, and their characteristic forms in a number of galaxies, are discussed in detail by McLaughlin (1994); for our purposes, it is sufficient to note that

$$\phi(\log L) \sim LN(L) \quad \text{and} \quad \psi(\log L) \sim L^2 N(L)\,. \qquad (2.1)$$

The distributions ϕ and ψ are the first two moments of the basic spectrum N, and respectively weight the number of clusters and the mass in clusters (per unit *logarithmic* mass). Thus, for an observed number N_{tot} of globulars in a GCS, with a combined mass M_{tot}, we have

$$\int N(L)dL \propto \int \phi(\log L)d\log L \propto N_{tot}$$

and

$$\int \phi(\log L)dL \propto \int \psi(\log L)d\log L \propto M_{tot}\,.$$

We show in Figures 1 and 2 the distribution of globular cluster luminosities—in terms of all three functions N, ϕ, and ψ—in the Milky Way, M31, and M87. (The mass-to-light ratio of the globulars, which is $\simeq 2$ on average in the Milky Way, is assumed to be roughly independent of cluster mass [e.g., Mandushev, Spassova, & Staneva 1991]. These luminosity distributions are then equivalent, aside from normalization, to the corresponding functions of mass.) Several features of the GCS mass spectra in Figures 1 and 2 are generic to those in many other galaxies:

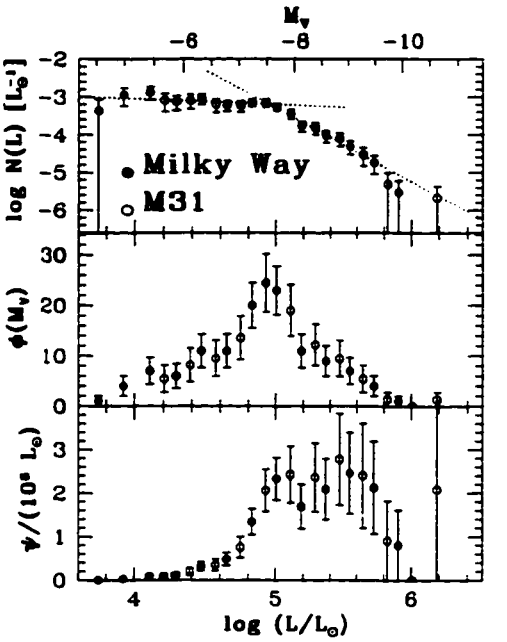

FIG. 1.—Globular cluster mass distributions $N(L) \sim mN(m)$, $\phi \sim N(m)$, and $\psi \sim m^2N(m)$ for the Milky Way and M31 GCSs. The data consist of 120 Milky Way globulars with Galactocentric radii $R_{gc} < 40$ kpc (from an updated version of the catalog used by HP and McLaughlin 1994), and 81 clusters from the M31 database of Reed, Harris, & Harris (1994), with $(m - M)_V = 24.6$ assumed. Broken lines in the top panel correspond to the parametric fits of eq. (2.2).

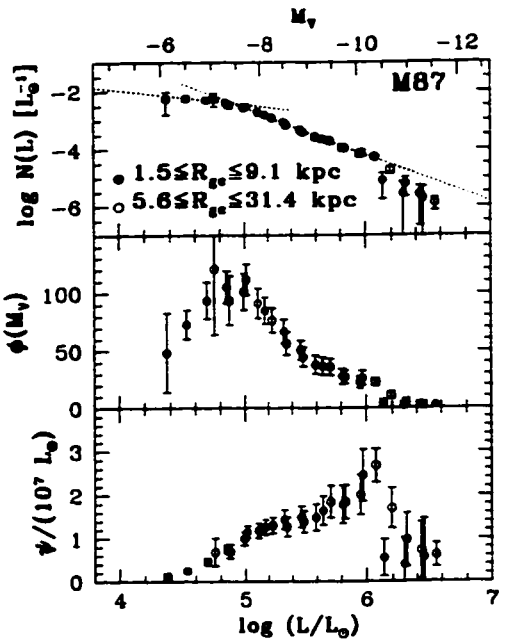

FIG. 2.—Functions N, ϕ, and ψ for the M87 GCS, with data taken from McLaughlin et al. (1994) (5.6 kpc $\leq R_{gc} \leq$ 31.4 kpc) and from Harris et al. (1995b) (1.5 kpc $\leq R_{gc} \leq$ 9.1 kpc); a Virgo distance modulus of $(m - M)_V = 31.0$ has been applied (Pierce et al. 1994; Freedman et al. 1994). The total number of globulars observed is ~3000. Broken lines correspond to the power-law fits of eq. (2.3).

1. There is a well-defined mass, which we label m_*, at which ϕ peaks. This mass,

$$m_* \simeq 1.6 \times 10^5\ M_\odot$$

(corresponding to $M_V = -7.4$ for a mass-to-light ratio of 2), is roughly the same in the three GCSs considered here, and in all others where it has been observed. Current observations allow for possible variations in m_* at the level of ~30% from galaxy to galaxy (e.g., Harris 1991; Fleming et al. 1995). The GCLF peak mass does *not* represent either an upper or a lower limit to allowed globular cluster masses, nor does it correspond to any maximum in the cluster number distribution $N(m)$. Technically, it is just that mass at which the logarithmic slope $\gamma \equiv d \log N/d \log m$ steepens, rather suddenly, from > -1 to < -1 (McLaughlin 1994, or eq. [2.1] above). This is easily seen if power laws are fitted to the mass spectra N of Figures 1 and 2. Then $N(L) \sim L^{\gamma}$, and we find for the Milky Way and M31 combined (see also Surdin 1979; Racine 1980; Richtler 1992; HP)

$$\gamma(\mathrm{MW/M31}) = \begin{cases} -0.15 \pm 0.15\,, & m \leq m_* \\ -1.95 \pm 0.15\,, & m \geq m_*\,. \end{cases} \qquad (2.2)$$

Similarly, *over a range of* 30 *kpc* in galactocentric radius within M87, the GCS mass spectrum is uniformly well fitted by (Harris, McLaughlin, & Harris 1995b)

$$\gamma(\mathrm{M87}) = \begin{cases} -0.5 \pm 0.2, & m \leq m_*\,, \\ -1.65 \pm 0.10, & m \geq m_*\,. \end{cases} \qquad (2.3)$$

This specific functional fit to the M87 $N(L)$ also roughly applies in two other Virgo ellipticals, so that in this sense the M87 GCS is not unlike those of other large, early-type galaxies (McLaughlin 1994).

The monotonic behavior of the mass spectrum N seen in these and other data suggests that globular cluster masses do not bracket one "characteristic" value (as implied in Peebles & Dicke 1968; Fall & Rees 1985; Kang et al. 1990; Murray & Lin 1992, 1993; Kumai, Basu, & Fujimoto 1993), but rather range continuously over several orders of magnitude. Evidently, whatever its origin, the mass m_* is very robust against such influences as galaxy luminosity or Hubble type, mean galaxy or GCS metallicity, and internal or external postformation cluster destruction mechanisms.

2. There is a second critical mass, say m_1, at which ψ peaks. In general (as seen in Figs. 1 and 2; also Harris 1991), m_1 is different from m_*, showing again that no preferred mass scale has been imprinted on any GCS. As with the peak in ϕ, a maximum in ψ corresponds to a steepening of the logarithmic mass spectral slope γ (now from > -2 to < -2, so that $m_1 > m_*$; see eq. [2.1]). The mass m_1 is *not* constant from galaxy to galaxy (see also McLaughlin et al. 1995), and the detailed shape of the GCS mass spectrum can vary between systems. Figures 1 and 2, and equations (2.2) and (2.3), provide a case in point: $N(L)$ is steeper above the GCLF peak mass in the Milky Way and M31 GCSs than in M87, and shallower below it. The LWLFs of these spiral GCSs are therefore somewhat flatter beyond m_*, and m_1 is relatively closer to m_*. We return to this point in § 4 below, but note here that, contrary to the suggestion of HP, there is no single γ which applies above m_* in all GCSs. Rather, a narrow but significant range, perhaps $\gamma \simeq -1.6$ to -2, is indicated by the present data.

3. Current data do not show a significant dependence of either the shape of $N(m)$ or the masses m_* and m_1 on galactocentric radius within any one system. (Fig. 2 shows this for M87 specifically; see also Harris et al. 1991; McLaughlin, Harris, & Hanes 1994; Harris et al. 1995b.) This implies that the external dynamical mechanisms that could potentially destroy globular clusters (particularly gravitational shocks, which are functions of cluster mass, galactocentric position, and details of the parent galaxy potential; e.g., Aguilar, Hut, & Ostriker 1988) have not seriously affected observed GCLFs in the mass ranges discussed here. As discussed below, the form of the mass spectrum of cores within two Galactic giant molecular clouds (GMCs) further suggests that internal processes (such as relaxation and evaporation) have not significantly altered the shape of the GCLF over a Hubble time (see also Murray & Lin 1992, 1993; Oh & Lin 1992). It may therefore be possible to explain much of the GCLF without considering the effects of postformation dynamical evolution.

4. The peak mass m_* of ϕ is quite insensitive to the metallicities of either the globulars in a GCS or the halo population in the parent galaxy. Moreover, this appears to be generally true for the *entire* GCS mass spectrum. Armandroff (1989) has shown this to be the case for the Milky Way; and the constancy of the GCLF over 30 kpc or so within M87, together with the existence of a significant metallicity gradient in the GCS (Lee & Geisler 1993; Harris, Harris, & McLaughlin 1995a), implies that $N(m)$ there is similarly impervious to chemical abundance. More explicitly, the globulars in each of M87, NGC 1399, and NGC 5128 fall into two or three distinct groups of different mean metallicity (Ashman 1994, private communication; cf. Lee & Geisler 1993; Ostrov, Geisler, &

Forte 1993; Harris et al. 1992). We have performed Kolmogorov-Smirnov tests on the GCLFs of the different metallicity groups within each of these galaxies, and find no significant differences among them.

As a corollary to this point, the ability of the protogalactic gas to form globular clusters is in no way compromised by the presence of heavy elements. Specifically, there is new evidence for the existence of many clusters with supersolar metal abundances in the center of M87 (Harris et al. 1995a), in the elliptical NGC 3923 (Zepf, Ashman, & Geisler 1995), and especially around the cD galaxy NGC 3311 (Secker et al. 1995). These objects pose a severe problem for any theory of cluster formation which requires a low protoglobular metallicity in order to delay the onset of fragmentation due to thermal instability (e.g., Fall & Rees 1985; Murray & Lin 1992, 1993; Richtler & Fichtner 1994; see the discussions of Ashman 1990 and HP).

5. As a whole, ϕ is always roughly symmetric about is peak. Within the parametric representation of $N(m)$ given by equations (2.2) and (2.3), the quantitative statement of this result is that the sum of the power-law slopes above and below m_* is always near -2 (McLaughlin 1994). The robustness of this rough GCLF symmetry implies that differences between the finer details of the distributions in Figures 1 and 2 (such as the *individual* slopes γ above and below m_*, or the value of m_1) are not due either to observational uncertainty or to very galaxy-specific factors such as dynamical evolution, total GCS population, or mean galaxy and GCS metallicity. At the same time, the LWLF is *not* symmetric about m_1. Thus, although the GCLF is often approximated by a Gaussian (see Harris 1991), such a fit has no physical significance: if ϕ truly were a normal distribution, then ψ would be also (Harris 1991; McLaughlin 1994).

There are some striking parallels between GCLFs and the mass functions of younger star clusters and cluster-forming regions. The luminosity spectra of LMC clusters and Galactic open clusters both follow power laws with $\gamma \simeq -1.5$ (Elson & Fall 1985; van den Bergh & Lafontaine 1984). Similarly, the young clusters in the merging galaxies NGC 4038/4039 (the Antennae) show $\gamma \simeq -1.8$ (Whitmore & Schweizer 1995). Also, the $N(L)$ of extragalactic giant H II regions (e.g., Banfi et al. 1993) is a power law of slope $\gamma = -1.8$ in the mean, apparently independent of parent galaxy metallicity. (It should be noted, however, that the forms of the underlying *mass* spectra are not necessarily clear in these cases.) Most compelling is the fact that the mass spectra of Galactic GMCs (e.g., Casoli, Combes, & Gerin 1984; Solomon et al. 1987; Williams & McKee 1995) and the dense cores within them (Loren 1989; Stutzki & Güsten 1990; Lada et al. 1991; Wood, Myers, & Daugherty 1994; Williams, de Geus, & Blitz 1994; and the review of Blitz 1991) also have roughly power-law shapes, with slopes $\gamma \simeq -1.4$ to -1.6.

The mass spectral slopes quoted in the literature for GMCs and cores typically apply over little more than a decade in mass because of incompleteness in the cloud counts at low masses (e.g., Williams & McKee 1995). This makes it difficult to determine whether or not there exists a low-mass breakpoint and change of slope in N (or peak in ϕ, i.e., an analog of the globular cluster m_*). However, the recent study of Williams et al. (1994) shows just such a feature in the mass spectrum of clumps in the Rosette and Maddalena GMCs. We plot N, ϕ, and ψ for these clumps in Figure 3. A peak in ϕ occurs at $m_* \simeq 50$–$60\ M_\odot$; a power-law fit to the mass spectrum,

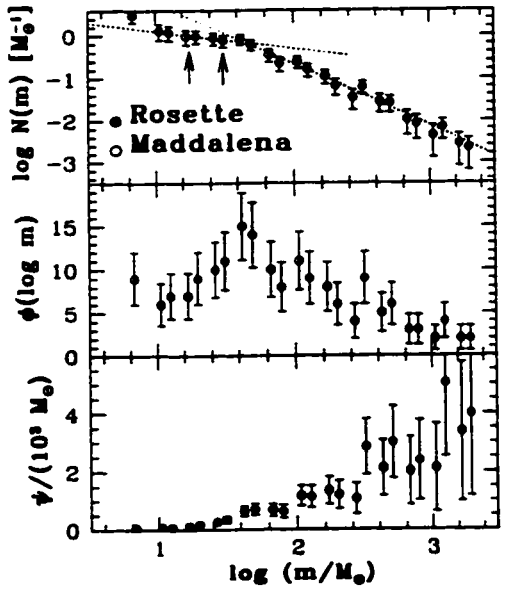

FIG. 3.—Mass spectrum N and corresponding ϕ, ψ for a collection of ~180 molecular cores in the Galactic Rosette and Maddalena GMCs (Williams et al. 1994). The Maddalena data have been scaled so that the maximum core mass is the same as in the Rosette; a Kolmogorov-Smirnov test then shows that the shapes of the mass spectra are identical above $m \simeq 10\ M_\odot$. Arrows in the top panel mark the completeness limits of the data (see Williams et al.). Note that the peak in ϕ occurs above these limiting masses. The power-law fits of eq. (2.4) are drawn in the top panel. Note the similarity especially to the M87 GCS data in Fig. 2.

$N(m) \sim m^\gamma$, then yields

$$\gamma(\text{cores}) = \begin{cases} -0.4 \pm 0.2\,, & m \le m_*\,, \\ -1.45 \pm 0.10\,, & m \ge m_*\,, \end{cases} \qquad (2.4)$$

remarkably similar to the results for the M87 GCS (eq. [2.3]). In particular, it is interesting that the sum of power-law slopes above and below m_* is $\simeq -1.9$, i.e., the core ϕ is roughly symmetric about its peak.

Any ISM ought to engage in cloud building of the most general type. Since it is in GMC cores that current star formation is proceeding in earnest, and since it seems unlikely that their mass function has evolved significantly away from the formation spectrum, a comparison of Figures 1, 2, and 3 suggests that *the overall form of the GCS mass spectrum may be attributed in large part to a robust formation mechanism.*

3. A STEADY STATE AGGLOMERATION MODEL

One way (Oort 1954) to interpret the mass spectrum of Galactic GMCs and cores is as that distribution which affords a steady state balance between the rates of cloud creation (by collisions between smaller clouds) and destruction (by the internal star formation process). Field & Saslaw (1965) were the first to offer a simple analytical realization of this picture for the case of strictly coalescent collisions. The model was developed in more detail by Field & Hutchins (1968), Penston et al. (1969), Taff & Savedoff (1973), Handbury, Simons, & Williams (1977), and especially Kwan (1979). Most recent work has concentrated on the buildup of GMCs in spiral arms

(Cowie 1981; Casoli & Combes 1982; Kwan & Valdes 1983, 1987; Tomisaka 1984, 1986) or in merging galaxies (Olson & Kwan 1990a, b). The steady state mass spectra obtained in these studies generally provide good descriptions of the observed GMC distribution. (There are, however, some claims to the contrary, which we discuss in § 4 below). Naturally, there are other theories of GMC formation (see, e.g., the review of Elmegreen 1993), but the collisional-growth model remains the one which most clearly leads to a well-defined spectrum of cloud masses.

Regardless of how an initial ensemble of clouds is created, collisional encounters must have some influence on its final state. In what follows, we investigate the role which such encounters between cores in the large protogalactic gas clouds of HP might have played in determining the mass spectra of GCSs. Following HP, we refer to the parental clouds as "supergiant molecular clouds," or SGMCs. As discussed in the introduction, these SGMCs and their cores are taken to be self-gravitating and magnetized. In addition, cores—the regions to which star formation is confined—are expected to be considerably less massive than their host SGMCs by factors typically of order 10^3 (as observed for modern GMCs and cores; see also Larson 1993 and HP). Protoglobular cores must have been only slightly more massive than the final clusters, which today have a mean mass of a few $10^5\ M_\odot$. We therefore adopt a fiducial SGMC mass of $7 \times 10^6\ M_\odot$ (HP).

Throughout this section, much of our discussion will involve just a set generic clouds, which could be taken to mean GMCs, SGMCs, the cores of either, or even, in some instances, entire protogalaxies. At various points we will establish direct connections with SGMC cores specifically, and hence GCSs, but on the whole the theory which develops is quite a general one.

3.1. *Basic Physics*

The original Oort model considers only coalescent collisions; collisional fragmentation is included in different ways in the studies of Taff & Savedoff (1973), Goldstein & Mazzella (1974), Handbury, Simons, & Williams (1979), Cowie (1980), Hausman (1982), and Nozakura (1990). If it occurs, fragmentation can inhibit the buildup of large clouds and strongly affect the final mass spectrum. It is therefore important to ask under what conditions colliding clouds will shatter rather than merge.

Two colliding bodies with masses $m_B \geq m_A$ and relative velocity v_{AB} can be expected to coalesce if the total energy of the pair is negative (Olson & Kwan 1990a), i.e., if

$$\frac{1}{2}\frac{m_A m_B}{m_A + m_B} v_{AB}^2 \leq \frac{G m_A m_B}{r_{AB}} + \frac{3}{5}\frac{G m_A^2}{R_A} + \frac{3}{5}\frac{G m_B^2}{R_B}$$

Here r_{AB} is the center-to-center separation of the clouds at the time of impact, and R_A, R_B are the radii of the individual clouds. If there is a minimum cloud mass m_0 and a cloud velocity spectrum $v_{AB} \simeq v_0 (m_A/m_0)^b$ (see eqs. [3.4] and [3.6] below), and if all clouds have the same column density $\Sigma = m/\pi R^2$ (a characteristic of self-gravitating structures), then this coalescence criterion becomes

$$3\left(\frac{m_B}{m_A}\right)^{3/2} + 8\left(\frac{m_B}{m_A}\right)^{1/2} + 5\left(\frac{m_B}{m_A}\right)^{-1/2} + 3\left(\frac{m_B}{m_A}\right)^{-1} \geq \frac{15\,\sigma^2}{G\sqrt{m_0 \pi \Sigma}}\left(\frac{m_A}{m_0}\right)^{2b-1/2} - 3\,. \quad (3.1)$$

where we have replaced r_{AB} by R_B (for a glancing collision) and v_0 by $6^{1/2}\,\sigma$, with σ the one-dimensional velocity dispersion of the cloud system.

According to HP (see their Table 3), a $7 \times 10^6\ M_\odot$ Galactic SGMC has an internal velocity dispersion $\sigma \simeq 25$ km s^{-1}, and each core within such a cloud has a column density $\Sigma \simeq 1.2 \times 10^3\ M_\odot$ pc^{-2}. We estimate a minimum core mass $m_0 \sim 10^3\ M_\odot$ (near the bottom of the range of Galactic globular cluster masses). Coalescence then obtains in collisions with minimum-mass cores (i.e., $m_A = m_0$) when $m_B \gtrsim 50 m_0$. Also, if kinetic energy is equipartioned among the cores (i.e., $b = -\frac{1}{2}$), then all encounters with $m_B \geq m_A \gtrsim 14 m_0$ will result in a merger. The surface pressure P_s on an SGMC affects both its internal velocity dispersion σ and the column density Σ of its cores, but in such a way that the combination $\sigma^2/\Sigma^{1/2}$ is independent of P_s (cf eq. [5.2] below). The critical coalescence ratios m_B/m_A are therefore the same for cores in an SGMC of given mass anywhere in a protogalaxy. They are, however, weakly dependent on the mass of the parent cloud: in a very large SGMC of $\sim 5 \times 10^9\ M_\odot$, m_B/m_A must be a factor of ~ 2 larger for a coalescent collision. At the same time, it should be noted that the condition (3.1) is conservative in that it does not account for any magnetic fields which may thread the colliding bodies and enhance the probability of coalescence.

Thus, energy considerations alone suggest that coalescence is the general rule for collisions between all but the least massive cores. To describe the mass spectra of globular cluster systems, we will therefore expand on the basic agglomeration model of Kwan (1979). That is, we allow for the disruption of massive cores in SGMCs by the act of star formation, but assume that all collisions are coalescent; a thorough treatment of fragmentation is left for future study. Our theory is therefore applicable at moderately high masses, in particular above the peak mass m_* of the globular cluster luminosity function, ϕ.

It is also essential that the SGMCs cradling the cores not be disrupted when they collide with one another. Using equation (3.1) with σ the velocity dispersion of the Galactic halo, and taking the minimum SGMC mass to be $\sim 10^6\ M_\odot$ (i.e., a factor of 10^3 larger than the minimum core mass), we find (again using Table 3 of HP) that two colliding Milky Way SGMCs with masses m_A and m_B will merge if $m_B \gtrsim 90 m_0$ when $m_A = m_0$, or more generally if $m_B \geq m_A \gtrsim 30 m_0$. Thus, parent-cloud collisions should not severely disturb the core agglomeration process within large SGMCs. In addition, however, the shock heating that results from collisions must not be allowed to vaporize the clouds. Since a typical collision will involve a near-minimum mass SGMC and a much larger one, it is sufficient to check that a $\sim 10^6\ M_\odot$ cloud will survive the event.

A cloud of mass m_{cl} and radius R_{cl} remains essentially intact as a shock moves through it if the cooling length L_c of the shock satisfies $L_c \ll R_{cl}$ (e.g., Seab & Shull 1983). If v_s is the typical shock speed through the cloud, and t_c the cooling time of the gas, then $L_c = v_s t_c$. Now, from HP we have $R_{cl} \simeq 35$ pc for an $m_{cl} = 10^6\ M_\odot$ SGMC; and $n_{cl} \simeq 106$ cm^{-3}. The next two paragraphs demonstrate that the cooling length is indeed negligible when compared to the size of these smallest colliding clouds.

The compression of *magnetized* gas due to the passage of a shock is much less than that due to purely hydrodynamic shocks. Specifically, the ratio of post- to preshock gas densities is given by Shull & Draine (1987) as $\rho_f/\rho_i \simeq 77 v_{s,7}$, where $v_{s,7} \equiv v_s/100$ km s^{-1}. For highly supersonic shocks, we expect speeds ranging from $\simeq 150$ km s^{-1} in the halo of the Milky

Way to $\simeq 300$ km s^{-1} in M87. Thus, we examine conditions bracketed by the two extremes in shock speed, $v_{s,7} = (1, 3)$. The corresponding density enhancement factors are (77, 230) for these two shock velocities, so that the gas densities in the shocks propagating in the SGMCs are $n_{s,3} \simeq (8.1, 24.4)$, respectively, in units of 10^3 cm^{-3}. We deduce the shock temperatures from the relation of Shull & Draine (1987) for strong shocks, $T_s = (3\,\mu_s v_s^2/16\,k_B) = 2.18 \times 10^5\, v_{s,7}^2$ K for $\mu_s = 0.965 m_H$. With densities and temperatures in hand, we can then roughly estimate the cooling rates of the shocked gas.

The calculations of Sutherland & Dopita (1993) are used to find the cooling time of low-density astrophysical plasmas at a fiducial SGMC metallicity of [Fe/H] $= -2$ (at the low end of the range of known GCS abundances: Harris 1991). Any increase in [Fe/H] will *shorten* the t_c (and L_c) we now derive. From Table 6 of Sutherland & Dopita, and the densities and temperatures from the preceding paragraph, we find t_c for a gas in collisional ionization equilibrium. (This will be an overestimate of the true timescale because some low-ionization species should remain in high-temperature, shock-heated plasmas, which should therefore have relatively higher cooling rates.) Thus, at $T_s = 2 \times 10^5$ K we have $t_c \simeq 2.4$ yr; and at 2×10^6 K, $t_c \simeq 58$ yr. These are infinitesimal in comparison to the free-fall time of $\sim 3 \times 10^6$ yr for SGMCs of mass $10^6\ M_\odot$. The associated cooling lengths are less than 10^{-3} of the size (35 pc) of a $10^6\ M_\odot$ cloud, and the condition $L_c \ll R_{cl}$ is well satisfied. Shocks that arise from collisions of magnetized, low-metallicity SGMCs therefore cool very rapidly, and the clouds survive collisions without vaporizing. Moreover, the collisions excite a considerable flux of Alfvén waves in the clouds, which probably provide additional support.

We may now return to the main issue, which is to compute the mass spectrum of cores within SGMCs when core growth and disruption are in equilibrium. Such a steady state $N(m)$ is of interest partly because it is independent of initial conditions. We therefore simplify our computations by supposing that cores of all masses are grown from an initial collection of objects which were all at the same minimum mass m_0. An explicit discussion of collision timescales is deferred to § 5, where we show that a steady state core spectrum can be achieved in a reasonable amount of time.

The conservation of mass is necessary for the establishment of a steady state distribution of clouds. It is significant, then, that GCSs constitute only a tiny fraction (~ 0.1–1%; Harris 1991) of their parent galaxies' total mass. Equivalently, any one SGMC can lose at most a few percent of its mass to globular clusters during a bout of star formation. To a very good approximation, then, the total gas mass of the core system which makes up an SGMC is conserved, and a steady state is possible in principle. This will always hold in a statistical sense, even though the odd core must lose quite a substantial fraction—likely $\gtrsim 50\%$—of its mass to stars if it is to form a bound cluster (Hills 1980; Lada, Margulis, & Dearborn 1984; Elmegreeen & Clemens 1985).

Such a high *local* star formation efficiency (SFE) in the *cluster-forming* cores guarantees both that the globulars will have the same masses (to within a factor of 2) as their progenitor cores, and that the core mass spectrum will be inherited by the emergent GCS. Elmegreen & Clemens (1985) suggest that cores of any mass are equally likely to have an SFE high enough to produce a bound cluster. The average SFE in such cores will then be indpendent of mass, so that *the GCS $N(m)$ is directly proportional to the core mass spectrum.* Since this presumably arises from an agglomeration process, it is explicitly independent of metallicity.

3.2. *A General Equation*

A full treatment of the agglomeration problem derives the cloud distribution function $f(m, r, v, t)$ (the number of bodies per unit mass and phase-space volume at time t). Such a distribution function evolves in time according to a general kinetic (Boltzmann) equation (Cowie 1980; Pumphrey & Scalo 1983), and as Pumphrey & Scalo argue, the best way to follow its development is through the use of N-body simulations. In this paper, however, we do not concern ourselves with the dynamics of SGMCs or their cores, but are ultimately interested only in the distribution of their masses. We therefore work explicitly with $N(m)$, the spatially averaged number density of clouds at mass m:

$$N(m) \equiv N(m, t) = \frac{1}{V} \iint f(m, r, v, t)\, dr\, dv\ .$$

Many studies show that the steady state mass spectra obtained by analytically or numerically following the evolution of $N(m)$ are generally in good agreement with the results from full-blown simulations which essentially yield the entire distribution function f (e.g., Wetherill 1990).

Without loss of generality, we can start by assuming an ensemble of clouds, all at the same mass m_0, that grows by binary collisions into a system with a wide range of masses. Since we consider only coalescent collisions, all clouds will ultimately have masses which are integer multiples of the fundamental building block m_0. There are then four processes which can change the number density of clouds at mass m:

1. Losses due to binary collisions with other clouds:

$$\left.\frac{\partial N(m)}{\partial t}\right|_L = -N(m) \sum_{m'=m_0}^{\infty} N(m')\sigma(m, m')v(m, m')\ .$$

Here σ is the cross section for the collision of the two clouds, and v is the relative velocity between the masses m, m'. Both quantities should be considered as appropriate averages over the cloud space and velocity distributions, and hence are functions of mass only.

2. Gains due to collision of two clouds with masses m' and $m - m'$:

$$\left.\frac{\partial N(m)}{\partial t}\right|_G = \frac{1}{2} \sum_{m'=m_0}^{m-m_0} N(m')N(m-m')\sigma(m', m-m')v(m', m-m')\ ,$$

where the factor $\frac{1}{2}$ accounts for the symmetry intrinsic to σ and v [i.e., $\sigma(m, m') = \sigma(m', m)$ and $v(m, m') = v(m', m)$].

3. Losses due to disruption by star (cluster) formation:

$$\left.\frac{\partial N(m)}{\partial t}\right|_D = -\frac{N(m)}{\tau(m)}\ ,$$

where $\tau(m)$ is the lifetime (disruption timescale) of a cloud at mass m and will, in general, be a function of m. The steady state mass spectrum does not depend on the details of the disruption mechanism, but just on the characteristic time $\tau(m)$ between cloud formation and destruction.

4. Gains of small clouds to cancel the loss of larger ones broken up by star formation:

$$\left.\frac{\partial N(m)}{\partial t}\right|_R = Ar(m)\ ,$$

where A is a normalization constant, and $r(m)$ is the "replenishment" mass spectrum of the new clouds. We assume that these clouds can only have masses which are integer multiples of m_0, and therefore that $r(m) \equiv 0$ for all $m < m_0$. In general, $r(m)$ governs the recycling of disrupted clouds *and* the replacement of any mass lost to newly formed stars (clusters). However, it is well known (e.g., Taff & Savedoff 1973; § 3.4 below) that the steady state $N(m)$ is insensitive to the details of $r(m)$, and we need not distinguish between its two contributions. The basic function of $r(m)$ is to conserve mass; just how this is done is largely irrelevant.

Generally, then, we have for each $m = m_0, 2m_0, \ldots$,

$$\frac{\partial N(m)}{\partial t} = \left.\frac{\partial N(m)}{\partial t}\right|_L + \left.\frac{\partial N(m)}{\partial t}\right|_G + \left.\frac{\partial N(m)}{\partial t}\right|_D + \left.\frac{\partial N(m)}{\partial t}\right|_R . \quad (3.2)$$

The product σv in the first two terms essentially measures the probability of a collision (and, by hypothesis, a coalescence), and is usually referred to as the coagulation or agglomeration kernel. Strictly, it is a function of the relative velocity and the masses of *both* colliding clouds; but to enable a semianalytical treatment which makes no appeal to N-body or Monte Carlo simulations, we formally separate this product and make a pair of simplifying assumptions (Kwan 1979):

$$\sigma(m, m') = \begin{cases} \sigma_{m'} , & m \le m' , \\ \sigma_m , & m > m' , \end{cases} \quad (3.3)$$

and

$$v(m, m') = \begin{cases} v_m , & m \le m' , \\ v_{m'} , & m > m' , \end{cases} \quad (3.4)$$

i.e., the collision cross section is approximated by that of the more massive cloud (appropriate enough if the cross sections are geometric), and the relative velocity is taken to be roughly the speed of the less massive cloud.

Given any set of functions σ_m, v_m, $\tau_m \equiv \tau(m)$, and $r_m \equiv r(m)$, we are interested in the *steady state* solution to equation (3.2) (such a solution will generally be unique, if it exists; see Taff & Savedoff [1973] for a proof of this in a simple case). Thus, we set $\partial N(m)/\partial t = 0$ for all m in equation (3.2) and divide both sides by $N^2(m_0)\sigma_{m_0} v_{m_0}$ to make it dimensionless. Denoting

$$x(m) \equiv \frac{N(m)}{N(m_0)} ,$$

we then have

$$0 = -x(m) \sum_{m'=m_0}^{\infty} x(m') \frac{\sigma(m, m')}{\sigma_{m_0}} \frac{v(m, m')}{v_{m_0}} + \frac{1}{2} \sum_{m'=m_0}^{m-m_0} x(m') x(m - m') \frac{\sigma(m, m - m')}{\sigma_{m_0}} \frac{v(m', m - m')}{v_{m_0}} - \frac{x(m)}{N(m_0)\sigma_{m_0} v_{m_0} \tau_*} \frac{\tau_*}{\tau_m} + \frac{A}{N^2(m_0)\sigma_{m_0} v_{m_0}} r_m , \quad (3.5)$$

where we have introduced a representative disruption timescale, τ_*, which *need not* be the lifetime of an m_0 cloud. The significance of τ_* is discussed in §§ 3.3 and 5 below. For now, it is more less an arbitrary scaling introduced to normalize τ_m on the way to a dimensionless agglomeration equation.

Equation (3.5) is further manipulated in Appendix A, which develops a recursive solution for the normalized mass spectrum $x(m)$. Two important dimensionless constants arise there:

$$\frac{\rho_c}{m_0 N(m_0)} \equiv \sum_{m'=m_0}^{\infty} \left(\frac{m'}{m_0}\right) x(m') \frac{\tau_*}{\tau_m}$$

and

$$\beta \equiv \frac{\rho_c \sigma_{m_0} v_{m_0} \tau_*}{m_0} = \frac{\tau_*}{\tau_{\rm fid}} ,$$

where $\tau_{\rm fid} \equiv m_0/\rho_c \sigma_{m_0} v_{m_0}$ is essentially a fiducial cloud-cloud collision timecale, to be discussed further in § 5. (Note, though, that the true collision time for any cloud is a function of its mass.) Our β is therefore qualitatively similar to (but quantitatively different from) that discussed by HP. The other quantity defined here, ρ_c, can be thought of as a measure of the average mass density in disrupted or disrupting clouds. ***The quantity β is one of the most important free parameters in our models and is key in determining the shape of the steady state mass spectrum.***

The solution for $x(m)$ obtained from equation (3.5) is completely determined by specifying each of

$$\frac{\sigma_m}{\sigma_{m_0}} , \quad \frac{v_m}{v_{m_0}} , \quad \frac{\tau_m}{\tau_*} , \quad \frac{r_m}{r_{m_0}} , \quad \text{and } \beta .$$

Of these quantities, only β is strictly a constant number; the other four are actually *arbitrary functions* of m. When all these functions are pure power laws, there are only five free model parameters (β and four power-law exponents); moreover, in such a case, the actual value of m_0 has no effect on the mass spectral shape, because of the dimensionless nature of our solution. The mass spectrum is then normalized by fixing the values of m_0 and $N(m_0)$ (or ρ_c, or any other quantity which essentially reflects the total number of clouds present).

Our formulation of this problem is more general than others in its explicit allowance for arbitrary mass dependences in the cloud lifetime τ_m and the replenishment function r_m. The agglomeration models of Kwan (1979) and Field & Saslaw (1965) (both of which are applied specifically to the mass distribution of Galactic GMCs) are easily obtained as special cases of our approach, as is a model in which no clouds are ever disrupted.

Kwan.—Set

$$\sigma_m/\sigma_{m_0} = (m/m_0)^a ,$$

$$v_m/v_{m_0} = (m/m_0)^b ,$$

$$\tau_*/\tau_m = H(m - m_*) \quad \text{(Heaviside function)} ,$$

$$r_m/r_{m_0} = \delta(m_0) \quad \text{(Kronecker delta)} .$$

In other words, the star formation in low-mass ($m < m_*$) clouds does not destroy them; and disrupted ($m \ge m_*$) clouds are replaced by a collection of m_0 objects. Thus, $R = 1$ and $\tau_*/\tau_{m_0} = 0$ (see eq. [A3]); and $\rho_c = \rho_*$, $\tau_* = \tau_0$ in Kwan's notation. Kwan denotes the critical mass m_* as m_1, but this is generally different from our m_1, which is the mass at which $\psi \sim m^2 N(m)$ peaks. Note that only the *ratio* m_*/m_0, and not the individual value of either, is important for the mass spectral shape, so long as σ and v are pure power laws. Finally, our parameter β is closely related, but not identical, to the quantity $\varkappa$ defined by Kwan.

Field & Saslaw.—This is a further specialization of Kwan's formulation. Set $a = b = 0$, and let $\tau_* \to 0$. Then $x(m) \to 0$ for all $m \ge m_*$, and $\rho_c \to 0$; however, because m_* is finite, we also have $\rho_c/\tau_* \to$ constant. Under these assumptions, the third

term on the right-hand side of equation (3.5) vanishes, and taking the first moment of the equation (i.e., insisting that mass be conserved) yields equation (6) of Field & Saslaw (1965). In this ideal case, all clouds have the same physical dimensions and move at the same speed, and those more massive than the critical limit m_* are disrupted immediately upon their formation. The steady state mass spectrum can then be found analytically using a generating-function approach (more or less a discrete Laplace transform; see Field & Saslaw).

Pure Agglomeration.—Regardless of the details of σ_m and v_m, if $m_* \to \infty$ then no clouds are ever allowed to be disrupted. That is, $\tau_m = \infty$ and $r_m = 0$ for all masses m, and only the first two terms on the right-hand side of equation (3.5) survive. In addition, a steady state is not possible, and the left-hand side of equation (3.5) is replaced by a more general term proportional to $\partial N(m)/\partial t$. The time evolution of $N(m)$ under these conditions has been studied analytically by van Dongen & Ernst (1988). A key result is that for large masses and times the mass spectrum takes the form of a Schechter function whose shape is determined by the forms of σ_m and v_m, and whose characteristic mass $M_*(t)$ (not to be confused with our m_*) grows with time. This scenario has therefore been proposed to account for the luminosity function of galaxies (e.g., Silk 1978; Silk & White 1978; Cavaliere, Colafrancesco, & Menci 1992; Shaviv & Shaviv 1993). Interesting variants on it have also been discussed in some theories of the stellar initial mass function (Nakano 1966; Silk & Takahashi 1979; Ferraioli & Virgopia 1979; Lejeune & Bastien 1986).

3.3. *Specifics*

We have investigated a family of agglomeration models which is just a slight generalization of that considered by Kwan (1979). In particular, we set

$$\frac{\sigma_m}{\sigma_{m_0}} = \left(\frac{m}{m_0}\right)^a \quad \text{and} \quad \frac{v_m}{v_{m_0}} = \left(\frac{m}{m_0}\right)^b , \tag{3.6}$$

after Kwan, but we also allow for the possibility of an arbitrary replenishment spectrum r_m (which turns out to have no real influence on our results; see § 3.4). Also, we define

$$\frac{\tau_m}{\tau_*} = \begin{cases} \infty , & m < m_* , \\ (m/m_*)^c , & m \geq m_* . \end{cases} \tag{3.7}$$

In § 2 we introduced m_* as the peak mass observed GCLFs [$\phi \sim mN(m)$]. We now propose that m_* is a critical mass above which the lifetime τ_m becomes finite, and SGMC cores are destroyed by the stars they form. Thus, τ_* is given significance here as the lifetime of a critical-mass core. A heuristic argument in favor of this idea is the fact that a prescription like equation (3.7) for τ_m leads to a discontinuity in $\partial N/\partial t$ at $m = m_*$. This, in turn, results in just the type of sudden steepening in $N(m)$ above m_* which is seen in the GCS data (cf. Figs. 1 and 2). We assume, without proof, that such an interpretation of the observed m_* is compatible with its very weak dependence on specific environmental factors, such as protogalaxy temperature and metallicity or the local background density.

Equation (3.7) touches on a long-standing issue in molecular cloud work; namely, it is not known precisely how the mass of a GMC affects its lifetime. There is some evidence that large GMCs are in fact shorter-lived than smaller ones, and there may even be a natural mass unit (of $\sim 5 \times 10^4\ M_\odot$) that marks a rather abrupt transition between small molecular clouds which do not form appreciable numbers of disruptive OB stars, and higher-mass GMCs which do (Williams & McKee 1995). Such a mass may be the analog of our m_*, justifying its introduction in τ_m to some extent. Above m_*, the power-law form of τ_m is chosen just for simplicity in the absence of any detailed empirical or theoretical information; but regardless of the true form of τ_m, its explicit dependence on mass is the most important new element of our agglomeration model, and is the feature which affords acceptable fits to the observed mass spectra of GCSs. (Kwan & Valdes 1987 and Olson & Kwan 1990a, b include mass-dependent cloud lifetimes in their N-body simulations of GMCs, but in quite a different conext than we have here). The behavior of τ_m below m_* is of less importance: even if τ_m/τ_* is a finite constant for $m < m_*$, the steady state mass spectrum which results is not significantly different from that obtained with τ_m as given by equation (3.7).

The power-law dependences of v_m and σ_m (eq. [3.6]) are physically motivated. If there is equipartition of kinetic energy in an ensemble of clouds, then $mv_m^2 \sim$ constant and $b = -\frac{1}{2}$. This scaling, or one very near it, results naturally from the conservation of momentum in coalescent cloud collisions (Penston et al. 1969; Handbury et al. 1977; Hausman 1982; Pumphrey & Scalo 1983). We therefore adopt $b = -\frac{1}{2}$ in the rest of what follows. Also, we assume throughout that the cloud collision cross section is just geometric, $\sigma_m \sim R_{cl}^2$, so that two obvious choices for a are $\frac{2}{3}$ ($m \sim R_{cl}^3$; all clouds have the same average density) and 1 ($m \sim R_{cl}^2$, as suggested by HP for SGMCs and their cores). In fact, $a = 1$ is observed in present-day molecular clouds and cores (Larson 1981; Wood et al. 1994), and can be understood in terms of the virial theorem if the clouds are self-gravitating (Elmegreen 1989a). We will confine our model to $a = 1$ in §§ 4 and 5, but keep it as a free parameter for the rest of this section. Our simple parameterization of σ_m does not allow for the possibilities of gravitational focusing or indirect cloud collisions resulting from the entanglement of magnetic fields (Clifford & Elmegreen 1983). However, these are both second-order effects, and for the sake of simplicity we ignore them here. The principal effect of including gravitational focusing in the cross section σ_m, for example, is apparently to drive the cloud system to a steady state on a shorter timescale, without significantly altering the final equilibrium $N(m)$ (e.g., Kirienko 1994).

A general constraint on the powers a and b is imposed by the possibility of gelation (also referred to as a merging runaway). The product σv of cross section and relative velocity is essentially a measure of the cloud collision probability. If this increases too strongly as a function, then the total mass of the cloud system will formally diverge in a finite time, forming a "gel" whose mass grows unchecked at the expense of an ordered "sol." This sort of phase transition is possible in the absence of any cloud disruption when, if $\sigma v(m_A, m_B) \sim m_A^a m_B^b$, it happens that $(a + b) > 1$ (e.g., van Dongen & Ernst 1988; Cavaliere et al. 1992); and it may occur even when massive clouds are allowed to self-destruct (see van Dongen & Ernst 1984 for an example in the context of chemical polymerization). Gelation leads to a decidedly *non*–steady state situation, just because the sol (which is what we are interested in) continually loses mass to the gel. Indeed, we are unable to find any solutions to equation (A2) whenever $(a + b) > 1$, apparently regardless of the value of c (i.e., no matter how quickly the most massive clouds are disrupted). This could be attributable to the onset of a gelation transition, although with $b = -\frac{1}{2}$ and $a = 1$, the possibility is clearly not a concern for our SGMCs and cores.

We now focus our attention on the properties of the steady state agglomeration spectrum at large masses. When $m > m_e$ is so large that the cloud replenishment spectrum $r_m \simeq 0$ and collisional gains contribute more to $\partial N(m)/\partial t$ than do collisional losses, we have (see Kwan 1979 for a sketch of the derivation)

$$\gamma \equiv \frac{d \log N}{d \log m} = -\frac{d \log \sigma_m}{d \log m} - \frac{1}{\beta} \frac{\rho_t}{\langle \rho \rangle} \frac{\sigma_{m_0}}{\sigma_m} \frac{\tau_e}{\tau_m} \frac{m}{m_0}$$

$$= -a - \frac{1}{\beta} \frac{\rho_t}{\langle \rho \rangle} \left(\frac{m}{m_0} \right)^{1-a} \left(\frac{m}{m_e} \right)^{-c} . \quad (3.8)$$

where we have made use of equations (3.6) and (3.7), and where

$$\frac{\langle \rho \rangle}{m_0 N m_0} \equiv \sum_{m' = m_0}^{\infty} \left(\frac{m'}{m_0} \right) x(m') \frac{v_{m'}}{v_{m_0}}$$

is the velocity-weighted average mass density of the cloud system. The influences of β, σ_m/σ_{m_0}, and τ_m/τ_e are seen explicitly in equation (3.8); v_m/v_{m_0} and r_m/r_{m_0} have a more subtle effect on the high-mass $N(m)$, through the ratio $\langle \rho \rangle / \rho_t$.

Clearly, in order for the total mass in clouds to be finite, there must be some mass above which $\gamma < -2$. This is just m_1, the peak mass of ψ. Note, however, that if $(a + c) > 1$, γ will eventually increase with m, and the total mass will diverge (unless $a > 2$, which seems unlikely if the collision cross sections are geometric). Thus, we must have

$$c \leq 1 - a . \quad (3.9)$$

Only a restricted range of positive c values is ever allowed, but any $c \leq 0$ will lead to a physically allowed steady state $N(m)$ when $a \leq 1$. Negative values of c are therefore more likely, and larger clouds should be shorter-lived than smaller ones. This can be understood if star formation becomes increasingly more vigorous in more massive clouds. Smaller clouds are then able to survive the process, but as it grows more powerful there eventually comes a mass, m_e, at which the destructive effects of cluster formation outweigh the containment afforded by the parent cloud. This imbalance grows with cloud mass, and larger ones are disrupted on ever shorter timescales τ_m. These ideas are broadly consistent with observations of the present-day ISM which show that, on average, more luminous OB associations are found in more massive GMCs (Williams & McKee 1995), and that the mass of the most massive (and presumably most disruptive) young star in a cluster-forming core increases with the mass of the core itself (Larson 1982).

The case $(a + c) = 1$ is of interest both because equation (3.9) shows it to be a limiting situation, and because HP suggest $a = 1$ and $c = 0$ to explain GCS mass spectra. By equation (3.8), γ is then a constant [i.e., $N(m)$ is a pure power law] at large masses; but we must have $\gamma < -2$, so

$$\beta \frac{\langle \rho \rangle}{\rho_t} \leq \beta \frac{\langle \rho \rangle}{\rho_t} \bigg|_{\max} \sim \frac{1}{2 - a} \left(\frac{m_e}{m_0} \right)^c . \quad (3.10)$$

Typically, $\langle \rho \rangle / \rho_t$ depends on β (see Appendix B for details), and the requirement of equation (3.10) effectively places an upper limit on $\beta = \tau_e/\tau_{fid}$ when $(a + c) = 1$. If the fiducial collision time is very short relative to τ_e, then massive clouds are formed too efficiently for their number to be held in check by internal destruction processes.

The observations reviewed in § 2 show that $m_1 > m_e$ in real GCSs (cf. Figs. 1 and 2). This fact provides an additional constraint on the parameters of our model. In particular, if β is smaller than some critical value β_{crit}, then $\gamma < -2$ for all $m > m_e$, and $m_1 = m_e$. Thus, only for $\beta \geq \beta_{crit}$ can we find an agglomeration model that matches the globular cluster data. The value of β_{crit} is estimated by setting $\gamma = -2$ in equation (3.8) to find

$$m_1 \sim (2 - a) m_0 \beta \frac{\langle \rho \rangle}{\rho_t} \frac{\sigma_{m_1}}{\sigma_{m_0}} \frac{\tau_{m_1}}{\tau_e} = (2 - a) \langle \rho \rangle \sigma_{m_1} v_{m_0} \tau_{m_1} , \quad (3.11)$$

or

$$\left(\frac{m_1}{m_e} \right)^{1-(a+c)} \sim (2 - a) \beta \frac{\langle \rho \rangle}{\rho_t} \left(\frac{m_e}{m_0} \right)^{a-1} . \quad (3.12)$$

Thus, in order to have $m_1/m_e \geq 1$, we require

$$\beta \frac{\langle \rho \rangle}{\rho_t} \geq \beta \frac{\langle \rho \rangle}{\rho_t} \bigg|_{crit} \sim \frac{1}{2 - a} \left(\frac{m_e}{m_0} \right)^{1-a} . \quad (3.13)$$

Exact expressions for β_{crit} are given in Appendix B, but we note here that a comparison of equations (3.13) and (3.10) shows that when $(a + c) = 1$, $\beta_{crit} \sim \beta_{max}$, so in such a case we always find $m_1 = m_e$. The mass dependences of the cloud cross sections σ_m and lifetimes τ_m must therefore satisfy the strict inequality $(a + c) < 1$ if these models are to describe the observations.

Equation (3.11) offers some physical insight into the critical mass m_1 (see also Kwan 1979). For very large m, there are many more clouds at masses $m' \ll m$ than there are with $m' \gtrsim m$. Thus, it is collisions with these smaller clouds (whose typical speeds are $\sim v_{m_0}$, and whose collective number density is therefore just $\sim \langle \rho \rangle$) which will dominate in the evolution of the larger body. The combination $m/\langle \rho \rangle \sigma_m v_{m_0}$ is therefore an estimate of the time required for a given cloud to double its mass by collisions in the steady state (see § 5 and Appendix C). The point m_1 is roughly the mass above which a cloud's growth (doubling) time exceeds its lifetime against disruption by star formation.

Finally, we can estimate the ratio $N(m_1)/N(m_e)$ by integrating equation (3.8):

$$\log \left[\frac{N(m_1)}{N(m_e)} \right] \sim -a \log \left(\frac{m_1}{m_e} \right) - \frac{1}{\ln 10} \frac{1}{\beta} \frac{\rho_t}{\langle \rho \rangle} \left(\frac{m_e}{m_0} \right)^{1-a}$$

$$\times \frac{1}{1 - (a + c)} \left[\left(\frac{m_1}{m_e} \right)^{1-(a+c)} - 1 \right] . \quad (3.14)$$

More accurate versions of this relation and of equation (3.12), based on a large number of model calculations, are given in Appendix B. The important point here is that these two equations together provide a conceptual link between the theory and the observations of GCS mass spectra: fixing any four of the six free parameters a, b, c, m_e/m_0, r_m/r_{m_0}, and β, and measuring m_1/m_e and $N(m_1)/N(m_e)$ directly from observations, allows for the remaining two model parameters to be estimated. In § 4, we specify a, b, r_m/r_{m_0}, and m_e/m_0 and then solve for c and β in the Milky Way, M31, and M87 GCSs. First, however, we consider in slightly more detail the generic features of our theoretical mass spectra.

3.4. *Numerical Results*

Figure 4 shows the quantities $x(m) \equiv N(m)/N(m_0)$, $\phi/\phi_0 \equiv \phi(\log m)/\phi(\log m_0)$, and $\psi/\psi_0 \equiv \psi(\log m)/\psi(\log m_0)$ as functions of m/m_0 for two different agglometration models: one

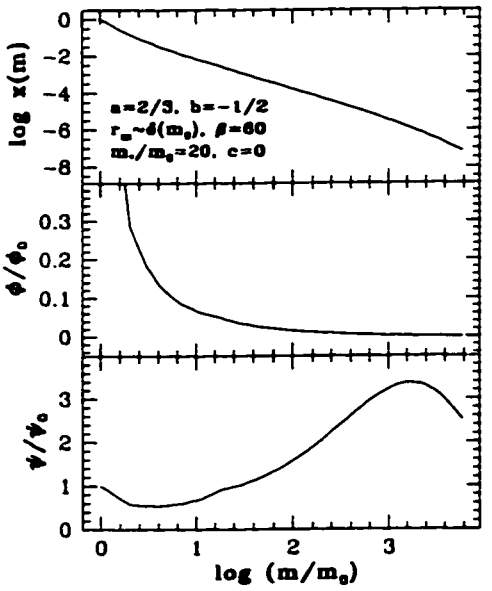

FIG. 4a

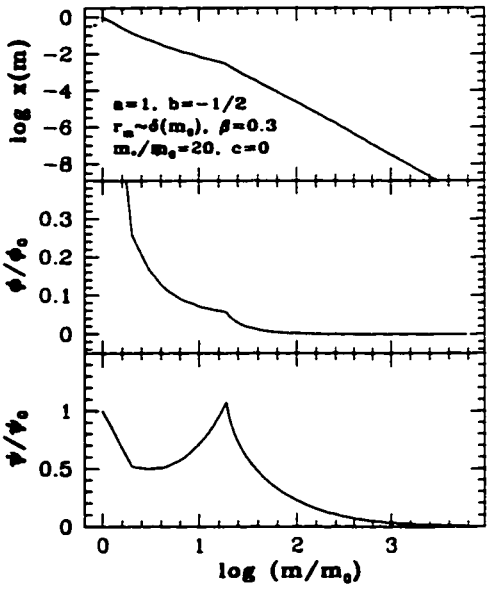

FIG. 4b

FIG. 4.—Model steady state mass distributions $x(m) = N(m)/N(m_0)$, $\phi(\log m)/\phi(\log m_0)$, and $\psi(\log m)/\psi(\log m_0)$. (*a*) Input parameters are $a = \frac{2}{3}$, $b = -\frac{1}{2}$, $c = 0$, $m_u/m_0 = 20$, $\beta = 60$, and $r_m/r_{m_0} = \delta(m_0)$. (*b*) Input $a = 1$ and $\beta = 0.3$, with other parameters the same as in (*a*).

with σ_m parameterized by $a = \frac{2}{3}$, and one with $a = 1$. We note here that ψ/ψ_0 is equivalent, aside from normalization, to the quantity $g(m)$ defined by Kwan (1979).

Most of the mass spectrum $x(m)$ in Figure 4*a* looks very much like a pure power law, and indeed a constant $\gamma = d \log N/d \log m \simeq -1.6$ to -1.7 roughly applies over two decades or so in mass. Such a close adherence to this simple approximation is, however, *not* the general rule. The slight cusp at m_u in the distributions of Figure 4*a* follows from the discontinuous definition of τ_m in equation (3.7), and is most apparent in ψ/ψ_0 in this case. Also, we have $m_1 > m_u$ (or $\beta > \beta_{crit}$) for this model: the LWLF ψ peaks around $1700m_0$, when the logarithmic slope $\gamma = -2$. The GLCF ϕ does not peak, but rises monotonically toward m_0; nowhere is $\gamma > -1$. This behavior may be connected to the model assumption that *all* collisions result in coalescence.

In Figure 4*b* we change a from $\frac{2}{3}$ to 1 and β from 60 to 0.3—recall that there is now an upper limit on β, since $(a + c) = 1$. As expected, the high-mass $N(m)$ is now just a pure power law (of slope -3 in this case), a limit which is achieved rather quickly after $m = m_u$. The cusp-like feature at m_u is obvious in all three distributions N, ϕ, and ψ, and the peak m_1 of ψ occurs at m_u because $\beta < \beta_{crit}$ necessarily when $(a + c) = 1$. There is significant curvature in $x(m)$ below m_u, in contrast to the conjecture (Kwan 1979) that $N(m)$ is just a pure power law of slope $\epsilon = -(3 + a + b)/2$ for $m < m_u$. In fact, even an approximate power-law behavior is only rarely realized at low masses in the exact solutions to equation (A2); and when it is, the slope need not correspond to the ϵ predicted by Kwan (1979). For example, with $a = 1$, $b = -\frac{1}{2}$, and $c = 0$, the coincidence of m_1 and m_u would lead us to identify m_u with the peak ψ rather than that of ϕ; and then we should also have $m_u/m_0 = m_1/m_0 \gtrsim 1000$, in order to include the full observed range of globular cluster masses. Kwan's formula would then give $\gamma = \epsilon = -1.75$ for the mass spectrum below m_1, which is what led HP to suggest this case as a viable GCS model. However, we find that γ is not constant at low masses, but approaches -1 from below as m increases to $m_u = m_1$. This is much shallower than the predicted ϵ, and does not apply anywhere in real GCS mass spectra. This situation cannot be remedied by any changes in β, b, m_u/m_0, or r_m; the specific $c = 0$ model of HP is not able to explain observed GCS mass spectra in detail. This is in line with the general result (eq. [3.9]) that since $a = 1$ for self-gravitating clouds, c must be strictly less than 0.

Figure 5*a* compares the mass spectrum obtained for a power-law replenishment spectrum, $r_m \sim m^{-3}$ (which is negligible even at $m = 20m_0$), with that corresponding to $r_m/r_{m_0} = \delta(m_0)$. Evidently, the dispersal of new clouds over a finite range in mass tends to "puff up" x, ϕ/ϕ_0, and ψ/ψ_0 everywhere, without really changing their gross shapes. This claim is rigorously proved by Taff & Savedoff (1972) specifically for the Field & Saslaw (1965) formulation of the agglomeration problem, and the work of Tomisaka (1984) suggests that it is quite generally true. In the absence of any information on what the form of r_m should be, and given the minor importance of this detail anyway, we adopt the simple δ-function formalism for the rest of what follows.

The results of varying the parameter $\beta = \tau_u/\tau_{fid}$ (or, more precisely, the ratio β/β_{crit}, where β_{crit} is the minimum ratio of timescales which allows for a separation of m_u and m_1) are illustrated in Figure 5*b*. A decrease in β corresponds to an increase in the fiducial collision time τ_{fid} and/or a decrease in the critical-mass lifetime m_u. It is then more difficult to form and/or maintain very large clouds, so the high-mass end of $x(m)$ steepens appreciably, and m_1 is brought closer to m_u. (In

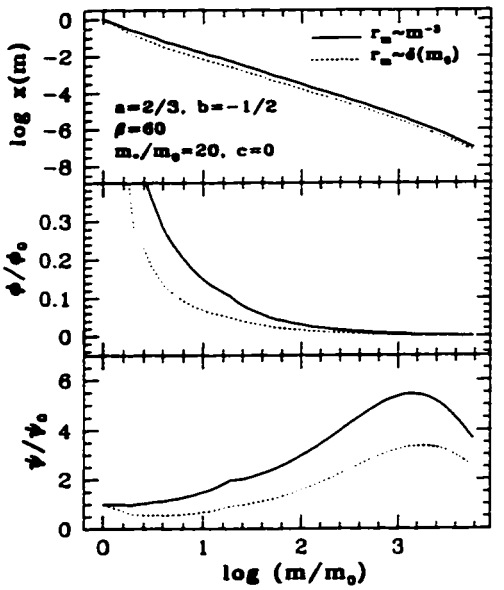

FIG. 5a

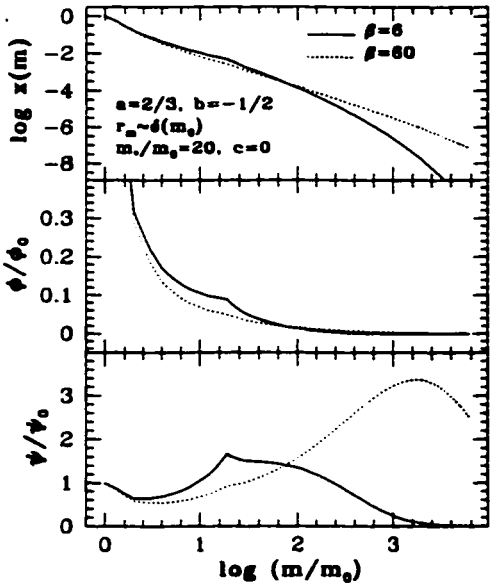

FIG. 5b

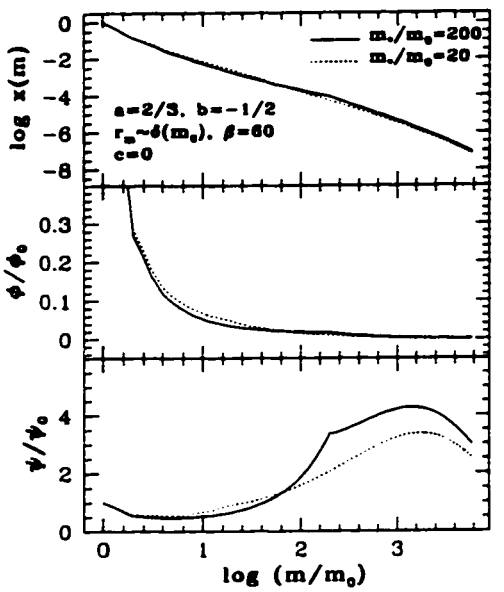

FIG. 5c

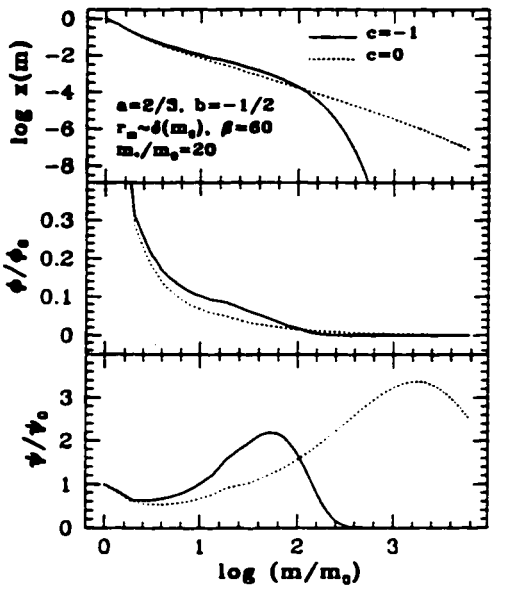

FIG. 5d

FIG. 5.—Generic effects of individual model parameters on the steady state mass spectrum. All models are computed with $a = \frac{1}{3}$ and $b = -\frac{1}{2}$, and the broken lines trace a convenient reference model with $c = 0$, $m_*/m_0 = 20$, $\beta = 60$, and $r_m/r_{m_*} = \delta(m_0)$ (i.e., the case illustrated in Fig. 4a). (*a*) Effect of varying the replenishment spectrum, r_m/r_{m_*}. (*b*) Effect of varying $\beta \equiv \tau_*/\tau_{\text{frag}}$. (*c*) Effect of varying the ratio m_*/m_0. (*d*) Effect of varying *c*, where the cloud disruption timescale $\tau_* \sim m^c$.

fact, by eq. [B2], $\beta_{crit} > 6$ for the models in Fig. 5*b*, so $m_1 = m_*$ for the solid curves there.) At the same time, intermediate- and low-mass clouds are able to exist longer without undergoing collisions, so that part of the mass spectrum is made shallower. The importance of β lies primarily in its influence on the observable ratio m_1/m_*.

Figure 5*c* shows the effect of increasing the ratio m_*/m_0 by an order of magnitude. This places relatively more clouds in the stable (infinitely long-lived) $m < m_*$ regime, which can only be done at the expense of the more massive clouds. $N(m)$ therefore steepens more quickly, and $\psi(\log m)$ peaks sooner, beyond m_*. Similar reasoning also explains why the value of β_{crit} (eqs. [3.13] and [B2]) must increase with the ratio m_*/m_0: when the numbers of high-mass clouds are relatively depleted, collision times must be shortened (relative to τ_*) to achieve $m_1 > m_*$.

Finally, Figure 5*d* contrasts the cloud distributions obtained when $c = 0$—in which case all clouds more massive than m_* have the same disruption timescale—with those for $c = -1$ (i.e., $\tau_m \sim m^{-1}$ for $m \geq m_*$). Because the largest clouds are shorter-lived than average when $c < 0$, and moderate-sized clouds are longer-lived, $N(m)$ is made steeper and shallower than "average" ($c = 0$) in those two mass regimes. The rapid destruction of massive clouds also causes m_1 to move closer to m_*, i.e., the timescales for cloud growth and disruption become comparable at lower masses. Evidently, if the two fundamental parameters a and b can be reasonably estimated (as we have argued they can), then the most important remaining elements of our theory are $\beta = \tau_*/\tau_{fld}$ and c.

In all we have computed ~500 steady state mass spectra with $b = -\frac{1}{2}$, $a = 1$ or $\frac{2}{3}$, a δ-function r_m, and a wide range of β, m_*/m_0, and c. These calculations are summarized in Appendix B. It is clear from them (as from the few models shown here) that a purely coalescent agglomeration scheme predicts too steep a slope at $m < m_*$ to be directly applied to real globular cluster systems. It is equally clear, however, that above m_*, where colliding clouds are indeed expected to merge (§ 3.1), our theory can provide a good description of observed GCS mass spectra.

4. FITTING THE LUMINOSITY FUNCTIONS

In this section and the next, we apply the theory of § 3 specifically to observations of GCS mass spectra. The agglomerating "clouds" discussed to this point are then understood to be the overdense cores of SGMCs. As discussed in § 3.1, the globular clusters formed by these cores are expected to inherit their systemic mass function.

While formally there are six free parameters in our theory—aside from the normalizations m_0 and $N(m_0)$, which do not affect the *shape* of the steady state mass spectrum—in practice, there are only two which cannot be specified *a priori*. The form of the replenishment function r_m is of little consequence, and we take it to be the simple δ-function. The relative value of the minimum mass for disruption is to some extent an unconstrained parameter; but we fix $m_*/m_0 = 200$, which is reasonable given the observed range in present-day globular cluster masses (recall $m_* \sim 1.6 \times 10^5\ M_\odot$). Equation (3.1) shows that all collisions involving cores with $m \geq m_*$ will then be coalescent. We can also identify probable values for the exponents a and b, which define collision cross sections and relative velocities. As discussed in § 3.3, we consider only $b = -\frac{1}{2}$ (equipartition of kinetic energy) on the basis of previous studies of agglomeration kinematics, and we assume purely geometric cross sections with $a = 1$ ($m \sim R^2$), which is understood in terms of the virial theorem for self-gravitating SGMCs and cores (this scaling is also consistent with the observation [Saito 1979] that the binding energy of globular clusters scales roughly as $m^{3/2}$).

This leaves us with only two free parameters: the mass dependence c of the disruption timescale (core lifetime: $\tau_m \sim m^c$ for $m \geq m_*$), and β (the ratio τ_*/τ_{fld} of characteristic disruption and collision times). To constrain these quantities, we make use of two independent observables: the ratios m_1/m_* and $N(m_1)/N(m_*)$. Best use is made of the data if both of these are estimated from the LWLF ψ, for the simple reason that m_1 stands out as the peak of this function (and m_* is clear as the peak of the GCLF ϕ). Once their values are known, it is possible to relate them to our agglomeration model, essentially through the use of equations (3.12) and (3.14) (see Appendix B for more details).

We have followed this procedure in fitting the shape of the M87 GCS spectrum. We estimate m_1/m_* and $\psi(m_1)/\psi(m_*)$ from Figure 2, and then solve equations (B3) and (B4) for c and β/β_{crit}; the results are listed in Table 1 and shown in Figure 6. Of particular note is the *negative value of* c (-0.6), as expected for $a = 1$ and $m_1 > m_*$. A generous estimate of the uncertainty in c is ± 0.3, based on the sensitivity to m_*/m_0 in the fitting equations given in Appendix B, and the observational uncertainties in m_1/m_* and $\psi(m_1)/\psi(m_*)$.

We fit the Milky Way and M31 GCS mass spectra in a slightly different manner. As Figure 1 shows, the LWLF there is rather flat at $m \geq m_*$, making it difficult to unambiguously pinpoint the peak mass m_1. However, if the core disruption

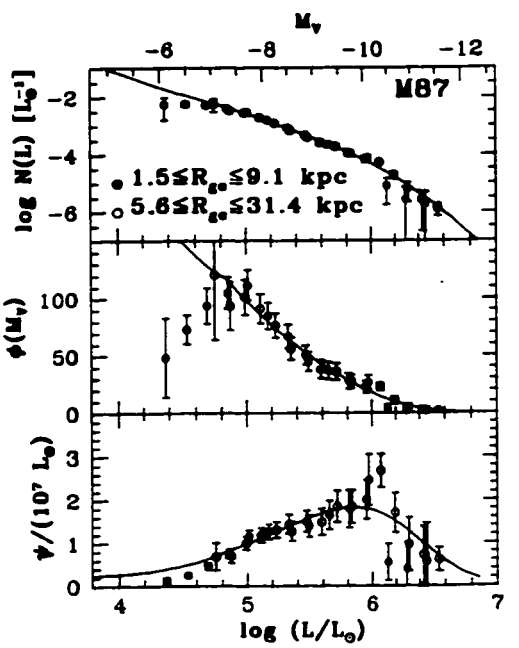

FIG. 6.—Model fits to the M87 GCS. We fix $a = 1$, $b = -\frac{1}{2}$, $r_m/r_{m_0} = \delta(m_0)$, and $m_*/m_0 = 200$. The observed $m_1/m_* = 10$ and $\psi(m_1)/\psi(m_*) = 2.2$ are then used to constrain c and β (Table 1). The model is scaled horizontally to match m_* with observed peak of the GCLF [$\log (L_*/L_\odot) = 4.9$] and vertically to match the value of $N(L)$ there.

TABLE 1

MODEL PARAMETERS FOR OBSERVED GCS MASS SPECTRA[a]

PARAMETER	$a = 1$		$a = \frac{1}{2}$	
	M87	Local Group[b]	M87	Local Group[b]
m_1/m_*	10	2.5	10	2.5
$\psi(m_1)/\psi(m_*)$	2.2	1.1	2.2	1.1
c	−0.6	−0.6	−0.25	−0.25
$\log(\beta/\beta_{crit})$	1.0	0.26	0.8	0.14

[a] $m_*/m_0 = 200$, $b = -\frac{1}{2}$, and $r_m \sim \delta(m_0)$ assumed throughout.
[b] Milky Way and M31 GCSs combined.

process depends largely on the physics of internal star formation and is relatively unaffected by external factors, then it may be that c (along with the GCLF peak m_*) is roughly the same from galaxy to galaxy. Under this assumption, we use the c values implied by the M87 data and estimate $\psi(m_1)/\psi(m_*)$ from Figure 1 to solve equations (B4) and (B3) for m_1/m_* and β. The results are given in Table 1, with the corresponding model curves drawn in Figure 7.

Although $a = 1$ is the natural choice of cross section here, setting $a = \frac{1}{2}$ allows for model fits of equal quality, and gives similar results overall (see Table 1). In particular, we still find $c < 0$, showing that, regardless of any assumptions on their mass-radius relation, the more massive cores of a given SGMC must be shorter-lived.

This theory of coalescent agglomeration can account for the shape of observed GCLFs over the full range of masses $m \geq m_*$.

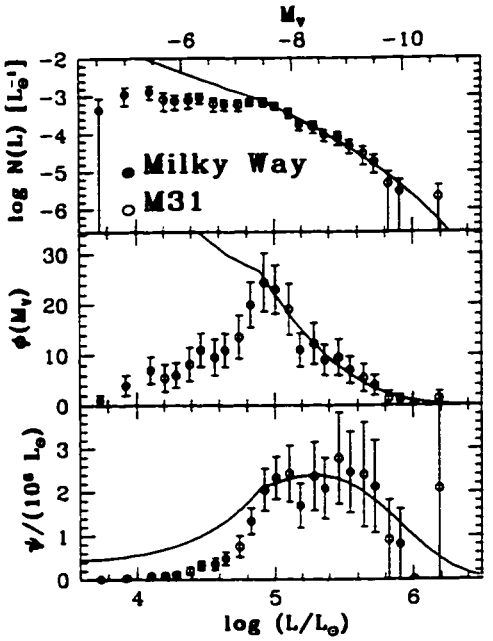

FIG. 7.—Model results for the Milky Way and M31 GCS mass spectra combined. Again, $a = 1$, $b = -\frac{1}{2}$, $r_m/r_{m_0} = \delta(m_0)$, and $m_*/m_0 = 200$ are fixed. The observed $\psi(m_1)/\psi(m_*) = 1.1$ and $c = -0.6$ (from Fig. 6) are then used to fit for m_1/m_* and β (Table 1). The model is scaled horizontally to match m_* with the observed peak of the GCLF [$\log(L/L_\odot) \simeq 4.9$] and vertically to match the value of $N(L)$.

Given the similarity between the mass spectra of GMC cores and the M87 GCS in particular (cf Figs. 2 and 3), our general model should also be able to explain the distribution of cloud masses in the present-day ISM. There are claims (e.g., Elmegreen 1989b) that agglomeration mass spectra (for $m < m_*$) are too steep to match Galactic GMC data. However, we would suggest that the GMC/core $N(m)$ be matched to the $m > m_*$ region of the models, where a mass-dependent cloud lifetime could bring the theory back into line with observation.

The assumption of purely coalescent collisions is not always valid for $m < m_*$, and the models in Figures 6 and 7 do not describe the data there. This is most evident in the GCLF itself (*middle panels*), emphasizing the need to consider *all three* of N and the moments ϕ and ψ when studying theoretical or observed GCS mass spectra. A careful reckoning of the effects of collisional fragmentation could go some way toward a successful model of the entire GCS mass spectrum, with a shallower low-mass slope (e.g., Goldstein & Mazzella 1974; Cowie 1980; Nozakura 1990). The best way to address this possibility is through the use of N-body or SPH simulations, which would have the additional advantage of self-consistently predicting the dynamics of a proto-GCS.

Figures 6 and 7 generally confirm our conclusion (§ 2; also McLaughlin 1994) that real differences exist between the mass spectra of the M87 and Local Group GCSs. Moreover, it is possible to explain these differences without compromising the universality of m_*. If indeed the mass dependence c of the core lifetime τ_m does not vary between SGMCs or between galaxies, then the ratio $\beta = \tau_*/\tau_{fid}$—which is decoupled from m_*—is the fundamental quantity which most affects the shape of the steady state core mass spectrum. Specifically, our analysis suggests that β was smaller for cores in the SGMCs of the Milky Way and M31 than for those in M87. The reason for this is still unclear, but it seems *not* to be an effect of Hubble type alone, and may have more to do with the generally sparser protogalactic environment in the Local Group. This view is supported by the observation of Local Group–like mass spectral slopes in the GCSs of two early-type galaxies by Kissler et al. (1994) ($\gamma = -1.9 \pm 0.1$ above m_* in NGC 4636, an elliptical galaxy in a sparse region of the Virgo Cluster) and Durrell et al. (1995) ($\gamma = -1.8 \pm 0.4$ for $m > m_*$ in the dwarf companion to the field S0 NGC 3115).

5. TIMESCALES: CONSEQUENCES FOR GALAXY FORMATION

5.1. *Collision Times*

Our models involve a fiducial collision time $\tau_{fid} = m_0/\rho_* \sigma_{m_0} v_{m_0}$. However, the true collision time for a core (i.e., the mean time between any two collisions) is a function of its mass. In Appendix C we give a general expression for this quantity (in units of τ_{fid}) in the steady state. There we also discuss the mass-doubling time (or growth time), which is important for understanding the peak of ψ. Figure 8 shows both of these timescales, as functions of cloud mass, for the specific ($a = 1$) models fitted to the GCS mass spectra of the Milky Way and M87.

The normalized collision time τ_{coll}/τ_{fid} is a decreasing function of mass, with a maximum of $(\beta/K)^{1/2}$ at $m = m_0$ (eq. [C2]; K^{-1} is the reduced mean free path defined in Appendix A). Table 2 lists $\tau_{coll}(m_0)/\tau_{fid}$, along with several other important quantities, for the agglomeration models of § 4. At large masses, we expect $\tau_{coll} \sim \sigma_m^{-1}$, which is seen in Figure 8. The relations given in Table 2 for $\tau_{coll}(m)$ are computed from equa-

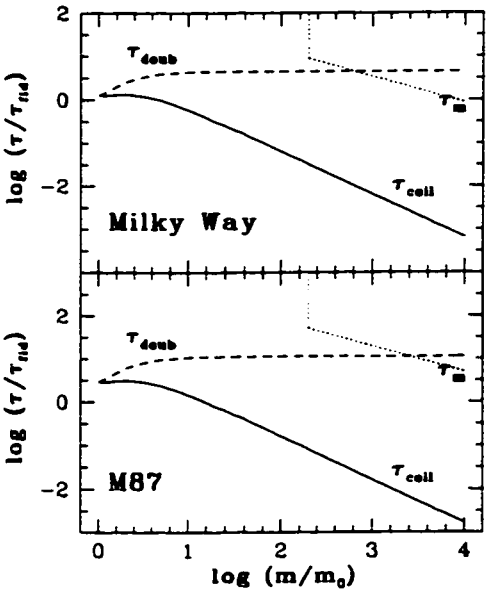

FIG. 8.—Dimensionless collision times τ_{coll}/τ_{fid}, doubling or growth times τ_{doub}/τ_{fid}, and disruption times τ_∞/τ_{fid} for the steady state agglomeration models which best fit the GCS mass spectra of the Milky Way (and M31) and M87. *Top panel:* Milky Way; $a = 1$, $b = -\frac{1}{2}$, $m_u/m_0 = 200$, $c = -0.6$, $r_\infty \sim \delta(m_0)$, and $\beta = 8.8$. *Bottom:* M87; $\beta = 51$. In both cases, $\tau_{doub} = \tau_\infty$ occurs near $m = m_*$, the peak mass of the LWLF ψ.

tion (C4), and for $m \geq 20m_0$ lie within 5% of the exact results of equation (C1).

The growth time τ_{doub}, also plotted in Figure 8, is calculated as per equation (C5). It is just equal to τ_{coll} for $m = m_0$, and scales roughly as $m\tau_{coll}$ ($\sim$constant for $a = 1$) at large masses (eq. [C6]; the velocity-weighted mean mass $\langle m \rangle$ is given in Table 2).

These dimensionless times are put on an absolute scale with a numerical estimate of τ_{fid}. The total mass density of a system of cores is ρ_{cl}, the internal density of the parent SGMC; similarly the one-dimensional velocity dispersion of the system is just σ_{cl}. Furthermore, with $a = 1$ all cores have the same column density Σ_{core}. Thus, by equation (C7) and Table 2,

$$\tau_{fid}(\text{cores}) \simeq \frac{1}{0.17\sqrt{\beta K}} \frac{\Sigma_{core}}{\rho_{cl}\sqrt{6}\,\sigma_{cl}} \qquad (5.1)$$

for each of the Milky Way/M31 and M87 GCSs. This estimate of τ_{fid} should be taken only as a rough guide, since the pure-coalescence mass spectra are steeper than observed GCS $N(m)$ below m_*. Consequently, the ratio of ρ_r to the total mass density of a cloud system will be larger in a more complete theory, and τ_{fid} shorter, by perhaps a factor of 2. The replenishment of small clouds over a finite mass range would also work to shorten τ_{fid}.

The core τ_{fid} depends on the properties of the parent cloud. In particular, since SGMCs and cores are self-gravitating, they obey the virial (Bonnor-Ebert) scalings (cf. eq. [5.2] of HP):

$$\sigma_{cl}^4 \sim m_{cl} P_s^{1/2}\,, \quad \rho_{cl}\sigma_{cl}^2 \sim P_s\,, \quad \Sigma_{cl} \sim P_s^{1/2}$$
$$\sigma_{core}^4 \sim m_{core} P_s^{1/2}\,, \quad \rho_{core}\sigma_{core}^2 \sim P_s\,, \quad \Sigma_{core} \sim P_s^{1/2}\,, \qquad (5.2)$$

where P_s is the surface pressure on the SGMC. Thus SGMCs or cores under the same P_s will have a constant column density Σ, i.e., $m \sim R^2$ and $a = 1$. (The surface pressure on the cores, which should really appear in the second line of equation [5.2], is just proportional to $\rho_{cl}\sigma_{cl}^2 \sim P_s$; see also HP.) Thus,

$$\tau_{fid}(\text{cores}) \sim \frac{\Sigma_{core}}{\rho_{cl}\sigma_{cl}} \sim \rho_{cl}^{-1/2} \sim m_{cl}^{1/4} P_s^{-3/8}\,. \qquad (5.3)$$

Now, magnetized SGMCs are expected to evolve on an *ambipolar diffusion* timescale, which scales with the dynamical time: $\tau_{AD,cl} \simeq 10\tau_{ff,cl} \sim \rho_{cl}^{-1/2}$. Equation (5.3) therefore shows that $\tau_{fid}/\tau_{AD,cl}$ is the same in every SGMC. Moreover, as we now show, this ratio is uniformly small, so the cores of any cloud should be able to evolve to a steady state $N(m)$.

For a Galactic SGMC of mass $m_{cl} = 7 \times 10^6\ M_\odot$ and Galactocentric distance $r_{gc} = 8$ kpc, HP estimate (see their Table 3) $\rho_{cl} = 0.23\ M_\odot\ \text{pc}^{-3}$ and $\sigma_{cl} = 25\ \text{km s}^{-1}$. Also, $\Sigma_{core} = 1200\ M_\odot\ \text{pc}^{-2}$ in such a cloud. Then from equations (5.1) and (5.3),

$$\tau_{fid}(\text{MW cores}) \simeq 6.9 \times 10^7\ \text{yr}\left(\frac{m_{cl}}{7 \times 10^6\ M_\odot}\right)^{1/4}\left(\frac{r_{gc}}{8\ \text{kpc}}\right)^{3/4},$$

where we have explicitly assumed that the parent SGMCs are embedded in a potential well filled with hot, isothermal gas such that $P_s \sim r_{gc}^{-2}$. Since isothermality further implies $P_s \sim \sigma_{gal}^4$, equations (5.1) and (5.3) also give

$$\frac{\tau_{fid}(\text{M87})}{\tau_{fid}(\text{MW})} = \left(\frac{\sigma_{gal,M87}}{\sigma_{gal,MW}}\right)^{-3/2}\left[\frac{(\beta K)_{M87}}{(\beta K)_{MW}}\right]^{-1/2} \simeq 0.1\,,$$

where we estimate $\sigma_{M87} \simeq 380\ \text{km s}^{-1}$ and $\sigma_{MW} \simeq 220/(2)^{1/2} \simeq 150\ \text{km s}^{-1}$.

We expect that a steady state distribution of core masses should be established within a few fiducial collision times. In the Milky Way, the ratio of SGMC ambipolar diffusion time to core τ_{fid} is $\tau_{AD,cl}/\tau_{fid} \simeq 2.5$; in M87, $\tau_{AD,cl}/\tau_{fid} \simeq 6.2$. The assumption that cores in an SGMC can attain a steady state mass spectrum is therefore a reasonable one.

We may also ask whether the SGMCs themselves can reach a collisionally induced steady state distribution of masses. A model-independent, order-of-magnitude estimate for the collision timescale of these larger entitites is just $\tau_{fid,cl} \sim \Sigma_{cl}/(\Gamma\rho_{gal}(6)^{1/2}\sigma_{gal})$, where ρ_{gal} and σ_{gal} are the total (gas + dark matter) mass density and one-dimensional dispersion in the potential well inhabited by the SGMCs, and Γ is the ratio of

TABLE 2

COMPUTED QUANTITIES FOR $a = 1$ GCS MODELS

Galaxies	β	K	$\rho_s/\langle\rho\rangle$	$\langle m\rangle/m_0$	$\bar{m}/m_0$	$N(m_0)/N_{tot}$	$\tau_{coll}(m_0)/\tau_{fid}$	$\tau_{coll}(m)/\tau_{fid}$*
Milky Way/M31	8.8	5.69	4.5	1.31	4.69	0.83	1.2	$6.7(m/m_0)^{-1}$
M87	51.0	6.27	12.1	1.26	5.28	0.85	2.9	$17.1(m/m_0)^{-1}$

* Large-mass ($m \geq 20m_0$) approximation: see eq. (C4).

gas (SGMC) to total mass. For conditions appropriate to the proto–Milky Way, we have $\Sigma_{cl} = 260(8 \text{ kpc}/r_{gc})\ M_\odot\ \text{pc}^{-2}$ (HP); $\rho_{gal} = V_c^2/4\pi G r_{gc}^2$ for an isothermal sphere; and $\sigma_{gal} = V_c/(2)^{1/2}$. Thus, $\tau_{fid,cl} \sim 4$–5×10^8 yr $(0.1/\Gamma)(r_{gc}/8 \text{ kpc})$. The Gyr timescales implied for the establishment of a steady state among the SGMCs could make it difficult for this to occur before the onset of large-scale collapse and galaxy formation.

5.2. *Disruption Times*

Figure 8 also shows the dimensionless disruption times τ_m/τ_{fid} for our GCS models (see eq. [3.7], and recall $\tau_*/\tau_{fid} = \beta$). For $m < m_* = 200m_\odot$, $\tau_m = \infty$; and for $m \geq m_*$ the power-law slope $c = -0.6$ of τ_m comes from the fits of § 4. The lifetime τ_m of a core equals its growth time τ_{doub} at $m \simeq m_1$ (the peak mass of ψ; cf. the values given in Table 1), in agreement with the analysis of § 3.3.

We anticipate that SGMCs are supported by turbulent, weak magnetic fields ($\sim$10–100 μG; HP), as is the case for molecular clouds in the present ISM. Modern theories of star formation (see the review of Shu, Adams, & Lizano 1987) posit that the star formation timescale is linked to the ambipolar diffusion time because it is the field slippage in magnetically supported clouds that allows the density to grow in cores. Thus, it is reasonable that core disruption times be linked to the ambipolar diffusion time of their parent SGMC: $\tau_* \sim \tau_{AD,cl} \sim \rho_{cl}^{-1/2}$ (but see Patel & Pudritz 1994). (This scaling sets the lifetimes of cores in *different* SGMCs in a protogalaxy. We still have from § 4 that within any *one* parent cloud, τ_m is a decreasing function of mass for $m_{core} \geq m_*$.)

This result and equation (5.3) together imply that, among the SGMCs of a given protogalaxy,

$$\beta(\text{cores}) = \frac{\tau_*}{\tau_{fid}} = \text{constant} .$$

That is, β is independent of SGMC mass or the surface pressure P_s, and every cloud produces globulars with the same $N(m)$. (However, as discussed in § 4, it is still not understood why β, and hence the shape of the GCS mass spectrum, varies *between* galaxies.) For a collection of SGMCs moving in an already well defined potential well, P_s will depend on galactocentric radius r_{gc}, so that

1. The invariance of GCS mass spectra with galactocentric radius arises from the fact that the (fiducial) core collision and disruption timescales are proportional to one another at every r_{gc}. Since β and m_* both are independent of r_{gc}, so too is the average globular cluster mass.

2. SGMCs, and therefore cores, under higher surface pressures evolve on shorter timescales. To the extent that higher pressures P_s obtain for clouds and cores nearer the center of a protogalactic potential well, this implies that GCS formation was an inside-out process.

Under the assumption of isothermality, $P_s \sim r_{gc}^{-2}$, the fact that the average cluster mass is independent of r_{gc} can be used (HP) to explain the observation (van den Bergh, Morbey, & Pazder 1991) that the half-light radii of Galactic globulars scale as $r_{gc}^{1/2}$.

The disruption timescale of a critical-mass (m_*) core is $\tau_* = \beta\tau_{fid}$. From the values given above for τ_{fid}, and with β from Table 2,

$$\tau_*(\text{MW cores}) \simeq 6.1 \times 10^8 \text{ yr} \left(\frac{m_{cl}}{7 \times 10^6\ M_\odot}\right)^{1/4} \left(\frac{r_{gc}}{8 \text{ kpc}}\right)^{3/4} ,$$

to within the same factor of $\sim$2 uncertainty which affects τ_{fid}. Also,

$$\frac{\tau_*(\text{M87})}{\tau_*(\text{MW})} = \frac{\tau_{fid}(\text{M87})}{\tau_{fid}(\text{MW})} \frac{\beta_{\text{M87}}}{\beta_{\text{MW}}} \simeq 0.6 .$$

The ratio $\tau_*/\tau_{AD,cl}$ is a constant 3.5 in the Milky Way, while for M87 it is 8.2

6. SUMMARY

We have further developed the theory of Harris & Pudritz (1994), which proposes that, much like presently forming star clusters, globulars were born in the dense cores of much larger, self-gravitating clouds (supergiant molecular clouds, or SGMCs). Specifically, we have derived the steady state mass spectrum, $N(m)$, which represents an equilibrium between the rates of creation of new large cores by collisions between smaller ones and disruption of existing cores by the side effects of internal star formation. This mass spectrum will then be passed on to a globular cluster system (GCS) by virtue of the very high ($\gtrsim$50%) star formation efficiency required of any core which is to form a bound star cluster. We have fitted theoretical spectra directly to observations in the Milky Way, M31, and M87 GCSs, as it seems plausible that the distributions there have not been significantly altered by dynamical evolution over a Hubble time. Our basic theory has no intrinsic mass scale, and so could also be used to interpret the $N(m)$ of present-day GMCs and their cores. In particular, there are striking similarities between the mass functions of clumps in the Rosette and Maddalena GMCs, and those of GCSs.

The models constructed here are based on the assumption that all collisions between protocluster cores will result in coalescence. This is an oversimplification in general, but true for massive, slow-moving cores. We therefore find that the models describe real GCS data only above the peak mass m_* of the globular cluster luminosity function $\phi \sim mN(m)$. [A peak in the moment ϕ corresponds only to a steepening of the fundamental $N(m)$, and does not point to any "characteristic" globular cluster mass.] Future work will examine the role of collisional fragmentation in determining the full GCS mass spectrum. The main results of this paper are as follows:

1. The peak m_* is observed to be nearly the same ($\simeq 1.6 \times 10^5\ M_\odot$) in galaxies of all types and sizes. We suggest that this critical mass marks a transition between low-mass cores which are able to contain the star formation proceeding within them, and high-mass ones which are destroyed by it. It remains to be shown that this interpretation is consistent with the overall insensitivity of GCS mass spectra to either cluster or galaxy metallicity.

2. The luminosity-weighted luminosity functions [$\psi \sim m^2N(m)$] of GCSs are observed to peak at masses $m_1 > m_*$ which can vary from galaxy to galaxy. Cores with $m \gtrsim m_1$ are disrupted (by star formation) before they can grow appreciably through more collisions. The ratio m_1/m_* in particular, and the shape of the GCS mass spectrum in general, are therefore determined primarily by the ratio $\beta = \tau_*/\tau_{fid}$ where τ_* is the lifetime of a critical-mass (m_*) core, and τ_{fid} measures a fiducial core-core collision time. This ratio can vary between galaxies independently of m_*: we find $\beta = 8.8$ for the Milky Way and M31 GCSs, and $\beta = 51$ in M87.

3. Within any one SGMC, the lifetimes of massive ($m > m_*$) cores must decrease with mass. Specifically, for a power-law

parameterization $\tau_m = \tau_e(m/m_e)^c$, our fits to the GCS data give $c \simeq -0.6$. The absolute scale τ_e is set by the ambipolar diffusion time ($\tau_{AD,cl} \simeq 10\tau_{ff,cl}$) of the parent SGMC. For cores in a cloud of mass m_{cl} and galactoctentric radius r_{gc}, we estimate

$$\tau_e \simeq 6.1 \times 10^8 \text{ yr } (m_{cl}/7 \times 10^8\ M_\odot)^{1/4}(r_{gc}/8 \text{ kpc})^{3/4}$$

in the Milky Way, and $\tau_e(\text{M87})/\tau_e(\text{MW}) \simeq 0.6$.

4. The fiducial core collision time is

$$\tau_{fid} \sim 6.9 \times 10^7 \text{ yr } (m_{cl}/7 \times 10^8\ M_\odot)^{1/4}(r_{gc}/8 \text{ kpc})^{3/4}$$

in Milky Way SGMCs; and $\tau_{fid}(\text{M87})/\tau_{fid}(\text{MW}) \simeq 0.1$. Thus, τ_e and τ_{fid} both increase with r_{gc}, suggesting an inside-out sequence of GCS formation.

5. The core timescales τ_e and τ_{fid} have identical dependences on the mass and galactocentric position of the parent SGMCs, so the ratio β is constant throughout a given protogalaxy. This explains the observed invariance of GCS mass spectra with galactocentric radius.

6. The ratio β is different in the Milky Way and M31 than in M87. This effect is not one of Hubble type alone, but is likely due more to the overall sparser environment of the Local Group.

We are grateful to Bill Harris for many interesting discussions on these topics. We also acknowledge the referee, Bruce Elmegreen, for useful comments which led to improvements in the paper. This work was supported by the Natural Sciences and Engineering Research Council of Canada, through a graduate fellowship to D. E. M. and an operating grant to R. E. P.

APPENDIX A

SCALED EQUATIONS

Equation (3.5) can be further simplified by working with a dimensionless mass (m/m_0) and replenishment spectrum (r_m/r_{m_0}), and by introducing the three dimensionless constants

$$\frac{\rho_r}{m_0 N(m_0)} \equiv \sum_{m'=m_0}^{\infty}\left(\frac{m'}{m_0}\right)x(m')\frac{\tau_e}{\tau_{m'}},$$

$$R \equiv \sum_{m'=m_0}^{\infty}\left(\frac{m'}{m_0}\right)\frac{r_{m'}}{r_{m_0}},$$

and

$$\beta \equiv \frac{\rho_r \sigma_{m_0} v_{m_0} \tau_e}{m_0}.$$

As discussed below equation (3.5), β is the ratio τ_e/τ_{fid} of fiducial disruption and collision timescales; ρ_r reflects the average mass density in disrupted or disrupting clouds; and R is related to the average density in newborn clouds. Both β and R are part of a model's specification (R being fixed by a choice of r_m), and $\rho_r/m_0 N(m_0)$ is then derived from the steady state mass spectrum which solves equation (3.5) (or [A2] below).

Mass is conserved in the steady state:

$$\sum_{m'=m_0}^{\infty} m' \frac{\partial N(m')}{\partial t} = 0,$$

so that taking the first moment of equation (3.2) (or eq. [3.5]) yields

$$A \sum_{m'=m_0}^{\infty} m' r_{m'} = \sum_{m'=m_0}^{\infty} m' N(m') \frac{1}{\tau_{m'}}.$$

The term on the right-hand side of this expression is just the total mass-loss rate due to star formation and cloud disruption; that on the left, the rate of replenishment required to balance these losses. The definitions of R and ρ_r then imply

$$A r_{m_0} = \frac{1}{R}\frac{\rho_r}{m_0 \tau_e}. \tag{A1}$$

Now we make use of equations (3.3) and (3.4) to rewrite the first term on the right-hand side of equation (3.5) (which is just proportional to $[\partial N(m)/\partial t]|_L$) as

$$-x(m)\left[\frac{\sigma_m}{\sigma_{m_0}}\sum_{m'=m_0}^{m-m_0} x(m')\frac{v_{m'}}{v_{m_0}} + \frac{v_m}{v_{m_0}}\sum_{m'=m_0}^{\infty} x(m')\frac{\sigma_{m'}}{\sigma_{m_0}} - \frac{v_m}{v_{m_0}}\sum_{m'=m_0}^{m-m_0} x(m')\frac{\sigma_{m'}}{\sigma_{m_0}}\right],$$

and define

$$K \equiv \sum_{m'=m_0}^{\infty} x(m')\frac{\sigma_{m'}}{\sigma_{m_0}}.$$

TABLE 3

PARAMETERS FOR SELECTED NUMERICAL MODELS[a]

	$K \equiv \sum_{m'=m_0}^{\infty} x(m')(\sigma_{m'}/\sigma_{m_0})$					
	$a = 1,\ c = -0.6$			$a = \frac{1}{3},\ c = -0.25$		
β/β^{*}_{crit}	$m_e/m_0 = 100$	$m_e/m_0 = 200$	$m_e/m_0 = 500$	$m_e/m_0 = 100$	$m_e/m_0 = 200$	$m_e/m_0 = 500$
0.....	4.306	4.773	5.376	3.435	3.652	3.893
1.....	5.079	5.524	6.111	3.750	3.922	4.115
2.....	5.265	5.710	6.312	3.824	3.985	4.172
5[b].....	5.545	6.005	6.600	3.931	4.078	4.250
10.....	5.785	6.240	6.840	4.016	4.156	4.309
20.....	6.057	6.515	7.149	4.103	4.234	4.387

[a] A δ-function r_m is assumed, and $b = -\frac{1}{2}$ is fixed throughout.
[b] β_{crit} is given by eq. (B2) of the text.

Since $[N(m)\sigma_m]^{-1}$ is the mean distance between collisions with clouds of mass m, K^{-1} can be viewed as a reduced mean free path, normalized by the length $[N(m_0)\sigma_{m_0}]^{-1}$.

Using equation (A1) and the definitions of K and β, equation (3.5) then becomes

$$0 = -x(m)\left[\frac{\sigma_m}{\sigma_{m_0}}\sum_{m'=m_0}^{m-m_0} x(m')\frac{v_{m'}}{v_{m_0}} - \frac{v_m}{v_{m_0}}\sum_{m'=m_0}^{m-m_0} x(m')\frac{\sigma_{m'}}{\sigma_{m_0}}\right] - x(m)\frac{v_m}{v_{m_0}}K + \frac{1}{2}\sum_{m'=m_0}^{m-m_0} x(m')x(m-m')\frac{\sigma(m', m-m')}{\sigma_{m_0}}\frac{v(m', m-m')}{v_{m_0}}$$

$$-\frac{1}{\beta}\left[\frac{\rho_\epsilon}{m_0 N(m_0)}\right]\frac{\tau_e}{\tau_m}x(m) + \frac{1}{\beta R}\left[\frac{\rho_\epsilon}{m_0 N(m_0)}\right]^2\frac{r_m}{r_{m_0}}. \quad \text{(A2)}$$

Note that $x(m_0) = 1$ by definition, so setting $m = m_0$ in equation (A2) gives

$$K = \frac{1}{\beta R}\left[\frac{\rho_\epsilon}{m_0 N(m_0)}\right]^2 - \frac{1}{\beta}\frac{\tau_e}{\tau_{m_0}}\left[\frac{\rho_\epsilon}{m_0 N(m_0)}\right]. \quad \text{(A3)}$$

which relation can be solved for $\rho_\epsilon/m_0 N(m_0)$ in terms of K.

By virtue of the way in which we have isolated the term K, the final, fully dimensionless equation (A2) affords a recursion relation for $x(m)$, $m \geq 2m_0$, given the trivial identity $x(m_0) = 1$. The parameter K is the only element of the equation which is not known *a priori*; it is determined self-consistently by iteratively adjusting its value and solving for the spectrum $x(m)$ until the two constraints

$$\sum_{m'=m_0}^{\infty} x(m')\frac{\sigma_{m'}}{\sigma_{m_0}} = K \quad \text{and} \quad \sum_{m'=m_0}^{\infty}\left(\frac{m'}{m_0}\right)x(m')\frac{\tau_e}{\tau_{m'}} = \frac{\rho_\epsilon}{m_0 N(m_0)}$$

are satisfied.

Table 3 lists the numerical values of K for a number of different agglomeration models (a, b, c, and m_e/m_0 are defined and discussed in § 3.3; see also § 4). These K values are accurate to better than 1%. Note that, in keeping with its definition as a reduced mean free path, K^{-1} decreases with each of a, β, and m_e/m_0.

APPENDIX B

DATA FITTING

Equations (3.12) and (3.14) both involve the quotient $\langle\rho\rangle/\rho_\epsilon$. We have computed this quantity for a total of ~500 model mass spectra with $a = \frac{1}{3}$ or $a = 1$; $b = -\frac{1}{2}$ and $r_m/r_{m_0} = \delta(m_0)$ always; m_e/m_0 ranging from 10 to 2000; and c between $+\frac{1}{3}$ (for $a = \frac{1}{3}$) and -1.3. To within ~10%, we find

$$a = 1 \Rightarrow \frac{\langle\rho\rangle}{\rho_\epsilon} = 1.20\left(\frac{m_e}{m_0}\right)^{-0.10}\beta^{-0.52},$$

$$a = \tfrac{1}{3} \Rightarrow \frac{\langle\rho\rangle}{\rho_\epsilon} = 1.35\beta^{-0.51}. \quad \text{(B1)}$$

By equation (A3), $\rho_\epsilon \sim (\beta)^{1/2}$ (which can also be understood as a consequence of the binary nature of the cloud collisions; see Kwan 1979), so the near-$\beta^{-1/2}$ dependence of $\langle\rho\rangle/\rho_\epsilon$ just reflects the fact that the velocity-weighted density $\langle\rho\rangle$ is determined primarily by the fast-moving, low-mass clouds whose distribution is quite insensitive to β or c.

The *critical* ratio of timescales, β_{crit} (where $m_1 > m_e$ for $\beta > \beta_{crit}$), is given by

$$a = 1 \Rightarrow \beta_{crit}^{0.48} = 1.26\left(\frac{m_e}{m_0}\right)^{0.10},$$

$$a = \tfrac{2}{3} \Rightarrow \beta_{crit}^{0.49} = 1.04\left(\frac{m_e}{m_0}\right)^{1/3} 10^{-0.07c}. \tag{B2}$$

The basic form of this relation can be understood in light of equations (3.13) and (B1). Since the sum $(a + b)$ governs the rate of collisional accretion, an increase in a with all other parameters fixed results in a more efficient buildup of massive clouds. Then $m_1 > m_e$ is more easily realized, and β_{crit} is smaller for $a = 1$ than for $a = \frac{2}{3}$. Although we work only with the equipartition velocity spectrum, $v_m \sim m^{-1/2}$, it is clear that any increase in b would similarly result in a lower β_{crit}.

Given the discussion leading to equation (3.12), and knowing the result of equation (B1), the ratio m_1/m_e of peak masses for ϕ and ψ is expected to be of the general form

$$\left(\frac{m_1}{m_e}\right)^{1-(a+c)} \sim \begin{cases} 1, & \beta < \beta_{crit}, \\ \left(\dfrac{\beta}{\beta_{crit}}\right)^{x}, & \beta \geq \beta_{crit}, \end{cases}$$

where β_{crit} is given by equation (B2), and where $x = 0.49$ for $a = 1$ or 0.48 for $a = \frac{2}{3}$. More exactly, the models we have computed (for which m_1 is determined precisely as that mass where $\gamma \equiv d \log N/d \log m = -2$) show that indeed $m_1/m_e = 1$ for $\beta < \beta_{crit}$, while for $\beta \geq \beta_{crit}$,

$$a = 1 \Rightarrow \left(\frac{m_1}{m_e}\right)^{1-(a+c)} = \left(\frac{\beta}{\beta_{crit}}\right)^{0.48}\left\{1 + 0.26 \exp\left[\frac{-0.002 \ln 10}{(\beta/\beta_{crit})^{0.48} - 1}\right]\right\},$$

$$a = \tfrac{2}{3} \Rightarrow \left(\frac{m_1}{m_e}\right)^{1-(a+c)} = \left(\frac{\beta}{\beta_{crit}}\right)^{0.49}\left\{1 + 0.67 \exp\left[\frac{-0.006 \ln 10}{(\beta/\beta_{crit})^{0.49} - 1}\right]\right\}. \tag{B3}$$

The exponential terms here account for the fact that $m_1 \sim m_e$ when $\beta \sim \beta_{crit}$, in which case equations (3.8) and (3.12), which hold in the limit of large masses, are not strictly valid at m_1.

Finally, once m_1/m_e is known, the ratio $N(m_1)/N(m_e)$ is calculable. Using equation (3.14) as a guide, and noting that the combination $(1/\beta)(\rho_d/\langle\rho\rangle)(m_e/m_0)^{1-a}$ is related to $(m_1/m_e)^{a+c-1}$, the exact $a = 1$ and $a = \frac{2}{3}$ models give

$$\log\left[\frac{N(m_1)}{N(m_0)}\right] = C_a\left[-a \log\left(\frac{m_1}{m_e}\right) + \left(\frac{m_1}{m_e}\right)^{0.81(a+c-1)} \frac{1 - (m_1/m_e)^{1-(a+c)}}{1 - (a + c)}\right], \tag{B4}$$

where, for $m_e/m_0 = 200$,

$$C_{a=1} = 0.63, \qquad C_{a=2/3} = 0.72.$$

Thus, to connect the observations of GCS mass spectra with our agglomeration model, we measure m_1/m_e as the ratio of the peak masses of the LWLF ψ and GCLF ϕ, and determine $N(m_1)/N(m_e)$ from the LWLF through

$$\frac{N(m_1)}{N(m_e)} = \frac{\psi(m_1)}{\psi(m_e)}\left(\frac{m_1}{m_e}\right)^{-2}.$$

Given these two quantities, and having already set a and m_e/m_0, equation (B4) is solved for the value of c, whereupon equation (B3) (along with eq. [B2]) yields the ratio β. The mean relations given here are all accurate to $\sim 10\%$ at worst for any one specific model, and therefore provide an excellent start to an iterative search for the model parameters which best fit a set of observations.

Although the ratio m_e/m_0 enters explicitly into the problem only through the expressions for β_{crit}, the constants C_a in equation (B4) also depend *very weakly* on m_e [the C_a scale roughly as $(m_e/m_0)^{-0.025}$]. However, the derived exponent c is quite sensitive even to small changes in C_a, because of the complicated relation between them (eq. [B4]); thus, if m_e/m_0 is changed by as much as an order of magnitude, c can also change appreciably (by perhaps $\sim 50\%$; see § 4).

APPENDIX C

STEADY STATE TIMESCALES

The reference time $\tau_{rfd} = m_0/\rho_s \sigma_{m_0} v_{m_0}$ appears as a natural scaling in our theory. Here we relate this quantity to the collision times and growth (mass doubling) times of clouds of various masses in a steady state distribution. We also show how τ_{rfd}, which involves the essentially unobservable ρ_s (defined in Appendix A), may be estimated empirically.

In the steady state, the mean time between collisions of a cloud at mass m with any other is (see § 3.2)

$$\tau_{coll}(m) = -N(m)\left[\frac{\partial N(m)}{\partial t}\bigg|_{L}\right]^{-1} = \left[\sum_{m'=m_0}^{\infty} N(m')\sigma(m, m')v(m, m')\right]^{-1}.$$

Given equations (3.3) and (3.4), and the definition of the inverse, reduced mean free path K in Appendix A, this can be written as

$$\frac{\tau_{coll}(m)}{\tau_{fld}} = \frac{\rho_\tau}{m_0 N(m_0)} \left[\frac{\sigma_m}{\sigma_{m_0}} \sum_{m'=m_0}^{m-m_0} x(m') \frac{v_{m'}}{v_{m_0}} - \frac{v_m}{v_{m_0}} \sum_{m'=m_0}^{m-m_0} x(m') \frac{\sigma_{m'}}{\sigma_{m_0}} + K \frac{v_m}{v_{m_0}} \right]^{-1}, \tag{C1}$$

where, as before, $x(m) \equiv N(m)/N(m_0)$. Evidently, τ_{coll} is a decreasing function of mass if σ_m is increasing, and

$$\frac{\tau_{coll}(m_0)}{\tau_{fld}} = \frac{1}{K} \frac{\rho_\tau}{m_0 N(m_0)}. \tag{C2}$$

Equation (A3) then gives $\rho_\tau/m_0 N(m_0)$ in terms of β and K. For $\tau_e/\tau_{m_0} = 0$ and a δ-function replenishment spectrum r_m, we have $\rho_\tau/m_0 N(m_0) = (\beta K)^{1/2}$.

Now consider the collision time τ_{coll} for a very large cloud, $m \gg m_0$. There are relatively few of these, so most of their collisions are with much smaller clouds. In particular, a typical encounter will involve a cloud at $\langle m \rangle$, a velocity-weighted mean mass defined by

$$\frac{\langle m \rangle}{m_0} \equiv \frac{\langle \rho \rangle}{m_0 N(m_0)} \frac{N(m_0)}{N_{tot}}, \tag{C3}$$

where $N_{tot} = \sum N(m)$, and $\langle \rho \rangle / m_0 N(m_0)$ is the velocity-weighted mean density defined below equation (3.8). Given the assumed equipartition velocity spectrum and the large number of low-mass clouds in the steady state, $\langle m \rangle / m_0$ is typically on the order of unity for the models we have computed. Thus, for $m \gg m_0$,

$$\frac{\tau_{coll}(m)}{\tau_{fld}} \to \frac{\langle m \rangle}{\langle \rho \rangle \sigma_m v_{\langle m \rangle}} \frac{\rho_\tau \sigma_{m_0} v_{m_0}}{m_0} = \frac{\rho_\tau}{\langle \rho \rangle} \left(\frac{\langle m \rangle}{m_0} \right)^{1-b} \left(\frac{m}{m_0} \right)^{-a}, \tag{C4}$$

which can be directly calculated from the dimensionless mass spectrum. (Recall that $\sigma_m \sim m^a$ and $v_m \sim m^b$.) As might have been expected, $\tau_{coll} \sim \sigma_m^{-1}$ for large clouds.

The growth, or doubling time τ_{doub} of a cloud is defined as the time for its mass to grow by order of itself, and can be approximated as

$$\frac{\tau_{doub}(m)}{\tau_{fld}} \approx \sum_{m'=m}^{2m-m_0} \frac{\tau_{coll}(m')}{\tau_{fld}}. \tag{C5}$$

This assumes that the only collisions are with m_0 clouds, and will therefore be an overestimate of the true doubling time; however, for $\langle m \rangle$ very near m_0, the discrepancy is not large. In § 5, equation (C5) is used to compute τ_{doub} for the fitted GCS models of § 4. It is found (cf. Fig. 8; also eq. [3.11] and the discussion following) that $\tau_m \simeq \tau_{doub}$ at $m \simeq m_1$.

Another estimate for τ_{doub}, valid at large masses, is

$$\frac{\tau_{doub}(m)}{\tau_{fld}} \approx \frac{m}{\langle m \rangle} \frac{\tau_{coll}(m)}{\tau_{fld}} \to \frac{\rho_\tau}{\langle \rho \rangle} \left(\frac{\langle m \rangle}{m_0} \right)^{-b} \left(\frac{m}{m_0} \right)^{1-a}, \tag{C6}$$

where the last step follows from equation (C4). Evidently, for large m, $\tau_{doub} \simeq m/\langle \rho \rangle \sigma_m v_{\langle m \rangle}$. This is again an overestimate of τ_{doub}, because it ignores the fact that τ_{coll} decreases as the cloud grows. Nevertheless, given equation (3.11), we see again that $\tau_m \sim \tau_{doub}$ for $m \sim m_1$.

To evaluate the fiducial collision time, we first write $\tau_{fld} = (\rho_{tot}/\rho_\tau)(m_0/\rho_{tot} \sigma_{m_0} v_{m_0})$. The total mass density of the cloud system, $\rho_{tot} = \sum mN(m)$, can be written as $\bar{m} N_{tot}$, with $\bar{m}$ the mean cloud mass. Since the cross sections σ_m are taken to be geometric, we also have $m_0/\sigma_{m_0} = \Sigma_{m_0}$, the column density of an m_0 cloud. And the relative velocity v_{m_0} may be estimated as $(6)^{1/2}\sigma_{1D}$, where σ_{1D} is the one-dimensional dispersion of the cloud system. Thus,

$$\tau_{fld} = \frac{\bar{m}}{m_0} \left[\frac{N(m_0)}{N_{tot}} \frac{\rho_\tau}{m_0 N(m_0)} \right]^{-1} \frac{\Sigma_{m_0}}{\rho_{tot} \sqrt{6} \sigma_{1D}}. \tag{C7}$$

The ratios $\bar{m}/m_0$ and $N(m_0)/N_{tot}$ are computed directly from a given dimensionless mass spectrum, and depend only weakly on β and K for a and b fixed. τ_{fld} therefore depends on the model parameters largely through the scaled ρ_τ [again, for $r_m \sim \delta(m_0)$ and $\tau_{m_0} \to \infty$, $\rho_\tau/m_0 N(m_0) = (\beta K)^{1/2}$; see eq. (A3)]. Σ_{m_0}, ρ_{tot}, and σ_{1D} are specified independently of the agglomeration model, as is done explicitly in § 5.

Table 2 above (§ 5) lists many of the quantities discussed here, as computed for the specific $a = 1$ models which best fit the GCS mass spectra of the Milky Way, M31, and M87.

REFERENCES

Aguilar, L., Hut, P., & Ostriker, J. P. 1988, ApJ, 335, 720
Armandroff, T. E. 1989, AJ, 97, 375
Ashman, K. M. 1990, MNRAS, 247, 662
Ashman, K. M., & Zepf, S. E. 1992, ApJ, 384, 50
Banfi, M., Rampazzo, R., Chincarini, G., & Henry, R. B. C. 1993, A&A, 280, 373
Blitz, L. 1991, in The Physics of Star Formation and Early Stellar Evolution, ed. C. J. Lada, & N. D. Kylafis (NATO ASI Ser.: Dordrecht: Kluwer), 3
Casoli, F., & Combes, F. 1982, A&A, 110, 287
Casoli, F., Combes, F., & Gerin, M. 1984, A&A, 133, 99
Cavaliere, A., Colafrancesco, S., & Menci, N. 1992, ApJ, 392, 41
Clifford, P., & Elmegreen, B. G. 1983, MNRAS, 202, 629
Cowie, L. L. 1980, ApJ, 236, 868
———. 1981, ApJ, 245, 66
Durrell, P. R., McLaughlin, D. E., Harris, W. E., & Hanes, D. A. 1995, ApJ., in press
Elmegreen, B. G. 1989a, ApJ, 338, 178
———. 1989b, ApJ, 347, 859
———. 1993, in Protostars and Planets III, ed. E. H. Levy & J. I. Lunine (Tucson: Univ. Arizona Press), 97
Elmegreen, B. G., & Clemens, C. 1985, ApJ, 294, 523
Elson, R. A. W., & Fall, S. M. 1985, PASP, 97, 692

Fall, S. M., & Rees, M. J. 1985, ApJ, 298, 18
Ferraioli, F., & Virgopia, N. 1979, Ap&SS, 60, 277
Field, G. B., & Hutchins, J. 1968, ApJ, 153, 737
Field, G. B. & Saslaw, W. C. 1965, ApJ, 142, 568
Fleming, D. E. B., Harris, W. E., Pritchett, C. J., & Hanes, D. A. 1995, AJ, 109, 1044
Freedman, W., et al. 1994, Nature, 371, 757
Goldstein, J. S., & Mazzella, A. J., Jr. 1974, Nuovo Cimento, 21B, 142
Handbury, M. J., Simons, S., & Williams, I. P. 1977, A&A, 61, 443
———. 1979, A&A, 77, 152
Harris, G. L. H., Geisler, D., Harris, H. C., & Hesser, J. E. 1992, AJ, 104, 613
Harris, W. E. 1991, ARA&A, 29, 543
Harris, W. E., Allwright, J. W. B., Pritchet, C. J., & van den Bergh, S. 1991, ApJS, 76, 115
Harris, W. E., Harris, G. L. H., & McLaughlin, D. E. 1995a, in preparation
Harris, W. E., McLaughlin, D. E., & Harris, G. L. H. 1995b, in preparation
Harris, W. E., & Pudritz, R. E. 1994, ApJ, 429, 177 (HP)
Hausman, M. A. 1982, ApJ, 261, 532
Heiles, C., Goodman, A. A., McKee, C. F., & Zweibel, E. G. 1993, in Protostars and Planets III, ed. E. H. Levy & J. I. Lunine (Tucson: Univ. Arizona Press), 279
Hills, J. G. 1980, ApJ, 225, 986
Kang, H., Shapiro, P. R., Fall, S. M., & Rees, M. J. 1990, ApJ, 363, 488
Katz, N., Hernquist, L., & Weinberg, D. H. 1992, ApJ, 399, L109
Kirienko, A. B. 1994, Astron. Lett., 20, 759
Kissler, M., Richtler, T., Held, E. V., Grebel, E. K., Wagner, S. J., & Capaccioli, M. 1994, A&A, 287, 463
Kumai, Y., Basu, B., & Fujimoto, M. 1993, ApJ, 404, 144
Kwan, J. 1979, ApJ, 229, 567
Kwan, J., & Valdes, F. 1983, ApJ, 271, 604
———. 1987, ApJ, 315, 92
Lada, C. J., Margulis, M., & Dearborn, D. 1984, ApJ, 285, 141
Lada, E. A., Bally, J., & Stark, A. A. 1991, ApJ, 368, 432
Larson, R. B. 1981, MNRAS, 194, 809
———. 1982, MNRAS, 200, 159
———. 1993, in ASP Conf. Ser. 48, The Globular Cluster–Galaxy Connection, ed. G. Smith & J. Brodie (San Francisco: ASP), 675
Lee, M. G., & Geisler, D. 1993, AJ, 106, 493
Lejeune, C., & Bastien, P. 1986, ApJ, 309, 167
Loren, R. B. 1989, ApJ, 338, 902
Mandushev, G., Spassova, N., & Staneva, A. 1991, A&A, 252, 94
McKee, C. F., Zweibel, E. G., Goodman, A. A., & Heiles, C. 1993, in Protostars and Planets III, ed. E. H. Levy & J. I. Lunine (Tucson: Univ. Arizona Press), 327
McLaughlin, D. E. 1994, PASP, 106, 47
McLaughlin, D. E., Harris, W. E., & Hanes, D. A. 1994, ApJ, 422, 486
McLaughlin, D. E., Secker, J., Harris, W. E., & Geisler, D. 1995, AJ, 109, 1033
Murray, S. D., & Lin, D. N. C. 1992, ApJ, 400, 265
———. 1993, in ASP Conf. Ser. 48, The Globular Cluster-Galaxy Connection, ed. G. Smith & J. Brodie (San Francisco: ASP), 738
Nakano, T. 1966, Prog. Theor. Phys., 36, 515
Nozakura, T. 1990, MNRAS, 243, 543
Oh, K.-S., & Lin, D. N. C. 1992, ApJ, 386, 519
Olson, K. M., & Kwan, J. 1990a, ApJ, 349, 480
———. 1990b, ApJ, 361, 426
Oort, J. H. 1954, Bull. Astron. Inst. Netherlands, 12, 177
Ostrov, P., Geisler, D., & Forte, J. C. 1993, AJ, 105, 1762
Patel, K. N., & Pudritz, R. E. 1994, ApJ, 424, 688
Peebles, P. J. E., & Dicke, R. H. 1968, ApJ, 154, 891
Penston, M. V., Munday, V. A., Stickland, D. J., & Penston, M. J. 1969, MNRAS, 142, 355
Pierce, M. J., Welch, D. L., McClure, R. D., van den Bergh, S., Racine, R., & Stetson, P. B. 1994, Nature, 371, 385
Pumphrey, W. A., & Scalo, J. M. 1983, ApJ, 269, 531
Racine, R. 1980, in IAU Symp. 85, Star Clusters, ed. J. E. Hesser (Dordrecht: Reidel), 369
Reed, L. G., Harris, G. L. H., & Harris, W. E. 1994, AJ, 107, 555
Rees, M. J., & Ostriker, J. P. 1977, MNRAS, 179, 541
Richtler, T. 1992, Habilitationsschrift zur Erlangung, Sternwarte Univ. Bonn
Richtler, T., & Fichtner, H. 1994, preprint
Saito, M. 1979, PASJ, 31, 181
Scoville, N. Z., & Sanders, D. B. 1978, in Interstellar Processes, ed. D. J. Hollenbach & H. A. Thronson (Dordrecht: Reidel), 21
Seab, C. G., & Shull, J. M. 1983, ApJ, 275, 652
Secker, J., Geisler, D., McLaughlin, D. E., & Harris, W. E. 1995, AJ, 109, 1019
Shaviv, N. J., & Shaviv, G. 1993, ApJ, 223, L59
Shu, F. H., Adams, F. C., & Lizano, S. 1987, ARA&A, 25, 23
Shull, J. M., & Draine, B. T. 1987, in Interstellar Processes, ed. D. J. Hollenbach & H. A. Thronson (Dordrecht: Reidel), 283
Silk, J. 1977, ApJ, 211, 638
———. 1978, ApJ, 220, 390
Silk, J., & Takahashi, T. 1979, ApJ, 229, 242
Silk, J., & White, S. D. 1978, ApJ, 223, L59
Silk, J., & Wyse, R. F. G. 1993, Phys. Rep., 231, 293
Solomon, P. M., Rivolo, A. R., Barrett, J., & Yahil, A. 1987, ApJ, 319, 730
Stutzki, J., & Güsten, R. 1990, ApJ, 356, 513
Surdin, V. G. 1979, Soviet Astron., 23, 648
Sutherland, R. S., & Dopita, M. A. 1993, ApJS, 88, 253
Taff, L. G., & Savedoff, M. P. 1972, MNRAS, 160, 89
———. 1973, MNRAS, 164, 357
Tomisaka, K. 1984, PASJ, 36, 457
———. 1986, PASJ, 38, 95
van den Bergh, S., & Lafontaine, A. 1984, AJ, 89, 1822
van den Bergh, S., Morbey, C., & Pazder, J. 1991, ApJ, 375, 594
van Dongen, P. G. J., & Ernst, M. H. 1984, J. Stat. Phys., 37, 301
———. 1988, J. Stat. Phys., 50, 295
Wetherill, G. W. 1990, Icarus, 88, 336
Whitmore, B. C., & Schweizer, F. 1995, AJ, 109, 960
Williams, J. P., de Geuss, E. J., & Blitz, L. 1994, ApJ, 428, 693
Williams, J. P., & McKee, C. F. 1995, ApJ, submitted
Wood, D. O. S., Myers, P. C., & Daugherty, D. A. 1994, in ASP Conf. Ser. 65, Clouds Cores and Low Mass Stars, ed. D. P. Clemens & R. Barvainis (San Francisco: ASP), 14
Zepf, S. E., Ashman, K. M., & Geisler, D. 1995, ApJ, 443, 570

Chapter 6

Summary and Discussion

We have attempted in this thesis to better understand some of the general aspects of the star formation process, first by zeroing in on the details of its initial conditions — as revealed particularly by the internal structures of the dense cores of molecular clouds in the Milky Way — and then by drawing back to take a broader look at some of its most conspicuous and robust final products — the systems of old globular star clusters that can be found in the halo of any large galaxy. Our main results have already been listed at the ends of Chapters 2, 3, and 5 (McLaughlin & Pudritz 1996b, 1997, 1996a). We recapitulate these now, and then go on to discuss some of what we see as the most interesting and immediate extensions of the ideas presented here.

6.1 Summary

As Chapters 1 and 2 discussed, Galactic GMCs and the dense, star-forming cores within them are known to be in a virial equilibrium (Larson 1981; Solomon et al. 1987; Bertoldi & McKee 1992) which relies, in part, on an internal turbulence that gives rise to total velocity dispersions which are *superthermal* $[\sigma > \sigma_{\rm T} = (kT/\mu m_H)^{1/2}]$ and *increasing outwards* within any given cloud or core. In particular, nonthermal linewidths ($\sigma_{\rm NT}^2 = \sigma^2 - \sigma_{\rm T}^2$) are observed to grow roughly as $\sigma_{\rm NT} \propto r^{0.5}$ inside low-mass ($M \leq 10 M_\odot$) cores, and as $\sigma_{\rm NT} \propto r^{0.25}$ or so in more massive ones (Fuller & Myers 1992; Caselli & Myers 1995). These scalings are observed both in cores that are known to contain young stars, and in those that appear to be quiescent. As such, they are evidently part of the initial

conditions for star formation; and they pose a clear challenge to standard theories of star formation that rely on models of isothermal spheres with constant velocity dispersions $\sigma = \sigma_T$ at all radii.

In Chapter 2, we therefore searched for a model of dense interstellar clouds that could be consistent both with these observations and with the empirical laws of Larson (1981) relating the *total* masses, radii, and linewidths of the largest cores and of entire GMCs: $M \propto R^2$ and $\sigma_{ave} \propto R^{1/2}$. Our approach was to specify an equation of state (EOS) to describe the density dependence of total (thermal plus turbulent) gas pressure, and then use this EOS to solve for the density profile — and hence for $\sigma^2(r) = P(r)/\rho(r)$ — of a self-gravitating, magnetized, and virialized sphere of gas. We showed that (1) *regardless of their EOS*, GMCs and the most massive cores must all be at their critical (Jeans) masses, in which case Larson's laws are automatically satisfied; and (2) the simplest EOS which both allows for this and matches the observed internal linewidth profiles in low- and high-mass cores alike, is a "pure logotrope:" $P/P_c = 1 + A \ln(\rho/\rho_c)$, which is a nontrivial modification of an EOS originally introduced by Lizano & Shu (1989). We then fit our EOS to the linewidth data in 38 cores to constrain its free parameter: $A \simeq 0.20 \pm 0.02$.

The physical basis of our logotrope is not yet understood, and it is still a phenomenological description of GMCs and cores. Nevertheless, with such a description in hand, some of the basic consequences of the turbulence in interstellar clouds can be investigated. Thus, in Chapter 3 we obtained semi-analytical solutions for the expansion-wave (inside-out) collapse, beginning from virial equilibrium, of a singular logotropic sphere. We found that the mass of the collapsed protostar at the center of such a sphere grows in time as $M_0 \propto t^4$. By contrast, the protostar in an expansion-wave collapse of a singular isothermal sphere grows only as $M_0 \propto t$ (Shu 1977). Thus, relative to an isothermal sphere, protostellar accretion in a logotrope is slower at first, and faster later on; low-mass stars take more time to form, and high-mass stars less time, than previously thought. Ultimately, this means that stars of *all* masses should form on fairly comparable (and observationally allowed) $\sim 1 - 3 \times 10^6$ yr timescales. Moreover, the long period of very slow infall which is implied by our theory, but which is absent in isothermal collapse, stands to at least qualitatively explain the apparent quiescence (i.e., the paucity of obvious collapse detections) in most molecular cores.

We then pointed out in Chapter 4 that, although the formation of a single star inside a molecular core rightly demands attention, the sizes of cores in Milky Way GMCs are such (up to

$M \sim 10^3 M_\odot$) that, by mass, most stars are forced to form in groups; and that the formation of bound stellar clusters in particular, although rare, is now and has always been a critical element of star and galaxy formation overall: Low-mass (open) clusters currently form in the Milky Way with an efficiency (in terms of the fraction of the total mass of active, star-forming gas that goes into such objects) of $f_{\rm cl} \sim 5 \times 10^{-3}$. Much more massive young star clusters, some of which are large and dense enough to survive the next ~10 Gyr essentially intact, are now being found in increasing numbers of starburst and merging galaxies. And old globular clusters are a ubiquitous presence in the halos of normal galaxies, where they typically account for fractions $f_{\rm cl}^{\rm glob} \sim 2 \times 10^{-3}$ of the total stellar mass. We argued that these points all suggest that globular cluster systems should be viewed as rather generic, even if especially convenient, manifestations of a most fundamental facet of star formation that has been well maintained over the past 15 Gyr.

Because a full theory for the formation even of *single* stars has not yet been developed from first principles, it seems most profitable to investigate the much more complicated (but at least equally important) *clustered* mode of star formation by extracting general constraints on it from observations of *both* present-day star-forming regions — GMCs and their cores — *and* the enduring progeny — globular cluster systems — of clouds long since gone. Thus, in Chapter 4 we identified several basic traits that are common to most GCSs; we argued that, even after 15 Gyr, these reflect the formation conditions in the systems, as opposed to their subsequent evolution; and we indicated how each may be best understood in terms of a formation scenario (Harris & Pudritz 1994) that connects explicitly with the same basic pattern of star formation that holds sway today (and with current ideas and observations of galaxy formation). Thus, the birth of globular clusters is put firmly in the dense cores of much larger, but subgalactic ($M \sim 10^8 - 10^9 M_\odot$), *supergiant molecular clouds* of gas that are in turn embedded in still larger, galaxy-sized gravitational wells.

One of the most fundamental characteristics of GCSs is their mass spectra, $N(m) = dN/dm$, which bear a striking likeness, above a cluster mass of $m_* \simeq 1.6 \times 10^5 M_\odot$, to the observed $N(m)$ in Galactic GMCs (e.g., Solomon et al. 1987) and cores (Blitz 1991). In Chapter 5, we exploited this fundamental similarity to develop the first quantitative theory of the GCS mass spectrum (or luminosity function). Following a suggestion by Harris & Pudritz (1994), we adapted an existing theory (Kwan 1979) for the mass spectra of Galactic GMCs: The masses of the protocluster cores

in a given SGMC are distributed so as to afford a steady-state balance between the rate of their growth by mutual collisions (assumed to be *coalescent*), and the rate of their self-destruction by the side-effects (winds, H II regions, supernovae) of internal massive-star formation. The protocluster $N(m)$ obtained in this way is ultimately inherited by the fully formed GCS, owing to the high ($\gtrsim$50%) cumulative star formation efficiency that is required of any body of gas if it is to form a bound cluster of stars. We found that the major influence on the shape of $N(m)$ is the ratio, β, of fiducial disruption and collision times for protocluster cores, and that it was necessary to allow for a *mass-dependent* protocluster disruption timescale, τ. We showed, through a combination of analysis and data-fitting, that (1) the ratio β is expected to be independent of the position of the cores' parent SGMC in any given protogalaxy, which explains the insensitivity of observed GCLFs to galactocentric radius; and (2) above m_*, more massive protoclusters self-destruct on progressively shorter timescales, viz. $\tau \propto m^{-0.6}$. Fits to the GCS $N(m)$ in the Milky Way, M31, and M87 all give excellent agreement between theory and observation, *for cluster masses in excess of* $m_* \simeq 1.6 \times 10^5 M_\odot$.

These results begin to answer some of the questions we started out with, but they also raise several new ones. We now briefly discuss a few of these.

6.2 Logotropic Clouds and Collapse

It goes almost without saying that the physical origin of the logotropic equation of state, with $A = 0.2$ (or of one close to it), has to be clarified. Even in the absence of such a fundamental understanding, however, there are a number of ways in which the model can be improved to provide still better descriptions of interstellar clouds.

First, giant molecular clouds are not spherical objects; and even though cores generally appear to be spheroidal, they are not perfectly round. Obviously, the assumption of spherical symmetry that facilitated the analyses of McLaughlin & Pudritz (1996b, 1997) has to be relaxed in future work. In addition, the representation of the mean magnetic fields in GMCs and cores as perfectly uniform, or poloidal, is quite idealized. Numerical models of cores should be built to allow for a nonspherical (axisymmetric) geometry and to solve simultaneously for a more realistic and self-consistent mean-field structure, while incorporating the effects of both modest rotation

and a logotropic equation of state (as a necessary description of the disordered component of **B**, or of whatever other physics gives rise to the nonthermal linewidths in cores and GMCs). The fundamental properties — internal density structures, critical masses, etc. — of such model clouds should then be examined in detail to confirm the results of McLaughlin & Pudritz (1996b), and carefully compared again with observational data. These models would provide the basis for more detailed investigations of cloud collapse.

But even without such realistic initial states, and in the idealized, spherically symmetric, non-rotating, and purely hydrodynamical (no mean **B**-field) limit considered by McLaughlin & Pudritz (1997), it is essential that the collapse of logotropes be studied numerically. It will be recalled that our semi-analytical similarity solutions for the collapse of non-isothermal spheres are, strictly speaking, valid only from the time ($t = 0$) when a cloud has evolved from its initial equilibrium configuration to achieve a formally infinite central density (i.e., when a central protostar is formed and begins to grow), to the time ($t = t_{\rm ew}$) when the expansion wave reaches the initial boundary of the cloud and is reflected by a constant surface pressure there. Even though this takes nearly half of the total collapse time in a logotrope specifically, *only ~3% of the total mass of such a cloud is accreted onto the protostar between* $t = 0$ *and* $t = t_{\rm ew}$. Thus, most of the mass of a star is gathered during a phase of accretion that cannot be described by the present collapse theory. Put another way, we expect even the smallest observable accreting protostars to generally be older than $t_{\rm ew}$. While it does seem plausible that the analytical protostellar accretion rate (i.e., $\dot{M}_0 \propto t^3$ in a logotrope) can be extrapolated beyond $t_{\rm ew}$ to provide a reasonable estimate of the total formation time of a star, there is no way to analytically obtain the velocity field and density profile in the collapsing cloud at such late times.

Thus, numerical hydrodynamics simulations should be employed to follow the full collapse of initially virialized spheres with non-isothermal equations of state. (In addition to the logotrope, it would be useful to consider the whole class of negative-index polytropes.) This exercise would give the protostellar mass M_0 (or accretion rate $\dot{M}_0$), velocity field $v(r)$, and density profile $\rho(r)$ as functions of time throughout the collapse, and thus would enable a direct check on the validity of our extrapolation of $\dot{M}_0$ to find the total formation times for stars of various masses. Moreover, and most importantly, it would then be possible to calculate a time sequence of emission-line profiles in

collapsing non-isothermal spheres. These could then be compared to the observed line profiles of individual young protostars (i.e., Class 0 sources such as B335 [Zhou et al. 1993]), both to gain some insight into the nature of these important objects (e.g., to estimate their ages), and also to test the logotropic model for GMCs and molecular cores in a way which is independent of the considerations of equilibrium clouds by McLaughlin & Pudritz (1996b).

6.3 Cluster Formation

On what is perhaps a more fundamental level, an explicit link has to be forged between the logotropic EOS and the formation of stars in groups and clusters, rather than just singly, inside molecular cores. There are at least three interwoven aspects of this process that should be carefully explored.

First, the logotropic model ultimately predicts nearly equal total accretion times for stars of essentially any mass (and a similar effect is expected, although to a lesser extent, for protostellar collapse inside clouds with any EOS that is softer than isothermal). As McLaughlin & Pudritz (1997) mentioned, this result has important implications for the form of the initial stellar mass function in a core [the IMF: roughly, $N(m) \propto m^{-2.35}$, as mentioned in §4.1]. To reiterate this point, if very many massive stars *start* collapsing too soon, then they will finish accreting and clear a region of gas (by their supernova explosions, if nothing else) before many low-mass stars have had time to form and fill out the low-mass end of the IMF. The origin of the stellar mass spectrum is a notoriously difficult problem that has gone 40 years unsolved, and it is still not clear how best to build a fundamental theory for it. However, in the case of *bound cluster* formation specifically, the requirement that the final star formation efficiency $[M_{\rm stars}/(M_{\rm stars}+M_{\rm gas})]$ be $\gtrsim$50% at the time of core disruption should serve, along with the predictions of stellar formation timescales that are now in hand for an array of non-isothermal core models, to constrain the number of stars that are *allowed* to form at any given mass before the feedback from the most massive ones puts an end to the whole process. That is, given an equation of state for the gas, it should be possible to theoretically bracket an allowed *range* of $N(m)$ in cluster-forming cores.

This touches on the second important issue, which is the question of how many cores can be expected to achieve a final SFE of ~50% or better. As we showed in Chapter 4, the fraction $f_{\rm cl}$ of such cores by mass is observed to be of order a few times 10^{-3}. An explanation of this fundamental

quantity, whose value is essentially the same now as it was when the old globular clusters formed, should come with a detailed investigation into the effects of massive-star winds, photoionization (H II regions), and supernova explosions on the gas in cores that form multiple stars. Many studies of the interaction of massive stars with the ISM have, of course, been carried out in the past, and technically it should not prove too difficult to adapt these in order to deduce the destructive effects of winds, H II regions, and supernovae *combined* in any single body of gas. In this context, the significance of the work presented here is that (1) it provides (through the logotropic EOS) for a realistic description of the *internal* density and velocity structures of star-forming clouds, which is crucial to quantifying the massive-star feedback; (2) it clarifies (through the generalized Bonnor-Ebert relations) the *average* properties of clouds, and so allows for calculations that should refer to a range of global conditions which mimic those observed (and that should then allow for statistical estimates of $f_{\rm cl}$ and its systematic dependences on cloud mass and environment); and (3) it isolates (through the consideration of globular clusters) those features of gas clouds that are important in *both* protogalactic *and* present-day settings, while also pointing up the universality of $f_{\rm cl} \sim 10^{-3}$ as a general empirical constraint on any theory of cluster formation.

This then relates directly to the third concern, which is the expected lifetime τ, against this disruption, of a cluster-forming core of any given mass. That is, the specification of a logotropic equation of state in the kinds of detailed calculations just suggested should allow for an independent check on whether protoglobular clusters indeed had $\tau \propto m^c$ and $c = -0.6 \pm 0.3$ for $m \geq m_* \simeq 1.6 \times 10^5 M_\odot$. In fact, given the very general framework within which this result was obtained (McLaughlin & Pudritz 1996a), we fully expect that it should hold as well — at the very least, insofar as $c < 0$ — among cores or GMCs in the Galaxy today. Our identification of m_*, as a universal mass below which star-forming clouds rather suddenly become much longer lived, should, of course, be qualitatively and quantitatively checked as part of this.

6.4 The Low-Mass End of the GCLF

To return to more specific considerations, recall that the agglomeration theory of McLaughlin & Pudritz (1996a) gives theoretical GCS mass spectra that compare well with observations at cluster masses $m \gtrsim 10^5 M_\odot$ (and therefore correctly locates most of the *mass* in GCSs); but that below

$m_* \simeq 1.6 \times 10^5 M_\odot$, our model $N(m)$ is too steep and predicts more clusters than are observed. The discrepancy at $m < m_*$ might be due *in part* to GCS erosion by the evaporation of low-mass clusters over ~15 Gyr, as discussed in §4.3 above; but this *cannot* be invoked to explain the entire effect.

Following Surdin (1979), there have been various recent claims to the contrary (e.g., Okazaki & Tosa 1995; Larson 1996; Elmegreen & Efremov 1997; Vesperini 1997). These authors specifically suggest that the shape of the Milky Way GCLF below m_* (or fainter than the turnover M_V^0), and even the very existence of a feature like m_* today, stem largely from the evaporation of a cluster population that initially included many more low-mass objects. [That is, the low-mass ends of GCS mass spectra are hypothesized to have begun as simple extensions of the $N(m) \propto m^\gamma$ behavior, with $\gamma \sim -1.6$ to -2.0, that is seen in their high-mass, $m \geq m_*$ regimes today — not too unlike the full, pure-coalescence spectra shown in Figs. 6 and 7 of McLaughlin & Pudritz (1996a).] The idea is that more massive globulars naturally have longer evaporation timescales and therefore evolve less in a given amount of time; specifically (e.g., Okazaki & Tosa 1995),

$$\tau_{\rm evap} \;=\; 4.1 \times 10^9 \text{ yr } \left(\frac{m}{10^5\ M_\odot}\right)^{1/2} \left(\frac{r_t/r_h}{10}\right) \left(\frac{r_h}{1 \text{ pc}}\right)^{3/2} . \qquad (6.1)$$

Here r_h is the half-light radius of a cluster with mass m, and r_t is its total radius. In this picture, then, the high-mass side of the GCLF is taken to be more or less identical to the initial distribution, which is in line with our arguments; the low-mass side of the GCLF is supposed to have been severely depleted by evaporation (together, in some cases, with other destruction mechanisms); and the turnover of the GCLF — or the mass m_* above which the slope of $N(m)$ rapidly steepens — is time-dependent, and *roughly* corresponds to the mass of the largest cluster that can possibly have evaporated during the life of a GCS.

As we said in Chapter 4, there are few data on the form of GCLFs at magnitudes fainter than M_V^0 in distant galaxies, so this sort of scenario cannot be entirely dismissed out of hand. We would note, though, that the low-mass ends of the Milky Way and M31 GCLFs [Fig. 1 of McLaughlin & Pudritz 1996a] are strikingly similar in appearance; and M_V^0 is, after all, not sensibly different in *any* galaxy. If these things were entirely due to the evaporation process, it would have to be quite remarkably robust. (Although evaporation *is*, in our view, the most robust dynamical destruction process, it does couple to the gravitational fields in galaxies, and is therefore not completely inde-

pendent of external environment; see, e.g., Oh & Lin 1992.) Even more, equation (6.1) shows that a pure-evaporation picture actually suggests that, contrary to observation, the Milky Way GCLF at least should vary measurably with Galactocentric distance.

To see this, we take stock of how cluster masses m, "concentrations" r_t/r_h, and half-light radii r_h depend on $R_{\rm gc}$ in our Galaxy: the first, as we have seen (and as is expected on the basis of our agglomeration theory for the GCLF) do not correlate at all with $R_{\rm gc}$; the second depend on it very weakly, if at all (the catalogue of Harris [1996b] for the parameters of Milky Way clusters shows that, to within factors of three, $r_t/r_h \approx 10$ throughout the halo); but the third, as has already been mentioned here (Chapter 4, and McLaughlin & Pudritz 1996a) increase with Galactocentric position: $r_h \propto R_{\rm gc}^{1/2}$ (van den Bergh et al. 1991). If, as seems likely (Murray & Lin 1992; Harris & Pudritz 1994), this is an initial condition on the clusters, then *evaporation timescales should increase with Galactocentric radius* as $\tau_{\rm evap} \propto R_{\rm gc}^{3/4}$. Thus, if m_* is interpreted roughly as the mass of a cluster for which $\tau_{\rm evap}$ is equal to the age of the Galaxy, then equation (6.1) yields $(m_* r_h^3) \simeq$ constant, whence $m_* \propto R_{\rm gc}^{-3/2}$ and the GCLF turnover should grow fainter with increasing $R_{\rm gc}$ [$M_V^0 = C - 2.5 \log_{10}(m_*/M_\odot) = C' + 3.75 \log_{10} R_{\rm gc}$]. By the same token, if the clusters in different galaxies have different characteristic r_h because of their different environments (as they should, if the arguments of Harris & Pudritz are correct), then M_V^0 would be expected to vary between galaxies in ways that are not observed.

Although this analysis is admittedly somewhat superficial, it does point up what could be a serious flaw in the idea that the low-mass ($m < m_*$) ends of GCS mass spectra are shaped entirely by evaporation. On the observational side, direct measurements of GCLFs to magnitudes significantly fainter then M_V^0, throughout many different galaxies, are now needed to check on the robustness of this part of the distribution. On the theoretical side, the types of evaporation models mentioned here have to be very carefully reconsidered. (And, more generally, *all* dynamical evolution calculations have to start allowing for the fact that some globular cluster properties are expected to vary with $R_{\rm gc}$, in any galaxy, *ab initio*.)

As another cautionary note, it is important to realize that the results of these evolutionary calculations are, perhaps not surprisingly, quite sensitive to the assumptions they make on the form of the initial GCS mass spectrum at low masses. For instance, Vesperini (1997) tracks the evolution

(by disk shocking and evaporation only) of a simulated GCS over 15 Gyr, and finds that when the initial $N(m)$ is taken to be a single power law at all masses, the cumulative loss of low-mass clusters leads to a final GCLF that looks much like the current distribution in the Milky Way. However, when he sets the *initial* GCLF to be almost identical to that observed now, he finds that *although the total population of the cluster system decreases by $\sim$70%, there is no significant change in the overall shape or the turnover magnitude of the GCLF* over 15 Gyr. This rather counterintuitive result is important for showing that *the entire GCLF could essentially be a formation relic*, even if severe globular cluster evolution has occurred. Whatever the true case is, it is evident that the form of the initial GCS mass spectrum has to be predicted *in full* and *from first principles* (i.e., without any extrapolations of its high-mass behavior to $m < m_*$) before evolutionary calculations can be viewed with any real confidence.

Thus, as was suggested in McLaughlin & Pudritz (1996a), the most logical next step, in the context of a collisional origin for the GCLF, is to relax the assumption that all collisions between all SGMC cores will result in coalescence; to instead allow for the fact that some encounters between low-mass ($m < m_*$) objects will lead to their fragmentation; and to quantify the "flattening" effect that this has on the GCS $N(m)$ at low cluster masses. Numerical simulations are again required to do this; but once completed, they would provide the first self-consistent model for the full initial $N(m)$ (as well as the initial dynamics) of GCSs. *Then*, perhaps, the amount and nature of their evolution over the past 15 Gyr can properly be inferred. Another interesting tie-in with the logotropic equation of state should come up here, as the outcome (i.e., coalescence vs. fragmentation) of a close encounter between any two cores in an SGMC will have to be decided in the simulations on a case-by-case basis, depending on the masses, radii, internal velocity dispersions, and approach velocity of the objects involved. Rules for this should ideally be drawn from new hydrodynamical simulations of collisions between self-gravitating logotropes (or other non-isothermal clouds). These results would then be of interest in connection with the mass spectra and dynamics of Galactic GMCs and cores as well.

6.5 Agglomeration and Fractal Cloud Structure

Finally, we return to a point that was raised in Chapter 1, in the discussion around Fig. 1.2. Specifically, it was noted there that the existence of apparently self-similar, clumpy substructure over a very wide range of scales in Galactic molecular clouds (from $R \sim 100$ pc down to $R \sim 0.01$ pc) has led in recent years to a *fractal* description of these structures. This description has been quantitatively developed, for example, by Elmegreen & Falgarone (1996), who use it to explain the mass spectra of GMCs and cores; and Elmegreen & Efremov (1997) have drawn on this to pursue the connection, discussed here and by Harris & Pudritz (1994), between the mass spectra of GMCs and GCSs.

In the extreme, the notion of a fractal ISM could be taken to imply, along the lines of Scalo (1985, 1990), that clouds and cores are elements of a self-similar hierarchy of structure that extends to much larger and smaller scales than have been observed, and that as such they are picked out as discrete objects only because of somewhat artificial biases intrinsic to the methods used to identify them. In such a case, the representation of the ISM as a collection of individual clouds and cores would be fallacious, and in fact this kind of argument has been used to challenge agglomeration models of cloud structure (which in turn casts doubt on the relevance of these models to the mass spectra of clouds, cores, or GCSs). Clearly, we do not share this extreme view: as we mentioned in §1.5.2, and as is discussed in more detail by, e.g., Blitz (1991) and Genzel (1992), there is good evidence that GMCs and their cores both are well defined and physically meaningful objects. Still, its fractal geometry is an interesting and important aspect of the ISM. We briefly address this now, to suggest that (1) some theoretical interpretations of it to date have involved some potentially rather serious oversimplifications, and (2) collisions and agglomeration in an ISM that consists of discrete clouds — whether now or 15 Gyr ago — are not only *consistent* with the possibility of fractal structure, but may in fact be a *contributing factor* in its development.

To this end, we first introduce the concept of the *capacity dimension* of an object, or of any abstract mathematical set. This is most easily understood as arising from a simple box-counting procedure (e.g., Lichtenberg & Lieberman 1991). Thus, imagine optimally and completely covering a subset of some N-dimensional space with a number $M(\varepsilon)$ of N-dimensional boxes, each of side ε. Evidently, the smaller ε, the more boxes are required to cover the set, and the capacity D_0 is thus

defined as

$$D_0 \equiv -\lim_{\varepsilon \to 0} \frac{\ln M(\varepsilon)}{\ln \varepsilon} . \tag{6.2}$$

To see the utility of this definition, consider that a single point can be covered by just one box of any size ε, in any N-dimensional space; thus, $M(\varepsilon) \equiv 1$, and $D_0 = 0$ for a point. Similarly, the capacity dimension of a "normal," Euclidean line is $D_0 = 1$ [$M(\varepsilon) \propto \varepsilon^{-1}$], which is just the same as its topological dimension; that of a Euclidean surface is $D_0 = 2$; and a solid three-dimensional body has $D_0 = 3$. Aside from some mathematical nuances that will not be important for us (see, e.g., Lichtenberg & Lieberman 1991), D_0 as defined here is essentially equivalent to what is called the *Hausdorff dimension*, or "the" *fractal dimension.*

There is, however, a large class of objects whose capacity, or Hausdorff, dimensions do not equal their topological dimensions. *A fractal set is by definition a set for which the Hausdorff dimension strictly exceeds the topological dimension* (Mandelbrot 1983). A famous example is the Koch snowflake (cf. Mandelbrot 1983), which is generated from an initially straight line (topological dimension 1), basically by superimposing a "kink" on it, and then kinks on the kink, ... , in a regular way such that $D_0 \simeq 1.26 > 1$ in the end. Thus, the Koch curve is *more convoluted* than a regular line; but since $D_0 < 2$, it is not so convoluted as to completely fill a 2-dimensional region of space. Similarly, a fractal surface with $2 < D_0 < 3$ is "crinkled," relative to a Euclidean plane or a spherical shell, but is not volume-filling.

These basic definitions have been brought up here because recent observations (e.g., Dickman, Horvath, & Margulis 1990; Falgarone et al. 1991, and references therein) have suggested that the perimeters of molecular clouds (i.e., the *projections* of their surfaces on the sky), have a fractal dimension of $D_0 \simeq 1.35$, which is generally thought to imply that *the GMC surfaces themselves are fractal, with* $D_0(\mathrm{GMC}) = 2.35$. The significance of this lies in the fact that the interfaces of turbulent flows in laboratory experiments are typically found to also have $D_0 \simeq 2.35$ (Sreenivasan 1991), as are (perhaps more to the point) the surfaces of clouds in the terrestrial atmosphere (Lovejoy 1982). It might appear at first, then, as if turbulent gas motions could be entirely responsible for the structure of interstellar clouds (and even of the ISM as a whole — including the intercloud medium — according to Elmegreen 1997).

In some — ***but not all*** — cases, fractal sets are intimately associated with *self-similarity,*

which is to say that they can be invariant under transformations in scale. Such behavior can manifest itself as power-law correlations between various properties of the set, as power laws are intrinsically scale-free in form. Thus, in the context of molecular clouds specifically, the existence of Larson's laws ($M \propto R^2$ and $\sigma_{\rm ave} \propto R^{1/2}$) has been cited by some (e.g., de Vega, Sánchez, & Combes 1996; Elmegreen 1997) as possible evidence for fractal structure on large scales. More recently, so has the power-law form, $N(m) \propto m^{\gamma}$, of the GMC/core mass spectrum (Elmegreen & Falgarone 1996).

Elmegreen & Falgarone argue that if the Galactic interstellar gas had a fractal dimension of $D_0 \simeq 2.3$, it would correspond to a self-similar hierarchy of clumps, cloud-like clusters of clumps, and clusters of clouds with an apparent mass spectrum that was a *perfect* power law, $N(m) \propto m^{-2}$. They claim that this is not inconsistent with observational constraints, and suggest that *"the mass distribution for molecular clouds is the result of fractal gas structure."* They also draw attention to the similar fractal dimension of (incompressible) laboratory turbulence, and propose that the cloudy structure of the ISM may therefore be the result of the (compressible) turbulent motions there. Elmegreen & Efremov (1997) then go on to suggest that the initial mass spectra of all bound stellar clusters (open and globular, young and old) should therefore also be of the form $N(m) \propto m^{-2}$, over the whole range of cluster masses, and thus that *"turbulence alone may produce star clusters in the sense that turbulence produces the scale-invariant gas structure that forms stars in hierarchical clusters."* The overall implication would appear to be that the broadest features of molecular clouds can be simply understood as almost trivial consequences of self-similarity.

We do not wish to challenge the existence of fractal structure *at some level* in the Galactic ISM; in particular, we find the results of Dickman et al. (1990) and Falgarone et al. (1991) fairly convincing. However, we do take a somewhat more skeptical view of the rather broader claims made by Elmegreen & Falgarone (1996) and Elmegreen & Efremov (1997), as the following points discuss.

First, it should be obvious that power-law scalings between molecular clouds do not automatically imply that they are indistinct or ill-defined parts of a global fractal network; after all, we (McLaughlin & Pudritz 1996b) and others (Chièze 1987; Elmegreen 1989) have derived Larson's laws from considerations of discrete clouds that are in virial equilibrium. Although neither Elmegreen & Falgarone nor Elmegreen & Efremov invoke Larson's laws as the main evidence for the putative large-scale fractality of the ISM, we mention them here to reinforce the basic point

that (as was mentioned in McLaughlin & Pudritz 1996b) such global correlations between clouds — or even between vaguer "elements" in a hierarchy of structure — do not necessarily offer a unique window on their dynamics. Moreover, the *failing* of the size-linewidth relation among low-mass cores in clouds, as well as the *different* internal $\sigma(r)$ profiles in low- and high-mass cores (Fuller & Myers 1992; Caselli & Myers 1995) show that the interstellar gas is *not* strictly self-similar on all scales, and that a distinction does have to be made between the interiors and exteriors of clouds. Of course, there has to be a limit to the extent of the scaling regime in any finite fractal structure, and it might just be argued the cores of GMCs represent this limit in the ISM. Whether this is the correct interpretation or not, the fact remains that the interiors of cores (on scales $\lesssim$1 pc) demand a "classical" description that does not refer to global scalings or self-similarity. This is just the approach we have taken throughout this thesis.

Second, and more fundamentally, it has to be stressed that the dimension D_0, and all of fractal geometry in general, is just that — a representation of the geometry of an object or a set of objects. Thus, there can be no such thing as a "fractal theory" of the ISM, only fractal *descriptions* to be explained by *dynamical* theories. However, nothing can be fully described just in terms of its geometry, so this can only work in one direction: the correct dynamics of the ISM has to account for whatever fractal structure is observed there, but (similar to what was said just above) considerations of fractal dimension alone cannot be used to uniquely infer the nature of the underlying dynamics. This is just another way of saying that fractal geometry is a purposely degenerate construct that is meant to provide a simplified characterization of complex systems, without having to refer to their often obscure dynamics. There is no doubt that turbulence is important in molecular clouds, but it is almost certainly just one of many different processes (see below) that are able to give rise to a capacity dimension $D_0 \sim 2$. In short, then, we would rephrase the statement of Elmegreen & Falgarone (1996), quoted above, as follows: *any fractal gas structure in the Milky Way is probably the result of the same physical processes that gave rise to the mass distribution for molecular clouds.*

This brings us to our third point, which is that the capacity dimension D_0 is an incomplete description of the geometry of an object or a set anyway (as a trivial example, note that cubes, spheres, and indeed any solid body, all have $D_0 = 3$). A more complete representation of a set is given by the spectrum of its *generalized fractal dimensions* D_q. To motivate the introduction of

these quantities, we allow now for the possibility of an *inhomogeneous* fractal, in which the density of points varies with location in the set. Then imagine again trying to cover such a set, embedded in an N-dimensional space and consisting of $\mathcal{N}$ points in total, with a number $M(\varepsilon)$ of N-dimensional boxes of side ε. Each box i will generally contain a different number n_i of points belonging to the set, and so will have a density $p_i = n_i/\mathcal{N}$. Then, by analogy with the definition (6.2), the generalized dimensions D_q can be defined as density-weighted capacities (Hentschel & Procaccia 1983):

$$D_q \equiv \frac{1}{q-1} \lim_{\varepsilon \to 0} \frac{\ln \sum_{i=1}^{M(\varepsilon)} p_i^q}{\ln \varepsilon} , \tag{6.3}$$

where q may take on any value whatsoever: $-\infty \leq q \leq \infty$. Three of the more physically transparent dimensions are obtained with $q = 0$ (in which case the capacity dimension D_0 of eq. [6.2] is regained), $q = 1$ (such that $D_1 = \lim_{\varepsilon \to 0} [\sum p_i \ln p_i / \ln \varepsilon]$ looks formally like an entropy, and is referred to as the *information dimension*), and $q = 2$ (which yields the *correlation dimension*, $D_2 = \lim_{\varepsilon \to 0} [\ln \sum p_i^2 / \ln \varepsilon]$). A mathematically more rigorous (but equivalent) definition of the D_q is given by Halsey et al. (1986), but the simple form written here is sufficient for our purposes. The important point is that when a fractal object is homogeneous [p_i = constant = $1/M(\varepsilon)$], it is easy to see that $D_q = D_0$ for all q, and therefore that a single fractal dimension characterizes the entire set. But in the more realistic case, when the fractal is inhomogeneous, each D_q is generally different from the next, and *the capacity D_0 is only one of an object's infinitely many fractal dimensions*; different subsets of the fractal are described by different fractal dimensions. Such a set is referred to as a *multifractal*, and can be thought of as an interwoven structure of infinitely many fractals. These objects need not display any strict self-similarity on all scales, as they come with a continuous spectrum of scaling exponents. Thus, D_0 is an even smaller piece of the full geometric and dynamical puzzle than before.

This somewhat technical issue actually is relevant here, because the claim of Elmegreen & Falgarone (1996), that the mass spectra of GMCs and cores are nothing more than reflections of "the" fractal dimension of the ISM (meaning D_0 specifically, in their paper), involves the implicit assumption that the ISM is a *homogeneous* fractal; that is, homogeneity gives rise to a strict self-similarity, and thus to a pure power-law mass spectrum whose exponent ($\gamma \simeq -2$, according to Elmegreen & Falgarone) is simply related to a single fractal dimension ($D_0 = 2.3 \pm 0.3$ in their

analysis). And it is the inference $D_0 = 2.3$ that leads to the identification, by both Elmegreen & Falgarone (1996) and Elmegreen & Efremov (1997), of turbulence as the driving force behind the supposed large-scale fractal structure and the mass spectra of molecular clouds and of cluster systems.

These claims are suspect, in our view, for three reasons: (1) As we have already discussed, D_0, whatever its value, is not a unique indicator of dynamics. (2) The extrapolation of the high-mass ends of the mass spectra of GMCs or of GCSs, where a *rough* power-law form obtains over *perhaps* a decade in mass, is not well justified. In the case of GCSs specifically, the idea that $N(m)$ started as a single power law over all masses is incompatible with the observation (cf. McLaughlin & Pudritz 1996a) that it actually steepens at high cluster masses, i.e., with the existence of m_1 and a peak in the luminosity-weighted luminosity functions of GCSs. At lower masses, the implication is that the peak in the GCLF, and the present behavior at $m < m_*$, had to have been carved out, over time, by dynamical destruction of the globulars; but this hypothesis faces its own difficulties, as we discussed in §6.4 above. In any case, the suggestion of Elmegreen & Efremov (1997) seems to be that the initial GCLF derived from a universal $N(m) \propto m^{-2}$ in *all* galaxies, which again is at odds with observations of real differences between the observed mass spectra of different GCSs (which are *not* all of the form m^{-2}; McLaughlin & Pudritz 1996a). And (3) it is well known (e.g., Sreenivasan 1991) that *laboratory turbulence is a multifractal phenomenon* (this relates to the fundamental *intermittency* of turbulence). That is, turbulent flows cannot be characterized by a single fractal dimension D_0, and there is no guarantee that they will give rise to scale-free cloud mass spectra that look like pure power laws [see Sylos-Labini & Pietronero (1996) for an example of how objects drawn from a multifractal set are given a non–power-law $N(m)$]. The connection made between turbulence and cloud or cluster mass spectra, based as it is on the assumption that the $N(m)$ are perfect power laws related to a single fractal dimension, is therefore not self-consistent. It is possible (again, see Sylos-Labini & Pietronero 1996) to use the full spectrum of generalized D_q for an underlying multifractal structure to infer the mass spectrum of a set of objects. But given the definition of the D_q (eq. [6.3]), and particularly their quantitative dependence on the inhomogeneity of the set (through the densities p_i), this procedure requires some *a priori* knowledge (or at least a model) of the dynamics giving rise to the fractal structure in the first place.

The fourth, and final, point to be made here is that the agglomeration process which we have credited with the formation of the observed mass spectra of GCSs and of modern-day cores and GMCs, could possibly lead, *even in the absence of any turbulence at all*, to the observed capacity dimension of individual clouds (i.e., $D_0 \sim 2.3$: Dickman et al. 1990; Falgarone et al. 1991), and even to a larger-scale fractal (or multifractal) structure in the ISM. There are two ways in which this could occur. First, simulations of the collisional evolution of astronomical cloud systems by Nozakura (1990), which take fragmentation into account, result in a fractal structure to the system, due largely to the clumping of the pieces of clouds that are collisionally disrupted. This process should be investigated in more detail, probably in tandem with the numerical simulations that are required for a self-consistent study of the low-mass end of the GCLF (§6.4). Second, the aggregation of small particles to form larger "clusters" (colloidal aggregates) has long been a topic of interest in the wider physics community (see, e.g., the review by Meakin 1986). Numerous laboratory experiments and computer simulations of the process have been performed, with some involving the agglomeration only of individual particles and others also allowing for interactions between the aggregates themselves. Depending on the specific case studied, and on the rules adopted to govern the kinetics of the reactions between particles and aggregates — so depending, for example, on whether or not their trajectories are ballistic, and whether their reactions are rapid (*diffusion limited*) or slow (*chemically limited*) — capacity dimensions in the range $D_0 \sim 1.8 - 2.5$ are found for the final clusters of particles (Meakin 1986).[1] *This range of dimensions includes the D_0 of GMC surfaces, as well as the D_0 suggested by Elmegreen & Falgarone (1996) for the Galactic cloud ensemble.* There are indications that these collisional aggregates, whether real or simulated, are actually multifractal in nature; but they bear as much of a superficial resemblance to clumpy GMCs as does any homogeneous fractal with $D_0 = 2.3$ (cf. Meakin & Donn 1988 and Elmegreen 1997).

Again, we are *not* trying to suggest that turbulence is unimportant in building up the structure in the ISM and inside clouds, but that *it need not have been alone in doing this.* To be sure, the extent to which the studies listed here (which really involve ***solid particles*** and microscopic

[1] A specific example in an astronomical context is provided by interstellar dust grains, which may be fractal objects with $D_0 \simeq 2$ (Wright 1987; Meakin & Donn 1988; Mathis 1996). Grain coagulation may be to blame for this, and it may have also helped shape the dust mass spectrum (Hayashi & Nakagawa 1975; Jura 1980; Weidenschilling & Ruzmaikina 1994; Kim, Martin, & Hendry 1994; Kim & Martin 1996). In any event, it seems certain that any fractal structure here cannot be traced back to turbulence.

aggregates) are relevant to the agglomeration process in *gaseous* GMCs or SGMCs, has to be carefully examined. But, as was mentioned at the beginning of this Section, it seems quite plausible that collisions between discrete and well defined clumps of gas not only can account for the mass spectra of molecular clouds and cores and globular cluster systems, but could also be fully consistent with — and even instrumental to — the development of complex and (multi)fractal geometry. It would be interesting to pursue this idea more quantitatively in future work, and to examine the relative contributions made by large-scale turbulent motions and simple agglomeration to the evolution of interstellar and protogalactic gas supplies.

Appendix A

Computer Codes

A.1 Hydrostatic Equilibrium

Following is a code (`poly.f`) which simultaneously solves the equation of hydrostatic equilibrium and Poisson's equation for a self-gravitating sphere of gas (see Appendix A of McLaughlin & Pudritz 1996b; Chapter 2 above). The user is asked to choose one of a number of possible barotropic equations of state (EOS), $\widetilde{P} = f(\widetilde{\rho})$, where $\widetilde{P} \equiv P/P_c$ and $\widetilde{\rho} \equiv \rho/\rho_c$. Currently available options for the EOS in `poly.f` are

$$f(\widetilde{\rho}) = \begin{cases} \widetilde{\rho} & \text{isothermal sphere} \\ 1 + A\ \ln\widetilde{\rho} & \text{"finite," or "pure" logotrope} \\ \ln(\ 1+\widetilde{\rho}\ )/\ln 2 & \text{"infinite" logotrope} \\ \widetilde{\rho}^{\ 1/n} & \text{negative-index polytrope: } n \equiv 1/\gamma \equiv N/(1+N), N < -1 \\ (\widetilde{\rho} + A\ \ln\widetilde{\rho} + C)/(1+C) & \text{combined isothermal sphere and logotrope; after Lizano \& Shu (1989)} \\ A\widetilde{\rho} + (1-A)\widetilde{\rho}^{\ 1/n} & \text{combined isothermal sphere and negative-index polytrope} \\ \widetilde{\rho}^{\ 1/2}\ \exp[A(1-\widetilde{\rho}^{\ -n})] & \text{"damped" } \gamma = 1/2 \text{ negative-index polytrope} \\ \widetilde{\rho}^{\ 1/n} + A\ \ln\widetilde{\rho} & \text{combined negative-index polytrope and logotrope .} \end{cases}$$

Printed to an output file are the quantities (see McLaughlin & Pudritz 1996b)

$\xi \equiv r/r_0$; $\widetilde{\rho}$; σ^2/σ_c^2; $\psi \equiv (\phi - \phi_c)/\sigma_c^2$; $d\psi/d\xi$; and $(\partial P_s/\partial R)_{M,\sigma_c}$ (to within a constant factor).

Given any EOS $f(\widetilde{\rho})$, the equation of hydrostatic equilibrium can be used to solve for (dimensionless) density as a function of (dimensionless) gravitational potential:

$$\frac{df}{d\xi} = -\widetilde{\rho}\,\frac{d\psi}{d\xi} \qquad \Longrightarrow \qquad \frac{df}{d\widetilde{\rho}}\,\frac{d\widetilde{\rho}}{\widetilde{\rho}} = -d\psi \qquad \Longrightarrow \qquad \widetilde{\rho} = \widetilde{\rho}(\psi)\ .$$

This can then be used in Poisson's equation,

$$\frac{d^2\psi}{d\xi^2} + \frac{2}{\xi}\frac{d\psi}{d\xi} = 9\tilde{\rho}(\psi) ,$$

to form a single, second-order differential equation for the gravitational potential ψ. This second-order equation (which is analogous to the classical Lane-Emden equation) is, of course, equivalent to a pair of first-order equations:

$$x \equiv \xi; \qquad \begin{array}{ll} y_1 = \psi & dy_1/dx = y_2 \\ y_2 = d\psi/d\xi & dy_2/dx = 9\tilde{\rho}(y_1) - 2y_2/x \end{array} .$$

It is this system which is actually solved (for ψ, which then yields $\tilde{\rho}$, and hence $\tilde{P}$ at every ξ) in `poly.f`. A fourth-order Runge-Kutta scheme with adaptive stepsize (based on code given in Press et al. 1992) is used to do this. The boundary ($x = 0$) conditions are just

$$\begin{array}{ll} y_1(0) = 0 & (dy_1/dx)_{x=0} = 0 \\ y_2(0) = 0 & (dy_2/dx)_{x=0} = 3 , \end{array}$$

where the last equality follows because we have, *for any EOS*, that $\psi \to 3\xi^2/2 + \mathcal{O}(\xi^4)$ as $\xi \to 0$.

Results obtained from `poly.f` are used in a separate code — `ave.f` below — to compute $P_{\rm ave}/P_c$, $\sigma^2_{\rm ave}/\sigma^2_c$, $\rho_{\rm ave}/\rho_c$, a, and α at every radius ξ in a hydrostatic-equilibrium gas cloud. Definitions and formulae for all of these quantities are given in McLaughlin & Pudritz (1996b).

A.1.1 poly.f

```
c
c     A program to compute the space density profile of a negative-
c     index polytrope, an isothermal sphere, a logotrope, or various
c     combinations of these (see McLaughlin & Pudritz 1996, ApJ, 469, 194)
c
      program poly
      EXTERNAL derivs1,derivs2,derivs3,derivs4,derivs5,derivs6,
     &         derivs7,derivs8,rkqs,func1,func2,func3,func4,func5
      PARAMETER (nmax=50,kmaxx=1000)
      real*8 xp(kmaxx),yp(nmax,kmaxx),ystart(nmax)
      real*8 rmax,x1,x2,eps,h1,hmin,dxsav,ak,rho,sig,index,ddx,
     &       rtbis,hmax,z1,z2,z,press,rsurf,ap,psi,adamp,gammp,
     &       ddamp1,ddamp2,lim1,lim2,a1,a2,apl,akk
      integer type1,type2,type,kmax,kount,nvar,nok,nbad,I
      character line*80
      logical done
      COMMON /path/ kmax,kount,dxsav,xp,yp,hmax
      COMMON /path2/ index,apl
      COMMON /path3/ rmax,press
      COMMON /path4/ ak,ap
      COMMON /path5/ psi
      COMMON /path6/ adamp,ddamp1,ddamp2,lim1,lim2,a1,a2
```

```
      COMMON /path7/ type,done
      COMMON /path8/ akk
c
      ddx=1.d-2
      hmax=2.0d-2
c      ddx=1.d-4
c      hmax=1.d-4
      akk=0.d0
c
      write(6,900) ' '
      write(6,900) 'Compute space density profile of: '
      write(6,900) '   (1) isothermal sphere'
      write(6,900) '   (2) logotrope'
      write(6,900) '   (3) negative-index polytrope'
      write(6,900) '   (4) combined isothermal sphere + logotrope'
      write(6,900) '   (5) combined isothermal sphere + polytrope'
      write(6,900) '   (6) DAMPED n=2 negative-index polytrope'
      write(6,900) '   (7) combined neg-index polytrope + logotrope'
5     write(6,900) 'Specify by number 1 to 7: '
      read(5,*) type1
      if(type1.eq.1) then
        type=1
      elseif(type1.eq.2) then
10      write(6,900) 'Finite (1) or infinite (2) logotrope: '
        read(5,*) type2
        if((type2.ne.1).and.(type2.ne.2)) goto 10
        if(type2.eq.1) type=2
        if(type2.eq.2) type=3
      elseif((type1.eq.3).or.(type1.eq.5)) then
15      write(6,900) 'Polytropic n = 1/gamma >= 1: '
        read(5,*) index
        if(index.lt.1.) goto 15
        if(type1.eq.3) type=4
        if(type1.eq.5) type=6
        if(index.eq.1.) type=1
      elseif(type1.eq.4) then
        type=5
      elseif(type1.eq.6) then
17      write(6,900) 'Damping factor exp(-A rho^{-n}); enter A, n: '
        read(5,*) adamp,index
        if((adamp.gt.1.).or.(adamp.le.0.).or.(index.lt.0.)) goto 17
        lim1=adamp/1.1
        lim2=adamp*1.d10
        a1=1.d0/(2.d0*index)
        a2=a1+1.d0
        ddamp1=gammp(a1,adamp)
        ddamp2=gammp(a2,adamp)
        rmax=1.d6
        type=7
```

```
      elseif(type1.eq.7) then
        write(6,900) 'P ~ rho^{1/n} + A ln(rho); enter n, A: '
        read(5,*) index,apl
        type=8
      else
        goto 5
      endif
      write(6,900) ' '
c
      if(type.eq.6) then
        write(6,910) 'P ~ A(rho/rho_0) + (1-A)(rho/rho_0)^{1/n}; ',
     &               'enter A: '
        read(5,*) ap
      endif
      if((type.ne.2).and.(type.ne.5).and.(type.ne.7)) then
        write(6,900) 'Maximum radius (in units of King radius r_0): '
        read(5,*) rmax
      elseif(type.eq.2) then
        write(6,900) 'P ~ 1 + A ln(rho/rho_0); enter A: '
        read(5,*) ak
        press=4.d0/ak
        rmax=rtbis(func1,1.d-10,1.d10,1.d-10)
        rmax=sqrt(2.*ak/9.)*exp(1./ak)
        rsurf=exp(-0.25)*rmax
      elseif(type.eq.5) then
        write(6,910) 'P ~ (rho/rho_0) + A ln(rho/rho_0) + C; ',
     &               'enter A, C: '
        read(5,*) ak,akk
        rmax=1.d5
      endif
      write(6,900) 'Output file: '
      read(5,1000) line
      open(7,file=line)
c
      kmax=1000
      dxsav=1.d0+ddx
      ystart(1)=0.
      ystart(2)=0.
      nvar=2
      x1=0.
      x2=rmax
      eps=1.d-8
      h1=1.d-8
      hmin=0.
      if(type.eq.1) then
         CALL odeint(ystart,nvar,x1,x2,eps,h1,hmin,nok,nbad,
     &               derivs1,rkqs)
         write(7,900) '#'
         write(7,910) '#     Space density profile of an isothermal ',
```

```
     &                'sphere'
          write(7,900) '#'
          write(7,900) '#     z1 = 18(P/P_0) - (d psi/d xi)^2'
          write(7,900) '#     z2 = 1 - 9(xi)(rho_s/rho_0)/(d psi/d xi)'
          write(7,900) '#'
          write(7,1500) '#','r/r_0','rho/rho_0','psi','d(psi)/d(xi)',
     &                  'z=z1/z2'
          write(7,900) '#'
          do 20 I=1,kount
            rho=exp(-yp(1,I))
            z1=18.*rho-yp(2,I)**2
            if(xp(I).eq.0.d0) then
              z2=-2.d0
            else
              z2=1.-9.*xp(I)*rho/yp(2,I)
            endif
            if(z2.eq.0.d0) then
              z=1.d20
            else
              z=z1/z2
            endif
            write(7,2000) sngl(xp(I)),sngl(rho),sngl(yp(1,I)),
     &                    sngl(yp(2,I)),sngl(z)
20        continue
       elseif(type.eq.2) then
          CALL odeint(ystart,nvar,x1,x2,eps,h1,hmin,nok,nbad,
     &                derivs2,rkqs)
          write(7,900) '#'
          write(7,910) '#     Space density profile of a finite ',
     &                 'logotrope'
          write(7,900) '#'
          write(7,920) '#           A = ',sngl(ak),' ===> P_0/P_s = ',
     &                 sngl(press)
          write(7,930) '#           A = ',sngl(ak),' ===> xi_max = ',
     &                 sngl(rmax),'; xi_s = ',sngl(rsurf)
          write(7,900) '#'
          write(7,900) '#     z1 = 18(P/P_0) - (d psi/d xi)^2'
          write(7,900) '#     z2 = 1 - 9(xi)(rho_s/rho_0)/(d psi/d xi)'
          write(7,900) '#'
          write(7,2500) '#','r/r_0','rho/rho_0','(sig)^2/(sig_0)^2',
     &                  'psi','d(psi)/d(xi)','z=z1/z2'
          write(7,900) '#'
          do 30 I=1,kount
            rho=1./(1.+yp(1,I)/ak)
            sig=(1.+ak*log(rho))/rho
            z1=18.*(1.+ak*log(rho))-yp(2,I)**2
            if(xp(I).eq.0.d0) then
              z2=-2.d0
            else
```

```
          z2=1.-9.*xp(I)*rho/yp(2,I)
        endif
        if(z2.eq.0.d0) then
          z=1.d20
        else
          z=z1/z2
        endif
        if(sig.lt.0.) sig=0.
        write(7,3000) sngl(xp(I)),sngl(rho),sngl(sig),
     &                sngl(yp(1,I)),sngl(yp(2,I)),sngl(z)
30    continue
      elseif(type.eq.3) then
        CALL odeint(ystart,nvar,x1,x2,eps,h1,hmin,nok,nbad,
     &              derivs3,rkqs)
        write(7,900) '#'
        write(7,910) '#     Space density profile of an infinite ',
     &               'logotrope'
        write(7,900) '#'
        write(7,900) '#     z1 = 18(P/P_0) - (d psi/d xi)^2'
        write(7,900) '#     z2 = 1 - 9(xi)(rho_s/rho_0)/(d psi/d xi)'
        write(7,900) '#'
        write(7,2500) '#','r/r_0','rho/rho_0','(sig)^2/(sig_0)^2',
     &                'psi','d(psi)/d(xi)','z=z1/z2'
        write(7,900) '#'
        do 40 I=1,kount
          rho=1./(2.*exp(yp(1,I)*log(2.))-1.)
          sig=log(1.+rho)/(log(2.)*rho)
          z1=18.*log(1.+rho)/log(2.)-yp(2,I)**2
          if(xp(I).eq.0.d0) then
            z2=-2.d0
          else
            z2=1.-9.*xp(I)*rho/yp(2,I)
          endif
          if(z2.eq.0.d0) then
            z=1.d20
          else
            z=z1/z2
          endif
          write(7,3000) sngl(xp(I)),sngl(rho),sngl(sig),
     &                  sngl(yp(1,I)),sngl(yp(2,I)),sngl(z)
40      continue
      elseif(type.eq.4) then
        CALL odeint(ystart,nvar,x1,x2,eps,h1,hmin,nok,nbad,
     &              derivs4,rkqs)
        write(7,900) '#'
        write(7,900) '#     Space density profile of a polytrope '
        write(7,940) '#          P ~ rho^{1/n}; n = ',sngl(index)
        write(7,900) '#'
        write(7,900) '#     z1 = 18(P/P_0) - (d psi/d xi)^2'
```

```
      write(7,900) '#     z2 = 1 - 9(xi)(rho_s/rho_0)/(d psi/d xi)'
      write(7,900) '#'
      write(7,2500) '#','r/r_0','rho/rho_0','(sig)^2/(sig_0)^2',
     &              'psi','d(psi)/d(xi)','z=z1/z2'
      write(7,900) '#'
      do 50 I=1,kount
        rho=1./((1.+(index-1.)*yp(1,I))**(index/(index-1.)))
        sig=rho**(1./index)/rho
        z1=18.*(rho**(1./index))-yp(2,I)**2
        if(xp(I).eq.0.d0) then
          z2=-2.d0
        else
          z2=1.-9.*xp(I)*rho/yp(2,I)
        endif
        if(z2.eq.0.d0) then
          z=1.d20
        else
          z=z1/z2
        endif
        write(7,3000) sngl(xp(I)),sngl(rho),sngl(sig),
     &                sngl(yp(1,I)),sngl(yp(2,I)),sngl(z)
50    continue
     elseif(type.eq.5) then
      CALL odeint(ystart,nvar,x1,x2,eps,h1,hmin,nok,nbad,
     &            derivs5,rkqs)
      write(7,900) '#'
      write(7,900) '#     Space density profile of a mixed '
      write(7,900) '#     isothermal sphere and logotrope'
      write(7,950) '#     P ~ (rho/rho_0) + A ln(rho/rho_0) + C; ',
     &             'A = ',sngl(ak),'; C = ',sngl(akk)
      write(7,900) '#'
      write(7,900) '#     z1 = 18(P/P_0) - (d psi/d xi)^2'
      write(7,900) '#     z2 = 1 - 9(xi)(rho_s/rho_0)/(d psi/d xi)'
      write(7,900) '#'
      write(7,2500) '#','r/r_0','rho/rho_0','(sig)^2/(sig_0)^2',
     &              'psi','d(psi)/d(xi)','z=z1/z2'
      write(7,900) '#'
      do 60 I=1,kount
        psi=yp(1,I)
        rho=rtbis(func2,1.d-30,1.1d1,1.d-10)
        sig=(1.d0+ak*log(rho)/rho+akk/rho)/(1.d0+akk)
        z1=18.*(rho+ak*log(rho)+akk)/(1.d0+akk)-yp(2,I)**2
        if(xp(I).eq.0.d0) then
          z2=-2.d0
        else
          z2=1.-9.*xp(I)*rho/yp(2,I)
        endif
        if(z2.eq.0.d0) then
          z=1.d20
```

```
        else
          z=z1/z2
        endif
        if(sig.lt.0.) sig=0.
        write(7,3000) sngl(xp(I)),sngl(rho),sngl(sig),
     &                sngl(yp(1,I)),sngl(yp(2,I)),sngl(z)
60      continue
      elseif(type.eq.6) then
        CALL odeint(ystart,nvar,x1,x2,eps,h1,hmin,nok,nbad,
     &              derivs6,rkqs)
        write(7,900) '#'
        write(7,900) '#     Space density profile of a mixed'
        write(7,900) '#     isothermal sphere and neg-index polytrope'
        write(7,940) '#     Polytropic index n = ',sngl(index)
        write(7,940) '#     Mixture parameter A = ',sngl(ap)
        write(7,900) '#'
        write(7,900) '#     z1 = 18(P/P_0) - (d psi/d xi)^2'
        write(7,900) '#     z2 = 1 - 9(xi)(rho_s/rho_0)/(d psi/d xi)'
        write(7,900) '#'
        write(7,2500) '#','r/r_0','rho/rho_0','(sig)^2/(sig_0)^2',
     &                'psi','d(psi)/d(xi)','z=z1/z2'
        write(7,900) '#'
        do 70 I=1,kount
          psi=yp(1,I)
          rho=rtbis(func3,1.d-30,1.1d1,1.d-10)
          sig=ap+(1.d0-ap)*(rho**(-1.+1./index))
          z1=18.*(ap*rho+(1.d0-ap)*(rho**(1./index)))-yp(2,I)**2
          if(xp(I).eq.0.d0) then
            z2=-2.d0
          else
            z2=1.-9.*xp(I)*rho/yp(2,I)
          endif
          if(z2.eq.0.d0) then
            z=1.d20
          else
            z=z1/z2
          endif
          write(7,3000) sngl(xp(I)),sngl(rho),sngl(sig),
     &                  sngl(yp(1,I)),sngl(yp(2,I)),sngl(z)
70      continue
      elseif(type.eq.7) then
        CALL odeint(ystart,nvar,x1,x2,eps,h1,hmin,nok,nbad,
     &              derivs7,rkqs)
        write(7,900) '#'
        write(7,900) '#     Space density profile of a damped n=2'
        write(7,900) '#          negative-index polytrope'
        write(7,900) '#     Damping term exp(-A rho^{-n})'
        write(7,920) '#          A = ',sngl(adamp),'; n = ',sngl(index)
        write(7,900) '#'
```

```
      write(7,900) '#     z1 = 18(P/P_0) - (d psi/d xi)^2'
      write(7,900) '#     z2 = 1 - 9(xi)(rho_s/rho_0)/(d psi/d xi)'
      write(7,900) '#'
      write(7,2500) '#','r/r_0','rho/rho_0','(sig)^2/(sig_0)^2',
     &              'psi','d(psi)/d(xi)','z=z1/z2'
      write(7,900) '#'
      do 80 I=1,kount
        psi=yp(1,I)
        rho=(adamp/rtbis(func4,lim1,lim2,1.d-10))**(2.d0*a1)
        sig=(1.d0/sqrt(rho))*exp(adamp*(1.d0-rho**(-index)))
        z1=18.*(rho*sig)-yp(2,I)**2
        if(xp(I).eq.0.d0) then
          z2=-2.d0
        else
          z2=1.-9.*xp(I)*rho/yp(2,I)
        endif
        if(z2.eq.0.d0) then
          z=1.d20
        else
          z=z1/z2
        endif
        write(7,3000) sngl(xp(I)),sngl(rho),sngl(sig),
     &                sngl(yp(1,I)),sngl(yp(2,I)),sngl(z)
80    continue
     elseif(type.eq.8) then
      CALL odeint(ystart,nvar,x1,x2,eps,h1,hmin,nok,nbad,
     &            derivs8,rkqs)
      write(7,900) '#'
      write(7,900) '#     Space density profile of a combined'
      write(7,900) '#       neg-index polytrope + logotrope'
      write(7,900) '#    P ~ (rho/rho_0)^{1/n} + A ln(rho/rho_0)'
      write(7,920) '#          A = ',sngl(apl),'; n = ',sngl(index)
      write(7,900) '#'
      write(7,900) '#     z1 = 18(P/P_0) - (d psi/d xi)^2'
      write(7,900) '#     z2 = 1 - 9(xi)(rho_s/rho_0)/(d psi/d xi)'
      write(7,900) '#'
      write(7,2500) '#','r/r_0','rho/rho_0','(sig)^2/(sig_0)^2',
     &              'psi','d(psi)/d(xi)','z=z1/z2'
      write(7,900) '#'
      do 90 I=1,kount
        psi=yp(1,I)
        rho=rtbis(func5,1.d-30,1.1d0,1.d-10)
        sig=(rho)**(1.d0/index-1.d0) + apl*log(rho)/rho
        z1=18.*(rho*sig)-yp(2,I)**2
        if(xp(I).eq.0.d0) then
          z2=-2.d0
        else
          z2=1.-9.*xp(I)*rho/yp(2,I)
        endif
```

```
          if(z2.eq.0.d0) then
            z=1.d20
          else
            z=z1/z2
          endif
          write(7,3000) sngl(xp(I)),sngl(rho),sngl(sig),
     &                  sngl(yp(1,I)),sngl(yp(2,I)),sngl(z)
90       continue
       endif
       close(7)
       write(6,900) ' '
       stop
900    FORMAT(A)
910    FORMAT(A,A)
920    FORMAT(2(A,F11.6))
930    FORMAT(3(A,F11.6))
940    FORMAT(A,F11.6)
950    FORMAT(A,A,F11.6,A,F11.6)
1000   FORMAT(A80)
1500   FORMAT(A1,5X,A5,9X,A9,9X,A3,7X,A12,6X,A7)
2000   FORMAT(5(3X,E12.6))
2500   FORMAT(A1,5X,A5,9X,A9,3X,A17,9X,A3,8X,A12,6X,A7)
3000   FORMAT(2(3X,E12.6),4X,E12.6,5X,3(3X,E12.6))
       end
c
c
c          The following function, for root-finding by bisection, is
c          modified from that given by Press et al. (1992, p. 347)
c
c
       REAL*8 FUNCTION rtbis(func,x1,x2,xacc)
       INTEGER JMAX
       REAL*8 x1,x2,xacc,func
       PARAMETER (JMAX=100)
       INTEGER j
       REAL*8 dx,f,fmid,xmid
       INTEGER type
       LOGICAL done
       COMMON /path7/ type,done
10     fmid=func(x2)
       f=func(x1)
       if(f*fmid.ge.0.) then
         if(type.eq.7) then
           done=.true.
           RETURN
         endif
         write(6,50) 'x1 x2 f(x1) f(x2): ',x1,x2,f,fmid
         write(6,100) 'New bracketing values for A: '
         read(5,*) x1,x2
```

```
        goto 10
      endif
      if(f.lt.0.)then
        rtbis=x1
        dx=x2-x1
      else
        rtbis=x2
        dx=x1-x2
      endif
      do 11 j=1,JMAX
        dx=dx*.5
        xmid=rtbis+dx
        fmid=func(xmid)
        if(fmid.le.0.)rtbis=xmid
        if(abs(dx).lt.xacc .or. fmid.eq.0.) RETURN
11    continue
      pause 'too many bisections in rtbis'
50    FORMAT(A,4F10.4)
100   FORMAT(A,$)
      end
c
c          Solver for rmax given A for a finite logotrope
c
      REAL*8 FUNCTION func1(z)
      real*8 z,f1,f2
      real*8 rmax,press,ak,ap
      COMMON /path3/ rmax,press
      COMMON /path4/ ak,ap
      f1=0.172975/((1.+(1./ak)*(z**2))**(3./2.))
      f2=0.827025/sqrt(1.+(1./ak)*((z/0.57)**2))
      func1=f1+f2-exp(-1./ak)
      RETURN
      end
c
c          Solver for rho/rho_0 given psi for isothermal sphere plus logotrope
c
      REAL*8 FUNCTION func2(z)
      real*8 z
      real*8 ak,ap,psi,akk
      COMMON /path4/ ak,ap
      COMMON /path5/ psi
      COMMON /path8/ akk
      func2=psi+(log(z)+ak*(1.-1./z))/(1.d0+akk)
      RETURN
      end
c
c          Solver for rho/rho_0 given psi for isothermal sphere plus
c          negative-index polytrope
c
```

```
      REAL*8 FUNCTION func3(z)
      real*8 z,fac
      real*8 index,apl,ak,ap,psi
      COMMON /path2/ index,apl
      COMMON /path4/ ak,ap
      COMMON /path5/ psi
      fac=(1.-ap)/(1.-index)
      func3=psi+ap*log(z)+fac*(z**(-1.+1./index))-fac
      RETURN
      end
c
c          Solver for adamp*(rho_0/rho)^{n} given psi for
c          DAMPED n=2 negative-index polytrope
c
      REAL*8 FUNCTION func4(z)
      real*8 z,gammp
      real*8 psi,adamp,ddamp1,ddamp2,lim1,lim2,a1,a2
      COMMON /path5/ psi
      COMMON /path6/ adamp,ddamp1,ddamp2,lim1,lim2,a1,a2
      func4=a1*exp(adamp)*(gammp(a1,z)-ddamp1)/(adamp**a1) +
     &         exp(adamp)*(gammp(a2,z)-ddamp2)/(adamp**a1) - psi
      RETURN
      end
c
c          Solver for rho/rho_0 given psi for logotrope plus
c          negative-index polytrope
c
      REAL*8 FUNCTION func5(z)
      real*8 z,fac
      real*8 index,apl,psi
      COMMON /path2/ index,apl
      COMMON /path5/ psi
      fac=1.-index
      func5=psi+apl*(1.d0-1.d0/z)-(1.d0-z**(fac/index))/fac
      RETURN
      end
c
c
c          The following subroutine, a driver for Runge-Kutta integration
c          of a system of ordibary differential equations, is a slightly
c          modified version of that given by Press et al. (1992, p. 714)
c
c
      SUBROUTINE odeint(ystart,nvar,x1,x2,eps,h1,hmin,nok,nbad,derivs,
     &                  rkqs)
      INTEGER nbad,nok,nvar,KMAXX,MAXSTP,NMAX
      REAL*8 eps,h1,hmin,x1,x2,ystart(nvar),TINY
      EXTERNAL derivs,rkqs
      PARAMETER (MAXSTP=10000,NMAX=50,KMAXX=1000,TINY=1.e-30)
```

```
      INTEGER i,kmax,kount,nstp
      REAL*8 dxsav,h,hdid,hnext,x,xsav,dydx(NMAX),xp(KMAXX),y(NMAX),
     &       yp(NMAX,KMAXX),yscal(NMAX),rat,hmax
      INTEGER type
      LOGICAL done
      COMMON /path/ kmax,kount,dxsav,xp,yp,hmax
      COMMON /path7/ type,done
      done=.false.
      x=x1
      h=sign(h1,x2-x1)
      nok=0
      nbad=0
      kount=0
      do 11 i=1,nvar
        y(i)=ystart(i)
11    continue
      if(kmax.gt.0) rat=2.*dxsav
      do 16 nstp=1,MAXSTP
        CALL derivs(x,y,dydx)
        do 12 i=1,nvar
          yscal(i)=abs(y(i))+abs(h*dydx(i))+TINY
12      continue
        if(kmax.gt.0)then
          if(rat.ge.dxsav) then
            if(kount.lt.kmax-1)then
              kount=kount+1
              xp(kount)=x
              do 13 i=1,nvar
                yp(i,kount)=y(i)
13            continue
              xsav=x
              if(x.lt.1.d-4) xsav=1.d-4
            endif
          endif
        endif
        if((x+h-x2)*(x+h-x1).gt.0.) h=x2-x
        CALL rkqs(y,dydx,nvar,x,h,eps,yscal,hdid,hnext,derivs)
        if(hdid.eq.h)then
          nok=nok+1
        else
          nbad=nbad+1
        endif
        if(((x-x2)*(x2-x1).ge.0.).or.(done))then
          do 14 i=1,nvar
            ystart(i)=y(i)
            if(type.eq.7) then
              ystart(i)=yp(kount,i)
            endif
14        continue
```

```
          if((kmax.ne.0).and.(type.ne.7))then
            kount=kount+1
            xp(kount)=x
            do 15 i=1,nvar
              yp(i,kount)=y(i)
15          continue
          endif
          return
        endif
        if(abs(hnext).lt.hmin) pause
     &           'stepsize smaller than minimum in odeint'
        if((abs(hnext).gt.(hmax*x)).and.(x.ge.1.d0)) hnext=hmax*x
        h=hnext
        rat=x/xsav
16    continue
      pause 'too many steps in odeint'
      RETURN
      end
c
c          System of ODE's for isothermal sphere:
c
      SUBROUTINE derivs1(x,y,dydx)
      real*8 x,y(50),dydx(50)
      if (x.eq.0.) then
        dydx(1)=0.
        dydx(2)=3.
      else
        dydx(1)=y(2)
        if(y(1).lt.0.) y(1)=0.
        dydx(2)=9.*exp(-y(1))-2.*y(2)/x
      endif
      RETURN
      end
c
c          System of ODE's for finite logotrope:
c
      SUBROUTINE derivs2(x,y,dydx)
      real*8 x,y(50),dydx(50),ak,ap
      COMMON /path4/ ak,ap
      if(x.eq.0.) then
        dydx(1)=0.
        dydx(2)=3.
      else
        dydx(1)=y(2)
        if(y(1).lt.0.) y(1)=0.
        dydx(2)=9./(1.+y(1)/ak)-2.*y(2)/x
      endif
      RETURN
      end
```

```
c
c          System of ODE's for infinite logotrope:
c
      SUBROUTINE derivs3(x,y,dydx)
      real*8 x,y(50),dydx(50)
      if(x.eq.0.) then
        dydx(1)=0.
        dydx(2)=3.
      else
        dydx(1)=y(2)
        if(y(1).lt.0.) y(1)=0.
        dydx(2)=9./(2.*exp(y(1)*log(2.))-1.)-2.*y(2)/x
      endif
      RETURN
      end
c
c          System of ODE's for negative-index polytrope, n = 1/gamma
c
      SUBROUTINE derivs4(x,y,dydx)
      real*8 x,y(50),dydx(50),index,apl
      COMMON /path2/ index,apl
      if(x.eq.0.) then
        dydx(1)=0.
        dydx(2)=3.
      else
        dydx(1)=y(2)
        if(y(1).lt.0.) y(1)=0.
        dydx(2)=9./((1.+(index-1.)*y(1))**(index/(index-1.))) -
     &          2.*y(2)/x
      endif
      RETURN
      end
c
c          System of ODE's for mixed isothermal sphere and logotrope
c
      SUBROUTINE derivs5(x,y,dydx)
      real*8 x,y(50),dydx(50),ak,ap,psi,rtbis
      EXTERNAL func2
      COMMON /path4/ ak,ap
      COMMON /path5/ psi
      if(x.eq.0.) then
        dydx(1)=0.
        dydx(2)=3.
      else
        dydx(1)=y(2)
        if(y(1).lt.0.) y(1)=0.
        psi=y(1)
        dydx(2)=9.*rtbis(func2,1.d-30,1.1d1,1.d-10) - 2.*y(2)/x
      endif
```

```
      RETURN
      end
c
c          System of ODE's for mixed isothermal sphere and
c          negative-index polytrope
c
      SUBROUTINE derivs6(x,y,dydx)
      real*8 x,y(50),dydx(50),ak,ap,psi,rtbis
      EXTERNAL func3
      COMMON /path4/ ak,ap
      COMMON /path5/ psi
      if(x.eq.0.) then
        dydx(1)=0.
        dydx(2)=3.
      else
        dydx(1)=y(2)
        if(y(1).lt.0.) y(1)=0.
        psi=y(1)
        dydx(2)=9.*rtbis(func3,1.d-30,1.1d1,1.d-10) - 2.*y(2)/x
      endif
      RETURN
      end
c
c          System of ODE's for DAMPED n=2 negative-index polytrope
c
      SUBROUTINE derivs7(x,y,dydx)
      real*8 x,y(50),dydx(50),psi,rtbis,adamp,ddamp1,ddamp2,
     &       lim1,lim2,a1,a2
      EXTERNAL func4
      COMMON /path5/ psi
      COMMON /path6/ adamp,ddamp1,ddamp2,lim1,lim2,a1,a2
      if(x.eq.0.d0) then
        dydx(1)=0.
        dydx(2)=3.
      else
        dydx(1)=y(2)
        if(y(1).lt.0.) y(1)=0.
        psi=y(1)
        dydx(2)=9.*(adamp/rtbis(func4,lim1,lim2,1.d-10))**(2.d0*a1)
     &          - 2.*y(2)/x
      endif
      RETURN
      end
c
c          System of ODE's for mixed logotrope and negative-index polytrope
c
      SUBROUTINE derivs8(x,y,dydx)
      real*8 x,y(50),dydx(50),index,apl,psi,rtbis
      EXTERNAL func5
```

```
      COMMON /path2/ index,apl
      COMMON /path5/ psi
      if(x.eq.0.) then
        dydx(1)=0.
        dydx(2)=3.
      else
        dydx(1)=y(2)
        if(y(1).lt.0.) y(1)=0.
        psi=y(1)
        dydx(2)=9.*rtbis(func5,1.d-30,1.1d0,1.d-10) - 2.*y(2)/x
      endif
      RETURN
      end
c
c
c          The following two subroutines -- which decide the (variable)
c          stepsize in the Runge-Kutta integration of ODEs -- may be taken
c          in their entirety from Press et al. (1992, pp. 712-713), with the
c          ONE MODIFICATION that all variables declared there as REAL must
c          now be designated REAL*8 (double precision)
c
c
      SUBROUTINE rkqs(y,dydx,n,x,htry,eps,yscal,hdid,hnext,derivs)
      SUBROUTINE rkck(y,dydx,n,x,h,yout,yerr,derivs)
c
c
c          The following functions and subroutines, which evaluate the
c          incomplete gamma function (required for analysis of the DAMPED
c          n=2 negative-index polytrope), may be taken in their entirety
c          from Press et al. (1992, pp. 211-213), with the ONE MODIFICATION
c          that all variables declared there as REAL must now be designated
c          REAL*8 (double precision)
c
c
      REAL*8 FUNCTION gammp(a,x)
      SUBROUTINE gser(gamser,a,x,gln)
      SUBROUTINE gcf(gammcf,a,x,gln)
      REAL*8 FUNCTION gammln(xx)
```

A.1.2 ave.f

```
c
c     A program to compute the mass-averaged velocity dispersion, virial
c     parameter alpha, and 'non-uniformity' parameter a of the gravitational
c     energy of a hydrostatic-equilibrium gas configuration; requires results
c     from poly.f as input (see McLaughlin & Pudritz 1996, ApJ, 469, 194)
c
```

```
      program ave
      EXTERNAL derivs1,derivs2,derivs3,rkqs
      PARAMETER (nmax=50,kmaxx=200)
      real*8 xp(kmaxx),yp(nmax,kmaxx),ystart(nmax)
      real*8 rad(2000),rho(2000),sig(2000),pot(2000),dpot(2000),
     &     rho2(2000),sig2(2000),dpot2(2000)
      real*8 yp1,yp2
      real*8 x1,x2,eps,h1,hmin,dxsav,press,rhoave,sigave,agrav
      integer kmax,kount,nvar,nok,nbad,I,J,tot,type
      character line*120,infile*120,outfile*120
      COMMON /path/ kmax,kount,dxsav,xp,yp
      COMMON /path2/ rad,rho,rho2,sig,sig2,dpot,dpot2,tot
c
      write(6,900) ' '
5     write(6,900) 'Isothermal sphere (1) or other (2)?'
      read(5,*) type
      if((type.ne.1).and.(type.ne.2)) goto 5
      if(type.eq.1) then
        write(6,900) 'Input file with (xi, rho, psi, dpsi): '
      elseif(type.eq.2) then
        write(6,900) 'Input file with (xi, rho, sigma, psi, dpsi): '
      endif
      read(5,1000) infile
      write(6,900) 'Output file: '
      read(5,1000) outfile
      write(6,900) ' '
c
      open(4,file=infile)
      open(7,file=outfile)
      write(7,900) '#'
      write(7,900) '#         Header from input file ---'
      write(7,900) '#'
      do 10 I=1,32767
        read(4,1000) line
        if(line(1:1).eq.'#') then
          write(7,1000) line
        else
          goto 20
        endif
10    continue
20    write(7,900) '#'
      write(7,900) '#'
      write(7,900) '#'
      write(7,1300) '#','Grav. Energy','Virial Param.'
      write(7,1600) '#','xi=r/r_0','P_ave/P_0','(<sig>/sig_0)^2',
     &              '<rho>/rho_0','a','alpha'
      write(7,900) '#'
      J=0
      do 30 I=1,32767
```

```
        J=J+1
        if(type.eq.1) then
          read(line,*) rad(J),rho(J),pot(J),dpot(J)
          sig(J)=1.d0
        elseif(type.eq.2) then
          read(line,*) rad(J),rho(J),sig(J),pot(J),dpot(J)
        endif
        read(4,1000,end=40) line
30    continue
40    close(4)
      tot=J
c
      yp1=1.e30
      yp2=1.e30
      CALL spline(rad,rho,tot,yp1,yp2,rho2)
      CALL spline(rad,sig,tot,yp1,yp2,sig2)
      CALL spline(rad,dpot,tot,yp1,yp2,dpot2)
c
      kmax=0
      dxsav=0.
      nvar=1
      hmin=0.
      do 50 I=1,tot
        if(rad(I).eq.0.) goto 50
        ystart(1)=0.
        x1=0.
        x2=rad(I)
        eps=1.d-7
        h1=1.d-5
        CALL odeint(ystart,nvar,x1,x2,eps,h1,hmin,nok,nbad,
     &              derivs1,rkqs)
        press=3.*ystart(1)/(rad(I)**3)
        ystart(1)=0.
        x1=0.
        x2=rad(I)
        eps=1.d-7
        h1=1.d-5
        CALL odeint(ystart,nvar,x1,x2,eps,h1,hmin,nok,nbad,
     &              derivs2,rkqs)
        rhoave=3.*ystart(1)/(rad(I)**3)
        sigave=press/rhoave
        alpha=5.*sigave/(rad(I)*dpot(I))
        ystart(1)=0.
        x1=0.
        x2=rad(I)
        eps=1.d-7
        h1=1.d-5
        CALL odeint(ystart,nvar,x1,x2,eps,h1,hmin,nok,nbad,
     &              derivs3,rkqs)
```

```
        agrav=15.*ystart(1)/((dpot(I)**2)*(rad(I)**3))
        write(7,2000) sngl(rad(I)),sngl(press),sngl(sigave),
     &                sngl(rhoave),sngl(agrav),sngl(alpha)
50     continue
       close(7)
       stop
900    FORMAT(A)
1000   FORMAT(A120)
1300   FORMAT(A1,62X,A12,3X,A13)
1600   FORMAT(A1,4X,A8,6X,A9,3X,A15,2X,A11,9X,A1,12X,A5)
2000   FORMAT(6(3X,E12.6))
       end
c
c
c          The following three subroutines, for Runge-Kutta integration of
c          a system of ODEs, may be taken in their entirety from Press et al.
c          (1992, pp. 712-715), with the ONE MODIFICATION that all variables
c          declared there as REAL must now be designated REAL*8 (double
c          precision)
c
c
       SUBROUTINE odeint(ystart,nvar,x1,x2,eps,h1,hmin,nok,nbad,derivs,rkqs)
       SUBROUTINE rkqs(y,dydx,n,x,htry,eps,yscal,hdid,hnext,derivs)
       SUBROUTINE rkck(y,dydx,n,x,h,yout,yerr,derivs)
c
c          System of ODEs required to compute average pressure at radius x
c
       SUBROUTINE derivs1(x,y,dydx)
       real*8 x,y(50),dydx(50)
       real*8 rhox,sigx
       real*8 rad(2000),rho(2000),rho2(2000),sig(2000),sig2(2000),
     &        dpot(2000),dpot2(2000)
       integer tot
       COMMON /path2/ rad,rho,rho2,sig,sig2,dpot,dpot2,tot
c
       if(x.eq.0.) then
         rhox=1.
         sigx=1.
       else
         CALL splint(rad,rho,rho2,tot,x,rhox)
         CALL splint(rad,sig,sig2,tot,x,sigx)
       endif
       dydx(1)=(x**2)*(rhox*sigx)
       RETURN
       end
c
c          System of ODEs required to compute average density at radius x
c
       SUBROUTINE derivs2(x,y,dydx)
```

```
      real*8 x,y(50),dydx(50)
      real*8 rhox
      real*8 rad(2000),rho(2000),rhc2(2000),sig(2000),sig2(2000),
     &       dpot(2000),dpot2(2000)
      integer tot
      COMMON /path2/ rad,rho,rho2,sig,sig2,dpot,dpot2,tot
c
      if(x.eq.0.) then
        rhox=1.
      else
        CALL splint(rad,rho,rho2,tot,x,rhox)
      endif
      dydx(1)=(x**2)*rhox
      RETURN
      end
c
c          System of ODEs required to compute non-uniformity factor a at
c          radius x
c
      SUBROUTINE derivs3(x,y,dydx)
      real*8 x,y(50),dydx(50)
      real*8 rhox,dpotx
      real*8 rad(2000),rho(2000),rho2(2000),sig(2000),sig2(2000),
     &       dpot(2000),dpot2(2000)
      integer tot
      COMMON /path2/ rad,rho,rho2,sig,sig2,dpot,dpot2,tot
c
      if(x.eq.0.) then
        rhox=1.
        dpotx=0.
      else
        CALL splint(rad,rho,rho2,tot,x,rhox)
        CALL splint(rad,dpot,dpot2,tot,x,dpotx)
      endif
      dydx(1)=(x**3)*rhox*dpotx
      RETURN
      end
c
c
c          The following two subroutines, which perform an interpolation
c          of tabulated densities, velocity dispersions, and potentials
c          as functions of radius (output from poly.f), may be taken in
c          their entirety from Press et al. (1992, pp. 109-110), with
c          the TWO MODIFICATIONS that (1) all variables declared there as
c          REAL must now be designated REAL*8 (double precision), and
c          (2) the parameter NMAX in SUBROUTINE spline must be set to
c          NMAX=2001
c
c
```

```
SUBROUTINE spline(x,y,n,yp1,ypn,y2)
SUBROUTINE splint(xa,ya,y2a,n,x,y)
```

A.2 Gravitational Collapse

Following are two programs, `sing.f` and `coll.f`, used to integrate the coupled, first-order differential equations (A4) and (A5) of McLaughlin & Pudritz (1997; Chapter 3 above), and thus to obtain similarity solutions for the gravitational collapse of polytropic and logotropic gas spheres. A change of variables has been implemented, and the differential equations formally manipulated, to (somewhat) facilitate the calculations here. Thus, in the current versions of these codes, we define (cf. Appendices A and B of McLaughlin & Pudritz 1997)

$$\mathrm{X} \equiv x\alpha^{(1-\gamma)/2} \qquad \mathrm{V} \equiv v\alpha^{(1-\gamma)/2} \qquad \chi \equiv (2-\gamma)\mathrm{X} - \mathrm{V},$$

and work with the logarithmic "density," $\ln\alpha$, as the independent variable, so that the equations to be solved are:

$$\frac{d\mathrm{X}}{d\ln\alpha} = \frac{\chi^2 - 1}{[\alpha/(4-3\gamma) + 2(1-\gamma) - 2\chi/\mathrm{X}]\chi + (1-\gamma)\mathrm{V}} + \frac{1-\gamma}{2}\,\mathrm{X}$$

$$\frac{d\mathrm{V}}{d\ln\alpha} = \frac{[\alpha\chi/(4-3\gamma) + (1-\gamma)\mathrm{V} - 2/\mathrm{X}]\chi + 2(1-\gamma)}{[\alpha/(4-3\gamma) + 2(1-\gamma) - 2\chi/\mathrm{X}]\chi + (1-\gamma)\mathrm{V}} + \frac{1-\gamma}{2}\,\mathrm{V}\,.$$

The code `sing.f` is used to integrate this system of equations *through* a singular point chosen by the user. It is easy to see that singular points, in terms of these new variables, satisfy the simple relation

$$\chi_* - 1 = (2-\gamma)\mathrm{X}_* - \mathrm{V}_* - 1 = 0\,,$$

and that, in the neighborhood of such points,

$$\frac{d\mathrm{X}}{d\alpha} = \frac{1-\gamma}{2}\,\frac{\mathrm{X}_*}{\alpha_*} + \alpha_*^{(1-\gamma)/2}\,\frac{1}{a_1} \qquad \frac{d\mathrm{V}}{d\alpha} = \frac{1-\gamma}{2}\,\frac{\mathrm{V}_*}{\alpha_*} + \alpha_*^{(1-\gamma)/2}\,\frac{b_1}{a_1}\,,$$

with a_1 and b_1 given by equations (B6), (B7) of McLaughlin & Pudritz (1997). Thus, the system of equations for X and V is solved by `sing.f` as follows. The user chooses a singular point x_* (in the original variables of McLaughlin & Pudritz 1997), and decides whether to compute the "plus" or "minus" solution which passes through that point. This implicitly picks out a unique value of the reduced central mass m_0 (or density normalization C). The density α_* corresponding to x_* is computed from equation (B2) of McLaughlin & Pudritz (1997), so that all of X_*, V_*, $d\mathrm{X}/d\alpha$ and $d\mathrm{V}/d\alpha$ are known. The code then integrates *away* from the singular point, in each of *two directions*:

(1) α is first slightly increased over α_*: `alph1=(1+step)*alstar` in the code, for some very small `step` value. This is equivalent to moving to x slightly smaller than x_*. Evidently, X at this new α is obtained as $\mathrm{X} = \mathrm{X}_* + (d\mathrm{X}/d\alpha)(\alpha - \alpha_*)$; and similarly for V. These provide the boundary conditions required to integrate the coupled fluid equations given just above, so the switch to $\ln\alpha$ as the independent variable is made and the integration carried out. For "minus" solutions, the integration is stopped at some pre-set, large $\ln\alpha$ (or, equivalently, some very small x); for "plus" solutions, it stops as soon as $v(x)$ becomes negative. In either case the values of the *usual* similarity variables x, $\alpha(x)$, $v(x)$, and $m(x)$ for all $x < x_*$ ($\alpha > \alpha_*$) are written to an output file.

(2) α is next set to be just less than α_*: `alph1=(1-step)*alstar`, which is equivalent to

moving to x slightly larger than the chosen x_*. The code variables X and V at this new α are determined in the same way as before, and integration towards smaller α-values can proceed. This time, a "minus" solution is stopped *either* when $v(x) = 0$, *or* when it tries to pass through a second critical point [signalled by a change in the sign of $(\chi - 1)$]; "plus" solutions are always continued to some pre-set, small value of α (large value of x). The resulting x, $\alpha(x)$, $v(x)$, and $m(x)$ — now for all $x > x_*$ — are then written to the same output file used in the previous step.

By construction, `sing.f` can only be used to find collapse solutions which pass through at least one critical point. Moreover, when the solution is a "minus" one, ***since the integration proceeds in a direction away from a user-specified critical point, this must be a saddle*** (integration away from a node is unstable; see the footnote in §2.3 of McLaughlin & Pudritz 1997). Thus, although `sing.f` allows the user to specify any starting critical point $x_* \leq x_{\rm ew}$, care must be taken to ensure that it is indeed a saddle. If so, then the minus solution will either lie to the left of the expansion wave in a $(-v, x)$ plot, or to the right of it (cf. Fig. 2 of McLaughlin & Pudritz 1997). In the former case, `sing.f` is able to find the entire collapse solution (or at least, that part of it which has $v < 0$). In the latter case, however, `sing.f` gives only a partial solution: it stops at the second critical point because this will be a node, and integration towards larger x, i.e., away from the node, would be unstable.

This second type of minus solution with singular points is an example of out-of-equilibrium ($C > C_{\rm HSE}$) collapse. It is continued to arbitrarily large x by matching to a solution generated with the program `coll.f`, which is also used to integrate those "minus" solutions which have $C > C_{\rm HSE}$ and pass through no singular points at all. `coll.f` employs the same X and V variables as `sing.f`, but starts integrating a solution at a pre-set x so large (and hence, $\ln\alpha$ so large and negative) that the asymptotic results (A10) of McLaughlin & Pudritz (1997) apply. The user specifies a polytropic index and a density normalization $C > C_{\rm HSE}$, thus defining an initial X and V. The integration goes in the direction of increasing $\ln\alpha$ (decreasing x), and stops *either* when a singular point is encountered [this will be a node, and an attempt to cross it will again cause a change in sign of $(\chi - 1)$], *or* when $\ln\alpha$ reaches some pre-set large value without coming across any singular point. In the latter case, the entire collapse solution [x, $\alpha(x)$, $v(x)$, and $m(x)$] is contained in the output from `coll.f`. But in the former case, `coll.f` gives just part of the "minus" solution: once a node is encountered, integration cannot continue towards still smaller x, i.e., away from the node (again, this is an unstable procedure). Thus, the entire solution for a $C > C_{\rm HSE}$ collapse with critical points must be obtained by combining the large-x results of `coll.f` with appropriate small-x results from `sing.f`, i.e., by starting from some saddle-like critical point at smaller x and integrating *towards* the same node met in `coll.f`. This procedure is in some sense one of trial and error, as it is not known *a priori* which saddle and node correspond to any single solution.

A.2.1 sing.f

```
c
c     A program to integrate the 'similarity' fluid equations of McLaughlin
c     & Pudritz (1997, ApJ, 476, 750), for collapse of a polytropic or
c     logotropic gas sphere through *one* singular point
c
      program sing
      EXTERNAL derivs1,stiff,alcrit
      PARAMETER (nmax=50,kmaxx=2000)
      real*8 xp(kmaxx),yp(nmax,kmaxx),ystart(nmax)
```

```
      real*8 x1,x2,eps,h1,hmin,dxsav
      real*8 index,power,alphew,xew,xcrit,alstar,vstar,a1,b1,c1,d1,
     &       k1,k2,dk,xless(kmaxx),alless(kmaxx),vless(kmaxx),
     &       mless(kmaxx),xmore(kmaxx),almore(kmaxx),vmore(kmaxx),
     &       mmore(kmaxx),mstar,step,rtbis,bigx,bigv,alph1
      integer type,kmax,kount,nvar,nok,nbad
      real*8 hmax
      character outfile*120,line*120
      COMMON /path/ kmax,kount,dxsav,xp,yp
      COMMON /path2/ index
      COMMON /path4/ hmax
      COMMON /path5/ xcrit
c
      step=1.d-6
      hmax=2.d-2
c
      write(6,100) ' '
      write(6,100) 'Collapse of gas sphere through a singular point'
      write(6,100) ' '
5     write(6,100) 'Gas polytropic index < 4/3 (0 = logotrope):'
      read(5,*) index
      if((index.ge.4.d0/3.d0).or.(index.lt.0.d0)) goto 5
      power=(index-1.d0)/2.d0
      alphew=2.d0*(4.d0-3.d0*index)
      xew=(alphew**power)/(2.d0-index)
      write(6,200) '        alpha_EW = ',alphew
      write(6,200) '            x_EW = ',xew
      line=' '
10    write(6,100) 'Singular point x_* <= x_EW (<return> for x_EW): '
      read(5,1000) line
      if(line.ne.' ') then
         read(line,*) xcrit
      else
         type=1
         xcrit=xew
      endif
      if(xcrit.le.0.d0) goto 10
      if(xcrit.gt.xew) goto 10
      if(xcrit.lt.xew) then
20      write(6,100) 'Minus (1) or Plus (2) solution? '
        read(5,*) type
        if((type.ne.1).and.(type.ne.2)) goto 20
      endif
      write(6,100) 'Output file: '
      read(5,1000) outfile
      write(6,100) ' '
c
      if(xcrit.eq.xew) then
        alstar=alphew
```

```
        vstar=0.d0
        if(index.gt.6.d-1) then
          if(type.eq.1) then
            a1=(3.d0*index-5.d0)*(alstar**(1.d0-power))/(1.d0+index)
            b1=(5.d0*index-3.d0)/(1.d0+index)
          elseif(type.eq.2) then
            a1=-2.d0*(alstar**(1.d0-power))
            b1=0.d0
          endif
        elseif(index.le.6.d-1) then
          if(type.eq.1) then
            a1=-2.d0*(alstar**(1.d0-power))
            b1=0.d0
          elseif(type.eq.2) then
            a1=(3.d0*index-5.d0)*(alstar**(1.d0-power))/(1.d0+index)
            b1=(5.d0*index-3.d0)/(1.d0+index)
          endif
        endif
      elseif(xcrit.lt.xew) then
        alstar=rtbis(alcrit,1.d-10,1.d10,1.d-10)
        vstar=(2.d0-index)*xcrit - alstar**power
        k1=8.d0*(alstar**power)/xcrit - (9.d0-7.d0*index)
        k2=2.d0*(1.d0-index)*(5.d0-3.d0*index) +
     &       6.d0*(((alstar**power)/xcrit)**2) -
     &         4.d0*(4.d0-3.d0*index)*(alstar**power)/xcrit + alstar
        dk=k1**2 - 4.d0*(1.d0+index)*k2
        if(type.eq.1) then
          a1=(-k1 + sqrt(dk))/(2.d0*(1.d0+index))
        elseif(type.eq.2) then
          a1=(-k1 - sqrt(dk))/(2.d0*(1.d0+index))
        endif
        b1=-2.d0*(1.d0-index) + 2.d0*(alstar**power)/xcrit + a1
        a1=a1*(alstar**(1.d0-power))
      endif
      bigx=xcrit/(alstar**power)
      bigv=vstar/(alstar**power)
      c1=-power*bigx/alstar + 1.d0/(a1*(alstar**power))
      d1=-power*bigv/alstar + b1/(a1*(alstar**power))
c
      open(7,file=outfile)
      write(7,100) '#'
      write(7,150) '#    Collapse of polytropic gas sphere through ',
     &             'a singular point'
      if(type.eq.1) then
        write(7,100) '#                 --- minus solution'
      elseif(type.eq.2) then
        write(7,100) '#                 --- plus solution'
      endif
      write(7,100) '#'
```

```
      write(7,300) '#      polytropic index: ',index
      write(7,300) '#                  x_EW: ',xew
      write(7,300) '#             alpha_EW: ',alphew
      write(7,100) '#'
      write(7,300) '#      singular point x_* = ',xcrit
      write(7,300) '#             alpha(x_*) = ',alstar
      write(7,300) '#                 v(x_*) = ',vstar
      write(7,100) '#'
      write(7,1100) '#','x','alpha(x)','v(x)','m(x)'
      write(7,100) '#'
c
      kmax=2000
      kount=0
      dxsav=1.d-4
      nvar=2
      hmin=0.d0
      alph1=(1.d0+step)*alstar
      x1=log(alph1)
      x2=35.d0
      eps=1.d-8
      h1=1.d-5
      ystart(1)=bigx + c1*(alph1-alstar)
      ystart(2)=bigv + d1*(alph1-alstar)
      CALL odeint(ystart,nvar,x1,x2,eps,h1,hmin,nok,nbad,derivs1,stiff)
      do 30 I=1,kount
        alless(I)=exp(xp(kount-I+1))
        xless(I)=yp(1,kount-I+1)*(alless(I)**power)
        vless(I)=yp(2,kount-I+1)*(alless(I)**power)
        mless(I)=alless(I)*(xless(I)**2)*
     &            ((2.d0-index)*xless(I)-vless(I))/(4.d0-3.d0*index)
        write(7,1200) xless(I),alless(I),vless(I),mless(I)
30    continue
c
      mstar=alstar*(xcrit**2)*((2.d0-index)*xcrit-vstar)/
     &      (4.d0-3.d0*index)
      write(7,1200) xcrit,alstar,vstar,mstar
c
      kmax=2000
      kount=0
      dxsav=1.d-4
      nvar=2
      hmin=0.d0
      alph1=(1.d0-step)*alstar
      x1=log(alph1)
      x2=-5.d0
      eps=1.d-8
      h1=1.d-5
      ystart(1)=bigx + c1*(alph1-alstar)
      ystart(2)=bigv + d1*(alph1-alstar)
```

```
      CALL odeint(ystart,nvar,x1,x2,eps,h1,hmin,nok,nbad,derivs1,stiff)
      do 40 I=1,kount
        almore(I)=exp(xp(I))
        xmore(I)=yp(1,I)*(almore(I)**power)
        vmore(I)=yp(2,I)*(almore(I)**power)
        mmore(I)=almore(I)*(xmore(I)**2)*
     &           ((2.d0-index)*xmore(I)-vmore(I))/(4.d0-3.d0*index)
        write(7,1200) xmore(I),almore(I),vmore(I),mmore(I)
40    continue
      close(7)
      stop
100   FORMAT(A)
150   FORMAT(A,A)
200   FORMAT(A,E15.7)
300   FORMAT(A,E)
1000  FORMAT(A120)
1100  FORMAT(A1,9X,A1,13X,A8,11X,A4,13X,A4)
1200  FORMAT(4(3X,E14.6))
      end
c
c
c          The function rtbis, which uses bisection to solve for the
c          density at a critical point, given the x-value of the point,
c          may be taken in its entirety from Press et al. (1992, p. 347),
c          with the ONE MODIFICATION that all variables declared there
c          as REAL must now be designated REAL*8 (double precision);
c          the argument 'func' is a dummy variable representing the
c          function 'alcrit' just below
c
c
      REAL*8 FUNCTION rtbis(func,x1,x2,xacc)
c
c
      REAL*8 FUNCTION alcrit(z)
      real*8 z,fac1,fac2,fac3,fac4,zpow,index,xcrit
      COMMON /path2/ index
      COMMON /path5/ xcrit
      zpow=(index-1.d0)/2.d0
      fac1=(z**(zpow+1.d0))/(4.d0-3.d0*index)
      fac2=(1.d0-index)*(z**zpow)
      fac3=-2.d0*(z**(2.d0*zpow))/xcrit
      fac4=(1.d0-index)*(2.d0-index)*xcrit
      alcrit=fac1+fac2+fac3+fac4
      RETURN
      end
c
c
c          This driver for integration of ODEs has been modified from that
c          given in Press et al. (1992, p. 714) to stop the integration
```

```
c          when the solution crosses the line of critical points
c
c
      SUBROUTINE odeint(ystart,nvar,x1,x2,eps,h1,hmin,nok,nbad,derivs,
     *steps)
      INTEGER nbad,nok,nvar,KMAXX,MAXSTP,NMAX
      REAL*8 eps,h1,hmin,x1,x2,ystart(nvar),TINY
      EXTERNAL derivs,stiff
      PARAMETER (MAXSTP=10000,NMAX=50,KMAXX=2000,TINY=1.e-30)
      INTEGER i,kmax,kount,nstp
      REAL*8 dxsav,h,hdid,hnext,x,xsav,dydx(NMAX),xp(KMAXX),y(NMAX),
     *yp(NMAX,KMAXX),yscal(NMAX)
      REAL*8 index,chix,ochix,hmax
      COMMON /path/ kmax,kount,dxsav,xp,yp
      COMMON /path2/ index
      COMMON /path4/ hmax
      x=x1
      h=sign(h1,x2-x1)
      nok=0
      nbad=0
      kount=0
      do 11 i=1,nvar
        y(i)=ystart(i)
11    continue
      if (kmax.gt.0) xsav=x-2.*dxsav
c
      ochix=0.d0
c
      do 16 nstp=1,MAXSTP
        CALL derivs(x,y,dydx)
        do 12 i=1,nvar
          yscal(i)=abs(y(i))+abs(h*dydx(i))+TINY
12      continue
        if(kmax.gt.0)then
          if(abs(x-xsav).gt.abs(dxsav)) then
            if(kount.lt.kmax-1)then
              kount=kount+1
              xp(kount)=x
              do 13 i=1,nvar
                yp(i,kount)=y(i)
13            continue
              xsav=x
            endif
          endif
        endif
        if((x+h-x2)*(x+h-x1).gt.0.) h=x2-x
        CALL steps(y,dydx,nvar,x,h,eps,yscal,hdid,hnext,derivs)
        if(hdid.eq.h)then
          nok=nok+1
```

```
        else
          nbad=nbad+1
        endif
c
        chix=(2.d0-index)*y(1)-y(2)-1.d0
c        if((chix*ochix).lt.0.d0) RETURN
c
        if(((x-x2)*(x2-x1).ge.0.).or.(y(2).gt.0.d0).or.
     &     ((chix*ochix).lt.0.d0))then
          do 14 i=1,nvar
            ystart(i)=y(i)
14        continue
          if(kmax.ne.0)then
            kount=kount+1
            xp(kount)=x
            do 15 i=1,nvar
              yp(i,kount)=y(i)
15          continue
          endif
          return
        endif
c
        ochix=chix
c
        if(abs(hnext).lt.hmin) pause
     &      'stepsize smaller than minimum in odeint'
        if(abs(hnext).gt.hmax) hnext=sign(hmax,x2-x1)
        h=hnext
16    continue
      pause 'too many steps in odeint'
      RETURN
      end
c
c
c         The following three subroutines, which together take a step in
c         the integration of stiff sets of ODEs, may be taken in their
c         entirety from Press et al. (1992, pp. 739, 39, 38), with the
c         ONE MODIFICATION that all variables declared there as REAL
c         must now be designated REAL*8 (double precision)
c
c
      SUBROUTINE stiff(y,dydx,n,x,htry,eps,yscal,hdid,hnext,derivs)
      SUBROUTINE lubksb(a,n,np,indx,b)
      SUBROUTINE ludcmp(a,n,np,indx,d)
c
c
c         System of ODEs (collapse equations) to be integrated
c
c
```

```
      SUBROUTINE derivs1(x,y,dydx)
      real*8 x,y(50),dydx(50)
      real*8 alph,dens,chi,denom,num1,num2
      real*8 index
      COMMON /path2/ index
      COMMON /path3/ dens,chi,denom
c
      alph=exp(x)
      dens=alph/(4.d0-3.d0*index)
      chi=(2.d0-index)*y(1)-y(2)
      denom=(dens-2.d0*chi/y(1))*chi + (1.d0-index)*(y(2)+2.d0*chi)
      num1=chi**2-1.d0
      num2=(dens*chi-2.d0/y(1))*chi + (1.d0-index)*(y(2)*chi+2.d0)
      dydx(1)=num1/denom + (1.d0-index)*y(1)/2.d0
      dydx(2)=num2/denom + (1.d0-index)*y(2)/2.d0
      endif
      RETURN
      end
c
c
c          Matrix of *second* derivatives of the system of ODEs, inverted
c          in SUBROUTINE stiff (see discussion and examples in Press et al.
c          1992, p. 727 ff.); the components of the vector f here are just
c          dydx(1) and dydx(2) from SUBROUTINE derivs1
c
c
      SUBROUTINE jacobn(x,y,dfdx,dfdy,n,nmax)
      INTEGER n,nmax
      REAL*8 x,y(50),dydx(50),dfdx(nmax),dfdy(nmax,nmax),
     &       fac,brak1,brak2,brak3,brak4
      REAL*8 index
      REAL*8 dens,chi,denom
      COMMON /path2/ index
      COMMON /path3/ dens,chi,denom
c
      CALL derivs1(x,y,dydx)
      fac = (1.d0-index)/2.d0
      brak1 = (2.d0-index)*dens + 2.d0*((chi/y(1))**2) -
     &         4.d0*(2.d0-index)*(chi/y(1)) +
     &            2.d0*(1.d0-index)*(2.d0-index)
      brak2 = -dens + 4.d0*(chi/y(1)) - (1.d0-index)
      brak3 = 2.d0*(2.d0-index)*dens*chi + 2.d0*chi/(y(1)**2) -
     &           2.d0*(2.d0-index)/y(1) + (1.d0-index)*(2.d0-index)*y(2)
      brak4 = -2.d0*dens*chi + 2.d0/y(1) + (1.d0-index)*(chi-y(2))
c
      dfdx(1) = -(dydx(1)-fac*y(1))*dens*chi/denom
      dfdx(2) = -(dydx(2)-fac*y(2)-chi)*dens*chi/denom
c
      dfdy(1,1) = fac - ((dydx(1)-fac*y(1))*brak1 -
```

```
     &              2.d0*(2.d0-index)*chi)/denom
      dfdy(1,2) = -((dydx(1)-fac*y(1))*brak2+2.d0*chi)/denom
      dfdy(2,1) = -((dydx(2)-fac*y(2))*brak1-brak3)/denom
      dfdy(2,2) = fac - ((dydx(2)-fac*y(2))*brak2-brak4)/denom
      RETURN
      end
```

A.2.2 coll.f

```
c
c     A program to integrate the 'similarity' fluid equations of McLaughlin
c     & Pudritz (1997, ApJ, 476, 750), for collapse of a polytropic or
c     logotropic gas sphere, starting from x=infinity (no passage through any
c     singular point)
c
      program coll
      EXTERNAL derivs1,stiff
      PARAMETER (nmax=50,kmaxx=2000)
      real*8 xp(kmaxx),yp(nmax,kmaxx),ystart(nmax)
      real*8 x1,x2,eps,h1,hmin,dxsav
      real*8 index,power,chse,alphew,xew,c,xx(kmaxx),alpha(kmaxx),
     &       vel(kmaxx),mass(kmaxx),hmax
      integer kmax,kount,nvar,nok,nbad
      character outfile*120
      COMMON /path/ kmax,kount,dxsav,xp,yp
      COMMON /path2/ index
      COMMON /path4/ hmax
c
      hmax=1.2d-2
c
      write(6,100) ' '
      write(6,100) 'Collapse of gas sphere just out of HSE'
      write(6,100) ' '
5     write(6,100) 'Gas polytropic index < 4/3 (0 = logotrope):'
      read(5,*) index
      if((index.ge.4.d0/3.d0).or.(index.lt.0.d0)) goto 5
      power=1.d0/(2.d0-index)
      chse=(2.d0*(4.d0-3.d0*index)/((2.d0-index)**2))**power
      power=(index-1.d0)/2.d0
      alphew=2.d0*(4.d0-3.d0*index)
      xew=(alphew**power)/(2.d0-index)
      write(6,200) '            x_EW = ',xew
      write(6,200) '        alpha_EW = ',alphew
      write(6,200) '          C(HSE) = ',chse
15    write(6,150) 'Density normalization C > C(HSE): '
      read(5,*) c
      if(c.le.chse) goto 15
```

```
      write(6,100) 'Output file: '
      read(5,1000) outfile
      write(6,100) ' '
c
      open(7,file=outfile)
      write(7,100) '#'
      write(7,150) '#    Collapse of polytropic gas sphere just out ',
     &             'of hydrostatic equilibrium'
      write(7,300) '#      polytropic index: ',index
      write(7,300) '#                  x_EW: ',xew
      write(7,300) '#              alpha_EW: ',alphew
      write(7,300) '#                C(HSE): ',chse
      write(7,100) '#'
      write(7,300) '#      density normalization C = ',c
      write(7,100) '#'
      write(7,1100) '#','x','alpha(x)','v(x)','m(x)'
      write(7,100) '#'
c
      kmax=5000
      kount=0
      dxsav=hmax
      nvar=2
      hmin=0.d0
      x1=-20.d0
      x2=35.d0
      eps=1.d-8
      h1=1.d-5
      ystart(1)=(2.d0-index)*log(c)/2.d0-x1/2.d0
      ystart(2)=log(2.d0-index) + log(c) - log(4.d0-3.d0*index) +
     &          log(1.d0-(chse/c)**(2.d0-index)) -
     &           index*ystart(1)/(2.d0-index) +
     &            (1.d0-index)*x1/(2.d0-index)
      ystart(1)=exp(ystart(1))
      ystart(2)=-exp(ystart(2))
      CALL odeint(ystart,nvar,x1,x2,eps,h1,hmin,nok,nbad,derivs1,stiff)
      do 50 I=1,kount
        alpha(I)=exp(xp(kount-I+1))
        xx(I)=yp(1,kount-I+1)*(alpha(I)**((index-1.d0)/2.d0))
        vel(I)=yp(2,kount-I+1)*(alpha(I)**((index-1.d0)/2.d0))
        mass(I)=alpha(I)*(xx(I)**2)*
     &          ((2.d0-index)*xx(I)-vel(I))/(4.d0-3.d0*index)
        write(7,1200) xx(I),alpha(I),vel(I),mass(I)
50    continue
      close(7)
      stop
100   FORMAT(A)
150   FORMAT(A,A)
200   FORMAT(A,E15.7)
300   FORMAT(A,E)
```

```
1000  FORMAT(A120)
1100  FORMAT(A1,9X,A1,13X,A8,11X,A4,13X,A4)
1200  FORMAT(4(3X,E14.6))
      end
c
c
c          The equations being integrated, and the method of integration,
c          are formally the same as those dealt with in the program sing.f.
c          The following subroutines, which complete the present code, are
c          IDENTICAL to those given in sing.f
c
c
      SUBROUTINE odeint(ystart,nvar,x1,x2,eps,h1,hmin,nok,nbad,derivs,steps)
      SUBROUTINE stiff(y,dydx,n,x,htry,eps,yscal,hdid,hnext,derivs)
      SUBROUTINE lubksb(a,n,np,indx,b)
      SUBROUTINE ludcmp(a,n,np,indx,d)
      SUBROUTINE derivs1(x,y,dydx)
      SUBROUTINE jacobn(x,y,dfdx,dfdy,n,nmax)
```

A.3 Collisional Mass Spectra

Following is a program (`spec.f`) to compute the steady-state mass spectrum of interstellar clouds which results from the kinetic equation (3.5) (or eqs. [A2], [A3]) of McLaughlin & Pudritz (1996a; Chapter 5 above). The quantities derived are:

$N(m)/[m_0 N(m_0)]$	=	number density of clouds per unit mass; dN/dm
$g(m)$	=	mass fraction of clouds at mass m [in a logarithmic mass interval; $g(m) \sim m^2 N(m)$]
$f(\leq m)$	=	fraction of mass (density) in clouds of mass $\leq m$
$n(\leq m)$	=	fraction of total number (density) in clouds of mass $\leq m$
$d\ \ln N/d\ \ln m$	=	logarithmic slope of mass spectrum
$\sigma(d\ \ln N/d\ \ln m)$	=	error in logarithmic slope $d\ \ln N/d\ \ln m$
$\rho_\tau/[m_0 N(m_0)]$	=	(normalized) average mass density in clouds more massive than m_* (i.e., the unstable, star-forming clouds)
$\langle\rho\rangle/[m_0 N(m_0)]$	=	(normalized) velocity-weighted average mass density of cloud system.

The following are required as input:

$\sigma(m,m')/\sigma(m_0)$	=	(normalized) cross-section for collision between masses m and m'
$v(m,m')/v(m_0)$	=	(normalized) relative velocity between clouds of mass m and m'
$\tau(m)/\tau_*$	=	(normalized) lifetime, against self-disruption, of a cloud at mass m
$r(m)/r(m_0)$	=	(normalized) replenishment spectrum; mass distribution of new clouds obtained from disrupted ones
β	=	$\rho_\tau \sigma(m_0) v(m_0) \tau_* / m_0$
$m_0, N(m_0)$	=	minimum (unit) cloud mass and number of clouds at that mass.

The *first five* of these inputs determine the *shape* of the steady-state mass spectrum, while the last pair provides the (essentially arbitrary) normalization.

The lifetime $\tau(m)$ and replenishment spectrum $r(m)$ can have *arbitrary* mass dependences, and may take any functional form whatsoever. So can the collision cross-section $\sigma(m,m')$ and velocity spectrum $v(m,m')$, just so long as it is assumed that

$$\sigma(m,m') = \begin{cases} \sigma(m) & \text{if } m > m' \\ \sigma(m') & \text{if } m < m' \end{cases} \qquad v(m,m') = \begin{cases} v(m') & \text{if } m > m' \\ v(m) & \text{if } m < m' \end{cases} .$$

That is, the collision cross-section is approximated by the (geometric) cross-section of the most massive cloud involved, and the relative approach velocity by the velocity of the least massive cloud. A few "standard" options are offered for each of these four functions in `spec.f`, and modification to any other desired form should be straightforward. (See the `REAL*8 FUNCTION`s `tau`, `f`, `sigma`, and `veloc`.)

The method of solution is an iterative one. Basically, the solution depends on knowing the value of

$$K = \sum_{m_0}^{\infty} [N(m)/N(m_0)][\sigma(m)/\sigma(m_0)] .$$

The value of this sum is fixed by the *shape* of the mass spectrum (i.e., by the first five "input" parameters listed above), and is therefore *not* a free parameter; but neither can it be known a priori, so the approach is to fix K at some value, solve for the normalized spectrum $N(m)/N(m_0)$ [denoted $x(m)$] via a straightforward recursion relation, and then check that the values of K *and* $\rho_\tau/[m_0 N(m_0)]$ are self-consistent, i.e., $K(\text{input}) = K(\text{derived})$ and $\rho_\tau[K(\text{input})] = \rho_\tau[K(\text{derived})]$. Iteration on the value of K continues until these constraints are satisfied. The final numerical solution strictly finds only the normalized spectrum, $N(m)/N(m_0) = x(m)$; but once this is obtained, it is trivial to find $N(m) = x(m)N(m_0)$ [remember, $N(m_0)$ is treated as an arbitrary normalization].

The iterative search for the correct value of K (i.e., correct given the input parameters listed above) can be rather tricky. Clearly, if either of the *calculated* values of K and ρ_τ (denoted `ktemp` and `rhotemp`) ever exceed their specified *input* values, then the input K should be increased and another solution attempted. However, since we are dealing with infinite series here, it is possible to guess a K which never allows one or both of `ktemp` and `rhotemp` to reach the required values $K(\text{input})$ and $\rho_\tau[K(\text{input})]$. Thus, it is necessary to be able to decide when the sums involved in the definitions of K and ρ_τ have converged; and if so, whether those convergent values, calculated from the derived mass spectrum, do indeed agree with the guessed input values.

In order to do this, a series can be formed which has the same asymptotic limit as the calculated ρ_τ and K, but which converges to that limit more rapidly. If $\{S_N\}$ is a sequence of partial sums, then under certain conditions an improved estimate of the large-N limit of S_N may be given by (see Press et al. 1992, p. 160)

$$S_N \longleftarrow S_{N+1} - \frac{(S_{N+1} - S_N)^2}{S_{N+1} - 2S_N + S_{N-1}} ,$$

which is computed in the `SUBROUTINE csum` below. If the fractional change between two terms of this "accelerated" series is less than the (user-set) parameter `crit1`, then convergence is said to have been achieved. Then, if the "accelerated" sums representing K and ρ_τ are both within a (user-set) factor of `(1+crit2)` of the input values, the current value of K is taken to be the correct one; otherwise, if they are smaller than the input values, K is decreased and a new solution attempted. In practice, this acceleration procedure is only useful if the series in question satisfies certain criteria (see Press et al.), and it is not always helpful for the mass spectra calculated here. Thus, `spec.f` offers the option of either forming or ignoring the super-convergent series. (When this "trick" is not used, the parameters `crit1` and `crit2` have the same meaning, but are used to test the convergence

of the *unaltered* sums representing K and ρ_τ.)

This iteration on the value of K (increasing or decreasing the guessed input value, as required) continues either until the calculated K and ρ_τ agree with the input values as described above, or until the fractional change in K is less than the parameter `crit3`. In this way, K can generally be determined to much better than 1% accuracy.

The logarithmic slope of the mass spectrum, $d \ln N/d \ln m$, is also calculated. This is done by interpolating the computed mass spectrum (which is directly known only at masses which are integer multiples of m_0; `SUBROUTINE spline` and `SUBROUTINE splint` from Press et al. [1992] are used for the interpolation), and then using the Press et al. (1992) `SUBROUTINE dfridr` to compute a numerical derivative. The estimated uncertainty in the derivative is also returned by this subroutine, and is constrained to be strictly less than 10^{-4}.

Finally, the normalized mean time between collisions, $\tau_{\rm coll}(m)/\tau_{\rm fid}$ is calculated according to equation (C1) of McLaughlin & Pudritz (1996a). The mass-doubling time (same reference, eq. [C5]) is then computed in a separate code, `time.f`, which is also given below.

A.3.1 spec.f

```
c
c     A program to compute the steady-state mass spectrum of interstellar
c     clouds which results from the kinetic equation of McLaughlin &
c     Pudritz (1996, ApJ, 457, 578)
c
      program spec
      implicit none
      INTEGER Imax
      PARAMETER (Imax=100000)
      REAL*8 rhotau,sigma,veloc,K,gains,losses,
     &       xtemp,xstar(Imax),suml(2),ratio,rhotemp,
     &       Kl,Ku,rhotot,rhocum(Imax),ktemp,tcoll(Imax),
     &       rpart(5),kpart(5),denom,ntot(Imax),ntotex,lmass(Imax),
     &       lnum(Imax),y2(Imax),dfridr,deriv,ederiv,step,fac,
     &       avrho(3),avrhoex,rhosum(2),ksum(2),kex,rhoex,crit1,
     &       crit2,crit3,beta,tau,f,R,rttl(3),zz,Rsum(5),Rex(2),
     &       avet1(3),avet2(3),taven,tavem
      INTEGER ctype,vtype,I,J,Npts,L,m1,fcut,tcut
      CHARACTER line*80,filename*80
      LOGICAL flag,done,iterate
      REAL*8 cslope,vslope,m0
      INTEGER ctype,vtype
      INTEGER tautype,redtype
      REAL*8 tslope,fslope
      LOGICAL accel
      COMMON /pathsv/ ctype,vtype,cslope,vslope
      COMMON /func/ lmass,lnum,y2,Npts
      COMMON /patha/ accel
      COMMON /pathm/ m0,m1
      COMMON /patht/ tautype,redtype,tslope,fslope,fcut,tcut
```

```
c
      write(6,900) ' '
      write(6,940) 'STEADY-STATE MASS SPECTRUM FOR KINETIC EQUATION ',
     &             'OF M&P (1996)'
c
      write(6,900) ' '
      m0=1.d0
      line=' '
5     write(6,2000) 'Unit cloud mass m_0 (in M_suns; CR for 1): '
      read(5,1000) line
      if(line.ne.' ') read(line,*) m0
      if(m0.le.0.) goto 5
c
      write(6,900) ' '
      write(6,900) 'Mass dependence of cloud destruction timescale: '
      write(6,900) '     1. Step function '
      write(6,900) '     2. Pure power law '
      write(6,900) '     3. Truncated power law: '
6     write(6,2000) 'Specify by number: '
      read(5,*) tautype
      if(tautype.eq.1) then
7       write(6,2500) 'Maximal stable cloud mass m_* (in units ',
     &                'of m0): '
        read(5,*) m1
        if(m1.lt.1) goto 7
        tcut=m1
      elseif(tautype.eq.2) then
        write(6,2000) 'Power-law slope: '
        read(5,*) tslope
      elseif(tautype.eq.3) then
8       write(6,2500) 'Power-law slope and lower mass cutoff m_* ',
     &                '(in units of m0): '
        read(5,*) tslope,tcut
        if(tcut.lt.1) goto 8
      else
        goto 6
      endif
c
      write(6,900) ' '
      write(6,900) 'Replenishment mass spectrum: '
      write(6,900) '     1. Delta function '
      write(6,900) '     2. Pure power law '
      write(6,900) '     3. Truncated power law: '
10    write(6,2000) 'Specify by number: '
      read(5,*) redtype
      if(redtype.eq.1) then
        R=1.d0
      elseif(redtype.eq.2) then
11      write(6,2000) 'Power-law slope: '
```

```
        read(5,*) fslope
        if(fslope.ge.-2.5d0) goto 11
        Rsum(1)=0.d0
        Rsum(2)=0.d0
        Rsum(3)=0.d0
        Rsum(4)=0.d0
        Rsum(5)=0.d0
        Rex(1)=0.d0
        Rex(2)=0.d0
        do 12 I=1,100001
          Rsum(1)=Rsum(2)
          Rsum(2)=Rsum(3)
          Rsum(3)=Rsum(4)
          Rsum(4)=Rsum(5)
          Rsum(5)=Rsum(5)+(1.d0*I)**(1.d0+fslope)
12      continue
        accel=.true.
        CALL csum(Rsum,Rex)
        accel=.false.
        R=1.d0/Rex(2)
      elseif(redtype.eq.3) then
13      write(6,2500) 'Power-law slope and upper mass cut-off ',
     &                '(in units of m0): '
        read(5,*) fslope,fcut
        if(fcut.lt.1) goto 13
        Rsum(5)=0.d0
        do 14 I=1,fcut
          Rsum(5)=Rsum(5)+(1.d0*I)**(1.d0+fslope)
14      continue
        R=1.d0/Rsum(5)
      else
        goto 10
      endif
c
      write(6,900) ' '
18    write(6,2000) 'Characteristic mass gain beta (in units of m0): '
      read(5,*) beta
      if(beta.le.0.d0) goto 18
c
      write(6,900) ' '
20    write(6,900) 'Mass dependence of cross-section...'
      write(6,900) '     1. Kwans parametrization'
      write(6,900) '     2. Pure power law'
      write(6,2000) 'Specify by number: '
      read(5,1000) line
      if(line(1:1).eq.'1') then
        ctype=1
      elseif(line(1:1).eq.'2') then
        ctype=2
```

```
        write(6,2000) 'Power-law index: '
        read(5,*) cslope
      else
        goto 20
      endif
c
      write(6,900) ' '
25    write(6,900) 'Mass dependence of velocity spectrum '
      write(6,900) '     1. Kwans parametrization'
      write(6,900) '     2. Pure power law'
      write(6,900) '     3. b=0 to m_*; b=-1/2 thereafter'
      write(6,2000) 'Specify by number: '
      read(5,1000) line
      if(line(1:1).eq.'1') then
        vtype=1
      elseif(line(1:1).eq.'2') then
        vtype=2
        write(6,2000) 'Power-law index: '
        read(5,*) vslope
      elseif(line(1:1).eq.'3') then
        vtype=3
      else
        goto 25
      endif
c
      write(6,900) ' '
30    write(6,900) 'Iterate to solve for K? (y/n): '
      read(5,1000) line
      if((line(1:1).eq.'y').or.(line(1:1).eq.'Y')) then
        iterate=.true.
      elseif((line(1:1).eq.'n').or.(line(1:1).eq.'N')) then
        iterate=.false.
        write(6,900) ' '
33      write(6,900) 'Specify fixed value of K: '
        read(5,*) K
        if(K.lt.1.d0) goto 33
      else
        goto 30
      endif
c
      if(iterate) then
        write(6,900) ' '
35      line=' '
        write(6,940) 'Bounds on K (lower,upper; CR to allow free ',
     &               'search): '
        read(5,1000) line
        if(line.eq.' ') then
          flag=.false.
          K1=1.d0
```

```
          K=3.d0
        else
          flag=.true.
          read(line,*) Kl,Ku
          if((Kl.gt.Ku).or.(Kl.lt.1.d0)) goto 35
          if(Kl.eq.Ku) then
            iterate=.false.
            K=Kl
            goto 37
          endif
          K=(Kl+Ku)/2.d0
        endif
c
        write(6,900) ' '
        crit1=5.d-5
        crit2=2.d-2
        crit3=1.d-4
        L=1
        line=' '
        write(6,940) 'Specify parameters crit1,crit2,crit3,L (CR for ',
     &               'default 5.d-5,2.d-2,1.d-4,1): '
        read(5,1000) line
        if(line.ne.' ') read(line,*) crit1,crit2,crit3,L
c
        write(6,900) ' '
36      write(6,900) 'Force accelerated convergence of series? (y/n): '
        read(5,1000) line
        if((line(1:1).eq.'y').or.(line(1:1).eq.'Y')) then
          accel=.true.
        elseif((line(1:1).eq.'n').or.(line(1:1).eq.'N')) then
          accel=.false.
        else
          goto 36
        endif
      endif
37    if(.not.iterate) then
        write(6,900) ' '
38      L=1
        line=' '
        write(6,900) 'Specify L (CR for L=1): '
        read(5,1000) line
        if(line.ne.' ') read(line,*) L
        if(L.lt.1) goto 38
      endif
c
      write(6,900) ' '
39    write(6,900) 'Maximum mass for output (in units of m0): '
      read(5,*) Npts
      if(Npts.ge.Imax) goto 39
```

```
c
      write(6,900) ' '
      write(6,900) 'Output file: '
      read(5,1000) filename
c
      write(6,900) ' '
      zz=tau(1)/(2.d0*R)
      if(.not.iterate) goto 60
      done=.false.
c
c
40    rhotau=zz+sqrt(zz*zz+(beta*K)/R)
      ratio=rhotau/beta
      suml(1)=0.d0
      suml(2)=0.d0
      do 45 I=2,Imax
        xstar(I)=0.d0
45    continue
      I=1
      xstar(I)=1.d0
      xtemp=1.d0
      rhotemp=tau(1)
      ktemp=1.d0
      rpart(1)=0.d0
      rpart(2)=0.d0
      rpart(3)=0.d0
      rpart(4)=0.d0
      rpart(5)=rhotemp
      rhosum(1)=0.d0
      rhosum(2)=0.d0
      kpart(1)=0.d0
      kpart(2)=0.d0
      kpart(3)=0.d0
      kpart(4)=0.d0
      kpart(5)=ktemp
      ksum(1)=0.d0
      ksum(2)=0.d0
c
50    continue
        I=I+1
        if(I.gt.Imax) then
          write(6,930) 'Could not converge with Imax=',Imax,
     &                 ' and K = ',sngl(K)
          stop
        endif
        gains=0.d0
        do 55 J=1,I/2-1
          gains=gains+xstar(J)*xstar(I-J)*sigma(J,I-J)*veloc(J,I-J)
55      continue
```

```
      fac=1.d0-((2*(I/2))/I)/2.d0
      gains=gains+fac*xstar(I/2)*xstar(I-I/2)*
     &       sigma(I/2,I-I/2)*veloc(I/2,I-I/2)
      suml(1)=suml(1)+(xtemp*veloc(I-1,I-1))
      suml(2)=suml(2)+(xtemp*sigma(I-1,I-1))
      losses=sigma(I,I)*suml(1)-veloc(I,I)*suml(2)
      denom=losses+K*veloc(I,I)+ratio*tau(I)
      if(denom.le.1.d-30) then
        Kl=K
        if(.not.flag) Ku=1.9d1*Kl
        K=(Kl+Ku)/2.d0
        if(abs((Ku-Kl)/K).lt.crit3) done=.true.
        if(.not.done) goto 40
      else
        xtemp=(gains+R*rhotau*ratio*f(I))/denom
      endif
      rhotemp=rhotemp+I*xtemp*tau(I)
      rpart(1)=rpart(2)
      rpart(2)=rpart(3)
      rpart(3)=rpart(4)
      rpart(4)=rpart(5)
      rpart(5)=rhotemp
      CALL csum(rpart,rhosum)
      ktemp=ktemp+xtemp*sigma(I,I)
      kpart(1)=kpart(2)
      kpart(2)=kpart(3)
      kpart(3)=kpart(4)
      kpart(4)=kpart(5)
      kpart(5)=ktemp
      CALL csum(kpart,ksum)
      xstar(I)=xtemp
c
      if((rhosum(1).gt.0.d0).and.(ksum(1).gt.0.d0))
     &     write(6,3000),sngl(K),sngl(1.d0*I),
     &     sngl(xtemp),sngl(rhosum(2)/rhosum(1)),
     &     sngl(ksum(2)/ksum(1)),sngl(rhosum(2)/rhotau),
     &     sngl(ksum(2)/K)
c
      if( ((rhosum(1).gt.0.d0).and.(ksum(1).gt.0.d0)) .and.
     &          (abs((rhosum(2)-rhosum(1))/rhosum(1)).lt.crit1) .and.
     &          (abs((ksum(2)-ksum(1))/ksum(1)).lt.crit1) .and.
     &          (rhosum(2).lt.rhotau) .and. (ksum(2).lt.K) ) then
        if( (((rhotau-rhosum(2))/rhotau).lt.crit2) .and.
     &          (((K-ksum(2))/K).lt.crit2) ) then
          done=.true.
        else
          flag=.true.
          Ku=K
          K=(Kl+Ku)/2.d0
```

```
          if(abs((Ku-Kl)/K).lt.crit3) done=.true.
          if(.not.done) goto 40
        endif
      endif
      if((.not.done) .and. ((rhotemp.gt.rhotau) .or.
     &             (ktemp.gt.K) .or. (rhosum(1).gt.rhotau) .or.
     &             (ksum(1).gt.K) .or. (rhosum(2).gt.rhotau) .or.
     &             (ksum(2).gt.K))) then
        Kl=K
        if(.not.flag) Ku=1.9d1*Kl
        K=(Kl+Ku)/2.d0
        if(abs((Ku-Kl)/K).lt.crit3) done=.true.
        if(.not.done) goto 40
      endif
    if(.not.done) goto 50
c
c
60    rhotau=zz+sqrt(zz*zz+(beta*K)/R)
      ratio=rhotau/beta
      suml(1)=0.d0
      suml(2)=0.d0
      do 70 I=2,Npts
        xstar(I)=0.d0
        rhocum(I)=0.d0
        ntot(I)=0.d0
        tcoll(I)=0.d0
70    continue
      I=1
      xstar(I)=1.d0
      rhocum(I)=1.d0
      ntot(I)=1.d0
      tcoll(I)=rhotau/K
      rhotemp=tau(1)
      ktemp=1.d0
      rpart(1)=0.d0
      rpart(2)=0.d0
      rpart(3)=0.d0
      kpart(1)=0.d0
      kpart(2)=0.d0
      kpart(3)=ktemp
      avrho(1)=0.d0
      avrho(2)=0.d0
      avrho(3)=1.d0
      rttl(1)=0.d0
      rttl(2)=0.d0
      rttl(3)=1.d0
      avet1(1)=0.d0
      avet1(2)=0.d0
      avet1(3)=tcoll(I)
```

```
      avet2(1)=0.d0
      avet2(2)=0.d0
      avet2(3)=tcoll(I)
c
      do 90 I=2,Npts+1
        gains=0.d0
        do 80 J=1,I/2-1
          gains=gains+xstar(J)*xstar(I-J)*sigma(J,I-J)*veloc(J,I-J)
80      continue
        fac=1.d0-((2*(I/2))/I)/2.d0
        gains=gains+fac*xstar(I/2)*xstar(I-I/2)*
     &        sigma(I/2,I-I/2)*veloc(I/2,I-I/2)
        suml(1)=suml(1)+(xstar(I-1)*veloc(I-1,I-1))
        suml(2)=suml(2)+(xstar(I-1)*sigma(I-1,I-1))
        losses=sigma(I,I)*suml(1)-veloc(I,I)*suml(2)
        xstar(I)=(gains+R*rhotau*ratio*f(I)) /
     &           (losses+K*veloc(I,I)+ratio*tau(I))
        tcoll(I)=rhotau/(losses+K*veloc(I,I))
        rhotemp=rhotemp+I*xstar(I)*tau(I)
        ktemp=ktemp+xstar(I)*sigma(I,I)
        ntot(I)=ntot(I-1)+xstar(I)
        rhocum(I)=rhocum(I-1)+I*xstar(I)
c
        write(6,4000) sngl(K),sngl(1.d0*I),sngl(xstar(I)),
     &                sngl(rhotemp/rhotau),sngl(ktemp/K)
c
        rpart(1)=rpart(2)
        rpart(2)=rpart(3)
        rpart(3)=rhotemp
        kpart(1)=kpart(2)
        kpart(2)=kpart(3)
        kpart(3)=ktemp
        avrho(1)=avrho(2)
        avrho(2)=avrho(3)
        avrho(3)=avrho(3)+I*xstar(I)*veloc(I,I)
        rttl(1)=rttl(2)
        rttl(2)=rttl(3)
        rttl(3)=rttl(3)+I*xstar(I)
        avet1(1)=avet1(2)
        avet1(2)=avet1(3)
        avet1(3)=avet1(3)+tcoll(I)*xstar(I)
        avet2(1)=avet2(2)
        avet2(2)=avet2(3)
        avet2(3)=avet2(3)+tcoll(I)*xstar(I)*I
90    continue
c
c
      do 100 I=1,Npts
        lmass(I)=log10(1.d0*I)
```

```
        lnum(I)=log10(xstar(I))
100   continue
      CALL spline(lmass,lnum,Npts,1.d30,1.d30,y2,Imax)
c
      denom=ntot(Npts+1)-2.d0*ntot(Npts)+ntot(Npts-1)
      if(denom.eq.0.d0) then
        ntotex=ntot(Npts+1)
      elseif(denom.ne.0.d0) then
        ntotex=ntot(Npts+1)-((ntot(Npts+1)-ntot(Npts))**2)/denom
      endif
c
      denom=avrho(3)-2.d0*avrho(2)+avrho(1)
      if(denom.eq.0.d0) then
        avrhoex=avrho(3)
      elseif(denom.ne.0.d0) then
        avrhoex=avrho(3)-((avrho(3)-avrho(2))**2)/denom
      endif
c
      denom=rttl(3)-2.d0*rttl(2)+rttl(1)
      if(denom.eq.0.d0) then
        rhotot=rttl(3)
      elseif(denom.ne.0.d0) then
        rhotot=rttl(3)-((rttl(3)-rttl(2))**2)/denom
      endif
c
      denom=rpart(3)-2.d0*rpart(2)+rpart(1)
      if(denom.eq.0.d0) then
        rhoex=rpart(3)
      elseif(denom.ne.0.d0) then
        rhoex=rpart(3)-((rpart(3)-rpart(2))**2)/denom
      endif
c
      denom=kpart(3)-2.d0*kpart(2)+kpart(1)
      if(denom.eq.0.d0) then
        kex=kpart(3)
      elseif(denom.ne.0.d0) then
        kex=kpart(3)-((kpart(3)-kpart(2))**2)/denom
      endif
c
      denom=avet1(3)-2.d0*avet1(2)+avet1(1)
      if(denom.eq.0.d0) then
        taven=avet1(3)
      elseif(denom.ne.0.d0) then
        taven=avet1(3)-((avet1(3)-avet1(2))**2)/denom
      endif
c
      denom=avet2(3)-2.d0*avet2(2)+avet2(1)
      if(denom.eq.0.d0) then
        tavem=avet2(3)
```

```
      elseif(denom.ne.0.d0) then
        tavem=avet2(3)-((avet2(3)-avet2(2))**2)/denom
      endif
c
      write(6,910) '(extrap. rho)/rhotau: ',rhoex/rhotau
      write(6,910) '(extrap. K)/K: ',kex/K
      write(6,900) ' '
      write(6,910) '   rhotau/[m0*N(m0)] = ',rhotau
      write(6,910) '  rho_tot/[m0*N(m0)] = ',rhotot
      write(6,910) '         <rho>/rhotau = ',avrhoex/rhotau
      write(6,910) '          N(m0)/N_tot = ',1.d0/ntotex
c
      open(7,file=filename)
      write(7,900) '#'
      write(7,2000) '#  Destruction timescale: '
      if(tautype.eq.1) then
        write(7,910) 'Step function m_*/m0: ',m1
      elseif(tautype.eq.2) then
        write(7,910) 'Pure power law slope: ',sngl(tslope)
      elseif(tautype.eq.3) then
        write(7,920) 'Truncated power law slope: ',sngl(tslope),
     &               '  m_cut/m0: ',tcut
      endif
      write(7,2000) '#  Replenishment spectrum: '
      if(redtype.eq.1) then
        write(7,910) 'Delta function m0: ',sngl(m0)
      elseif(redtype.eq.2) then
        write(7,910) 'Pure power law slope: ',sngl(fslope)
      elseif(redtype.eq.3) then
        write(7,920) 'Truncated power law slope: ',sngl(fslope),
     &               '  m_cut/m0: ',fcut
      endif
      write(7,910) '#       R = ',1.d0/R
      write(7,910) '#  beta = ',beta
      write(7,2000) '#  Cross Section: '
      if(ctype.eq.1) then
        write(7,900) 'Kwans parametrization'
      elseif(ctype.eq.2) then
        write(7,910) ' power law slope ',sngl(cslope)
      endif
      write(7,2000) '#  Velocity Spectrum: '
      if(vtype.eq.1) then
        write(7,900) 'Kwans parametrization'
      elseif(vtype.eq.2) then
        write(7,910) ' power law slope ',sngl(vslope)
      elseif(vtype.eq.3) then
        write(7,900) ' power law b=0 to m_*; b=-1/2 thereafter'
      endif
      write(7,900) '#'
```

```
      write(7,910) '#                    K = ',K
      write(7,910) '#   rhotau/[m0*N(m0)] = ',rhotau
      write(7,910) '#  rho_tot/[m0*N(m0)] = ',rhotot
      write(7,910) '#        <rho>/rhotau = ',avrhoex/rhotau
      write(7,910) '#      rho_tot/rhotau = ',rhotot/rhotau
      write(7,910) '#         N(m0)/N_tot = ',1.d0/ntotex
      write(7,900) '#'
      write(7,910) '#   (extrap. K)/K: ',kex/K
      write(7,910) '#   (extrap. rho)/rhotau: ',rhoex/rhotau
      write(7,900) '#'
      write(7,900) '#     col.1:  m/m0'
      write(7,900) '#     col.2: log(m/m0)'
      write(7,900) '#     col.3: log{N(m)/[m0*N(m0)]} (per M_sun)'
      write(7,900) '#     col.4: g(m)'
      write(7,900) '#     col.5: mass fraction of clouds <=m'
      write(7,900) '#     col.6: number fraction of clouds <=m'
      write(7,900) '#     col.7: d(ln N)/d(ln m) (numerical)'
      write(7,900) '#     col.8: 10^5 x error in slope of col.7'
      write(7,900) '#     col.9: t(collision)/t(fiducial)'
      write(7,900) '#'
      write(7,910) '#     m0 (solar masses) = ',m0
      write(7,900) '#'
      write(7,910) '#     number-weighted mean t(coll)/t(fid): ',
     &              taven/ntotex
      write(7,910) '#     mass-weighted mean t(coll)/t(fid):   ',
     &              tavem/rhotot
      write(7,900) '#'
      write(7,910) '#  ',m0
      do 150 I=1,Npts
        if((I.le.(tcut+50)).or.(I.eq.Npts).or.((L*(I/L)).eq.I)) then
          deriv=0.d0
          ederiv=0.d0
          step=1.d-1
          do 130 J=1,100
            deriv=dfridr(lmass(I),step,ederiv,Imax)
            if(ederiv.lt.1.d-4) goto 140
            step=step/1.d1
130       continue
140       write(7,5000) I, lmass(I), lnum(I)-log10(m0),
     &                  ((1.d0*I)**2)*xstar(I)/rhotot,
     &                  rhocum(I)/rhotot, ntot(I)/ntotex,
     &                  deriv, ederiv*1.d5,tcoll(I)
        endif
150   continue
      close(7)
      stop
900   FORMAT(A)
910   FORMAT(A,F)
920   FORMAT(A,F,A,F)
```

```
930   FORMAT(A,I,A,F)
940   FORMAT(A,A)
1000  FORMAT(A80)
2000  FORMAT(A,$)
2500  FORMAT(A,A,$)
3000  FORMAT(7(E11.5,2X))
4000  FORMAT(5(E11.5,2X))
5000  FORMAT(I7,F11.6,F12.6,3(F11.6),F12.6,F8.4,F13.6)
      end
c
c         Normalized effective cloud cross-section
c
      REAL*8 FUNCTION sigma(ma,mb)
      implicit none
      INTEGER ma,mb
      REAL*8 mass
      REAL*8 cslope,vslope,m0
      INTEGER tautype,redtype,fcut,tcut
      REAL*8 tslope,fslope
      INTEGER ctype,vtype,m1
      COMMON /pathsv/ ctype,vtype,cslope,vslope
      COMMON /pathm/ m0,m1
      COMMON /patht/ tautype,redtype,tslope,fslope,fcut,tcut
c
      mass=max(1.d0*ma,1.d0*mb)
      if(ctype.eq.1) then
        if((mass*m0).le.5.d2) then
          sigma=(mass)**(5./3.)
        elseif((mass*m0).gt.5.d2) then
          sigma=(mass)**(2./3.)
          if(m0.lt.5.d2) sigma=sigma*(5.d2/m0)
        endif
      elseif(ctype.eq.2) then
        if(cslope.lt.0.d0) mass=min(1.d0*ma,1.d0*mb)
        sigma=(mass)**cslope
      endif
      RETURN
      end
c
c         Normalized cloud velocity spectrum
c
      REAL*8 FUNCTION veloc(ma,mb)
      implicit none
      INTEGER ma,mb
      REAL*8 mass
      REAL*8 cslope,vslope,m0
      INTEGER tautype,redtype,fcut,tcut
      REAL*8 tslope,fslope
      INTEGER ctype,vtype,m1
```

```
      COMMON /pathsv/ ctype,vtype,cslope,vslope
      COMMON /pathm/ m0,m1
      COMMON /patht/ tautype,redtype,tslope,fslope,fcut,tcut
c
      mass=min(1.d0*ma,1.d0*mb)
      if(vtype.eq.1) then
        if((mass*m0).le.5.d2) then
          veloc=1.d0
        elseif((mass*m0).gt.5.d2) then
          veloc=sqrt(1.d0/mass)
          if(m0.lt.5.d2) veloc=veloc*sqrt(5.d2/m0)
        endif
      elseif(vtype.eq.2) then
        if(vslope.gt.0.d0) mass=max(1.d0*ma,1.d0*mb)
        veloc=(mass)**vslope
      elseif(vtype.eq.3) then
        if(mass.le.(1.d0*tcut)) then
          veloc=1.d0
        elseif(mass.gt.(1.d0*tcut)) then
          veloc=sqrt((1.d0*tcut)/mass)
        endif
      endif
      RETURN
      end
c
c          Normalized replenishment spectrum
c
      REAL*8 FUNCTION f(ma)
      implicit none
      INTEGER ma
      REAL*8 m0,tslope,fslope
      INTEGER m1,tautype,redtype,fcut,tcut
      COMMON /pathm/ m0,m1
      COMMON /patht/ tautype,redtype,tslope,fslope,fcut,tcut
c
      if(redtype.eq.1) then
        if(ma.eq.1) then
          f=1.d0
        elseif(ma.gt.1) then
          f=0.d0
        endif
      elseif(redtype.eq.2) then
        f=(1.d0*ma)**fslope
      elseif(redtype.eq.3) then
        if(ma.le.fcut) then
          f=(1.d0*ma)**fslope
        else
          f=0.d0
        endif
```

```
      endif
      RETURN
      end
c
c          Normalized mass dependence of (inverse) cloud lifetime
c
      REAL*8 FUNCTION tau(ma)
      implicit none
      INTEGER ma
      REAL*8 m0,tslope,fslope
      INTEGER m1,tautype,redtype,fcut,tcut
      COMMON /pathm/ m0,m1
      COMMON /patht/ tautype,redtype,tslope,fslope,fcut,tcut
c
      if(tautype.eq.1) then
        if(ma.lt.m1) then
          tau=0.d0
        elseif(ma.ge.m1) then
          tau=1.d0
        endif
      elseif(tautype.eq.2) then
        tau=(1.d0/ma)**tslope
      elseif(tautype.eq.3) then
        if(ma.lt.tcut) then
          tau=0.d0
c          tau=1.d0
        elseif(ma.ge.tcut) then
          tau=((1.d0*tcut)/ma)**tslope
        endif
      endif
      RETURN
      end
c
c
      SUBROUTINE spline(x,y,n,yp1,ypn,y2,Imax)
      implicit none
      INTEGER n,NMAX,Imax
      REAL*8 yp1,ypn,x(n),y(n),y2(n)
      PARAMETER (NMAX=100000)
      INTEGER i,k
      REAL*8 p,qn,sig,un,u(NMAX)
      if(NMAX.ne.Imax) then
        write(6,99) 'Parameters Imax in main and NMAX in spline ',
     &              'do not agree'
        stop
      endif
c
c          The body of this subroutine may be taken from Press et al.
c          (1992, p. 109) without further modification
```

```
c
      RETURN
99    FORMAT(A,A)
      end
c
c
      SUBROUTINE splint(xa,ya,y2a,n,x,y)
      implicit none
      INTEGER n
      REAL*8 x,y,xa(n),y2a(n),ya(n)
      INTEGER k,khi,klo
      REAL*8 a,b,h
c
c         The body of this subroutine may be taken from Press et al.
c         (1992, p. 110) without further modification
c
      RETURN
      end
c
c         The following function, which computes numerical derivatives,
c         is slightly modified from that given in Press et al. (1992,
c         p. 182)
c
      REAL*8 FUNCTION dfridr(x,h,err,Imax)
      implicit none
      INTEGER NTAB
      REAL*8 err,h,x,CON,CON2,BIG,SAFE,func1,func2
      PARAMETER (CON=1.4,CON2=CON*CON,BIG=1.E30,NTAB=10,SAFE=2.)
      INTEGER i,j,Nmax,Imax
      REAL*8 errt,fac,hh,a(NTAB,NTAB)
      PARAMETER (Nmax=100000)
      REAL*8 lmass(Nmax),lnum(Nmax),y2(Nmax)
      INTEGER Npts
      COMMON /func/ lmass,lnum,y2,Npts
      if(Nmax.ne.Imax) then
        write(6,*) 'Parameters Imax in main and Nmax in dfridr ',
     &             'do not agree'
        stop
      endif
      if(h.eq.0.) then
        write(6,*) 'h must be nonzero in dfridr'
        stop
      endif
      hh=h
      CALL splint(lmass,lnum,y2,Npts,x+hh,func1)
      CALL splint(lmass,lnum,y2,Npts,x-hh,func2)
      a(1,1)=(func1-func2)/(2.0*hh)
      err=BIG
      do 12 i=2,NTAB
```

```
        hh=hh/CON
        CALL splint(lmass,lnum,y2,Npts,x+hh,func1)
        CALL splint(lmass,lnum,y2,Npts,x-hh,func2)
        a(1,i)=(func1-func2)/(2.0*hh)
        fac=CON2
        do 11 j=2,i
          a(j,i)=(a(j-1,i)*fac-a(j-1,i-1))/(fac-1.)
          fac=CON2*fac
          errt=max(abs(a(j,i)-a(j-1,i)),abs(a(j,i)-a(j-1,i-1)))
          if (errt.le.err) then
            err=errt
            dfridr=a(j,i)
          endif
11      continue
        if(abs(a(i,i)-a(i-1,i-1)).ge.SAFE*err)return
12    continue
      RETURN
      end
c
c          Calculation of super-convergent series; various procedures
c          are allowed for here.
c
      SUBROUTINE csum(xpart,xsum)
      implicit none
      REAL*8 xpart(5),xsum(2),hold(2),denom,temp
      LOGICAL accel
      COMMON /patha/ accel
c
      temp=xsum(2)
c
      if(accel) then
c        denom=xpart(3)-2.d0*xpart(2)+xpart(1)
c        if(denom.eq.0.d0) then
c          hold(1)=xpart(2)
c        elseif(denom.ne.0.d0) then
c          hold(1)=xpart(3)-((xpart(3)-xpart(2))**2)/denom
c        endif
c
c        denom=xpart(4)-2.d0*xpart(3)+xpart(2)
c        if(denom.eq.0.d0) then
c          xsum(1)=xpart(3)
c        elseif(denom.ne.0.d0) then
c          xsum(1)=xpart(4)-((xpart(4)-xpart(3))**2)/denom
c        endif
c
        denom=xpart(5)-2.d0*xpart(4)+xpart(3)
        if(denom.eq.0.d0) then
          hold(2)=xpart(4)
        elseif(denom.ne.0.d0) then
```

```
          hold(2)=xpart(5)-((xpart(5)-xpart(4))**2)/denom
        endif
c
c        denom=hold(2)-2.d0*xsum(1)+hold(1)
c        if(denom.eq.0.d0) then
c          xsum(2)=xsum(1)
c        elseif(denom.ne.0.d0) then
c          xsum(2)=hold(2)-((hold(2)-xsum(1))**2)/denom
c        endif
c
        xsum(2)=hold(2)
      elseif(.not.accel) then
        xsum(2)=xpart(5)
      endif
      xsum(1)=temp
      RETURN
      end
```

A.3.2 time.f

```
c
c     A program to compute the mean mass-doubling time, tau_doub, of a
c     cloud of mass m (McLaughlin & Pudritz 1996, ApJ, 457, 578); input
c     file must be output directly from spec.f
c
      program time
      implicit none
      INTEGER Nmax1,Nmax2
      PARAMETER (Nmax1=30000,Nmax2=15000)
      REAL*8 a4,a5,a6,a7,a8
      REAL*8 t(Nmax1),tg(Nmax2),m(Nmax1),num(Nmax1)
      INTEGER I,J,maxmas
      CHARACTER line*100,infile*100,outfile*100
c
      write(6,900) 'Input file: '
      read(5,1000) infile
      open(4,file=infile)
      J=0
      do 10 I=1,100000
        read(4,1000,end=15) line
        if(line(1:1).ne.'#') then
          J=J+1
          if(J.gt.Nmax1) then
            write(6,950) 'Overfilled arrays. Increase parameters ',
     &                   'Nmax1 and Nmax2'
            stop
          endif
```

```
          read(line,*) maxmas,m(J),num(J),a4,a5,a6,a7,a8,t(J)
          num(J)=10.d0**num(J)
        endif
10    continue
15    close(4)
      if(maxmas.ne.J) then
        write(6,950) 'Bad input file ',infile
        stop
      endif
      write(6,900) 'Output file: '
      read(5,1000) outfile
      open(7,file=outfile)
      write(7,900) '#'
      write(7,950) '#   Collisional mass-doubling times (equation ',
     &             'C5 of McLaughlin & Pudritz 1996)'
      write(7,900) '#'
      write(7,950) '#   Input steady-state mass spectrum: ',infile(1:35)
      write(7,900) '#'
      write(7,900) '#      Column 1: log (m/m_0)'
      write(7,900) '#      Column 2: log (tau_doub/tau_fid)'
      write(7,900) '#'
      do 30 I=1,maxmas/2
        tg(I)=0.d0
        do 20 J=I,2*I-1
          tg(I)=tg(I)+t(J)
20      continue
        if((I.le.200).or.(100*(I/100).eq.I)) then
          write(7,1100) sngl(m(I)),sngl(log10(tg(I)))
        endif
30    continue
      close(7)
      stop
900   FORMAT(A)
950   FORMAT(A,A)
1000  FORMAT(A100)
1100  FORMAT(2F11.6)
      end
```

Appendix B

Bureaucracy

Following are Publication Agreements for each of the three articles reprinted from the Astrophysical Journal in this thesis:

McLaughlin, D. E., & Pudritz, R. E. 1996a, ApJ, 457, 578
McLaughlin, D. E., & Pudritz, R. E. 1996b, ApJ, 469, 194
McLaughlin, D. E., & Pudritz, R. E. 1997, ApJ, 476, 750

PUBLICATION AGREEMENT
American Astronomical Society

Date: July 14, 1995

To: Dr. Dean E. McLaughlin
Department of Physics and Astronomy
McMaster University
Hamilton, ON, Canada L8S 4M1

E-Number: 32114J
(January 10, 1996 issue of Ap. J.)

Dear Colleague:

With regard to your original and previously unpublished paper entitled: THE FORMATION OF GLOBULAR CLUSTER SYSTEMS. I. THE LUMINOSITY FUNCTION
written by you and Ralph E. Pudritz

which has been accepted for publication in our journal, the following terms are submitted for your consideration. If these terms are satisfactory, please sign below and return this agreement to us. We cannot publish your paper without this approval.

Copyright Assignment: Because the Society, acting through the University of Chicago Press, is undertaking to publish this paper, and because you desire to have this paper so published, you grant and assign the entire copyright for this paper exclusively to the Society. The copyright consists of all rights protected by the copyright laws of the United States and of all foreign countries, in all languages and forms of communication.

The Society, in turn, grants to you the non-exclusive right of republication, subject only to your giving appropriate credit to the Journal. To protect the copyright in this paper, the original copyright notice as it appears in the Journal should be included in the credit.

Compensation and Subsidiary Rights: It is understood that you will receive no monetary compensation from the Society for the assignment of copyright and publication of the paper. Please note, however, that you may grant or deny requests to reprint this paper in books or journals, and you may retain all fees from such reprinting. We will forward such requests to you.

Who Should Sign: The agreement should be signed by at least one of the authors (who agrees to inform the others, if any) or, in the case of a "work made for hire," by the employer.

An author who is a U.S. Government officer or employee *and* who prepared the paper as part of his or her official duties does not own any copyright in it. If at least one of the authors is not in this category, that author should sign below. If all the authors are in this category, please return this form unsigned.

FOR THE AMERICAN ASTRONOMICAL SOCIETY:

Helmut A. Abt, Managing Editor
The Astrophysical Journal, Part I
and *The Astrophysical Journal*
Supplement Series

A. Dalgarno, Letters Editor
The Astrophysical Journal, Part II

ACCEPTED AND APPROVED FOR THE AUTHOR(S)

Author's signature

DATE: JULY 18/95

Our address is printed on the other side; you need only fold and fasten this sheet and attach a stamp.

PUBLICATION AGREEMENT
American Astronomical Society

Date: April 11, 1996

To: Dr. Dean E. McLaughlin
Department of Physics and Astronomy
McMaster University
Hamilton, ON, Canada L8S 4M1

E-Number: 33750
(October 1, 1996 issue of Ap. J.)

Dear Colleague:

With regard to your original and previously unpublished paper entitled: A MODEL FOR THE INTERNAL STRUCTURE OF MOLECULAR CLOUD CORES
written by you and Ralph E. Pudritz

which has been accepted for publication in our journal, the following terms are submitted for your consideration. If these terms are satisfactory, please sign below and return this agreement to us. We cannot publish your paper without this approval.

Copyright Assignment: Because the Society, acting through the University of Chicago Press, is undertaking to publish this paper, and because you desire to have this paper so published, you grant and assign the entire copyright for this paper exclusively to the Society. The copyright consists of all rights protected by the copyright laws of the United States and of all foreign countries, in all languages and forms of communication.

The Society, in turn, grants to you the non-exclusive right of republication, subject only to your giving appropriate credit to the Journal. To protect the copyright in this paper, the original copyright notice as it appears in the Journal should be included in the credit.

Compensation and Subsidiary Rights: It is understood that you will receive no monetary compensation from the Society for the assignment of copyright and publication of the paper. Please note, however, that you may grant or deny requests to reprint this paper in books or journals, and you may retain all fees from such reprinting. We will forward such requests to you.

Who Should Sign: The agreement should be signed by at least one of the authors (who agrees to inform the others, if any) or, in the case of a "work made for hire," by the employer.

An author who is a U.S. Government officer or employee *and* who prepared the paper as part of his or her official duties does not own any copyright in it. If at least one of the authors is not in this category, that author should sign below. If all the authors are in this category, please return this form unsigned.

FOR THE AMERICAN ASTRONOMICAL SOCIETY:

Helmut A. Abt, Managing Editor
The Astrophysical Journal, Part I
and *The Astrophysical Journal Supplement Series*

A. Dalgarno, Letters Editor
The Astrophysical Journal, Part II

ACCEPTED AND APPROVED FOR THE AUTHOR(S)

Author's signature

DATE: APRIL 16/96

Our address is printed on the other side; you need only fold and fasten this sheet and attach a stamp.

PUBLICATION AGREEMENT
American Astronomical Society

Date: September 16, 1996

To: Dr. Dean E. McLaughlin
Department of Physics and Astronomy
McMaster University
Hamilton, ON, Canada L8S 4M1

E-Number: 34766
(February 20, 1997 issue of ApJ0

Dear Colleague:

With regard to your original and previously unpublished paper entitled: GRAVITATIONAL COLLAPSE AND STAR FORMATION IN LOGOTROPIC AND NON-ISOTHERMAL SPHERES
written by you and Ralph E. Pudritz

which has been accepted for publication in our journal, the following terms are submitted for your consideration. If these terms are satisfactory, please sign below and return this agreement to us. We cannot publish your paper without this approval.

Copyright Assignment: Because the Society, acting through the University of Chicago Press, is undertaking to publish this paper, and because you desire to have this paper so published, you grant and assign the entire copyright for this paper exclusively to the Society. The copyright consists of all rights protected by the copyright laws of the United States and of all foreign countries, in all languages and forms of communication.

The Society, in turn, grants to you the non-exclusive right of republication, subject only to your giving appropriate credit to the Journal. To protect the copyright in this paper, the original copyright notice as it appears in the Journal should be included in the credit.

Compensation and Subsidiary Rights: It is understood that you will receive no monetary compensation from the Society for the assignment of copyright and publication of the paper. Please note, however, that you may grant or deny requests to reprint this paper in books or journals, and you may retain all fees from such reprinting. We will forward such requests to you.

Who Should Sign: The agreement should be signed by at least one of the authors (who agrees to inform the others, if any) or, in the case of a "work made for hire," by the employer.

An author who is a U.S. Government officer or employee *and* who prepared the paper as part of his or her official duties does not own any copyright in it. If at least one of the authors is not in this category, that author should sign below. If all the authors are in this category, please return this form unsigned.

FOR THE AMERICAN ASTRONOMICAL SOCIETY:

Helmut A. Abt, Managing Editor
The Astrophysical Journal, Part I
and *The Astrophysical Journal*
Supplement Series

A. Dalgarno, Letters Editor
The Astrophysical Journal, Part II

ACCEPTED AND APPROVED FOR THE AUTHOR(S)

Author's signature

DATE: SEPT. 24/96

Our address is printed on the other side; you need only fold and fasten this sheet and attach a stamp.

References

Adams, W. S. 1941, ApJ, 93, 11

Aguilar, L., Hut, P., & Ostriker, J. P. 1988, ApJ, 335, 720

Ajhar, E. A., Blakeslee, J. P., & Tonry, J. L. 1994, AJ, 108, 2087

Arons, J., & Max, C. E. 1975, ApJ, 196, L77

Ashman, K. M. 1990, MNRAS, 247, 662

Ashman, K. M., & Bird, C. M. 1993, AJ, 106, 2281

Ashman, K. M., & Zepf, S. E. 1992, ApJ, 384, 50

Baade, W. 1944a, ApJ, 100, 137

Baade, W. 1944b, ApJ, 100, 147

Barnard, E. E. 1919, ApJ, 49, 1

Barrett, A. H., Ho, P. T. P., & Myers, P. C. 1971, ApJ, 211, L39

Bates, D. R., & Spitzer, L. 1951, ApJ, 113, 441

Baum, W. A. 1955, PASP, 67, 328

Beichman, C. A., Myers, P. C., Emerson, J. P., Harris, S., Benson, P. J., & Jennings, R. E. 1986, ApJ, 307, 337

Beers, T. C., & Geller, M. J. 1983, ApJ, 274, 491

Bertoldi, F., & McKee, C. F. 1992, ApJ, 395, 140

Binney, J., & Tremaine, S. 1987, Galactic Dynamics (Princeton: Princeton Univ. Press)

Blaauw, A. 1991, in The Physics of Star Formation and Early Stellar Evolution, ed. C. J. Lada and N. D. Kylafis (Dordrecht: Kluwer), 125

Blitz, L. 1991, in The Physics of Star Formation and Early Stellar Evolution, ed. C. J. Lada and N. D. Kylafis (Dordrecht: Kluwer), 3

Blitz, L., & Stark, A. A. 1986, ApJ, 300, L89

Bloemen, J. B. G. M., Strong, A. W., Mayer-Hasselwander, H. A., Blitz, L., Cohen, R. S., Dame, T. M., Grabelsky, D. A., Thaddeus, P., Hermsen, W., & Lebrun, F. 1986, A&A, 154, 25

Bohlin, R. C., Savage, B. D., Drake, J. F. 1978, ApJ, 224, 132

Bonnor, W. B. 1956, MNRAS, 116, 351

Boulares, A., & Cox, D. P. 1990, ApJ, 365, 544

Bransden, B. H., & Joachain, C. J. 1989, Introduction to Quantum Mechanics (Hong Kong: Longman)

Brodie, J. P., & Huchra, J. 1991, ApJ, 379, 157

Burton, W. B., Gordon, M. A., Bania, T. M., & Lockman, F. J. 1975, ApJ, 202, 30

Caputo, F., & Castellani, V. 1984, MNRAS, 207, 185

Capuzzo-Dolcetta, R. 1993, ApJ, 415, 616

Carruthers, G. R. 1970, ApJ, 161, L81

Caselli, P., & Myers, P. C. 1995, ApJ, 446, 665

Chaboyer, B., Demarque, P., & Sarajedini, A. 1996, ApJ, 459, 558

Chandrasekhar, S., & Fermi, E. 1953, ApJ, 118, 116

Charlton, J. C., & Laguna, P. 1995, ApJ, 444, 193

Chernoff, D. F., & Shapiro, S. L. 1987, ApJ, 322, 113

Chernoff, D. F., & Weinberg, M. D. 1990, ApJ, 351, 121

Cheung, A. C., Rank, D. M., Townes, C. H., Thornton, D. D., & Welch, W. J. 1968, Phys. Rev. Lett., 21, 1701

Chièze, J. P. 1987, A&A, 171, 225

Clark, B. G. 1965, ApJ, 142, 1398

Clemens, D. P., Sanders, D. B., Scoville, N. Z., & Solomon, P. M. 1986, ApJS, 60, 297

Cohen, R. S., & Thaddeus, P. 1977, ApJ, 199, L105

Combes, F. 1991, ARA&A, 29, 195

Crutcher, R. M., Troland, T. H., Goodman, A. A., Heiles, C., Kazès, I., & Myers, P. C. 1993, ApJ, 407, 175

Dame, T. M., Ungerechts, H., Cohen, R., de Geus, E., Grenier, I., May, J., Murphy, D., Nyman, L. A., & Thaddeus, P. 1987, ApJ, 322, 706

de Vega, H. J., Sánchez, N., & Combes, F. 1996, Nature, 383, 56

Dickman, R. L. 1978, ApJS, 37, 407

Dickman, R. L., Horvath, M. A., & Margulis, M. 1990, ApJ, 365, 586

Dickman, R. L., Snell, R. L., & Schloerb, F. P. 1986, ApJ, 309, 326

Djorgovski, S. 1993, in ASP Conf. Ser. 50, Structure and Dynamics of Globular Clusters, ed. S. G. Djorgovski and G. Meylan (San Francisco: ASP), 373

Djorgovski, S. G., & Davis, M. 1987, ApJ, 313, 59

Djorgovski, S. G., & Meylan, G. 1994, AJ, 108, 1292

Dressler, A. 1980, ApJ, 236, 351

Duley, W. W., & Williams, D. A. 1984, Interstellar Chemistry (Oxford: Academic Press)

Dunham, T. 1937, PASP, 49, 26

Durrell, P. R., Harris, W. E., Geisler, D., & Pudritz, R. E. 1996, AJ, 112, 972

Durrell, P. R., McLaughlin, D. E., Harris, W. E., & Hanes, D. A. 1995, ApJ, 463, 543

Ebert, R. 1955, Z. Astrophys., 37, 217

Eddington, A. S. 1937, Observatory, 60, 99

Efremov, Y. N. 1995, AJ, 110, 2757

Eggen, O. J., Lynden-Bell, D., & Sandage, A. 1962, ApJ, 136, 748

Elmegreen, B. G. 1983, MNRAS, 203, 1011

Elmegreen, B. G. 1985, in Protostars & Planets II, ed. D. C. Black and M. S. Matthews (Tucson: Univ. of Arizona Press), 33

Elmegreen, B. G. 1989, ApJ, 338, 178

Elmegreen, B. G. 1991, in The Physics of Star Formation and Early Stellar Evolution, ed. C. J. Lada and N. D. Kylafis (Dordrecht: Kluwer), 35

Elmegreen, B. G. 1997, ApJ, 477, 196

Elmegreen, B. G., & Clemens, C. 1985, ApJ, 294, 523

Elmegreen, B. G., & Efremov, Y. N. 1997, ApJ, 480, 235

Elmegreen, B. G., & Falgarone, E. 1996, ApJ, 471, 816

Elson, R. A. W., & Schade, D. J. 1994, ApJ, 437, 625

Evans, N. J. 1991, in ASP Conf. Ser. 20, Frontiers of Stellar Evolution, ed. D. L. Lambert (San Francisco: ASP), 45

Ewen, H. I., & Purcell, E. M. 1951, Nature, 168, 356

Faber, S. M., & Gallagher, J. S. 1979, ARA&A, 17, 135

Faber, S. M., Dressler, A., Davies, R. L., Burstein, D., Lynden-Bell, D., Terlevich, R., & Wegner, G. 1987, in Nearly Normal Galaxies, ed. S. M. Faber (New York: Springer-Verlag), 175

Falgarone, E. 1995, in ASP Conf. Ser. 80, The Physics of the Interstellar Medium and Intergalactic Medium, ed. A. Ferrara, C. F. McKee, C. Heiles, and P. R. Shapiro (San Francisco: ASP), 158

Falgarone, E., Phillips, T. G., & Walker, C. K. 1991, ApJ, 378, 186

Fall, S. M., & Rees, M. J. 1977, MNRAS, 181, 37P

Fall, S. M., & Rees, M. J. 1985, ApJ, 298, 18

Fall, S. M., & Rees, M. J. 1988, in IAU Symposium No. 126, Globular Cluster Systems in Galaxies, ed. J. E. Grindlay and A. G. D. Philip (Dordrecht: Kluwer), 323

Federman, S. R., Glassgold, A. E., & Kwan, J. 1979, ApJ, 227, 466

Field, G. B. 1965, ApJ, 142, 531

Field, G. B., & Saslaw, W. C. 1965, ApJ, 142, 568

Field, G. B., Goldsmith, D. W., & Habing, H. J. 1969, ApJ, 155, L149

Fleck, R. C. 1980, ApJ, 242, 1019

Fleck, R. C. 1981, ApJ, 246, L151

Fleming, D. E. B., Harris, W. E., Pritchet, C. J., & Hanes, D. A. 1995, AJ, 109, 1044

Forbes, D. A., Brodie, J. P., & Grillmair, C. J. 1997, AJ, 113, 1652

Forbes, D. A., Franx, M., Illingworth, G. D., & Carollo, C. M. 1996, ApJ, 467, 126

Frenk, C. S., & White, S. D. M. 1980, MNRAS, 193, 295

Frerking, M. A., Langer, W. D., & Wilson, R. W. 1982, ApJ, 262, 590

Fuller, G. A., & Myers, P. C. 1992, ApJ, 384, 523

Geisler, D., & Forte, J. C. 1990, ApJ, 350, L5

Geisler, D., Lee, M. G., & Kim, E. 1996, AJ, 111, 1529

Genzel, R. 1992, in The Galactic Interstellar Medium, by W. B. Burton, B. G. Elmegreen, and R. Genzel (Berlin: Springer-Verlag), 275

Gerhard, O. E., & Binney, J. 1985, MNRAS, 216, 467

Gnedin, O. Y., & Ostriker, J. P. 1997, ApJ, 474, 223

Goldreich, P., & Kwan, J. 1974, ApJ, 189, 441

Goldsmith, P. F., & Arquilla, R. 1985, in Protostars & Planets II, ed. D. C. Black and M. S. Matthews (Tucson: Univ. of Arizona Press), 137

Goldsmith, P. F., & Langer, W. D. 1978, ApJ, 222, 881

Gomez, M., Hartmann, L., Kenyon, S. J., & Hewett, R. 1993, AJ, 105, 1927

Goodman, A. A., & Heiles, C. 1994, ApJ, 424, 208

Goodman, A. A., Benson, P. J., Fuller, G. A., & Myers, P. C. 1993, ApJ, 406, 528

Grillmair, C. J., Faber, S. M., Lauer, T. R., Baum, W. A., Lynd, C. R., O'Neil, E. J., & Shaya, E. J. 1994, AJ, 108, 102

Gunn, J. E., & Griffin, R. F. 1979, AJ, 84, 752

Habing, H. J. 1968, B.A.N., 19, 421

Halsey, T. C., Jensen, M. H., Kadenoff, L. P., Procaccia, I., & Shraiman, B. I. 1986, Phys. Rev. A, 33, 1141

Hanes, D. A. 1971, MSc Thesis, University of Toronto

Hanes, D. A. 1977a, MNRAS, 179, 331

Hanes, D. A. 1977b, Mem. R. Astron. Soc., 84, 45

Hanes, D. A., & Whittaker, D. G. 1987, AJ, 94, 906

Harris, G. L. H., Geisler, D., Harris, H. C., & Hesser, J. E. 1992, AJ, 104, 613

Harris, W. E. 1976, AJ, 81, 1095

Harris, W. E. 1986, AJ, 91, 822

Harris, W. E. 1991, ARA&A, 29, 543

Harris, W. E. 1995, in IAU Symposium No. 164, Stellar Populations, ed. P. C. van der Kruit and G. Gilmore (Dordrecht: Kluwer), 85

Harris, W. E. 1996a, in ASP Conf. Ser. 92, The Formation of the Galactic Halo....Inside and Out, ed. H. Morrison and A. Sarajedini (San Francisco: ASP), 231

Harris, W. E. 1996b, AJ, 112, 1487

Harris, W. E., & Pudritz, R. E. 1994, ApJ, 429, 177

Harris, W. E., & Racine, R. 1979, ARA&A, 17, 241

Harris, W. E., & van den Bergh, S. 1981, AJ, 86, 1627

Harris, W. E., Harris, G. L. H., & McLaughlin, D. E. 1997, AJ, submitted

Harris, W. E., Pritchet, C. J., & McClure, R. D. 1995, ApJ, 441, 120

Harris, W. E., Allwright, J. W. B., Pritchet, C. J., & van den Bergh, S. 1991, ApJS, 76, 115

Harris, W. E., Phelps, R. L., Madore, B. F., Pevunova, O., & Skiff, B. A. 1997, AJ, 113, 688

Hartmann, J. 1904, ApJ, 19, 268

Hartwick, F. D. A., & Sargent, W. L. W. 1978, ApJ, 221, 512

Hayashi, C., & Nakagawa, Y. 1975, Prog. Theor. Phys., 54, 93

Heiles, C., Goodman, A. A., McKee, C. F., & Zweibel, E. G. 1993, in Protostars and Planets III, ed. E. H. Levy and J. I. Lunine (Tucson: Univ. of Arizona Press), 279

Henriksen, R. N. 1991, ApJ, 377, 500

Henriksen, R. N., & Turner, B. E. 1984, ApJ, 287, 200

Hentschel, H. G. E., & Procaccia, I. 1983, Physica D, 8, 435

Herbst, E., & Klemperer, W. 1973, ApJ, 185, 505

Hilker, M., & Kissler-Patig, M. 1996, A&A, 314, 357

Hills, J. G. 1980, ApJ, 225, 986

Ho, P. T. P., & Townes, C. H. 1983, ARA&A, 21, 239

Hodge, P. 1988, PASP, 100, 568

Hollenbach, D. J., & Salpeter, E. E. 1971, ApJ, 163, 155

Hollenbach, D. J., Werner, M. W., & Salpeter, E. E. 1971, ApJ, 163, 165

Holtzman, J. A., et al. 1992, AJ, 103, 691

Holtzman, J. A., et al. 1996, AJ, 112, 416

Hubble, E. 1932, ApJ, 76, 44

Hunter, D. A., Shaya, E. J., Holtzman, J. A., Light, R. M., O'Neil, E. J., & Lynds, R. 1995, ApJ, 448, 179

Ibata, R. A., Gilmore, G., & Irwin, M. J. 1994, Nature, 370, 194

Jacoby, G. H., Branch, D., Ciardullo, R., Davies, R. L., Harris, W. E., Pierce, M. J., Pritchet, C. J., Tonry, J. L., & Welch, D. L. 1992, PASP, 104, 599

Jenkins, E. B., & Meloy, D. A. 1974, ApJ, 193, L121

Johnstone, D. 1993, AJ, 105, 155

Jura, M. 1974, ApJ, 191, 375

Jura, M. 1980, ApJ, 235, 63

Kang, H., Shapiro, P. R., Fall, S. M., & Rees, M. J. 1990, ApJ, 363, 488

Katz, N. 1992, ApJ, 391, 502

Katz, N., & Gunn, J. E. 1991, ApJ, 377, 365

Kavelaars, J. J., & Hanes, D. A. 1997, MNRAS, 285, L31

Kennicutt, R. C. 1983, ApJ, 272, 54

Kenyon, S. J., Hartmann, L. W., Strom, K. M., & Strom, S. E. 1990, AJ, 99, 869

Kim, S.-H., & Martin, P. G. 1996, ApJ, 462, 296

Kim, S.-H., Martin, P. G., & Hendry, P. D. 1994, ApJ, 422, 164

King, I. R. 1966, AJ, 71, 64

Kippenhahn, R., & Weigert, A. 1990, Stellar Structure and Evolution (Berlin: Springer-Verlag)

Kissler-Patig, M. 1997, A&A, 319, 83

Kissler-Patig, M., Richtler, T., & Hilker, M. 1996, A&A, 308, 74

Kormendy, J., & Richstone, D. 1995, ARA&A, 33, 581

Kraft, R. P. 1994, PASP, 106, 553

Kulkarni, S. R., & Heiles, C. 1988, in Galactic and Extragalactic Radio Astronomy, Second Edition, ed. G. L. Verschuur and K. I. Kellerman (New York: Springer-Verlag), 95

Kumai, Y., Basu, B., & Fujimoto, M. 1993a, ApJ, 404, 144

Kumai, Y., Hashi, Y., & Fujimoto, M. 1993b, ApJ, 416, 576

Kundić, T., & Ostriker, J. P. 1995, ApJ, 438, 702

Kwan, J. 1979, ApJ, 229, 567

Lada, E. A. 1992, ApJ, 393, L25

Lada, E. A., Bally, J., & Stark, A. A. 1991a, ApJ, 368, 432

Lada, E. A., DePoy, D. L., Evans, N. J., & Gatley, I. 1991b, ApJ, 371, 171

Lada, E. A., Strom, K. M., & Myers, P. C. 1993, in Protostars and Planets III, ed. E. H. Levy and J. I. Lunine (Tucson: Univ. of Arizona Press), 245

Laird, J. B., Carney, B. W., Rupen, M. P., & Latham, D. W. 1988, AJ, 96, 1908

Lang, K. R. 1980, Astrophysical Formulae, Second Edition (New York: Springer-Verlag)

Langer, W. D., Velusamy, T., Kuiper, T. B. H., Levin, S., Olsen, E., & Migenes, V. 1995, ApJ, 453, 293

Larson, R. B. 1981, MNRAS, 194, 809

Larson, R. B. 1982, MNRAS, 200, 159

Larson, R. B. 1988, in IAU Symposium No. 126, Globular Cluster Systems in Galaxies, ed. J. E. Grindlay and A. G. D. Philip (Dordrecht: Kluwer), 311

Larson, R. B. 1990, in Physical Processes in Fragmentation and Star Formation, ed. R. Capuzzo-Dolcetta, C. Chiosi, & A. Di Fazio (Dordrecht: Kluwer), 389

Larson, R. B. 1992, in Star Formation in Stellar Systems, ed. G. Tenorio-Tagle, M. Prieto, and F. Sanchez (Cambridge: Cambridge Univ. Press), 125

Larson, R. B. 1993, in ASP Conf. Ser. 48, The Globular Cluster-Galaxy Connection, ed. G. H. Smith and J. P. Brodie (San Francisco: ASP), 675

Larson, R. B. 1996, in ASP Conf. Ser. 92, Formation of the Galactic Halo....Inside and Out, ed. H. Morrison and A. Sarajedini (San Francisco: ASP), 241

Lauer, T. R., & Kormendy, J. 1986, ApJ, 303, L1

Lee, H. M., & Goodman, J. 1995, ApJ, 443, 109

Lee, M. G., & Geisler, D. 1993, AJ, 106, 493

Leisawitz, D., Bash, F. N., & Thaddeus, P. 1989, ApJS, 70, 731

Leung, C. M. 1985, in Protostars & Planets II, ed. D. C. Black and M. S. Matthews (Tucson: Univ. of Arizona Press), 104

Lichtenberg, A. J., & Lieberman, M. A. 1991, Regular and Chaotic Dynamics, Second Edition (New York: Springer-Verlag)

Lizano, S., & Shu, F. H. 1989, ApJ, 342, 834

Longair, M. S. 1994, High-Energy Astrophysics, Second Edition, Volume 2: Stars, the Galaxy and the Interstellar Medium (Cambridge: Cambridge Univ. Press)

Loren, R. B. 1989a, ApJ, 338, 902

Loren, R. B. 1989b, ApJ, 338, 925

Lovejoy, S. 1982, Science, 216, 185

Lynds, B. T. 1962, ApJS, 7, 1

Maddalena, R., & Thaddeus, P. 1985, ApJ, 294, 231

Majewski, S. R. 1993, in ASP Conf. Ser. 49, Galaxy Evolution: The Milky Way Perspective, ed. S. R. Majewski (San Francisco: ASP), 5

Majewski, S. R., Hawley, S. L., & Munn, J. A. 1996, in ASP Conf. Ser. 92, Formation of the Galactic Halo....Inside and Out, ed. H. Morrison and A. Sarajedini (San Francisco: ASP), 119

Mandelbrot, B. B. 1983, The Fractal Geometry of Nature (New York: Freeman)

Mandushev, G., Spassova, N., & Staneva, A. 1991, A&A, 252, 94

Mathis, J. S. 1990, ARA&A, 28, 37

Mathis, J. S. 1996, ApJ, 472, 643

McKee, C. F. 1989, ApJ, 345, 782

McKee, C. F. 1995, in ASP Conf. Ser. 80, The Physics of the Interstellar Medium and Intergalactic Medium, ed. A. Ferrara, C. F. McKee, C. Heiles, and P. R. Shapiro (San Francisco: ASP), 292

McKee, C. F., & Ostriker, J. P. 1977, ApJ, 218, 148

McKee, C. F., & Zweibel, E. G. 1995, ApJ, 440, 686

McKee, C. F., Zweibel, E. G., Goodman, A. A., & Heiles, C. 1993, in Protostars and Planets III, ed. E. H. Levy and J. I. Lunine (Tucson: Univ. of Arizona Press), 327

McKellar, A. 1940, PASP, 52, 187

McLaughlin, D. E. 1994, PASP, 106, 47

McLaughlin, D. E. 1995, AJ, 109, 2034

McLaughlin, D. E., & Pudritz, R. E. 1996a, ApJ, 457, 578

McLaughlin, D. E., & Pudritz, R. E. 1996b, ApJ, 469, 194

McLaughlin, D. E., & Pudritz, R. E. 1997, ApJ, 476, 750

McLaughlin, D. E., Harris, W. E., & Hanes, D. A. 1993, ApJ, 409, L45

McLaughlin, D. E., Harris, W. E., & Hanes, D. A. 1994, ApJ, 422, 486

McLaughlin, D. E., Secker, J., Harris, W. E., & Geisler, D. 1995, AJ, 109, 1033

Meakin, P. 1986, in On Growth and Form: Fractal and Non-Fractal Patterns in Physics, ed. H. E. Stanley and N. Ostrowsky (Dordrecht: Kluwer), 111

Meakin, P., & Donn, B. 1988, ApJ, 329, L39

Merrill, P. W. 1934, PASP, 46, 206

Merrill, P. W. 1936, ApJ, 83, 126

Meurer, G. R., Heckman, T. M., Leitherer, C., Kinney, A., Robert, C., & Garnett, D. A. 1995, AJ, 110, 2665

Meylan, G., & Heggie, D. C. 1997, A&A Rev., 8, 1

Mihalas, D., & Binney, J. 1981, Galactic Astronomy: Structure and Kinematics (New York: Freeman)

Miller, G. E., & Scalo, J. M. 1979, ApJS, 41, 513

Minniti, D. 1996, ApJ, 459, 175

Minniti, D., Meylan, G., & Kissler-Patig, M. 1996, A&A, 312, 49

Moore, B. 1996, ApJ, 461, L13

Morris, M., Zuckerman, B., Palmer, P., & Turner, B. E. 1973, ApJ, 186, 501

Mouschovias, T. Ch. 1976a, ApJ, 206, 753

Mouschovias, T. Ch. 1976b, ApJ, 207, 141

Mouschovias, T. Ch. 1987, in Physical Processes in Interstellar Clouds, ed. G. E. Morfill & M. Scholer (Dordrecht: Reidel), 453

Mouschovias, T. Ch., & Spitzer, L. 1976, ApJ, 210, 326

Murali, C., & Weinberg, M. D. 1997, MNRAS, in press

Murray, S. D., & Lin, D. N. C. 1989a, ApJ, 339, 933

Murray, S. D., & Lin, D. N. C. 1989b, ApJ, 346, 155

Murray, S. D., & Lin, D. N. C. 1990, ApJ, 357, 105

Murray, S. D., & Lin, D. N. C. 1992, ApJ, 400, 265

Murray, S. D., & Lin, D. N. C. 1993, in ASP Conf. Ser. 48, The Globular Cluster-Galaxy Connection, ed. G. H. Smith and J. P. Brodie (San Francisco: ASP), 738

Myers, P. C. 1985, in Protostars & Planets II, ed. D. C. Black and M. S. Matthews (Tucson: Univ. of Arizona Press), 81

Myers, P. C., & Benson, P. J. 1983, ApJ, 266, 309

Myers, P. C., & Goodman, A. A. 1988a, ApJ, 326, L27

Myers, P. C., & Goodman, A. A. 1988b, ApJ, 329, 392

Myers, P. C., Goodman, A. A., Güsten, R., & Heiles, C. 1995, ApJ, 442, 177

Norman, C., & Silk, J. 1980, ApJ, 238, 158

Nozakura, T. 1990, MNRAS, 243, 543

O'Connell, R. W., Gallagher, J. S., & Hunter, D. A. 1994, ApJ, 433, 65

O'Connell, R. W., Gallagher, J. S., Hunter, D. A., & Colley, W. S. 1995, ApJ, 446, L1

Oh, K. S., & Lin, D. N. C. 1992, ApJ, 386, 519

Okazaki, T., & Tosa, M. 1995, MNRAS, 274, 48

Ostriker, J. P., Binney, J., & Saha, P. 1989, MNRAS, 241, 849

Ostriker, J. P., Spitzer, L., & Chevalier, R. A. 1972, ApJ, 176, L51

Ostrov, P., Geisler, D., & Forte, J. C. 1993, AJ, 105, 1762

Palla, F., & Zinnecker, H. 1988, in IAU Symposium No. 126, Globular Cluster Systems in Galaxies, ed. J. E. Grindlay and A. G. D. Philip (Dordrecht: Kluwer), 697

Pascarelle, S. M., Windhorst, R. A., Keel, W. C., & Odewahn, S. C. 1996, Nature, 383, 45

Peebles, P. J. E. 1984, ApJ, 277, 470

Peebles, P. J. E., & Dicke, R. H. 1968, ApJ, 154, 891

Pesce, E., Capuzzo-Dolcetta, R., & Vietri, M. 1992, MNRAS, 254, 466

Phelps, R. L., & Lada, E. A. 1997, ApJ, 477, 176

Press, W. H., Teukolsky, S. A., Vetterling, W. T., & Flannery, B. P. 1992, Numerical Recipes in Fortran, Second Edition (Cambridge, MA: Cambridge Univ. Press)

Pryor, C., & Meylan, G. 1993, in ASP Conf. Ser. 50, Structure and Dynamics of Globular Clusters, ed. S. G. Djorgovski and G. Meylan (San Francisco: ASP), 357

Pudritz, R. 1990, ApJ, 350, 195

Racine, R. 1968a, PASP, 80, 326

Racine, R. 1968b, JRASC, 62, 367

Rees, M. J., & Ostriker, J. P. 1977, MNRAS, 179, 541

Richer, H. B., Crabtree, D. R., Fabian, A. C., & Lin, D. N. C. 1993, AJ, 105, 877

Richer, H. B., et al. 1996, ApJ, 463, 602

Richstone, D. O., & Tremaine, S. 1986, AJ, 92, 72

Rosenblatt, E. I., Faber, S. M., & Blumenthal, G. R. 1988, ApJ, 330, 191

Russell, H. N. 1935, MNRAS, 95, 635

Saha, M. N. 1937, Nature, 139, 840

Salpeter, E. E. 1955, ApJ, 121, 161

Sandage, A. 1953, AJ, 58, 61

Sandage, A. 1990, JRASC, 84, 70

Sanders, D. B., Clemens, D. P., Scoville, N. Z., & Solomon, P. M. 1986, ApJS, 60, 1

Sanders, D. B., Scoville, N. Z., & Solomon, P. M. 1985, ApJ, 289, 373

Sarajedini, A., & King, C. R. 1989, AJ, 98, 1624

Savage, B. D., Bohlin, R. C., Drake, J. F., & Budich, W. 1977, ApJ, 216, 291

Scalo, J. M. 1985, in Protostars & Planets II, ed. D. C. Black and M. S. Matthews (Tucson: Univ. of Arizona Press), 201

Scalo, J. M. 1986, Fund. Cosmic Phys., 11, 1

Scalo, J. 1990, in Physical Processes in Fragmentation and Star Formation, ed. R. Capuzzo-Dolcetta, C. Chiosi, and A. de Fazio (Dordrecht: Kluwer), 151

Scalo, J. M., & Pumphrey, W. A. 1982, ApJ, 258, L29

Scheffler, H., & Elsässer, H. 1988, Physics of the Galaxy and Interstellar Matter (Berlin: Springer-Verlag)

Schwartz, P. R., Wilson, W. J., & Epstein, E. E. 1973, ApJ, 186, 529

Schweizer, F. 1987, in Nearly Normal Galaxies, ed. S. M. Faber (New York: Springer-Verlag), 18

Schweizer, F., Miller, B. W., Whitmore, B. C., & Fall, M. S. 1996, AJ, 112, 1839

Scoville, N. Z., & Sanders, D. B. 1987, in Interstellar Processes, ed. D. J. Hollenbach and H. A. Thronson (Dordrecht: Reidel), 21

Scoville, N. Z., & Solomon, P. M. 1975, ApJ, 199, L105

Scoville, N. Z., Yun, M. S., Clemens, D. P., Sanders, D. B., & Waller, W. H. 1987, ApJS, 63, 821

Searle, L., & Zinn, R. 1978, ApJ, 225, 357

Secker, J. 1992, AJ, 104, 1472

Secker, J., & Harris, W. E. 1993, AJ, 105, 1358

Secker, J., Geisler, D., McLaughlin, D. E., & Harris, W. E. 1995, AJ, 109, 1019

Shapiro, P. R., & Kang, H. 1987, ApJ, 318, 32

Shapley, H. 1918, ApJ, 48, 89

Shu, F. H. 1992, The Physics of Astrophisics, Volume 2: Gas Dynamics (Mill Valley: University Science Books)

Shull, J. M., & Beckwith, S. 1982, ARA&A, 20, 163

Silk, J. 1977, ApJ, 211, 638

Solomon, P. M., Sanders, D. B., & Rivolo, R. 1985, ApJ, 292, L19

Solomon, P. M., Rivolo, A. R., Barrett, J., & Yahil, A. 1987, ApJ, 319, 730

Spitzer, L. 1956, ApJ, 124, 20

Spitzer, L. 1978, Physical Processes in the Interstellar Medium (New York: Wiley)

Spitzer, L. 1987, Dynamical Evolution of Globular Clusters (Princeton: Princeton Univ. Press)

Spitzer, L., & Chevalier, R. A. 1973, ApJ, 183, 565

Sreenivasan, K. R. 1991, Ann. Rev. Fluid Mech., 23, 539

Stetson, P. B., VandenBerg, D. A., & Bolte, M. 1996, PASP, 108, 560

Strittmatter, P. A. 1966, MNRAS, 132, 359

Strong, A. W., Bloemen, J. B. G. M., Dame, T. M., Grenier, I. A., Hermsen, W., Lebrun, F., Nyman, L.-A., Pollock, A. M. T., & Thaddeus, P. 1988, A&A, 207, 1

Stutzki, J., & Güsten, R. 1990, ApJ, 356, 513

Suntzeff, N. 1993, in ASP Conf. Ser. 48, The Globular Cluster-Galaxy Connection, ed. G. H. Smith and J. P. Brodie (San Francisco: ASP), 167

Surdin, V. G. 1979, Sov. Astron., 23, 648

Swings, P. 1937, MNRAS, 97, 212

Swings, P., & Rosenfeld, L. 1937, ApJ, 86, 483

Sylos-Labini, F., & Pietronero, L. 1996, ApJ, 469, 26

Taillet, R., Salati, P., & Longaretti, P.-Y. 1996, ApJ, 461, 104

Tielens, A. G. G. M., & Hollenbach, D. 1985, ApJ, 291, 722

Tomisaka, K., Ikeuchi, S., & Nakamura, T. 1988a, ApJ, 326, 208

Tomisaka, K., Ikeuchi, S., & Nakamura, T. 1988b, ApJ, 335, 239

Tomisaka, K., Ikeuchi, S., & Nakamura, T. 1989, ApJ, 341, 220

Tremaine, S. D. 1976, ApJ, 203, 345

Tremaine, S. D., Ostriker, J. P., & Spitzer, L. 1975, ApJ, 196, 407

Trimble, V. 1987, ARA&A, 25, 425

Troland, T. H. 1990, in IAU Symposium No. 140, Galactic and Extragalactic Magnetic Fields, ed. R. Beck, P. Kronberg, and R. Wielebinski (Dordrecht: Kluwer), 293

Turner, B. E., & Ziurys, L. M. 1988, in Galactic and Extragalactic Radio Astronomy, Second Edition, ed. G. L. Verschuur and K. I. Kellerman (New York: Springer-Verlag), 200

van de Hulst, H. C. 1945, Ned. Tijdsch. Natuurk, 11, 201

van den Bergh, S. 1975, ARA&A, 13, 217

van den Bergh, S., Morbey, C., & Pazder, J. 1991, ApJ, 375, 594

van Dishoeck, E. F., & Black, J. H. 1986, ApJS, 62, 109

VandenBerg, D. A., Bolte, M. J., & Stetson, P. B. 1990, AJ, 100, 445

VandenBerg, D. A., Bolte, M., & Stetson, P. B. 1996, ARA&A, 34, 461

Vesperini, E. 1997, MNRAS, in press (preprint astro-ph 9702067)

Vietri, M., & Pesce, E. 1995, ApJ, 442, 618

Watson, A. M., et al. 1996, AJ, 112, 534

Watson, W. D. 1976, Rev. Mod. Phys., 48, 513

Watson, W. D., & Salpeter, E. E. 1972a, ApJ, 174, 321

Watson, W. D., & Salpeter, E. E. 1972b, ApJ, 175, 659

Weidenschilling, S. J., & Ruzmaikina, T. V. 1994, ApJ, 430, 713

Weinberg, M. D. 1994a, AJ, 108, 1398

Weinberg, M. D. 1994b, AJ, 108, 1403

Weinberg, M. D. 1994c, AJ, 108, 1414

Weinreb, S., Barrett, A. H., Meeks, M. L., & Henry, J. C. 1963, Nature, 200, 829

West, M. J. 1993, MNRAS, 265, 755

West, M. J., Côté, P., Jones, C., Forman, W., & Marzke, R. O. 1995, ApJ, 453, L77

White, S. D. M., & Frenk, C. S. 1991, ApJ, 379, 52

White, S. D. M., & Rees, M. J. 1978, MNRAS, 183, 341

Whitmore, B. C., & Schweizer, F. 1995, AJ, 109, 960

Whitmore, B. C., Schweizer, F., Leitherer, C., Borne, K., & Robert, C. 1993, AJ, 106, 1354

Whitmore, B. C., Sparks, W. B., Lucas, R. A., Machetto, F. D., & Biretta, J. A. 1995, ApJ, 454, L73

Wilking, B. A., Lada, C. J., & Young, E. T. 1989, ApJ, 340, 823

Williams, J. P., & McKee, C. F. 1997, ApJ, 476, 166

Williams, J. P., Blitz, L., & Stark, A. A. 1995, ApJ, 451, 252

Williams, J. P., de Geus, E. J., & Blitz, L. 1994, ApJ, 428, 693

Williamson, F. O., Sanders, W. T., Kraushaar, W. L., McCammon, D., Borken, R., & Bunner, A. N. 1974, ApJ, 193, L133

Wilson, R. W., Jefferts, K. B., & Penzias, A. A. 1970, ApJ, 161, L43

Wilson, T. L., & Walmsley, C. M. 1989, A&A Rev., 1, 141

Wright, E. L. 1987, ApJ, 320, 818

York, D. G. 1974, ApJ, 193, L127

Zepf, S. E., & Ashman, K. M. 1993, MNRAS, 264, 611

Zepf, S. E., Ashman, K. M., & Geisler, D. 1995, ApJ, 443, 570

Zhou, S., Evans, N. J., Kömpe, C., & Walmsley, C. M. 1993, ApJ, 404, 232

Zinn, R. 1980, ApJ, 241, 602

Zinn, R. 1985, ApJ, 293, 424

Zinn, R. 1993, in ASP Conf. Ser. 48, The Globular Cluster-Galaxy Connection, ed. G. H. Smith and J. P. Brodie (San Francisco: ASP), 302

Zinn, R., & West, M. J. 1984, ApJS, 55, 45

Zinnecker, H., McCaughrean, M. J., & Wilking, B. A. 1993, in Protostars and Planets III, ed. E. H. Levy and J. I. Lunine (Tucson: Univ. of Arizona Press), 429

Zuckerman, B., & Evans, N. J. 1974, ApJ, 192, L149

Zuckerman, B., & Palmer, P. 1974, ARA&A, 12, 279

Zweibel, E. G. 1990, ApJ, 348, 186

IMAGE EVALUATION TEST TARGET (QA-3)

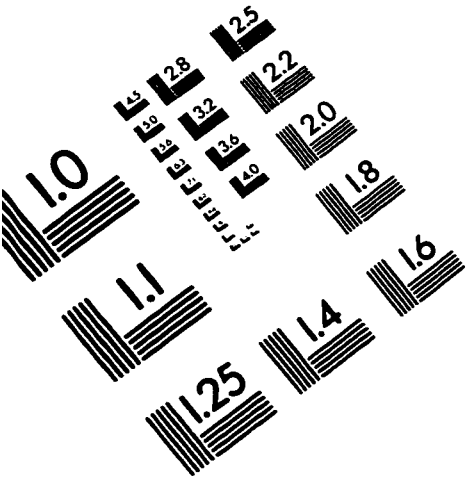

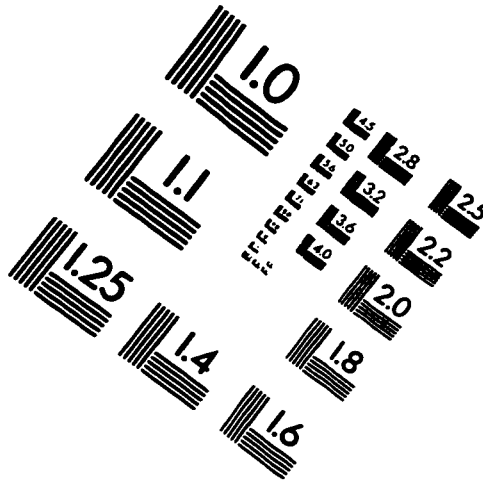

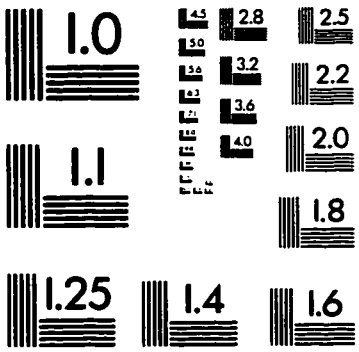

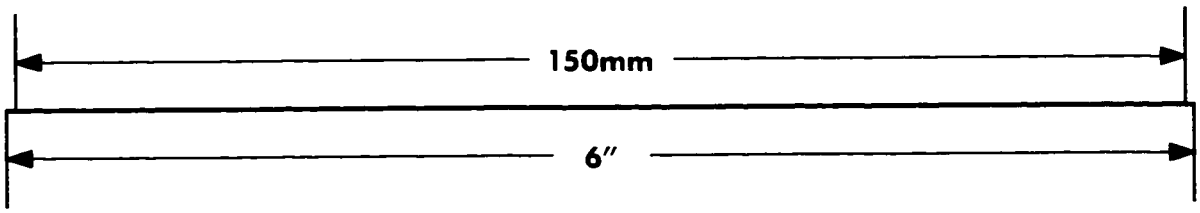

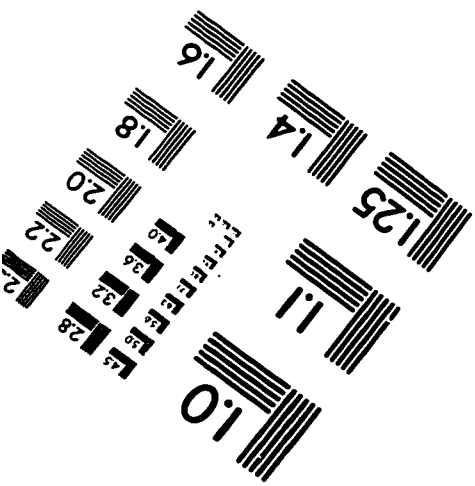

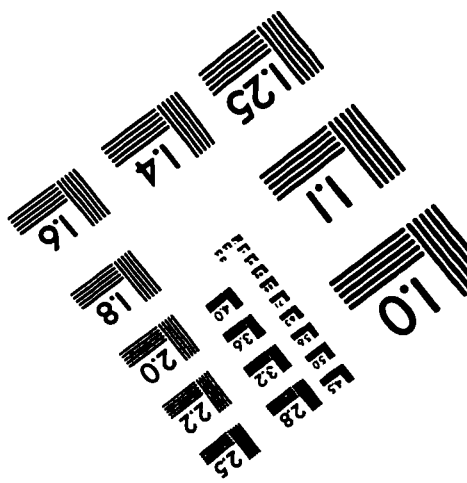

APPLIED IMAGE, Inc
1653 East Main Street
Rochester, NY 14609 USA
Phone: 716/482-0300
Fax: 716/288-5989